CANMET

Canadian Rockburst Research Program

Phase II

SEPTEMBER 1998

FINAL REPORT

EDITORS:

Parviz Mottahed

and

James B. Vance

SP98-017E

Natural Resources Canada | Ressources naturelles Canada

Canada

Catalogue No. M38-15/98-017E

ISBN 0-660-17551-7

This publication is available from:

CANMET

Minerals and Metals Sector

Natural Resources Canada

Ottawa, Ontario

K1A 0E4

Telephone: (613) 992-1285

Facsimile: (613) 947-6606

Cette publication est également disponible en français sous le titre *Programme canadien de recherche sur les coups de toit, Phase II : 1990-1995, Rapport final*

Nº de catalogue : M38-15/98-017F

ISBN 0-660-96017-6

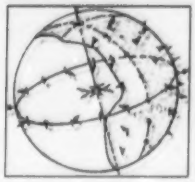

Preface

Rockbursts, witnessed as sudden and explosive ejections of rock accompanied by a release of seismic energy, have been a concern in Canada's hard rock mines ever since extraction has been carried out at moderate and deeper levels. Rockbursts are not linked to one mining area of the country but occur in widely separated regions. Rockbursts are hazardous to human life and detrimental to mining activity, and these things are driving the quest to predict them.

However, the predictability of such occurrences — the "where" and the "when" — still eludes us. Not surprisingly, many aspects of the mine extraction environment (rock mass stiffness, distribution of the natural stress field, the effects of major geological structures, the geometry and arrangement of underground openings, and extraction advance speed and quantity) will have an effect on the location and magnitude of rockbursting events. Many fields of study are required to evaluate, understand and develop solutions to this major impediment to deep mining: induced stress behaviour, ground control, rock mass and rock material behaviour, and integrity monitoring.

Phase II of the Canadian Rockburst Research Program, for which this report was prepared, was organized as a co-operative venture between industry, universities, the Government of Ontario and CANMET. Its objective was to develop practical engineering technologies and methods for mine operators to reduce and mitigate the effects of rockbursts in Canadian mines.

CANMET's contribution to this program, in line with its mandate to improve health and safety conditions for mine workers, centred on the monitoring of mining-induced seismic events. Several technologies were perfected: notably, an advanced algorithm for source location of events; state-of-the-art monitoring seismic systems and analysis software for additional capability in the analyses of full waveforms; and the regional seismic system, known as the CANMET Digital Seismograph Network (CDSN). CANMET also continued to monitor and analyze major seismic events in support of individual mining operations.

This report, outlining the technological developments related to CANMET's contribution, is a substantial work on the subject of seismic monitoring. It should be invaluable to the industry and to others who are now routinely using this technology to address mining under high ground stresses.

CANMET is proud of the role it has played in the project, and the contribution of its staff under the technical leadership of Dr. Parviz Mottahed, in developing needed technologies for the understanding and alleviation of rockbursts.

Marc Bétournay

Dr. Marc C. Bétournay
Manager
Mining Laboratories
CANMET

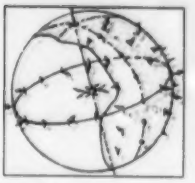

Foreword

The *Rockburst Handbook for Ontario Mines* was published following successful completion of Phase I of the Rockburst Research Program.

In 1990, the decision was made to proceed with Phase II of the research for another five years. The participants were CANMET, the Ontario Ministry of Northern Development and Mines, and 12 Ontario mines through the Mining Research Directorate (MRD, since renamed the Canadian Mining Research Organization (CAMIRO)). When Chile's CODELCO joined the program, the number of mines participating rose to 13.

Twelve million dollars was committed to the project, focused on four main areas of research:

- new data-acquisition systems;
- application of seismic data to mine design;
- source mechanisms of mining-induced seismicity; and
- characterization of cemented rockfill.

In addition, funding for applied research into more site-specific rockburst problems resulted in technical papers and reports on the findings.

In 1993, another rockburst research program was initiated, this time between the Province of Quebec, Quebec mine operators and the Government of Canada. The program was funded under Entente auxiliaire sur le développement minéral (EADM). The focus was on narrow-vein mining, commonly practised in Quebec, but the work was mostly contemporaneous with the research in Ontario.

The completion of Phase I and Phase II of rockburst research enabled microseismic monitoring to be applied to mine design with a higher degree of confidence than before. Ground-control engineers routinely include seismic monitoring equipment in their work and, with a better understanding of seismic sources, mine safety and productivity have improved.

CAMIRO has published the results of research by the other partners, which was co-ordinated through the Project Management Committee of the Canadian Rockburst Research Program (CRRP).

Jim Vance
Manager
Ground Control Program
CANMET

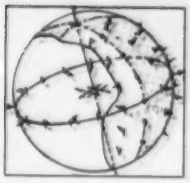

Acknowledgements

This publication is a result of five years of research by a dedicated team of scientists, engineers and technical support staff from CANMET's Mining and Mineral Sciences Laboratories (formerly Mining Research Laboratories). The various chapters have been prepared by several members of the group, whose contribution is gratefully acknowledged.

- Chapter 1: John E. Udd.
- Chapters 2, 3 and 6: Shahriar Talebi.
- Chapter 4, and appendices I and II: Paul Rochon and Denis Lebel.
- Chapter 5, and appendices III, IV and V: Maochen Ge.

In addition to this final report, CANMET produced many reports, publications and conference presentations of value to the mining industry during the program. These are listed in Appendix VI.

We gratefully acknowledge the contribution of the following individuals or organizations to the success of the program:

- The Canadian mining industry, for their support of this project.
- The Board of Directors of the Mining Research Directorate.
- The management committee of the Canadian Rockburst Research Program.
- All the ground-control and rock-mechanics staff of Mining Research Laboratories, particularly Behrouz Arjang, Martin Côté, Catherine Galley, Louise Laverdure, Michel Plouffe, Chris Pritchard and Maxine Lewis, who diligently and patiently typed the manuscript.

We also wish to thank Robert Lauriault, Manager, Communications, Mining and Mineral Sciences Laboratories–CANMET, and the publication production staff: Adèle Lessard, production co-ordinator and French editor; Jean MacGillivray, English editor; and Debra Seguin, graphic design and layout.

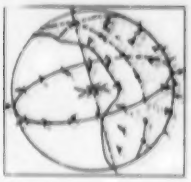

Canadian Rockburst Research Program

Partners in Funding the Program

Brunswick Mining & Smelting Ltd.
CANMET
CODELCO (El Teniente) Chile
Corona Corporation
Falconbridge Ltd.
Inco Ltd.
Lac Minerals Ltd.
Minnova Inc.
Noranda Minerals Inc.
Ontario Ministry of Northern Development and Mines
Placer Dome Inc.
Rio Algom Ltd.
Westmin Resources Ltd.

Members of the Project Management Committee

Charles Graham
Tony McKuch
Doug Morrison
Parviz Mottahed
Michel O'Flaherty
Yves Potvin
Bill Quesnel
Graham Swan

Mining Research Directorate

Peter Calder
John Gordon
Charles Graham
John Kelly
Michael Klugman
Sandy MacIntosh
Patrick Reed
John Udd

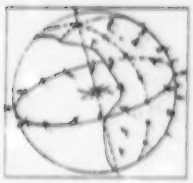

Table of Contents

History of Rockburst Research in Canada

1.1 Introduction

In the past few decades our understanding of the natural stresses that occur in the Earth's crust, and of the effect that these may have on man-made structures, has increased enormously. It is not so long ago that Wegener's Theory of Continental Drift was greeted with great scepticism, and the common view in mining was that the loads on underground structures were primarily of a superincumbent nature. When the first measurements of in situ stresses were made in Canada, by CANMET staff in the early 1960s, and when these disclosed that the principal stresses in rock masses were horizontal, they, too, were met with scepticism.

Today, in the late-1990s, it is well understood that the Earth's crust is in motion and that the natural stress field is dynamic. Scientists and engineers now recognize that the state of stress which occurs locally is a product of the geological environment, and is often related to the principal local structures and to past tectonic activity. Consequently, in mine design, it is generally accepted that the measurement of in situ stresses is a necessary element in the design of underground structures.

Equally, our understanding of rock mechanics has improved to the point where we know that whatever we do underground, vis-à-vis cutting excavations into the rock mass, will have an effect upon the pre-existing state of natural stress. Mine openings, as with any other openings in a stressed medium, cause the pre-existing stress field to be perturbed and the stresses to be concentrated around the openings. Stress concentrations and stress trajectories are part of the lexicon of today's mining engineer.

Knowing that what we do will affect the stability of the rock mass around mine openings, we also accept that, occasionally, a sudden redistribution of stresses can cause the strength of the rock mass to be exceeded so rapidly that an explosive failure of the rock can result. Rockbursts, as these events are called, are not acts of God, but rather the results of acts of man. Some circumstance, often unforeseen, has caused a local failure of the rock mass; be this the spalling of highly stressed rock at a point of concentration on the surface or an opening, the crushing of a pillar, or movement along a fault which has become unclamped. The latter are by far the most potentially dangerous because of the enormous amount of energy that can be released when a large volume of rock becomes suddenly de-stressed.

In the design of a system of underground openings, then, today's engineer must ponder not only the influences that man-made structures will have on the pre-existing state of stress, but also whether or not failures are a possibility. Analyses of the distributions of stresses, in both two and three dimensions, using a variety of numerical techniques, are a modern feature of both the design and the post-excavation monitoring of structures in rock. The objective of ground control is just exactly that!

1.2 Rockbursting in Canadian Mines

In his classic "Report on the Rockburst Situation in Ontario Mines," the late Professor R.G.K. Morrison reported that rockbursts had occurred intermittently since 1929, and possibly 1928 (Morrison, 1942). Commencing in 1934, however, bursting which caused concern to the mine operator began to take place in the Lake Shore Mine of the Kirkland Lake mining camp. According to W.T. Robson (Robson, 1946) the principal areas of concern were floor pillars: pillars, especially those in a branching vein structure; in an area of a complex fracture system; and in an area where a parallel and branching vein structure persisted vertically for over 1,100 feet.

From then on until 1940, the problem became much more acute in mines in several Ontario mining camps, notably Kirkland Lake; Larder Lake; the Porcupine; Sudbury; Little Long Lac; Pickle Lake; Uchi Lake; McKenzie Island; and Red Lake (Morrison, 1942). Several technical papers were published by the Canadian Institute of Mining and Metallurgy (as it was then known) during this period (Hodgson, 1943; Christian, 1939; Robertson, 1939; Langford, 1941; Robson, 1940). Many ideas were put forward to explain the phenomenon, but none of these addressed the possibility of the cause being the excessive stress concentrations caused by the mining practices of the day, especially a lack of sequencing in the extraction of the ore. It should be recalled that highly selective narrow-vein mining in hard, brittle and elastic rocks, and without any sequencing of stope and pillar extraction, was characteristic of the mines of the day in the mining camps mentioned.

It was Professor Morrison, drawing upon his experiences in the mines of the Kolar Gold Field in Mysore Sate, South India, who introduced the concept of a dome, or zone of de-stressed rock, around an opening in a stressed rock mass. He suggested that an appropriate strategy would be to control a gradual growth of the doming process, and to combine sequencing and support in order to reduce the effects. His intuitive grasp of the principles of stress analysis was simply phenomenal and he was years ahead of the field in promoting the concepts of stress control in mining. He is regarded as the father of rock mechanics in Canada.

From the mid-1940s, there was more "science" and less "art" in the design of underground mines. The concept of sequencing was generally accepted throughout the industry and the problem of rockbursting gradually abated. The first seismic monitoring system to be installed in a Canadian mine, based on a design by the United States Bureau of Mines, was in the Lake Shore Mine, in 1942 (Hodgson, 1943).

From then on, the implementation of improved mine design resulted in a dramatic reduction in the frequency of rockbursting. With the exception of three periods when there were increased fatalities, in the early 1950s and again in the early 1960s and the mid-1980s, the frequency has continued to decline (Hedley, 1992).

During the past three decades, however, the mining industry around the world has been introducing advanced mechanization and automation at an ever-increasing rate. This has been driven by several factors, including the need to remain competitive in international markets into which many more producers have entered; cost-efficiency and the relentless drive to greater productivity; and advances in equipment technology. Some of the results have been the replacement of high-cost selective methods of mining with lower-cost bulk mining methods and the larger production openings which were necessary. This, in turn, brought challenges to the established principles of design and practice.

In 1984, the rockburst problem in Ontario mines once again reached crisis proportions as a result of occurrences in both the Sudbury and Elliot Lake mining areas. In Sudbury, major rockbursts took place in both Falconbridge's Falconbridge Mine and Inco's Creighton Mine. In the former, four

miners were killed and the mine subsequently closed, resulting in the disruption of the work of 400 workers. In the latter, a part of the mine was severely damaged. At Elliot Lake, a series of rockbursts took place in the barrier pillar area between Rio Algom's Quirke Mine and the Denison Mine. Great concern was expressed about the possibility of an expanding zone of pillar collapse in these room-and-pillar operations.

1.3 The Canada-Ontario-Industry Rockburst Project, 1985-1990

As a result of these incidents, CANMET proposed a major tripartite research project to address the re-emerging rockburst problem (Udd, 1984). In this five-year, $4.2-million project, the largest collaborative mining research project ever undertaken in Canada up to that time, the federal government, through CANMET, agreed to fund a one-third share through the provision of the technical staff to perform the research. Equal contributions were made by the Government of Ontario, through the Ministry of Labour, for the purchase of equipment; and by the Ontario mining industry, through several companies and the Mining Research Directorate, for the on-site support necessary to effect local installations. The objectives were to improve the interpretation of microseismic signals and the accuracy of determining microseismic source locations; to improve evaluation of the effect of mining methods on local and regional stability conditions; and to develop leading-edge scientific capabilities in Canada and foster the spread of that technology throughout the industry.

By the conclusion of what became the first phase of a longer project, in 1990, all of the objectives had been achieved. It was particularly noteworthy that microseismic monitoring systems had been installed at all such mines where these were required. Local coverage across the province, at some 16 mines, was virtually complete; additional seismograph stations were installed in four mining areas to complement and fill in the existing stations of the Eastern Canada Grid of the Geological Survey of Canada (GSC). The accuracy of locating events and the speed of doing this were both greatly improved; macroseismic systems were developed as systems intermediate to the above, and were installed in major mines. These systems, which record waveforms, provide data for determining the source mechanisms; trials of de-stress blasting techniques and support systems for rockburst damage containment were made.

Equally important, though, was the higher level of expertise in Canada, achieved through the creation of teams of outstanding specialists at CANMET, at Queen's University at Kingston and Laurentian University in Sudbury, and in several mining organizations. By 1990, Canada's national rockburst expertise was second only to that of South Africa — a tremendous leap in only five years and a clear demonstration of the great benefits to be derived from collaborative research.

1.4 The Canadian Rockburst Research Program, 1990-1995

By 1990, largely as a result of increased expertise having been developed in Canada and the Canadian mining industry taking a more active role in the formulation of its research needs, the Mining Research Directorate of Sudbury assumed management of the program, at the request of industry. This organization, funded through the Ontario Mining Association, was established to act as a broker, to determine the needs of the companies participating and then arrange for the research to be delivered by other bodies — more or less along the lines that had been developed by the Australian Mineral Industries Research Association Limited (AMIRA).

At the beginning of the second phase of the work, the Project Management Committee defined both the strategic and tactical goals that were to be addressed during the next five years. Among the former were to improve the understanding of the rockburst phenomenon, and to use seismic and microseismic information in mine design (Project Management Committee, 1994). Among the latter were to improve the safety in and survivability of rockburst-prone excavations; to set design criteria for support; and to study the contribution of backfill to mine stability (Project Management Committee, 1994). In addition, the Management Committee determined that increasing the participation of industry in the program and broadening the participation to include research capabilities from all sources would also be non-technical objectives.

During 1990, five research projects were identified. These were the development of a data-acquisition system; an investigation of the source mechanisms for rockbursts; the use of full-wave data as a tool for better mine design, in order to alleviate rockbursts; support for use in rockburst-prone ground; and the use of stiff backfill for the support of rockburst-prone ground. The first three projects were proposed by the Seismology Group of the Department of Geology at Queen's University, Kingston; while the fourth, on support, was proposed by the Geomechanics Research Centre of Laurentian University, at Sudbury. The final proposal was made by Lac Minerals and Dr. D.G.F. Hedley, now acting as a private consultant.

During the second phase, CANMET maintained the macroseismic systems which had been installed at four mines; continued to analyze the data being gathered at the microseismic stations; maintained and upgraded the Sudbury Local Telemetered Network (SLTN) and the three other seismograph stations which had been installed at Elliot Lake, and the Macassa and Campbell Red Lake mines; and continued to conduct basic research on the causes and control of rockbursts. In addition, the Backfill Group, also at CANMET's Sudbury Laboratory, conducted investigations in support of the project on stiff backfills.

By the conclusion of the CRRP, in late 1995, the Project Management Committee considered that the technical objectives had been achieved, particularly in ground support and backfill; the operation of full-wave microseismic systems and analysis of the resulting data; the upgrade of the SLTN; and the application of full-wave data to numerical modelling for mine design (Project Management Committee, 1994). However, it was not clear if there should be a third phase to the work and, if so, how it would be organized. After ten years of research, the feeling seemed to be (understandably) that the work was becoming mature and that the focus should be on practical applications: applying what had been learned to operating mines, and defining the rockburst hazard in the context of overall mining risks and costs (Udd, 1984).

This volume contains a summary of the work that has resulted from CANMET's contributions to the CRRP from 1990 to 1995. It is organized in six chapters. In order to provide the reader with a general background in seismology and the seismological methodology used in the analysis of the data, Chapter 2 of this report reviews the definition and concepts in mine seismology. Chapter 3 discusses the history of the SLTN and its upgrade during Phase II of the rockburst research. Chapter 4 deals with the development and upgrade of CANMET's macroseismic hardware and complementary software. The efforts of CANMET's personnel in developing of the new source-location algorithm, ADASLS, is discussed in Chapter 5, with associated case studies which appear in the appendices. The seismic source studies over a broad magnitude range are discussed in Chapter 6 of this report, using the captured seismic data from Ontario mines. CANMET's software graphics, the list of publications by CANMET personnel during Phase II of rockburst research and the list of rockbursts recorded in Ontario mines by CANMET's macroseismic system appear in the appendices.

1.5 References

Christian, J.D. (1939). *Rockbursts at the Teck-Hughes Mine.* CIM Transactions 42:550-567.

Hedley, D.G.F. (1992). *Rockburst Handbook for Ontario Hardrock Mines.* CANMET Special Report SP 92-1E.

Hodgson, Ernest A. (1943). *Recent Developments in Rockburst Research at Lake Shore Mines.* CIM Transactions 45:313-324.

Langford, G.B. (1941). *The Rockburst Problem.* CIM Transactions 44:169-182.

Morrison, R.G.K. (1942). *The Rockburst Situation in Ontario Mines.* CIM Transactions 45:225-272.

Project Management Committee (1994). *Cooperative Rockburst Research — A Review of the Canadian Rockburst Research Program 1990-1995 and a Proposal for Further Research.* Mining Research Directorate, Sudbury, Ontario. 11 pages.

Robertson, A.F. (1939). *Rockbursts at Wright–Hargreaves Mine.* CIM Transactions 42:538-592.

Robson, W.T. (1946). *Rockburst Incidence, Research and Control Measures.* CIM Transactions 59:347-374.

Robson, W.T., Adamson, J.C. and Selnes, W.E. (1940). *Rockbursts at Lake Shore Mines.* CIM Transactions 43:7-30.

Udd, John E. (1984). *A Proposal for a Major Research Project on Rockbursts.* CANMET Report MRP/MRL 84-84 (TR). 18 pages.

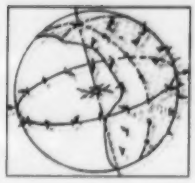

Definitions and Concepts in Mine Seismology

2.1 Introduction

This chapter provides a summary of the seismological terms and techniques used in mine seismology, particularly in the analysis of mine-induced seismicity and rockbursts. An attempt has been made to maintain descriptive language in defining the relevant terms and techniques as they appear throughout the text. Section 2 of this chapter deals with the definition of general terms used in this field, e.g. seismic methods, induced seismicity, monitoring and rockbursts; while Section 3 deals with the properties of body waves (P and S) in rocks. Source-location techniques are discussed Section 4, and Section 5 deals with different methods used in the analysis of the source mechanism of seismic events. Source-parameter determination is discussed in Section 6. Section 7 deals with geotomography, followed by the summary of some of the techniques used in seismic hazard assessment.

2.2 Definitions

Geophysics is a branch of physics whose objective is to study the Earth by using the methods and tools available in physics. The application of geophysics to the search for minerals by the mining industry dates back to the initial steps taken in the past century in Europe to measure variations of the Earth's magnetic field caused by the magnetic properties of ore bodies. Later, variations in the other properties of rocks, such as their elastic properties, electrical conductivity, gravity, magnetism and radioactivity, were used to gain information about the subsurface in the search for different types of minerals.

2.2.1 Seismology and Seismic Methods

Seismology is primarily the study of earthquakes using seismograms, the waveforms recorded at sensor locations following earthquake sequences. Seismic methods are used to extract information about the geometry of a subsurface structure and/or the nature of a seismic source from seismograms recorded by sensors located in appropriate locations relative to the area of study. Following Kasahara (1981), three principal groups of study can be distinguished in seismology:

- exploration of the Earth's subsurface structure and deep interior;
- investigation of the processes of occurrence and the sources of earthquakes; and
- application of seismological knowledge to human activities.

Earthquake seismology, which deals with the first two topics, employs passive methods of investigation which are based on seismograms from earthquakes. These earthquakes are mainly caused by the propagation of fractures within the Earth when rocks at the opposite sides of a fracture move relative to each other. The principal objective of this discipline is to study the nature of seismic events — a question of fundamental relevance in seismological studies. This area of research covers several aspects, including the analysis of individual earthquakes, a better understanding of the occurrence of

seismic events (e.g. source mechanism and parameter studies), and the analysis of seismic activity as a whole, including the mutual relationship between seismic events, tectonics and geology.

The third topic covers a number of applications of seismic methods, such as disaster prevention, seismic prospecting of natural resources and detection of underground nuclear explosions. Exploration seismology is based on using artificial sources to study subsurface structures and makes use of active methods of investigation. In recent times, seismic methods have been among the most widely used geophysical methods in mineral exploration. This is because of their high accuracy, high resolution and large penetration depths in comparison with other geophysical methods. Seismic methods are used in a variety of situations to define the geometry of the subsurface; for example, geological structures associated with oil and gas reservoirs (faults, anticlines and synclines) and the depth of the bedrock for the construction of large man-made structures. Some seismological studies, however, call upon more than one topic as classified above and thus cannot be limited to only one of the above topics. For example, mine seismology consists of the application of seismological techniques to mines and, as such, can be considered to be part of the third topic. However, the rapid expansion of this field of research in the last two decades has required the use of a large number of seismological techniques included in the first two topics.

2.2.2 Induced Seismicity

Induced seismicity generally defines seismicity caused by human activity, i.e. not originating directly from natural processes. This phenomenon is caused in a number of ways, including:

- removal of part of a rock mass (mining, tunnelling);
- perturbation of the natural hydraulic regime (fluid injection/extraction, dam construction); and
- perturbation of rock temperature (thermal cracking).

In all cases, the stress field in a rock mass is perturbed and the redistribution of stresses which follows can induce instabilities, particularly in highly stressed fractured rock masses. This phenomenon is observed over a wide range of magnitude, from acoustic emission in laboratory samples under loading to the large mine-induced seismic events observed around deep mines (Talebi, 1994).

Different terms are used to define instabilities or events caused by rock fracturing at different scales (see Figure 2.1). For example, in mine seismology, large events in the seismic range are often called mine tremors or mine-induced seismic events. Smaller events often located close to active mine stopes are usually defined as microseismic events because of their much smaller magnitudes. At the lowest end of the magnitude spectrum, acoustic emission is often used to indicate high-frequency emissions or rock noise monitored in rock samples under loading in the laboratory or observed in localized failure areas within a mine. The boundaries between these different categories are not very well

Figure 2.1 Monitoring frequency ranges of earthquakes, macro-/microseismic activity, acoustic emission and associated fields of study/domains of research

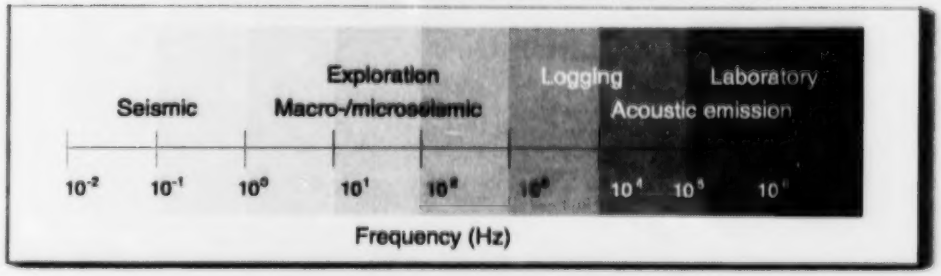

defined and many authors use the term acoustic emission — microseismic, or simply AE/MS, to refer to the latter two categories in a general manner.

2.2.3 Mine-induced Seismicity

Excavation of large volumes of rock at depth and the resulting stress redistribution can give rise to crack propagation and movement along pre-existing fracture planes. This process is usually accompanied with the generation of seismic waves and is known as mine-induced seismicity. Different classifications have been made of the events induced by mining. For example, Hasegawa et al. (1989) provided six conceivable models for such events (Figure 2.2). A cavity collapse results from either a rockburst in a mine ceiling or the fall of a loosened piece of rock under the pull of gravity (rockfall). A pillar burst is caused by convergent forces related to stope advance and time-dependent effects. The most common types of seismic events, however, are caused by movement along pre-existing faults and are commonly called fault-slip events.

Figure 2.2 Schematic diagram of six conceivable models for mine-induced events. Solid arrows show the direction of motion in a rock associated with the seismic event

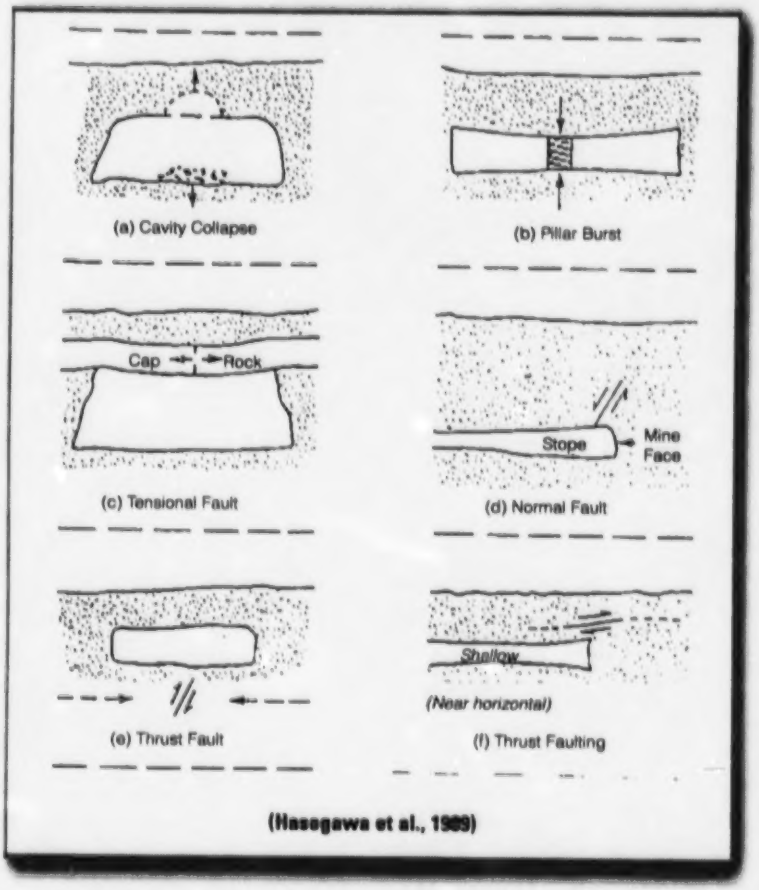

Gibowicz (1990) distinguished two types of seismic events in mines: those directly related to mining operations and caused by the sudden failure of brittle rock due to stress concentrations around the stope area; and those not directly related to mining operations and caused by movements on major faults and other discontinuities due to the interaction of tectonic stresses and mine-induced stresses. Although this is a rather general classification, it represents a definite trend observed in many mines. Gibowicz observed a bimodal distribution and a different behaviour of these two types of events from a probabilistic analysis. The most damaging rockbursts are usually associated with the second type of seismic events (i.e. fault-slip).

2.2.4 Monitoring Mine-induced Seismicity

Since mine-induced seismicity occurs over a broad range of magnitude, different monitoring systems sensitive in different magnitude/frequency ranges are used to monitor them (Figure 2.3).

Seismographic systems are normally used to detect seismic events having magnitudes larger than 2.5. They are used in seismological research of earthquakes and large mine-induced tremors.

Macroseismic systems cover the magnitude range from 0 to 3, where the most common mine-damaging rockbursts have been observed.

Microseismic systems cover the magnitude range from -4 to 0.

Figure 2.3 Three magnitude/frequency ranges of full-waveform monitoring of mine-induced seismicity in Canada

There are other types of systems that operate within or slightly below the ranges mentioned above. For example, portable high-frequency systems covering the magnitude range from -6 to -3 can be used to record acoustic emissions originating from active mining areas. In most cases, a number of sensors are installed, around and within an area of interest, to record seismic signals which represent ground movements at sensor locations. These signals contain information about the source of the waves, as well as the path through which they travel, including the local site conditions at the sensor location. It is, therefore, of utmost importance to take all these factors into account during the processing of seismic signals.

2.2.5 Rockbursts

Rockbursts are particular cases of seismic events induced by mining activity and generally cause disturbance and loss of production to a mine. The definition of a rockburst, according to Hedley (1992), is "a seismic event which causes injury or damage to equipment or the displacement of more than five tonnes of rock" in a mine. It is noteworthy that this definition does not relate rockbursts to a particular magnitude range of seismicity in a straightforward manner. Indeed, large seismic events do not necessarily generate rockbursts although, often, small seismic events are associated with considerable damage (Gibowicz, 1990).

2.3 Body Waves (P and S)

Two types of body waves can propagate in solids: one corresponds to the dilatational component; and the other, to the rotational component of motion, as outlined by the wave equation theory. The first type of wave is known under a variety of names, including dilatational, compressional, longitudinal, irrotational and, most often, as the P (Primary) wave. The latter name is attributed to the fact that, following an earthquake, this type of wave is generally the first one recorded. The second type is also known under different names, such as shear, transverse, rotational or S (Secondary) wave.

2.3.1 Velocities

The velocities of the P- and S-waves in an elastic homogeneous isotropic rock mass are as follows:

$$Cp = ((\lambda + 2\mu) / \rho)^{0.5} \quad (1)$$

$$Cs = (\mu / \rho)^{0.5} \quad (2)$$

where: Cp is P-wave velocity
Cs is S-wave velocity
λ is Lamé constant
μ is shear modulus of the rock
ρ is rock density

The ratio of S-wave to P-wave velocities ranges from zero to about 0.7. As fluids have no resistance to shear, μ is zero and, therefore, S-waves do not propagate through fluids.

Most rocks, however, cannot be considered to be homogeneous isotropic media. Figure 2.4 shows velocities obtained for different types of rocks, as reported by Birch (1966). The wide range of values obtained for the same type of rock can be explained by the fact that rocks are made of mineral grains with voids between them. Indeed, these voids are the main contributing factor to rock porosity, a determining factor in rock properties such as P- and S-wave velocities. Moreover, since these pores are often filled with fluids, seismic velocities are even more affected (Telford et al., 1990).

2.3.2 Attenuation

There are different types of mechanisms causing a decrease in the amplitude of seismic waves as they propagate through rocks.

- Geometrical spreading originates from the expansion of the wavefront in a spherical manner (also called spherical divergence). As the wave propagates, the wavefront expands and wave amplitude decreases with distance since the total energy should remain the same. The energy density in this case decreases inversely as a function of the square of the distance from the source.
- Scattering is responsible for the disappearance of part of the energy. Indeed, rock materials are often associated with the presence of

Figure 2.4 P-wave velocity in different types of rock

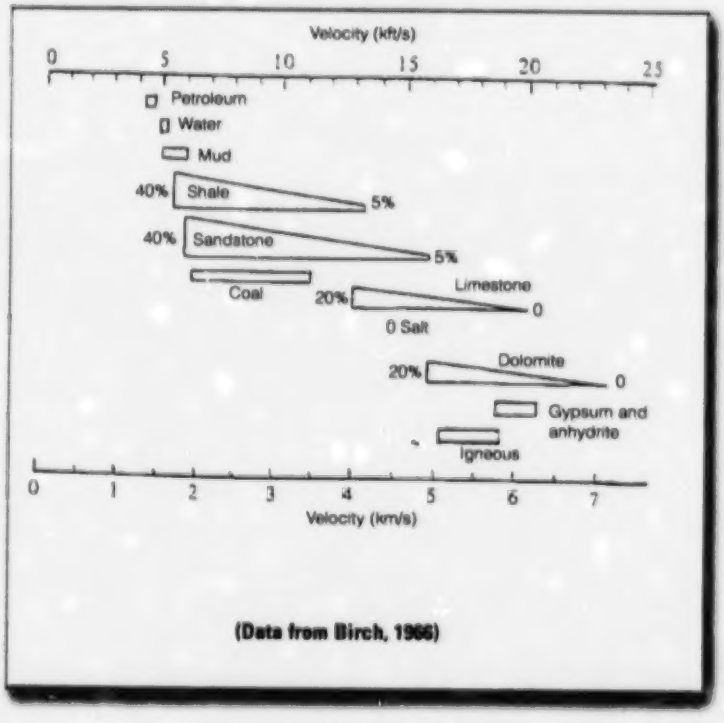

(Data from Birch, 1966)

discontinuities of different sizes. Reflection of body waves on such discontinuities causes part of their energy to be lost.

- Absorption or attenuation. A part of the energy of body waves is absorbed by the medium and ultimately transformed into heat. This phenomenon is responsible for wave distortion and sometimes complete wave disappearance.

Attenuation is a fundamental aspect of body-wave propagation in rocks. It consists of selective filtering of frequencies within the body wave. This is due to the inelastic nature of real Earth materials imposing energy losses on seismic waves during their propagation. The mechanism by which energy loss is produced is attributed to several factors, including internal friction along joints and discontinuities, viscosity and flow of fluids present in pores and fractures. The exact mechanism by which this phenomenon occurs is not yet well understood and a combination of the above factors in some cases could not be excluded. However, internal friction, along with loss of energy involved in the creation of new fractures, are believed to be major causes of this occurrence.

The direct measurement of attenuation is very difficult and laboratory results cannot easily be applied to in situ situations. Field measurements can be made, provided seismic waves pass through a homogeneous rock mass and appropriate corrections are made for any reflection and refraction effects. The energy loss varies exponentially with distance and is often described as follows:

$$A_1 = A_2 \exp(-\alpha x) \tag{3}$$

where A_1 and A_2 are wave amplitudes at two points at a distance x from each other and α is the attenuation parameter. The quality factor Q is often used to describe wave attenuation. This parameter is related to the attenuation parameter as follows:

$$Q = \pi f/\alpha C \tag{4}$$

where f is the wave frequency. Numerous experiments have shown that the attenuation parameter is proportional to frequency and that the quality factor is independent of frequency. Most observations indicate that the quality factors for rocks fall roughly in the range 20 to 150. Much higher values have been obtained for competent rocks at great depths.

2.3.3 Polarization

The propagation of P- and S-waves in homogeneous isotropic media occurs according to two distinct modes. If the movement of particles at the tip of an expanding wavefront is considered, in the case of P-waves, the particles move back and forth in a direction parallel to the direction of wave propagation (Figure 2.5). This fundamental property is sometimes used to extract further information about the medium or the orientation of the sensors. In the case of S-waves, however, the particle movement is in a plane perpendicular to the direction of propagation.

In the presence of anisotropy, or layering within the medium, the S-wave is decoupled into two orthogonal components propagating at two different speeds. This phenomenon is called shear-wave splitting or birefringence. In isotropic solids, however, these two components of S-waves have the exact same properties and travel at the same speed and, as a result, cannot be distinguished from one another. These components for seismic waves often consist of SH- and SV-waves. The SH component is horizontal, while SV is in a vertical plane and perpendicular to the seismic ray.

2.4 Source Location

Although Chapter 5 fully discusses the theory of source location and the common methodology used in the industry, for the sake of completeness a brief description will be given in this section.

Figure 2.5 Particle motion caused by a spherical P-wave. Circles represent the expanding wavefront and arrows show the direction of motion of P-waves as they travel further from the source. λ here represents the wavelength

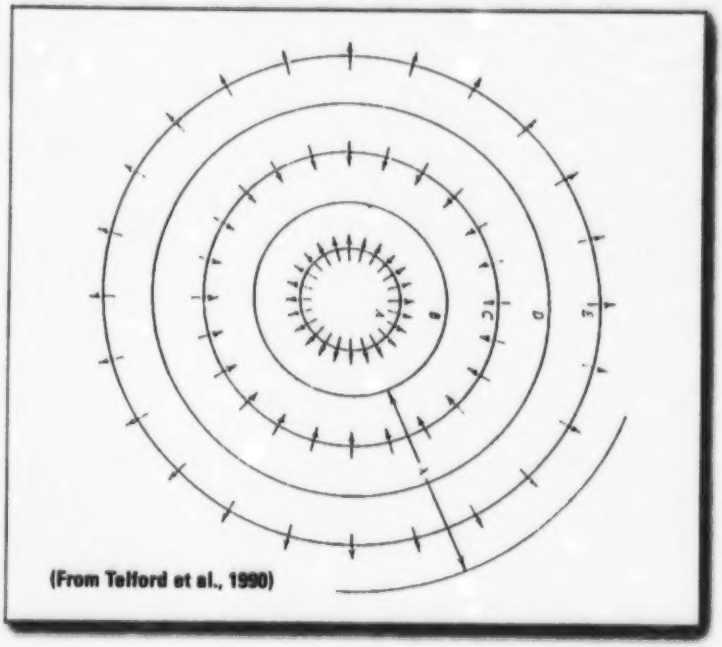

(From Telford et al., 1990)

2.4.1 Source Region

The most fundamental piece of information about a seismic event consists of the co-ordinates of the location where it occurs. The *focus,* or *hypocentre,* specifies the location from which seismic waves are radiated. More specifically, the hypocentre corresponds to the geometrical point where rupture initiates and from which the earliest P-waves are radiated. The projection of this point on the surface is called the *epicentre*. Due to the extent of the area of rupture associated with a seismic event, the source area cannot always be assumed to be a geometrical point and, often, the term *source region* or *focal region* should be used as a more appropriate term. It is important to note that the term *source location,* as determined and used in some studies to define the area where the rupture occurs, is, in fact, the equivalent of hypocentre; i.e. the point of rupture initiation. Only in cases where the source can be considered to be a point, i.e. where the dimensions of the rupture area are very small relative to the distance to the observation point, does source location correspond exactly to the general area where rupture happened.

2.4.2 Source-Location Techniques

These techniques attempt to determine the exact locations of the hypocentres of seismic events. The parameters usually used to achieve this objective are, in order of their frequency of use, P-wave arrival times, S-wave arrival times, and P/S-wave polarization properties. The procedure often implies the determination of four parameters: the co-ordinates of the source point (x, y and z) and its origin time (t). The source-sensor travel times of body waves within the rock mass are related to these four parameters in a non-linear manner, leading to a non-linear system of equations that has to be solved to determine the source location. Source-location techniques operate in two different ways from the point of view of the computational procedure. *Direct methods* consist of linearizing the non-linear system of equations and then solving the linear system in one step to obtain x, y, z and t. The USBM method is based on this approach. *Iterative methods,* on the other hand, use an iterative approach to find the final solution to a quasi-linear or non-linear system of equations. Usually, a trial solution is used to initiate the procedure and this trial solution is improved, following a scheme, until it satisfies a pre-set condition. Geiger's method and the Simplex method are examples of this approach (Ge, 1988).

The iterative search undertaken in iterative source-location methods consists of comparing the arrival times of a new solution with those observed for the waveforms originating from the source. These methods attempt to find the best source location by minimizing a quantity representing the difference between observed and calculated arrival times. The source location corresponds to the point where this quantity is as small as required. *Error space analysis*, often used in conjunction with the Simplex method, consists of calculating the value of the misfit function for a grid network in space. Error space here consists of attributing the value of error to each point in the space, i.e. a spatial error distribution. The misfit function is usually of L1 norm (absolute deviation estimator) or L2 norm (least-squares estimator). This approach has the advantage of visualizing the local areas where the misfit function is a minimum and therefore can be used for a reliable source location. However, it is also cumbersome.

2.4.3 USBM Method

The USBM method was established in the early 1970s and has been widely used in mining applications in North America ever since. This direct method has the advantage of being simple and straightforward. Additionally, it involves the least-squares technique and is more efficient than other direct methods. The method requires data from at least five transducers to uniquely define the source location.

2.4.4 Geiger's Method

This method dates back to the early 20th Century and is now the method of choice for seismologists in locating earthquakes. It has also found wide application in mining situations. Geiger's method is a very sophisticated and powerful source-location technique, and it gives accurate results when the algorithm converges satisfactorily. The iterative process in this method consists of calculating an adjustment vector (Δx, Δy, Δz, Δt) using least squares and adding it to the solution obtained from the previous iteration. The source location is found when a pre-set condition on the misfit value is met.

2.4.5 Simplex Method

This method has been known for more than two decades as a mathematical tool to optimize the solution of over-determined systems, and was introduced by Gendzwill and Prugger (1985) in recent years for source location. Although this method is an iterative one, it is entirely different from Geiger's method. The search process here consists of finding the point of minimum error in an error space. This is achieved by setting an initial Simplex (i.e. a geometric figure with one more vertex than the dimensions of the space to search), calculating the errors for all vertices, and forming a new vertex by moving the vertex with the largest error to a position with a smaller error. As the process is repeated, the Simplex moves through the error space expanding, contracting, shrinking and turning towards the minimum error point; i.e. source location (Ge, 1988).

2.5 Source Mechanism

The determination of the process of failure at the origin of seismic events is a fundamental aspect of research in earthquakes as well as mine-induced seismology. It has long been known that friction between fault surfaces is often unstable, that sudden slip movements along faults could generate seismic waves, and that this slip mechanism is responsible for most of the observed earthquakes. This mechanism, however, is not the only possible mechanism at the origin of seismic events, and an exact knowledge of the process of fracturing at the source is needed in order to define an adequate strategy to assess the seismic hazard and to define rock-mass-support requirements.

2.5.1 Seismic Moment Tensor

The relative importance of the different components of failure at the source of seismic events can be estimated using a ***moment tensor inversion*** technique. Such inversions could be attempted provided that two basic conditions are met: the source is a point source, i.e. only wavelengths much larger than the source dimension are used; and the effects of wave propagation within the medium are properly modelled.

The moment tensor is a second-order symmetrical tensor with six independent components, which contains all of the information about a point-source mechanism. In general, seismic radiation from any source can be calculated using a space-time convolution of a ***slip function*** with a ***Green's function***. The slip function describes the fault displacement during failure as a function of time and position on the fault plane, whereas Green's function represents the response of the earth to the slip. The slip function and Green's function, therefore, quantitatively express the source and propagation effects on seismic motion, respectively. To date, the use of these concepts in the study of mine-induced seismicity has been rather limited.

2.5.2 Radiation Pattern

The radiation pattern of the waves generated by seismic events is one of their most widely used properties in the study of the source mechanism of the seismic wave. Except for a few studies focusing on seismic waves recorded in the near field (i.e. at distances from the source, much smaller than the actual wavelengths), radiation pattern and other source properties have been generally studied in the far field. This concept implies that the observation point is several wavelengths away from the source, so that the contribution of the near field terms of motion can safely be neglected. Figure 2.6 shows radiation patterns for four types of seismic-source mechanisms. It is noteworthy to describe the link between these basic radiation patterns and different types of mine-induced events (Figure 2.2). For example, Figure 2.6(a) depicts the radiation pattern for a single force corresponding to cavity collapse shown on Figure 2.2(a), whilst Figure 2.6(b) shows the same for a dipole, which characterizes a pillar burst, similarly shown on Figure 2.2(b). Figure 2.6(c) corresponds to a tensional fault, such as that shown on Figure 2.2(c), whilst Figure 2.6(d) corresponds to the different types of faulting shown in figures 2.2(d), 2.2(e) and 2.2(f). The basic properties used from such patterns are the amplitude and polarization direction of P- and S-wave components at

Figure 2.6 Normalized far-field P- and S-wave radiation pattern (solid arrows) for four types of point sources shown in Figure 2.2. Open arrows show the point force system at the source (see text for more details)

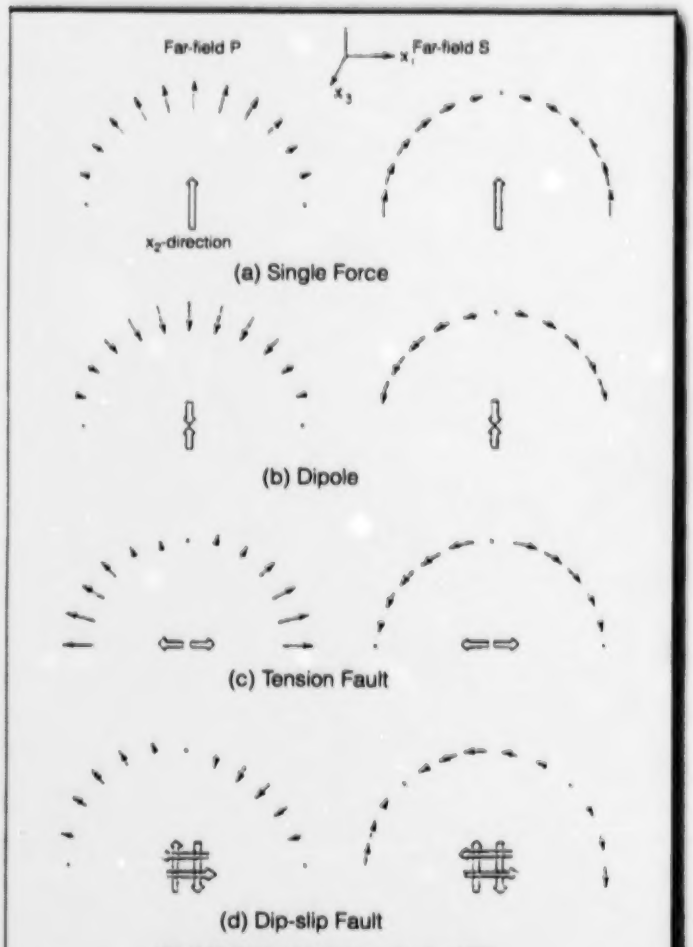

Figure 2.7 Radiation pattern of P- and S-waves from a double-couple source. Arrows on the surface of the spheres show polarization directions

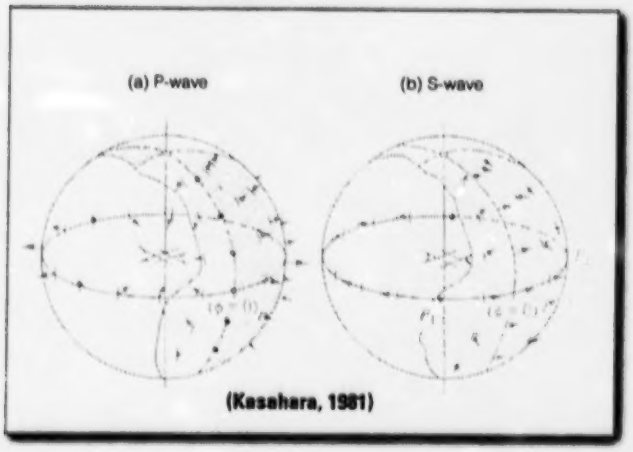

(Kasahara, 1981)

different points around the source. It follows that the difference between radiation patterns from different types of source mechanisms should allow the distinction between different sources if measurements of P- and S-wave amplitudes are available. The polarity of the initial P-wave pulse is a popular and simple parameter to use: pointing either towards the hypocentre or away from it, indicating a dilatational or compressional first motion, respectively.

Studies of mine-induced events observed around mining openings have shown that most of these events are caused by shear failure along fault planes or pre-existing weakness planes in the rock mass (Spottiswoode and McGarr, 1975; McGarr et al., 1979). These studies have also shown that there does not seem to be any fundamental difference between naturally occurring earthquakes and mine-induced events. The basic source model for such a mechanism could be approximated by a double couple, as is the case for earthquakes. This conclusion has led the way for a great use of the techniques of earthquake research in the study of mine-induced events. Two such techniques of particular relevance are fault-plane solution or focal mechanism determination, and spectral analysis. The first technique is usually based on using the radiation pattern of P-waves, whilst the second method uses the properties of the radiated seismic signals in the frequency domain.

Figure 2.8 Focal mechanism for a shear event induced by fluid injection: (a) P-wave first motions; and (b) S-wave polarization

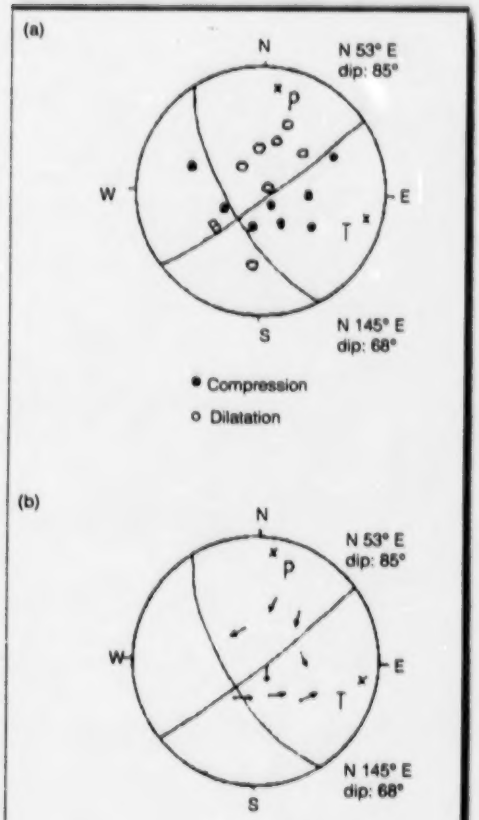

(Talebi and Cornet, 1987)

2.5.3 Focal Mechanism

It has long been known that the radiation pattern for a shear-type event approximates a double couple and is very characteristic (Figure 2.7). The space around the source is divided into four quadrants: two quadrants of compression and two quadrants of dilatation, with respect to the sense of first motion of P-waves radiated by the source. The determination of focal mechanism or fault-plane solution could be utilized in the analysis if a sufficient number of sensors are located around the source to permit the plotting of the sense of first motion of P-waves on a stereonet, and determining the two nodal planes separating the quadrants of compression and dilatation. P- and S-wave amplitudes and S-wave polarization directions have also been used by some authors to determine focal mechanism. One of the two nodal planes corresponds to the actual fracture plane and the other is called the auxiliary plane. An example of such determinations is shown on Figure 2.8. Three axes are defined from a focal mechanism: the pressure axis (P) and the tension axis (T), which correspond, respectively, to the directions where dilatational and compressional motions are a maximum and minimum; and the null axis (B), which corresponds to the intersection of the two nodal planes (Figure

2.8(a)). The polarization directions of S-waves diverge from the P-axis, converge towards the T-axis and are perpendicular to the nodal planes (Figure 2.8(b)).

Focal mechanism determinations are particularly informative since the three axes, P, T and B, can contribute to the evaluation of the in situ principal stress orientations, implying that the fault plane solutions are powerful tools in assessing the conditions in the source region. However, this technique has certain limitations. First of all, the data are generally contaminated by noise, causing a certain inaccuracy of the results. Also, two possible planes of faulting are defined, but the fault plane cannot be uniquely defined without using other tools or observations. But, in general, fault plane solutions are valuable tools in remotely determining the stress regime in a certain area of a rock mass. Figure 2.9 shows three basic types of focal mechanisms corresponding to three different stress regimes.

Figure 2.9 Elementary types of focal mechanism: (a) strike-slip; (b) reverse dip-slip; and (c) normal dip-slip

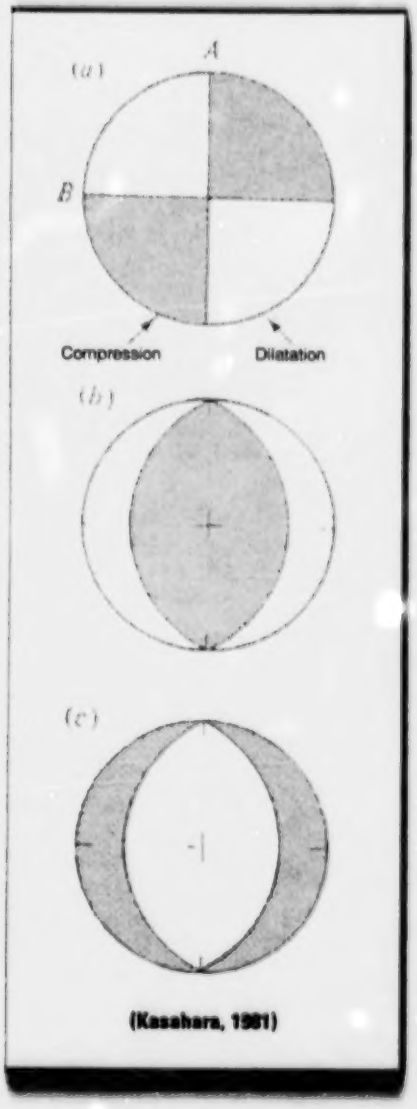

(Kasahara, 1981)

2.5.4 Source Modelling

Two basic shear failure-type models are widely used in seismology to describe seismic events: kinematic models and quasi-dynamic models. In the first case, a dislocation occurs along some planar fault and the source-time function is defined arbitrarily, while in the second case a crack propagates and the model attempts to take into account the rupture process at the source. Two currently used models are the kinematic model of Brune (1970, 1971) and the quasi-dynamic model of Madariaga (1976), with both models assuming a circular failure area. Although different approaches have been used, the resulting properties of far-field radiation from these two models are similar in nature. The main difference is the dependence of the resulting source properties on the azimuth of observation in the latter case, in comparison to the former, which produces azimuth-independent results.

2.5.5 Homogeneous and Inhomogeneous Models

The models presented in the previous section are sometimes called homogeneous models since they assume a homogeneous stress release over the source area when the rupture is completed. There is an increasing interest, however, in using inhomogeneous models; assuring inhomogeneous stress release over the source area, to describe a more complex seismic event experienced. The laboratory experiments on rock friction have shown that for two rock faces in contact, the real contact area can be a very small fraction of the total surfaces. Such contact areas in earthquake theory are called asperities, regions of high-stress release where most of the seismic energy caused by earthquakes is generated. In simple terms, seismic energy is radiated from the breaking of such patches on the fault surface with strong resistance to shear movements. Such a concept has been adopted in seismic source studies by a number of authors (McGarr, 1981). A related concept was used by Aki (1979), who used the concept of barriers defined as areas which resist the rupture front and remain unbroken following the failure process. In the asperity model, stress concentrations exist before failure, and, as the asperities are broken, the stress on the fault tends to

become uniform at the end of the failure process. In the barrier model, stress along the fault is uniform prior to failure, but becomes irregular after the failure has taken place because of the presence of barriers (Gibowicz, 1990).

The analysis of inhomogeneous models becomes more relevant when near-field strong ground motion is studied. Indeed, the peak ground motion is associated with deformation over only a fraction of the fault area, the asperity area. Assessments of near-field strong ground-motion parameters permit the estimation of the size and other characteristics of the source process describing asperities within the overall source area. Although most studies in this field indicate that a homogeneous shear failure model is usually adequate to describe simple events, complex events have been reported by a number of authors and the use of a simple model to describe them is rather questionable. On the other hand, it is well known that some after-shocks occur off the main fault planes during earthquake sequences, which result in complex events and implies that, in such cases, at least part of the complexity of seismic radiation cannot be attributed to the main event, as assumed in inhomogeneous models (Scholz, 1990).

2.6 Source Parameters

The parameters characterizing the source of induced seismic events are commonly called source parameters. Basically, these parameters could be calculated in time and frequency domains and measure three properties (Figure 2.10): the strength of an event (seismic moment, magnitude and seismic energy); source dimensions (source and asperity radii); and estimates of stress release (static, dynamic or rms stress drop, and apparent stress). These parameters are routinely used by seismologists in the field of induced seismicity to analyze seismic events. The most commonly used parameters are magnitude and seismic moment, which measure the strength of an event.

Most seismic models, kinematic or quasi-dynamic, predict the flat low-frequency trend of the far-field displacement spectra and a descending trend at high frequencies, inversely proportional to some power of frequency (Brune, 1970; Madariaga, 1976). Three parameters are routinely used to describe the far-field displacement spectra: the low-frequency level; the slope of the high-frequency fall-off; and the "corner frequency," which is defined as the intersection of the low- and high-frequency trends (Figure 2.11). At low frequencies, the flat portion of the spectra is controlled by seismic moment and the source can be approximated as a point. A decrease in amplitude is observed near the corner frequency. This region is dominated by frequencies with wavelengths related to the duration of

Figure 2.10 Three types of seismic-source parameters

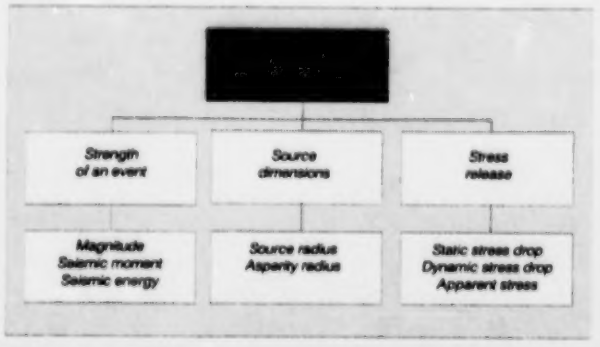

Figure 2.11 Schematic far-field displacement spectra of P- and S-waves

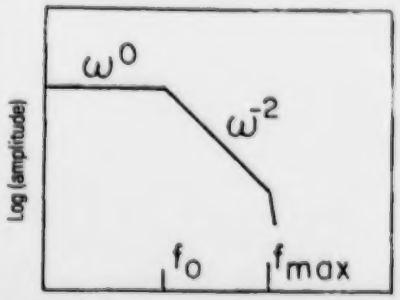

rupture on the fault. For a constant rupture speed, the corner frequency is inversely proportional to the fault dimension. Finally, a high-frequency descending trend of the spectra is observed with a slope of -2 or lower. Spectral analysis has become a routine technique in the study of small events. Several authors have shown in their pioneer studies that this technique can be successfully used to analyze seismic events induced by mining (Spottiswoode and McGarr, 1975; Gibowicz et al., 1977).

2.6.1 Magnitude

The most popular parameter describing the size of an event is magnitude. Magnitude is calculated on a logarithmic scale based on the maximum amplitude of a seismic wave at a particular frequency, corrected for source-sensor distance and instrument response. There are many types of magnitude scales in different situations; for example:

- M_L is the local magnitude scale introduced by Richter and used by most seismologists, particularly for seismic events in the western part of North America
- m_N is the local magnitude scale introduced by Nuttli for eastern North America, east of the Rockies
- M_S is the magnitude scale based on surface waves
- M_A is the magnitude scale based on maximum acceleration
- M_D is the magnitude scale based on duration of coda waves

Indeed, variations of magnitude determinations for the same event at different stations are to be expected because of different radiation coefficients and the properties of the source-sensor path. Events of similar magnitude could differ significantly in radiated seismic energy. Dziewonski and Woodhouse (1983) described magnitude as "a hopelessly inadequate measure of the size of an earthquake." Even in the best cases, errors of 0.2-0.3 units in a calculated magnitude are to be expected (Bath, 1973). Moreover, magnitude scales tend to saturate with increasing event size as the largest portion of the radiated energy, in this case, will be outside the frequency content of the instrumentation.

In recent years, moment magnitude M has been used more often to estimate the strength of the source, as this parameter can be used over a broad range of source strength. It has been simply defined by Hanks and Kanamori (1979) as:

$$M = 2/3 \log M_0 - 6.0 \qquad (5)$$

where M_0 is seismic moment in Newton-meters.

2.6.2 Seismic Moment

Seismic moment is a more adequate measurement of earthquake strength than magnitude. This parameter has a distinct physical interpretation, regardless of the specific source model adopted. In general, the equivalent force system acting at the source can be described by a second-order symmetric tensor with six independent components called the moment tensor. In the case of a

double-couple source, only the off-diagonal terms in the seismic moment tensor are non-zero and a scalar is often used:

$$M_0 = \mu A u \qquad (6)$$

where, μ is the modulus of rigidity at the source
A is the seismic source area
u is the average slip on the fault plane

This relationship can be used to calculate seismic moment from field data, whenever the average displacement along the fracture or fault plane can be measured. In practice, however, due to the inaccessibility of the source area for direct observations, seismic moment is usually calculated from the low-frequency horizontal trend of corrected displacement spectra of P- or S-waves, as follows:

$$M_0 = \frac{4 \pi \rho C^3 R |\Omega_0|}{F_C R_C} \qquad (7)$$

where, ρ is the rock density
C is the P- or S-wave velocity
R is the source-sensor distance
$|\Omega_0|$ is the modulus of the plateau level of the displacement spectrum
F_C is the P- or S-wave radiation coefficient
R_C is the free surface amplification factor

If the focal mechanism of the event is not known, average values of 0.52 and 0.63 are used for (F_C) in the case of P- and S-waves, respectively (Boore and Boatwright, 1984). The free-surface coefficient (R_C) can be safely neglected for sensors installed down boreholes in underground mines.

2.6.3 Source Dimensions

Estimation of source dimensions from seismic spectra necessitates some assumptions about the failure process, making it more model-dependent. It is generally accepted that the dimensions of the failure area depend inversely on the corner frequency. For example, in Brune's (1970) model, the corner frequency (f_0) is interpreted as being inversely proportional to the rupture duration. Taking a circular source and a constant rupture velocity, source radius is calculated from the corrected displacement spectra of S-waves as:

$$r_0 = 2.34 C / 2 \pi f_0 \qquad (8)$$

In the quasi-dynamic model of Madariaga (1976), corrections are needed for the angle between the normal to the fault and the ray take-off angle. Source radii calculated from this model are about half the size of those calculated from Brune's model (Gibowicz, 1990). However, Brune's model continues to be widely used because of its simplicity.

The determination of corner frequency (f_0) can be undertaken in a number of ways. One possible approach is that of Snoke (1987), which consists of calculating two independent parameters directly from the corrected displacement spectra of S-waves: (Ω_0), the level of the low-frequency constant trend; and (J_C), the energy flux being the integral of the squared particle velocity for the S-wave window. Two frequencies (f_1 and f_2) are defined in this approach as the limits of the spectral

bandwidth over which the calculation of energy flux is performed. The method assumes a constant spectral amplitude of the displacement spectrum for frequencies below f_1 and a f^{-2} fall-off for frequencies above f_2 (Gibowicz, 1990). Corner frequencies can then be calculated from the following relationship:

$$f_0 = (J_c / 2\pi^3 \Omega_0^2)^{1/3} \quad (9)$$

2.6.4 Stress Release

There are many different measurements of stress release caused by a seismic event (e.g. static and dynamic stress drop). These values can agree in some particular cases, but are not necessarily comparable as they correspond to different models of stress release along the failure area. Indeed, estimates of stress release are among the most model-dependent source parameters and should be taken with caution. However, when a particular parameter is estimated for several events, the relative difference of the results can be discussed (Scholz, 1990).

The most used estimate of stress release is the "static stress drop," defined as the average difference between the initial and final stress levels over the fault plane. For a complete stress release along the fault surface, stress drop can be calculated from the estimations of seismic moment (M_0) and source radius (r_0), according to Brune (1970, 1971) as:

$$\Delta\sigma = 7 M_0 / 16 r_0^3 \quad (10)$$

This represents a uniform reduction of stress along the fault, taken as an approximation of static stress drop.

Two estimates of dynamic stress release can be deduced from the ground velocity and acceleration. The dynamic stress drop (σ_d) is calculated based on the initial slope of the far-field velocity signal (Boatwright, 1980) or the maximum acceleration of the S-waves (McGarr, 1981). The second (σ_{rms}) is calculated from the root mean square of the acceleration averaged over the duration of the S-wave arrival (Hanks and McGuire, 1981), representing an averaged dynamic stress release. When the rupture process is simple, i.e. a constant rupture velocity, the above estimates should agree reasonably well (Gibowicz, 1990); otherwise, the results will differ significantly due to the complexity of the rupture process. The ratios of various estimates of stress release are used to characterize the rupture complexity associated with seismic events.

2.6.5 Scaling Relations of Seismic Sources

Scaling relations of seismic sources are the relationships between the estimates of the two first types of source parameters, i.e. those between source strength and source dimensions. More precisely, a source scaling relation describes the manner in which source duration or source dimension increases with increasing seismic moment. The significance of this type of analysis in the study of mine-induced events is that these events are recorded over a broad frequency and magnitude range; thus the question of whether or not they have the same behaviour over the full range of magnitude has important consequences, from a practical point of view, on the manner in which they can be analyzed and handled.

Figure 2.12 Seismic moment versus radius — source for small earthquakes

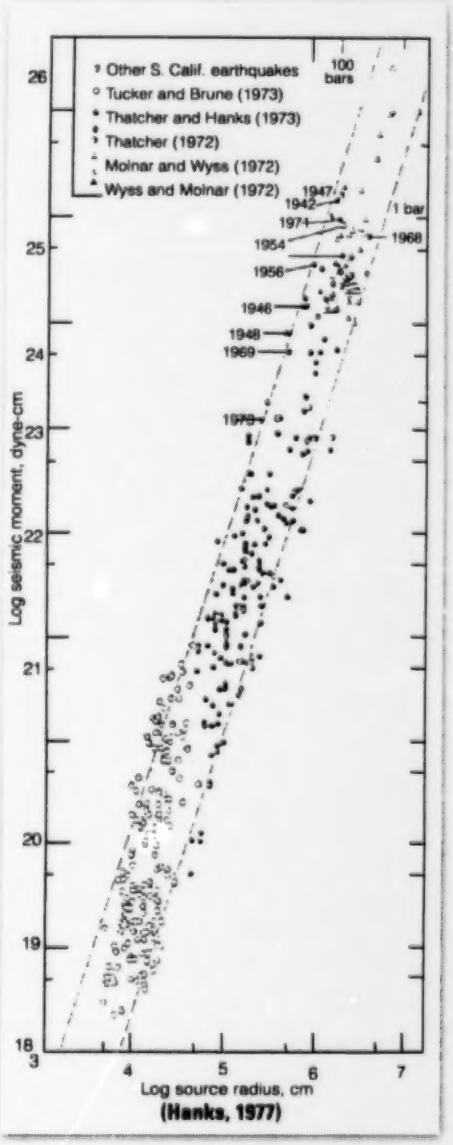

In studies of source parameters for a large number of seismic events over a broad range of magnitude, it has been observed that stress drop is roughly independent of magnitude and ranges mostly between 0.1 and 10 MPa. A dependence of seismic moment on r_0^3 is clearly observed in Figure 2.12 (Hanks, 1977). This pattern has been confirmed by many studies for seismic and volcanic events, after-shock sequences and mine tremors in South Africa and Poland, etc. (Gibowicz, 1990). A constant stress drop model implies a self-similar rupture process regardless of the size of the seismic events — indicating, in simple terms, that earthquakes, mine tremors and microseismic events are generated in a similar manner, but along different sized failure areas.

In contrast to the general observation of similarity of the failure process over a broad range of magnitude, there is growing evidence of a breakdown of this similarity for very small events, as observed by a marked decrease of stress drop with decreasing seismic moment. This effect, observed at the lower end of the spectrum, consists of seismic moment decreasing much faster than r_0^3, suggesting that there might be a lower limit to source dimensions (Gibowicz et al., 1991; Hasegawa, 1983). This observation can be explained by any phenomenon at the source, in the medium or the recording system, causing the reduction in the high-frequency content in the recorded signals. Seismologists have proposed two different explanations for this observation, provided the influence of the recording system can be neglected. Hanks (1982) argues that this is a propagation effect and that there is a maximum frequency limit (f_{max}) to what can be detected. This is because of the high attenuation levels in the medium close to the surface of the Earth, where seismographic stations used for earthquake monitoring are installed. Aki (1984), on the other hand, argues that this represents a true source effect and that there is a minimum limit to the dimension of the source (Scholz, 1990). Recent results favour the attenuation as the origin of this effect.

2.6.6 Path Effects

Seismic signals contain useful information about the source and the medium which the waves propagate through. In some situations, the latter effects can be neglected due to the high quality of the medium. Recent studies have shown, however, that path effects cannot always be neglected, especially when dealing with high-

frequency microseismic studies. This subject becomes more noteworthy in mine-induced seismology and particularly for signals recorded at short distances from the source, as the mine is generally an inhomogeneous environment because of the presence of areas of backfill, openings, etc. which affect the seismic-wave propagation.

Seismic spectra, hence, must be corrected for attenuation caused by wave propagation along the source-sensor path. Such corrections are of utmost importance for proper retrieval of source parameters of small events, even if they are recorded at short distances. The effects of attenuation on seismic and microseismic signals and the need for proper correction have been pointed out by several authors (Talebi and Cornet, 1987; Cranswick and Sembera, 1989; Spottiswoode, 1993). To correct for attenuation along the path, the spectra should be multiplied by the exponential term $\exp(\pi f R / C Q)$ where R is the source-sensor distance and C is the velocity of the body wave under consideration.

2.7 Geotomography

Tomography could be described as a methodology for reconstructing some property of an object along a cross-section of it by measuring, on the perimeter of the object, the energy passing through it. The mathematical framework of tomography was demonstrated early this century and the method has found widespread application in a number of disciplines. For example, X-ray tomography has had huge success in medicine with the use of CAT scan. Geophysicists have taken advantage of this method to extract useful information about the Earth, and the technique is generally referred to as geotomography.

The application of geotomography in mining is based on seismic or electromagnetic waves. Images or maps of physical properties of a rock mass are constructed to provide information in order to address mining-related problems, such as the delineation of lithological boundaries, detection of fractures and fluids, evaluation of stress levels or the effectiveness of de-stress blasting operations.

2.7.1 Tomographic Imaging

Tomographic imaging can be carried out according to two different principles. *Transmission tomography* uses the properties of waves passing through the object, while *diffraction tomography* uses the properties of waves that have been scattered by discontinuities in the medium. The latter method, depending on the circumstance under investigation, has advantages in the detection of anomalies, but its application is somewhat difficult because of the need to detect the scattered waves. Transmission tomography, however, can be performed using the properties of the first arriving waves, which is much more practical; and the method has found much more widespread application. The procedure consists of placing a number of sources and receivers of energy on the perimeter of an object. As the waves propagate through the object from each source location to each sensor location, the waves are affected by the properties of the medium. Each projection contains information about the object along its corresponding ray path. Such information is then extracted from the waveforms and a tomographic image is produced using mathematical techniques. This image provides information about the physical properties of the internal structure of the medium.

2.7.2 Inversion Techniques

The two principal characteristics of the transmitted waves include wave travel time and wave amplitude. The former depends on the path length and velocity along the path, and these data are used to produce an image of the velocity distribution within the object. Since seismic velocity is sensitive to elastic properties of the medium and the presence of discontinuities, such properties can be imaged. For

example, an adequate data set of P- and S-wave waveforms can be used to image the elastic properties of the object, such as the elastic modulus and Poisson's ratio. Amplitude, on the other hand, depends on the path length and attenuation properties of the medium, and is much more sensitive to the presence of areas with discontinuities and can be used to image them. However, this approach often proves to be impractical because of the difficulty of proper measurement of attenuation.

The travel time between each source and receiver location can be described as a line integral:

$$t = \int s \, . \, dl \qquad (11)$$

where (s) is slowness at each travel point (the inverse of velocity) and (dl) is the path increment. Usually, the function s is approximated as a set of discrete elements or pixels, each having a uniform slowness or velocity. For a complete data set, the above relationship is then transformed into a number of linear relationships expressed in matrix form:

$$T = D \, . \, S \qquad (12)$$

where T is a vector containing the travel time information for all the source-sensor paths and S is a vector containing all slowness information for the model. D is a rectangular matrix representing a linear transformation of the slowness model to the data; i.e. path lengths within the pixels. The objective of inversion is to find a model S given a set of travel time data T that satisfies the above equation. This procedure requires that the matrix D be calculated. This is a simple problem of geometry in cases where seismic rays could be assumed to be straight. In practice, the existence of significant velocity contrasts leads to refraction and ray bending, hence ray geometry has to be calculated according to the velocity model to achieve the final objective.

A detailed technical discussion of inversion techniques is beyond the scope of this document, thus only the principles of some popular techniques are discussed.

Direct inversion of equation 12 can be performed, but this is a very time-consuming process requiring a large number of matrix operations.

Back projection is an approximate solution to the problem of inversion. Here, a transpose of the matrix D, rather than the inverse of it, is obtained by dividing each row of D by the square of the path length. This procedure does not provide very accurate solutions, but the results can be used as a starting point for more sophisticated inversion techniques.

Least-squares techniques attempt to find a solution by minimizing the difference between measured and calculated travel times. In practice, *damped least-squares methods* are usually more successful and applicable. *Single value decomposition (SVD)* is another method used to handle singular matrices.

Alternatives to the direct inversion techniques mentioned above are:

Algebraic Reconstruction Techniques (ART). This is an iterative process based on the reduction of the travel-time residual along each ray where a velocity model is modified until it converges to a solution.

Simultaneous Iterative Reconstruction Techniques (SIRT) provide another iterative process in data inversion. ART and SIRT techniques are easy to use and computationally less intensive than direct-inversion techniques.

2.7.3 Experimental Set-up and Resolution

The resolution of tomographic imaging depends primarily on the wavelength utilized. In general, the shorter the wavelength, the smaller the feature that could be resolved; however, the short wavelengths are more strongly attenuated than long wavelengths and there is a limit to their range of propagation. This leads to a trade-off between the degree of the resolution of the feature under investigation and the range of investigation. Another limitation to resolution is caused by ray bending when strong velocity contrasts are present. Moreover, the use of travel-time data as an input, in most cases, causes a bias in the type of anomaly that could be detected. Indeed, high-velocity anomalies affect the arrival times much more than low-velocity anomalies, which makes the first type of anomaly much easier to detect than the second type.

The best practical configuration for tomographic experiments would be the inclusion of sources and receivers in the whole surrounding area of investigation to ensure the sampling of the entire rock mass under study by seismic rays. Such an approach is possible in certain circumstances, e.g. for a mine pillar. A more common procedure consists of using one or more boreholes and an opening for source and receiver positions. Cross-hole geometry is widely used in order to avoid attenuation caused by the rock close to the surface or the mine opening. In any event, the resolving power of an experimental set-up can be estimated using numerical simulation before the experiment takes place.

An example of such an approach is provided by Jackson and Tweeton (1994) in Figure 2.13, which shows the ray path coverage using three different experimental configurations using the same spacing between different stations. It is clear that the resolution of different areas of these configurations is not identical and depends primarily on how well each zone is criss-crossed by ray paths. Figure 2.14(a) depicts a trial model for which travel times can be calculated and used for the three configurations shown on Figure 2.13. The resolving power of each set-up can be estimated by inverting the synthetic data obtained in this way for each geometry. Obviously, the better the configuration, the more the agreement between the image produced and the initial model. Figures 2.14(b), 2.14(c) and 2.14(d) show the images obtained for the three configurations shown on figures 2.13(a), 2.13(b) and 2.13(c), respectively. A complete coverage provides an accurate image of the anomaly's position, size, shape and magnitude (Figure 2.14(b)). When only three sides are covered (Figure 2.14(c)), a somewhat degraded image is obtained, in that the size, shape and magnitude of the anomaly are distorted. With only two sides of the object covered (Figure 2.14(d)), the results are even more distorted. This problem is not related to poor ray coverage, but rather to the limited viewing angles; a reconstruction using the same geometry but a ray path density increased by a factor of 9 would not be significantly different from Figure 2.14(d) (Jackson and Tweeton, 1994). The above examples show the

Figure 2.13 Ray path coverage associated with three experimental configurations: (a) complete coverage on four sides; (b) coverage on three sides; and (c) coverage

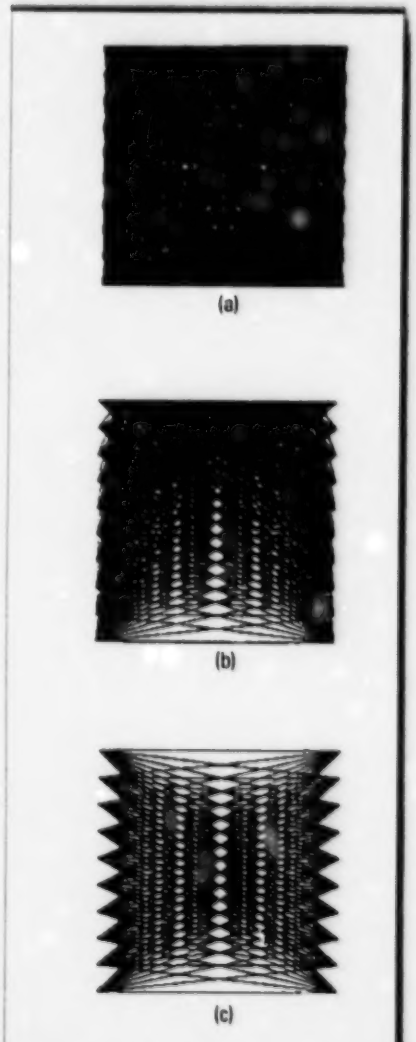

(a)

(b)

(c)

(After Jackson and Tweeton, 1994)

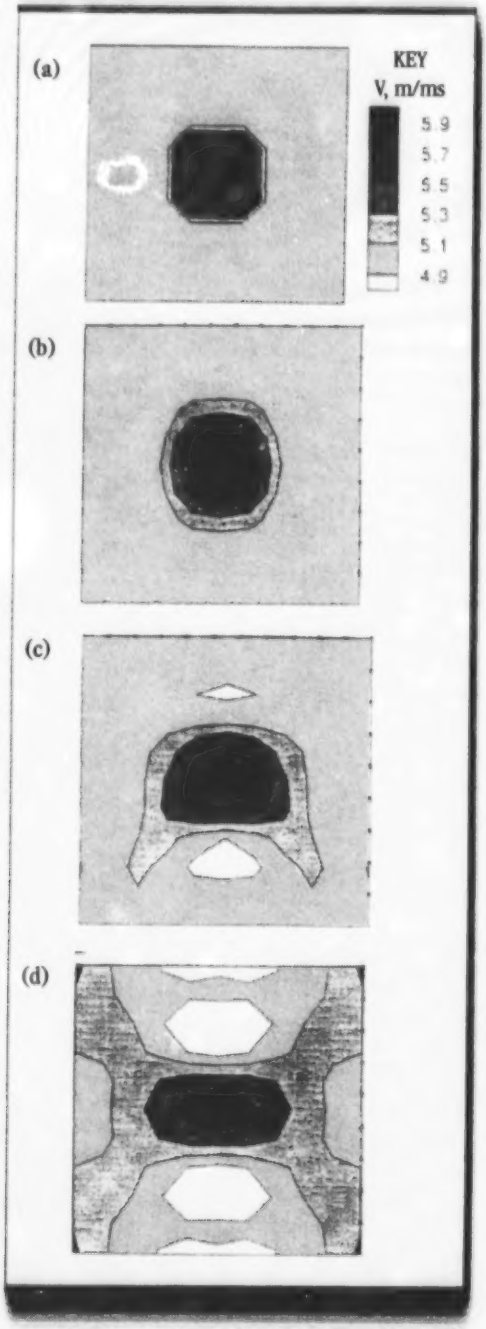

Figure 2.14 Resolution test with synthetic data: (a) the velocity model; (b) reconstruction using complete coverage of Figure 2.13(a); (c) reconstruction using coverage on three sides of Figure 2.13(b); and (d) reconstruction using coverage on two sides of Figure 2.13(c)

extreme importance of a proper design of source-sensor arrays for seismic tomographic experiments.

2.8 Seismic Hazard

The most important socio-economic implication of research into mine-induced seismicity is to use the knowledge generated in the reduction of the hazards caused by rockbursts. Recent decades have seen numerous attempts to predict natural earthquakes, with very limited success. The concepts and methods of earthquake prediction are, for the time being, far from being reliable or directly applicable to predict mine-induced seismicity. The major fundamental difference between the two fields of study, earthquake versus mining-induced seismology, is that earthquakes are caused by natural processes involving no direct interference from man, while rockbursts and mine-induced seismic events are caused by human activity.

This section discusses some basic concepts used in earthquake prediction. These methods are related to naturally occurring earthquakes and are *not* directly applicable to the problem of rockbursts. The objective of this section is to provide the reader with a basic framework about this area of seismological research.

2.8.1 Earthquake Seismic Cycle

Analysis of historical data on earthquake activity has shown the cyclical nature of the occurrence of earthquakes on faults or sections of a fault. Earthquake recurrence refers to the time interval between subsequent rupture episodes in a certain area, i.e. the period of the loading cycle prior to earthquakes. Historical records for several seismogenic areas of the Earth support this idea. The seismic cycle is sometimes divided into four basic phases of inter-seismic, pre-seismic, co-seismic and post-seismic activity.

2.8.2 Earthquake Prediction

Earthquake prediction usually describes the forecasting of the place, the size and the time of an expected earthquake. However, difficulties arise in cases of inaccurate information, whose use becomes generally impractical because the predicted parameters are inaccurate. The first step in this endeavour is usually *statistical prediction*, which is based on the assumption that earthquakes occur with a statistical character that does not change with time. The second stage is *tectonic prediction*, in which the magnitude and tectonic information of an earthquake are aimed at but the precise time information is not a concern. *Physical prediction* is concerned with the precise determination of all three factors (time, place and size) of an earthquake.

Earthquake prediction can be broken into three main categories: long-term, intermediate-term and short-term. Long-term implies years to a decade; intermediate-term implies a few weeks to a few years; and short-term implies hours to a few weeks (Scholz, 1990). Long-term prediction takes advantage of the repetition of the seismic cycle for earthquakes and is based on calculating the recurrence time of earthquakes on a fault and determining the approximate time for the next earthquake. This area of research has been progressing steadily in the past decades. Intermediate- and short-term prediction, on the other hand, are based on precursory phenomena of different kinds. Progress in this area of research has been unsatisfactory.

2.8.3 Precursory Phenomena

Precursory phenomena deal with anomalous signals, observed close and prior to earthquakes, but do not necessarily imply the imminence of an earthquake. Scholz (1990) indicates that the observation of precursors in the past has been a matter of chance and their identification has been made after the fact. Such observations are subject to many interpretations, and the models used have risen and fallen in their acceptability in scientific circles. The existence of precursory phenomena is supported by most of the evidence, but it is difficult to designate a single precursor that can be universally accepted. At the same time, a credible search for precursors cannot be undertaken without the prior determination of the area of investigation using long-term methods.

A whole range of precursory phenomena have been reported and analyzed. They are related to different aspects and properties of the source region; for example:

- anomalous land deformations, e.g. as recorded by tiltmeters and strainmeters;
- seismicity patterns based on observations during seismic periods, particularly foreshocks prior to the main event and other properties, such as b-value;
- changes in P- and S-wave velocities and their ratio;
- changes in hydrochemical and geochemical properties of subsurface water, oil or gas (e.g. pressure, flow rate, colour, taste, smell and chemical composition); and
- changes in electrical resistivity or magnetic field of the Earth.

The most obvious precursors of earthquakes are foreshocks, or lower magnitude seismic activity observed before earthquakes. Jones and Molnar (1979) have shown that 60-70% of all earthquakes larger than magnitude 7 recorded since 1950 were preceded by foreshocks. This activity becomes evident a few days before the main event and accelerates up to its initiation. The main difficulty of using foreshocks in prediction is their lack of recognizable distinction from other earthquakes (Scholz, 1990).

2.8.4 Modelling Precursory Phenomena

Two types of models can be distinguished: nucleation and dilatancy modes. The former are those based on fault constitutive relations which predict shear failure behaviour, but not the change in the properties of the rock surrounding the fault area; while the latter are based on bulk rock constitutive relations, which predict the changes in the physical properties of the rock surrounding the fault area. The growth of a slipping patch up to the point of instability is called nucleation, which has been modelled using crack models or frictional models.

- **Nucleation models.** Both crack and frictional models predict that failure will not occur until slip has taken place over a fault patch of a critical radius, which is a function of the fault strength,

state of stress and elastic properties of surrounding rocks (Scholz, 1990). As nucleation is an essential part of the instability, prediction may be a possibility if some geophysical properties of the nucleation process can be detected. In reality, however, the problem has many practical hurdles, e.g. the lack of information on the size of the event, even if the nucleation was properly detected.

- **Dilatancy models** are based on changes of the properties of the rock within or outside the rupture zone. They are of two types: volume dilatancy models and fault-zone dilatancy models. To date, several precursory phenomena have been observed to precede earthquakes but no universal mechanism for them has yet been proposed.

2.8.5 Seismic Hazard Estimation

Seismic hazard estimation is a worthwhile objective of seismicity studies. Traditional methods used in this field are often based on the results of the observations of past seismicity in a certain area. This assumes that future seismicity will be similar to past seismicity. This assumption can be valid with two conditions: recurrence of the seismic activity is established, and the time period under study is longer than the actual recurrence time of the fault area. In practice, these conditions are rarely met, even for earthquake studies. Also, although the nature of small and large earthquakes is believed to be similar, according to scaling laws, extrapolation between these two families is not possible for hazard-estimation purposes. There is, however, sufficient ground for long-term hazard estimates if geological data such as fault-slip rates are considered. Further consideration of the seismic cycle can form the basis for extending the results to the time factor. A contributing factor in such endeavours can be the improvement of models of estimating strong ground motion. Better understanding of site response can allow such predictions to be converted into estimations of damage (Scholz, 1990).

2.9 References

Aki, K. (1979). "Characterization of Barriers on an Earthquake Fault." *J. Geophys. Res.* 84:6140-6148.

Aki, K. (1984). "Asperities, Barriers and Characteristics of Earthquakes." *J. Geophys. Res.* 89:5867-5872.

Bath, M. (1973). "Introduction to Seismology." *Natur Och Kultur,* Stockholm, p. 395.

Birch, F. (1966). "Compressibility; Elastic Constants" in *Handbook of Physical Constants, Geological Society of America Memoir 97*, Clark, S.P., ed., pp. 97-173.

Boatwright, J. (1980). "A Spectral Theory for Circular Seismic Sources: Simple Estimates of Source Dimension, Dynamic Stress Drop and Radiated Seismic Energy." *Bull. Seism. Soc. Am.* 70:1-27.

Boore, D.M. and Boatwright, J. (1984). "Average Body-Wave Radiation Coefficients." *Bull. Seism. Soc. Am.* 74:1615-1621.

Brune, J.N. (1970). "Tectonic Stress and the Spectra of Seismic Shear Waves from Earthquakes." *J. Geophys. Res.* 75:4997-5009.

Brune, J.N. (1971). "Correction." *J. Geophys. Res.* 76:5002.

Cranswick, E. and Sembera, E. (1989). "Earthquake Site/Source Studies in the AE/MS Domain." Proceedings of the 4th Conference on AE/MS Activity in Geological Structures and Materials. Trans-Tech Publications, pp. 375-402.

Dziewonski, A. and Woodhouse, J.H. (1983). " Studies of Seismic Source Using Normal-Mode Theory" in *Earthquakes, Observations, Theory and Interpretation.* H. Kanamori and Boschi, E., ed., North Holland, pp. 45-137.

Ge, M.C. (1988). "Optimization of Transducer Array Geometry for Acoustic Emission/Microseismic Source Location." Ph.D. thesis, Pennsylvania State University, 237 pages.

Gendzwill, D.J. and Prugger, A.F. (1985). "Algorithms for Microearthquake Locations." Proceedings of the 4th Symposium on AE/MS, Pennsylvania State University. Trans-Tech Publications, pp. 601-615.

Gibowicz, S.J. (1990). "Keynote Lecture: The Mechanism of Seismic Events Induced by Mining: A Review." Proceedings of the 2nd International Symposium on Rockbursts and Seismicity in Mines, University of Minnesota, pp. 3-27.

Gibowicz, S.J., Cichowicz, A. and Dybel, T. (1977). "Seismic Moment and Source Size of Mining Tremors in Upper Silesia, Poland." *Acta Geophys. Pol.* 25:201-218.

Gibowicz, S.J., Young, R.P., Talebi, S. and Rawlence, D.J. (1991). "Source Parameters of Seismic Events at the Underground Research Laboratory in Manitoba, Canada: Scaling Relations for Events with Moment Magnitude Smaller than -2." *Bull. Seism. Soc. Am.* 81(4):1157-1182.

Hanks, T.C. (1977). "Earthquake Stress Drops, Ambient Tectonic Stresses, and Stresses that Drive Plates." *Pure and Applied Geophysics* 115:441-458.

Hanks, T.C. (1982). "F_{max}." *Bull. Seism. Soc. Am.* 72:1867-1880.

Hanks, T.C. and Kanamori, H. (1979). "A Moment Magnitude Scale." *J. Geophys. Res.* 84:2348-2350.

Hanks, T.C. and McGuire, R.R. (1981). "The Character of High-Frequency Strong Ground Motion." *Bull. Seism. Soc. Am.* 71:2071-2096.

Hasegawa, H.S. (1983). "Lg Spectra of Local Earthquakes Recorded by the Eastern Canada Telemetered Network and Spectral Scaling." *Bull. Seism. Soc. Am.* 73:1041-1061.

Hasegawa, H.S. Wetmiller, R.J. and Gendzwill, D.J. (1989). "Induced Seismicity in Canada – An Overview" in *Seismicity in Mines,* Reprints from PAGEOPH 129(3/4), Birkhauser Verlag Basel publishers.

Hedley, D.G.F. (1992). *Rockburst Handbook for Ontario Hardrock Mines.* CANMET Special Report SP 92-1E, 305 pages.

Jackson, M.J and Tweeton, D.R. (1994). *Migratom – Geophysical Tomography Using Wavefront Migration and Fuzzy Constraints.* U.S. Bureau of Mines Report of Investigations RI 9497, 35 pages.

Jones, L. and Molnar, P. (1979). "Some Characteristics of Foreshocks and Their Possible Relationship to Earthquake Prediction and Premonitory Slip on Faults." *J. Geophys. Res.* 84:3596-3608.

Kasahara, K. (1981). *Earthquake Mechanics.* Cambridge University Press.

Madariaga, R. (1976). "Dynamics of an Expanding Circular Fault." *Bull. Seism. Soc. Am.* 66:639-666.

McGarr, A. (1981). "Analysis of Peak Ground Motion in Terms of a Model of Inhomogeneous Faulting." *J. Geophys. Res.* 86:3901-3912.

McGarr, A., Spottiswoode, S.M., Gay, N.C. and Ortlepp, W.D. (1979). "Observations Relevant to Seismic Driving Stress, Stress Drop and Efficiency." *J. Geophys. Res.* 84:2251-2261.

Scholz, C.H. (1990). *The Mechanics of Earthquakes and Faulting.* Cambridge University Press, 439 pages.

Spottiswoode, S.M. (1993). "Seismic Attenuation in Deep-Level Mines." Proceedings of the 3rd International Symposium on Rockbursts and Seismicity in Mines, pp. 409-414.

Spottiswoode, S.M. and McGarr, A. (1975). "Source Parameters of Tremors in a Deep-Level Gold Mine." *Bull. Seism. Soc. Am.* 65:93-112.

Snoke, J.A. (1987). "Stable Determination of (Brune) Stress Drop." *Bull. Seism. Soc. Am.* 77(2):530-538.

Talebi, S. (1994). *Source Studies of Mine-Induced Seismic Events Over a Broad Magnitude Range (- 4 <M< +4).* CANMET Report MRL 94-030(CL), 55 pages.

Talebi, S. and Cornet, F.H. (1987). "Analysis of the Microseismicity Induced by a Fluid Injection in a Granitic Rock Mass." *Geophys. Res. Lett.* 14(3):227-230.

Telford, W.M., Geldart, L.P. and Sheriff, R.E. (1990). *Applied Geophysics.* Cambridge University Press.

CANMET Digital Seismograph Network

3.1 Introduction

The Sudbury Local Telemetered Network (SLTN) became operational in 1987 as part of the Canada-Ontario-Industry Rockburst Research Project (COIRRP). SLTN's main objective was to improve detection and source-location capabilities for mine-induced seismic events and rockbursts within the Sudbury Basin. The network used three one-component, short-period seismograph stations located around the rim of the Basin.

During the Phase II rockburst project (Canadian Rockburst Research Program, 1990-1995), the seismograph network operated by CANMET in northeastern Ontario and northwestern Quebec, of which SLTN is part, was reviewed and a decision was made to upgrade this network to improve its capabilities and to make it more efficient. Installation of the upgraded SLTN started in July 1993 and data were rerouted to the CANMET Sudbury Laboratory for processing. This upgraded network included four one-component seismograph sensors and a triaxial seismograph station.

The latest expansion of the CANMET Digital Seismograph Network in November 1994 consisted of the inclusion of a network of three new stand-alone, single-component digital seismograph stations in Kirkland Lake, Ontario, and in Matagami and Val d'Or, Quebec. This expansion became possible as the funds through Quebec Rockburst Research Program, which was initiated in early 1993, became available. Through the expansion, it became possible to monitor a larger area of northeastern Ontario and northwestern Quebec — from the Elliot Lake mining camp in Ontario to the Matagami mining district in Quebec, with the heart of the network being located in Sudbury.

Figure 3.1 Location of seismograph stations in Northern Ontario

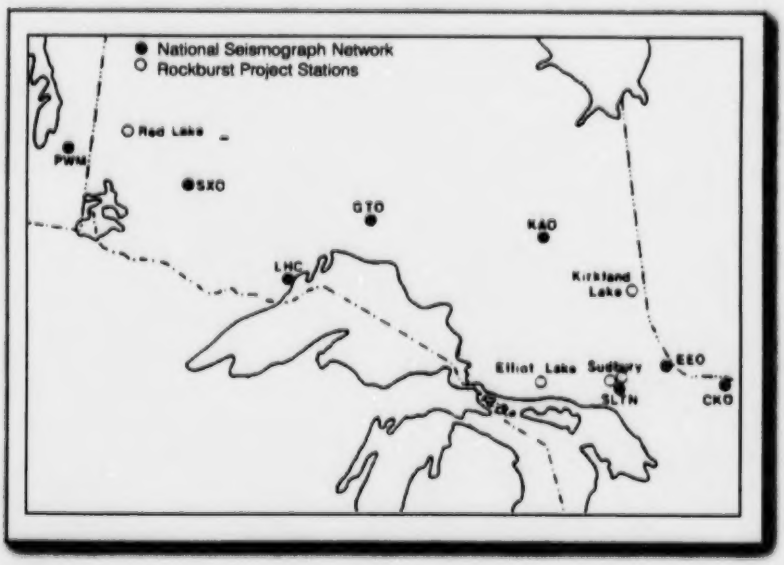

This report summarizes the objectives of installation and different components of the CDSN network, as well as its operations and rockburst monitoring during Phase II of the rockburst research program.

3.2 Background

Most hard-rock mining districts in Northern Ontario are located within the seismically stable Precambrian Shield. Because of the lack of significant

seismicity in this part of Canada, the coverage by seismic stations has been historically poor, with only one seismograph station having been installed in Kirkland Lake in the 1940s to record rockburst activity in the local gold mines. The coverage has improved significantly since 1982 when the Canadian Nuclear Fuel Waste Management Program, operated by Atomic Energy of Canada Ltd., supported the operation of six seismograph stations in Northern Ontario and Manitoba to provide data for regional seismic hazard estimates (Figure 3.1). These stations are part of the National Seismograph Network (NSN) operated by the Geophysics Division of the Geological Survey of Canada, which also operates the Canadian Seismograph Network for earthquake detection across the country. At most stations, only the analog signal used to be recorded by a helicorder, involving the change of paper chart on a daily basis (Hedley, 1992).

Because of the industry's pressing needs for more numerical data following an event, one of the first tasks undertaken in the COIRRP five-year program was to increase the number of seismograph stations around the Sudbury Basin from one to three, in order to increase the range of recorded events and to provide source-location capabilities for some previously unlocatable rockbursts. The network, known as SLTN, became fully operational in 1987. The original SLTN network provided coverage to the mines within the Sudbury area and consisted of three stations located around the rim of the basin (Figure 3.2).

Seismograph stations were also installed at Elliot Lake, Red Lake and Kirkland Lake (Plouffe et al., 1990). All of these consist of a vertical single-component, one-second period, Teledyne Geotech S13 seismometer, usually recording in the frequency range of 1 to 16 Hz. Signals from the seismographs were digitized at each station and transmitted by dedicated telephone lines to Science North, a public science centre in Sudbury. A processor at Science North saved triggered seismic events and sent these automatically over a dedicated telephone line to the Geological Survey in Ottawa, where they were processed and catalogued.

Hedley (1992) notes that while, in some cases, it was possible to differentiate between rockbursts and blasts, the task was difficult in others. Figure 3.3 shows seismic records for two rockbursts and two blasts recorded on the Elliot Lake seismograph. The distinction between rockbursts and blasts is rather easy when they are monitored at close distances (figures 3.3(a) and 3.3(b)), because of the different signatures produced and the fact that central blasts initially occur at specific times each day. However, at greater distances (figures 3.3(c) and 3.3(d)), the task becomes more difficult and events have to be confirmed by mine operators. It is interesting to note the great improvement in data quality when analog records, such as

Figure 3.2 Location of the seismograph stations around the Sudbury Basin and data transfer of the original SLTN network

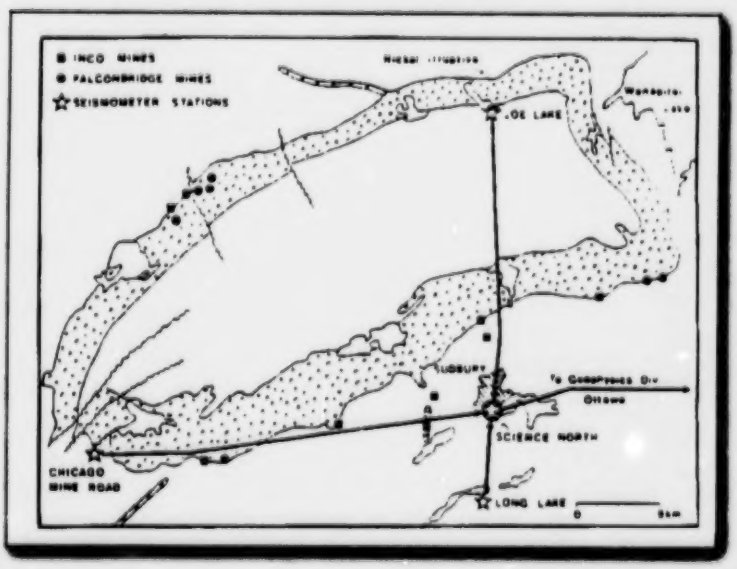

those depicted, are compared to digital records as recorded by the CANMET CDSN presented in this report. Figure 3.4 shows a histogram of large seismic events ($m_N > 2.0$) in Sudbury mines from 1984-1990, using the old system.

3.3 Upgrading the Network

In 1991, during the second phase of the rockburst project, the seismograph station network operated by CANMET in Northern Ontario was reviewed and a proposal was made to upgrade it (Mottahed, 1991). The intent was to use the more efficient Remote Seismograph Digitizer stations, such as those supplied by Nanometrics Inc. of Ottawa, instead of the conventional systems used at the time. The main objective of the change-over was to improve the network's capabilities and to make it more efficient. This was also compatible with the Geological Survey's plans to modify the National Seismograph Network in a similar manner. The following describes the objectives of the change-over (Pritchard and Talebi, 1994):

- To continue to direct the data from the three one-component stations of the original SLTN network installed around the Sudbury Basin to the central acquisition unit in Science North in Sudbury.
- To convert the Elliot Lake analog seismograph into a digital seismograph, with the data being transferred to Science North and being merged with the data from the original SLTN seismograph stations.
- To install a three-component seismograph station within the Sudbury Basin, with the data also being transferred to Science North and merged with the data from the original SLTN seismograph stations.
- To increase the sampling rate from 60 Hz to 100 Hz for a better quality of data.
- To proceed with data processing and magnitude determinations at the CANMET Elliot Lake Laboratory. This modification alone made possible a significant saving on the cost of the dedicated telephone lines formerly used to transit data to Ottawa.
- To plan the conversion of the analog stations at Red Lake and Kirkland Lake into digital seismographs, with the option of continuous transmission being postponed to a later date.

Figure 3.3 Analog seismic signals of blasts and rockbursts recorded on the Elliot Lake seismograph

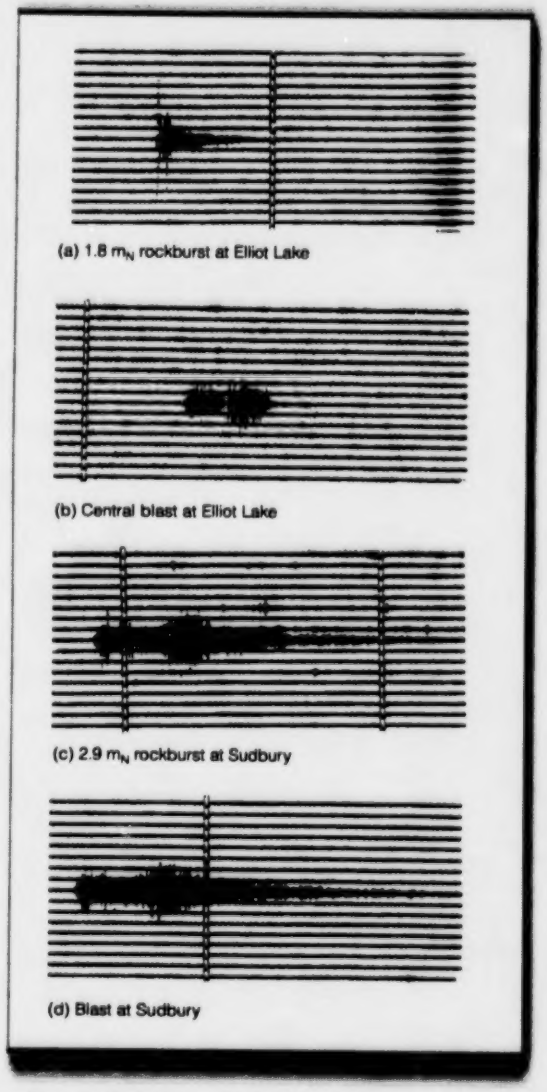

Figure 3.4 Histogram showing the number of seismic events (m_N>2.0) in Sudbury mines during the period 1984-1990

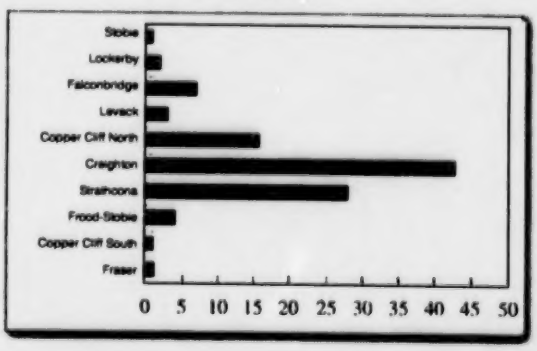

- To use state-of-the-art computer and digital technologies with improved analysis and communications software capabilities.

The CANMET Rockburst Group moved from Elliot Lake to Sudbury during 1993, so the final destination of the data and the processing unit was the Sudbury Laboratory. Installation of the upgraded SLTN started in July 1993, when CANMET assumed full responsibility for it. The upgraded SLTN then consisted of five seismograph stations (including Elliot Lake), with seven components in total (four one-component and one three-component sensors), covering the Sudbury and Elliot Lake mining districts (Figure 3.5). A triaxial station located in the Dowling area in the Sudbury district is composed of three orthogonal sensors: one in the vertical direction and two in the horizontal plane (one North–South and one East–West).

The improvements made as a result of the upgrade of SLTN can be summarized as follows:

- increased sampling rate from 60 Hz to 100 Hz for a better quality of digital data;
- improved event detection and location capabilities;
- cost reduction for data transfer since processing would be done at Sudbury;
- full-time supervision and maintenance;
- an increased number of sensors for better source-location accuracy;
- a three-component sensor providing better coverage and data available for in-depth research studies;
- expansion capabilities for the future across Ontario and Quebec; and
- improved data quality, data analysis and communications software capabilities.

In November 1994, the CDSN was expanded to include three new stand-alone, single-component digital seismograph stations in Kirkland Lake, Ontario, and in Matagami and Val d'Or, Quebec. This expansion was possible through the financial support of the Quebec Rockburst Research Program (QRRP) through the Mineral Development Agreement (MDA) between the governments of Canada and Quebec. The additional coverage has made it possible to monitor a larger area of northeastern Ontario and northwestern Quebec and to determine magnitudes for mine-induced events occurring in those Quebec mines. It has also added some redundancy to the calculation of magnitudes within the network. The CANMET Digital Seismograph Network now has the potential to cover a significant part of northeastern Ontario and northwestern Quebec — from Elliot Lake, Ontario, to Matagami, Quebec, with the heart of the network being the Sudbury mining district (Figure 3.6).

Figure 3.5 Location of the seismograph stations of the upgraded SLTN network

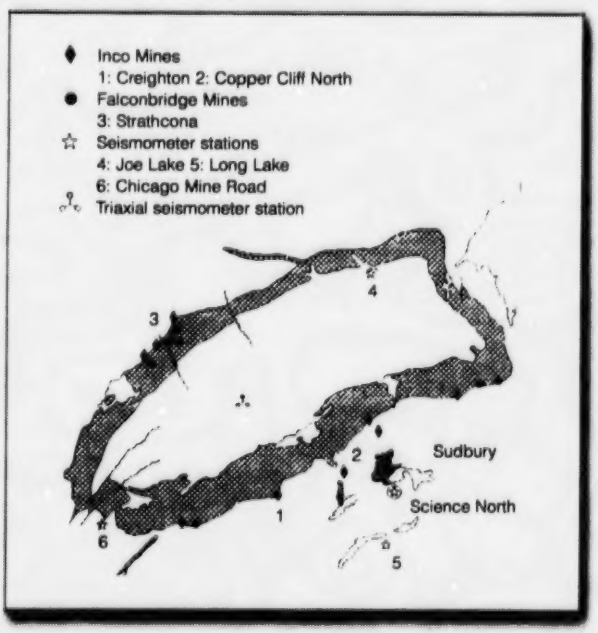

3.4 Overview of the System

This section reviews the technical details of the CDSN network, as well as the procedures used for data acquisition and processing. Figures 3.7 and 3.8 show the schematic procedures for data transfer and data processing used in this system.

Figure 3.8 Map showing the extent of the coverage provided by the CANMET Digital Seismograph Network

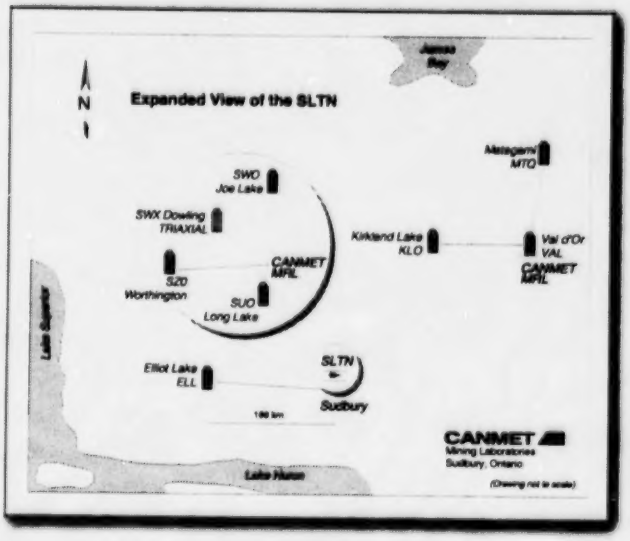

3.4.1 Hardware

As described earlier, two types of sensors – single component and three-component – are employed. Whilst the single-component sensors are one-second period, using Teledyne Geotech S13 seismometer units (which are used in numerous seismological applications around the world), the three-component sensor consists of three single-component, short-period seismometer units mounted orthogonally to each other, on surface, in a sealed vault. Each sensor operates with a minimum detectable ground motion of 2 nanometers per second (nm/s). This resolution is equivalent to the amplitude of a magnitude 1.5 m_N earthquake located at 100 km distance. The frequency range of these sensors covers the 0.5-40 Hz range and the sensors are designed to operate reliably at temperatures as low as -40°C. The analog signals generated by the sensors on site are filtered and converted to digital signals using an RD3 100-Hz digitizer. The continuous digital signals are transmitted via high-speed modem and dedicated phone lines to CANMET's Sudbury Laboratory for analysis.

The communications processor package consists of several hardware and software components. Dedicated high-speed modems receive data from the remote sensor sites and transfer these to a Front-End Processor (FEP). Each FEP is then linked to the communications processor, which is configured specifically for seismograph operations. The processor is responsible for the reception and decoding of incoming data and the trigger-detector information. A Global Positioning Satellite (GPS) master clock links all the incoming data in real time, with an accuracy to four decimal points. A software program called Network AcQuisition Software (NAQS) is the primary data-acquisition program which runs the host computer at the Sudbury Laboratory (Figure 3.7). Any triggered event is simultaneously stored in a large ring-buffer or hard-disk partition on the main acquisition computer. The event data are then transferred to a dedicated computer for data processing.

During the initial installation and network set-up, Nanometrics Inc. performed a system calibration to determine the frequency response of the system. This calibration demonstrated that the SLTN sensors were responding well to the signals generated within the expected frequency band determined by the manufacturer (0.5Hz-40 Hz). A calibration in a broader frequency range (0.5-100 HZ) was also performed on the Elliot Lake sensor by CANMET personnel to determine the response of the seismograph used for magnitude determinations.

3.4.2 Software

The Wide Area Seismic Protocol (WASP) software package is operated from the central station for automatic data transfer from individual seismograph stations (figures 3.7 and 3.8). Dial-up messages requesting data on triggered events are sent out from the central station to remote sites, which then

Figure 3.7 Schematic diagram of data transfer procedure of the upgraded SLTN

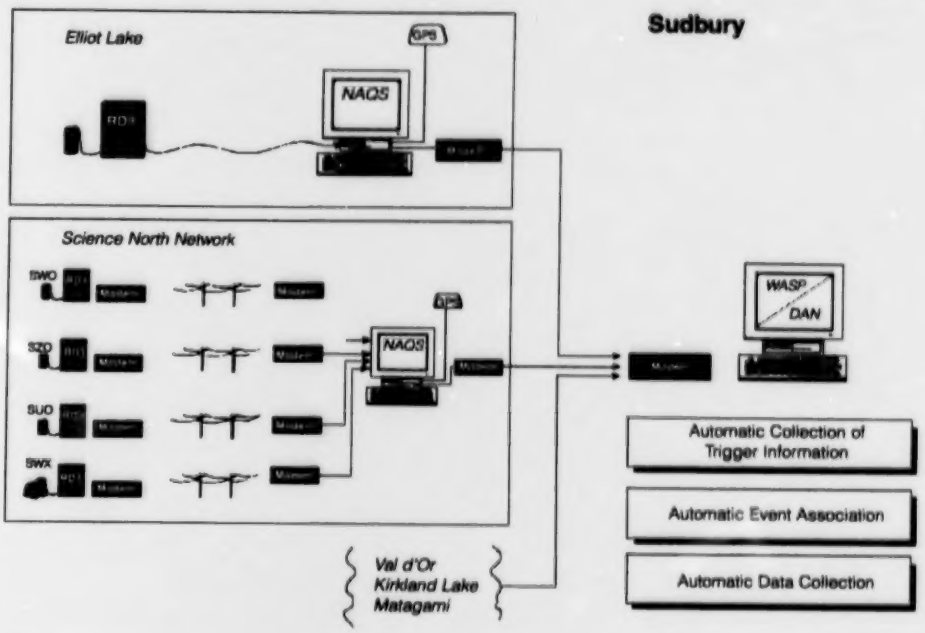

Figure 3.8 Schematic diagram of data processing procedure for the upgraded SLTN

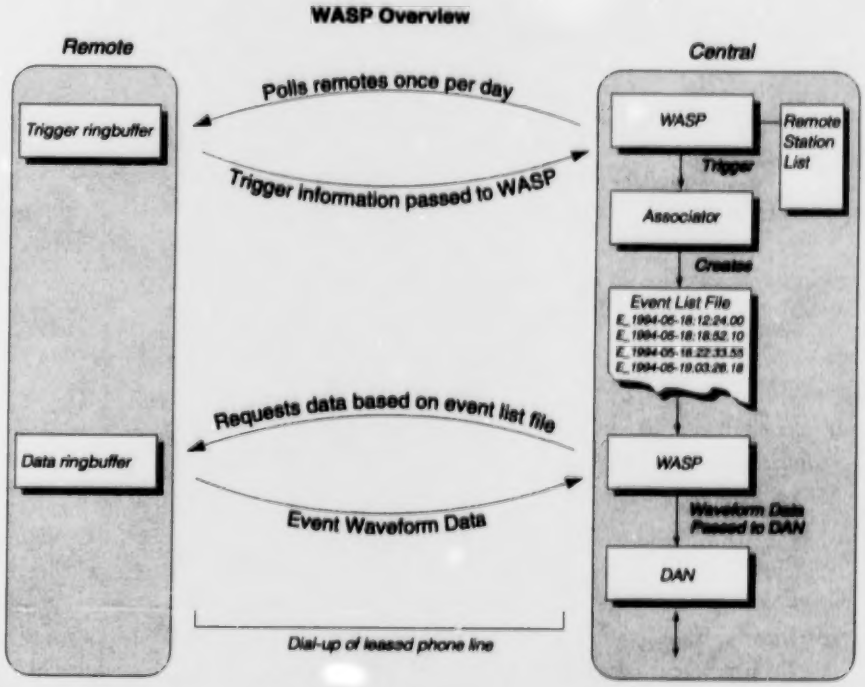

send the requested data to the central computer for processing and analysis. The change-over from the previous system to this automatic procedure has been a major improvement, and has helped save considerable time since manual handling of the data was virtually eliminated and calls could be completed in off-peak hours. With WASP being operational, dial-ups were completed automatically, and the data stored on the computer were ready for review and processing early every morning.

3.4.3 Daily procedure

After the events recorded by the host system are transferred via dedicated phone to the processing computer, the event-trigger files are collected and a review of each event is completed on a daily basis. These events are usually classified into four categories:

- Blasts: Related to mining and construction activities (figures 3.9 and 3.10).
- MIS events: Mining-induced seismic events confirmed by mine operators, either using an operating microseismic system in the mine or by underground observations (figures 3.11, 3.12, 3.13 and 3.14).
- Possible events: Events not recorded on a microseismic monitoring system, nor felt by mine operators in the absence of such a system at the mine.
- Global events: Large-scale, high-energy distant teleseisms from outside the Sudbury Basin (figures 3.15 and 3.16).

When the event trigger was classified as an MIS event, the following steps were completed:

- P- and S-wave arrival times were determined for each sensor site and the source location algorithm was used to determine event-source locations based on P- and S-wave arrival times. Events within the CDSN array are the most easily and accurately located.
- The remote seismographs such as the Elliot Lake remote site (ELL) were linked to the network via modem and the data were extracted for the same time window as for the recorded event. All the recorded files were then merged and magnitude determination was completed.

Figure 3.9 Example of a blast signal recorded on the SLTN

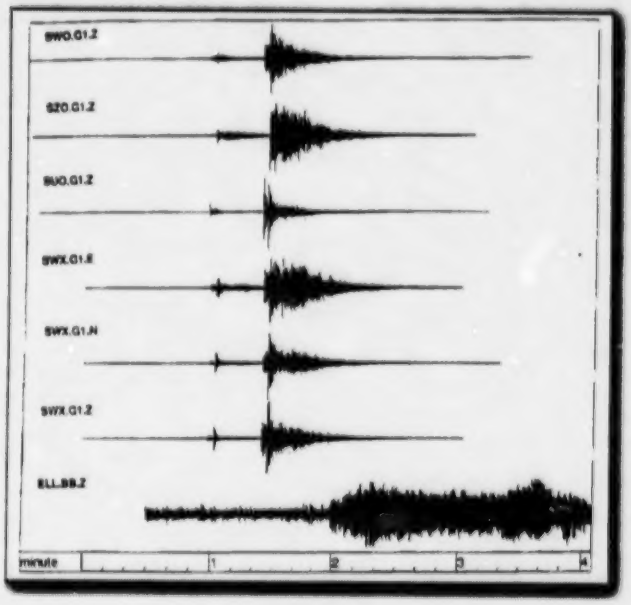

Figure 3.10 Example of signals from a blast using long delays, followed by a mine-induced event

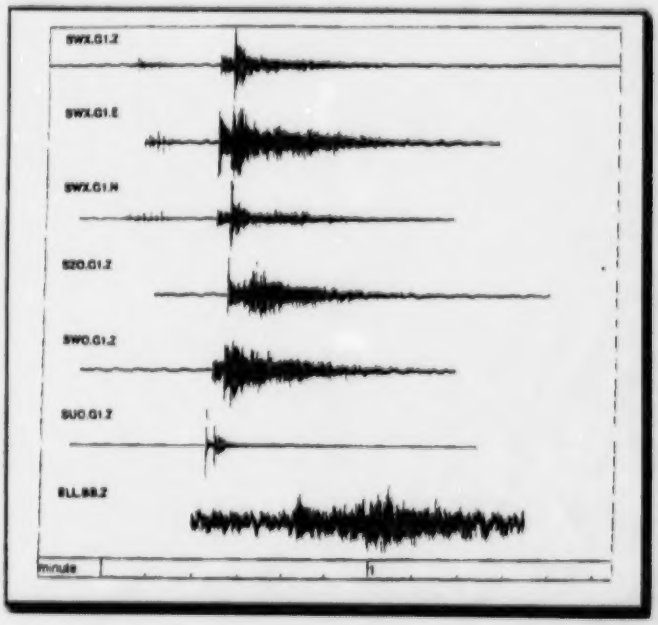

Figure 3.11 Example of a mine-induced seismic event from Inco's Creighton mine, as recorded by the SLTN, with the associated source-location plan

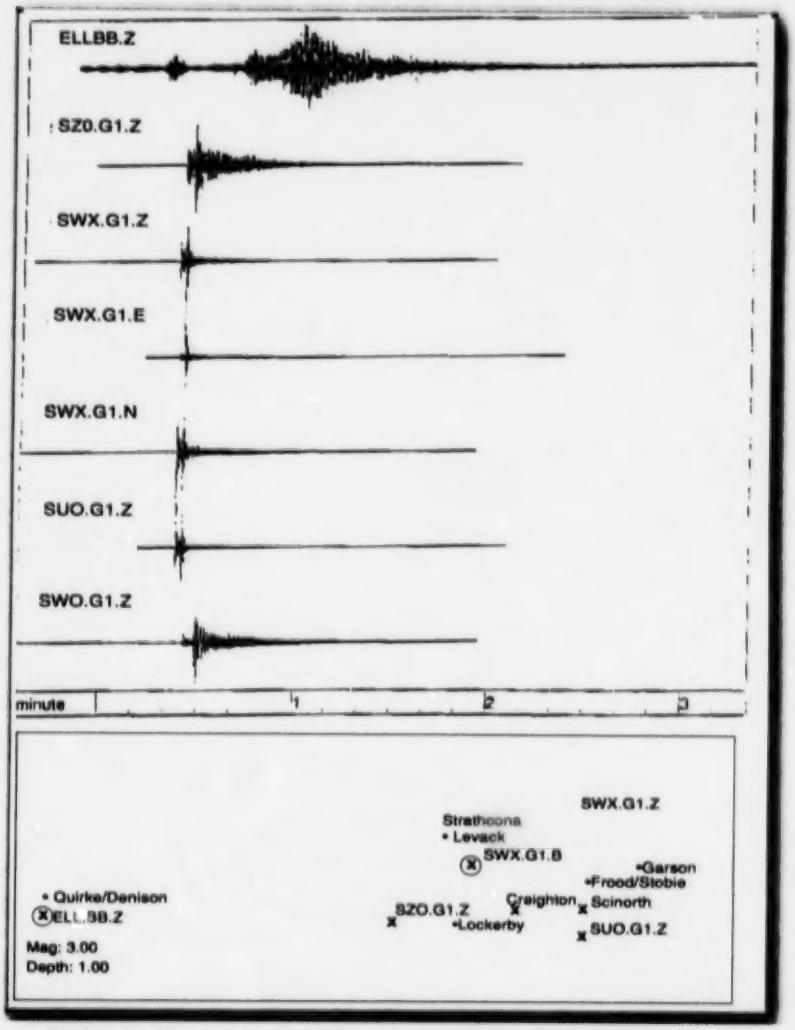

Figure 3.12 Signals recorded by the SLTN for the Nov. 26, 1993, fatal rockburst at Macassa mine in Kirkland Lake, Ontario

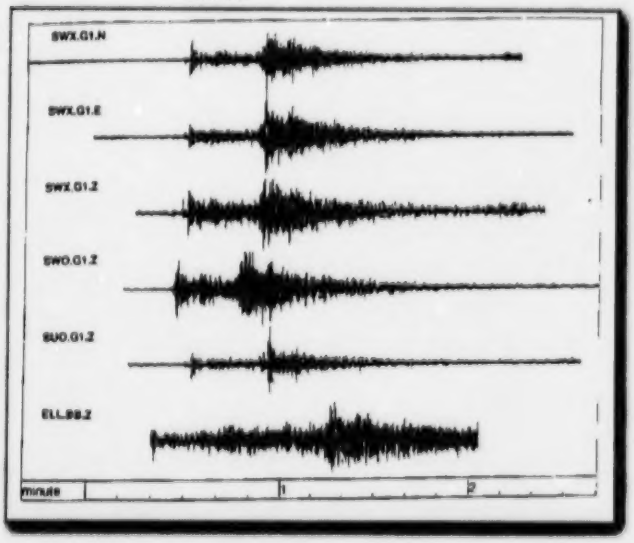

- The final product was a location plan showing the triggered sensor sites, the event-source locations in global co-ordinates and the magnitude of the event (see figures 3.14 and 3.16).

The location of each event was confirmed by mine operators provided there was an on-site microseismic monitoring system. The CDSN source-location accuracy was then compared to the one from the on-site monitoring system. Epicentres — the projection of event-source locations on surface — are typically determined with an accuracy of about 1.0 km. A print-out of the event waveforms showing P- and S-wave arrivals is completed and, if requested, the package is sent to the mine ground control department for their records. Also, the event and its associated parameters were added to the data base on a spreadsheet. At the end of each week, all the event data for that week were copied to an optical disk for permanent storage. A list of the MIS signals for each mine was also kept.

3.5 Summary of Operations

Since the first stage of the SLTN upgrade in July 1993, a number of practical problems have had to be resolved before the network could become fully operational. At the end of December 1993, the system had become operational for approximately 80% of the time. Downtime, particularly since July 1993, was a result of the problems with software, hardware and phone-line difficulties. However, in spite of the difficulties, some significant rockburst activities were recorded during this time period, including the fatal rockburst at Macassa mine in November 1993 (Figure 3.12). The new WASP communication software was installed in two steps, in February 1994 and June 1994. This operation was not totally satisfactory and persistent software conflicts made it necessary to

manually retrieve the data. In August 1994, as part of the overall upgrade plan, it was decided to relocate the main acquisition hardware from Science North to CANMET's Sudbury Laboratory. Hence, it became possible to provide a more reliable and timely response to system difficulties. It is interesting to note that the hardware and software difficulties experienced since the upgrade did not include the ELL sensor site, based on the same system logic, where the acquisition computer had worked for the two previous years with less than three days of total downtime.

Tables 3.1, 3.2 and 3.3 provide listings of mine-induced seismic events in Northern Ontario since September 1992, as recorded by the CANMET macroseismic monitoring systems, the CANMET Digital Seismograph Network and the seismograph network operated by the Geophysics Division of the Geological Survey of Canada. The lower limit of magnitude of these events corresponds to a magnitude of 1.5 m_N. Table 3.1 summarizes mine-induced seismic events from September 1992 to June 15, 1993, when Sudbury Laboratory took over the operation of this network. Table 3.2 lists the events from June 15, 1993, to December 31, 1993, and Table 3.3 summarizes the events from January 1, 1994, to December 31, 1994 (Talebi et al., 1994).

Some significant events recorded during the Phase II rockburst project are presented in figures 3.11 to 3.16. For example, Figure 3.13 shows waveforms from a significant seismic event (magnitude 2.7 m_N) at the Macassa mine in Kirkland Lake, Ontario, recorded on December 25, 1994. The location of the source and the magnitude determination for the same seismic event are presented on Figure 3.14, whilst Figure 3.15 depicts waveforms from a small earthquake located in the Kapuskasing area of Northern Ontario on December 25, 1994. Source location and magnitude determination for this event is presented on Figure 3.16.

Figure 3.13 Waveforms from a recent significant seismic event (magnitude 2.7 m_N) at Macassa Mine in Kirkland Lake, Ontario, recorded on Dec. 25, 1994

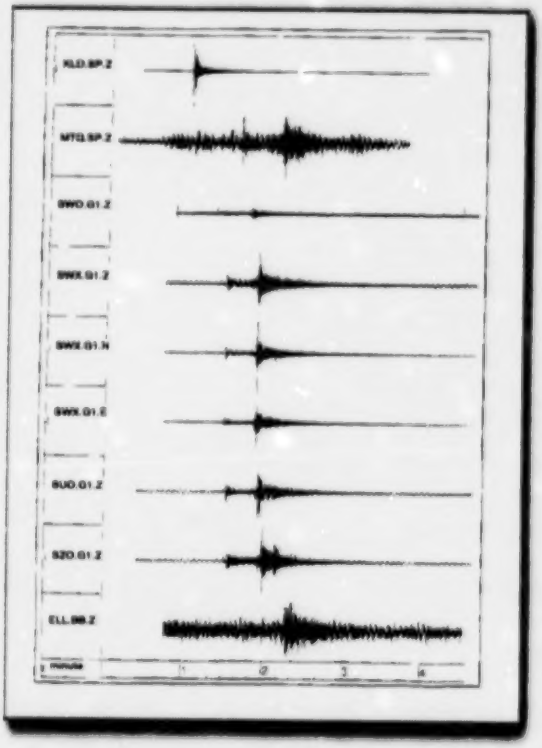

Figure 3.14 Source location and magnitude determination from the Dec. 25, 1994, seismic event at Macassa mine

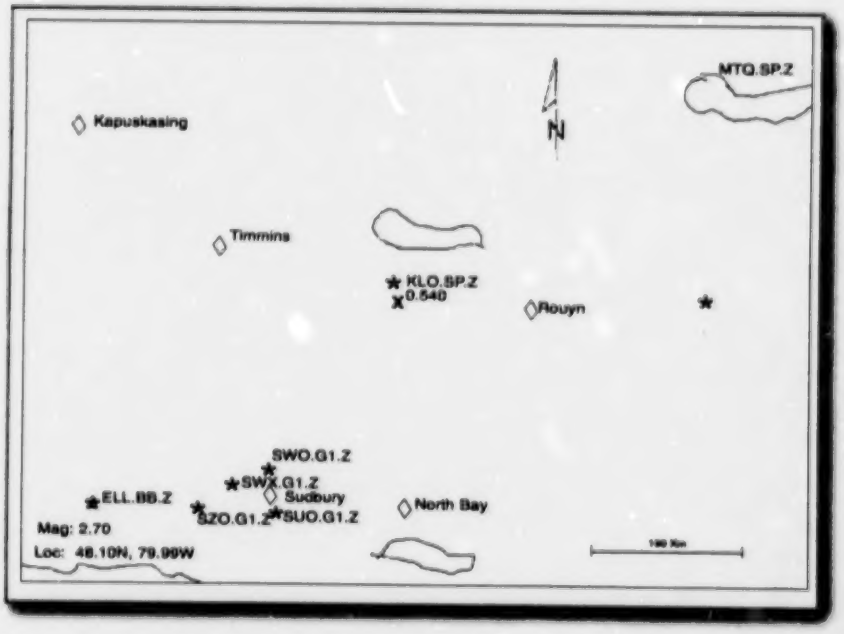

3.6 Data and Requests

Requests for information are also received from numerous sources, including the Geological Survey in Ottawa, contractors performing blasting operations for road construction and repairs around the Sudbury Basin, and a concerned or curious public, as well as the media and the universities. Information exchange has occurred frequently between the Geophysics Division of the Geological Survey of Canada in Ottawa and CANMET's Sudbury Laboratory, regarding rockburst monitoring — primarily to compare magnitude determinations of the CDSN with those of the Eastern Canada Telemetered Network (ECTN). The results of the two networks are typically within the acceptable range of ± 0.3 m_N throughout the monitoring range of the CDSN. The GSC have occasionally requested earthquake data recorded on CDSN for their archives. One of the most significant global events recorded by the SLTN was the magnitude 8.2 deep-focus (500 km) earthquake of June 9, 1994, in Bolivia, South America. This particular event was widely felt in the Northern hemisphere, even in Northern Ontario.

Figure 3.15 Waveforms from a small earthquake located in the Kapuskasing area of Northern Ontario, on Dec. 25, 1994

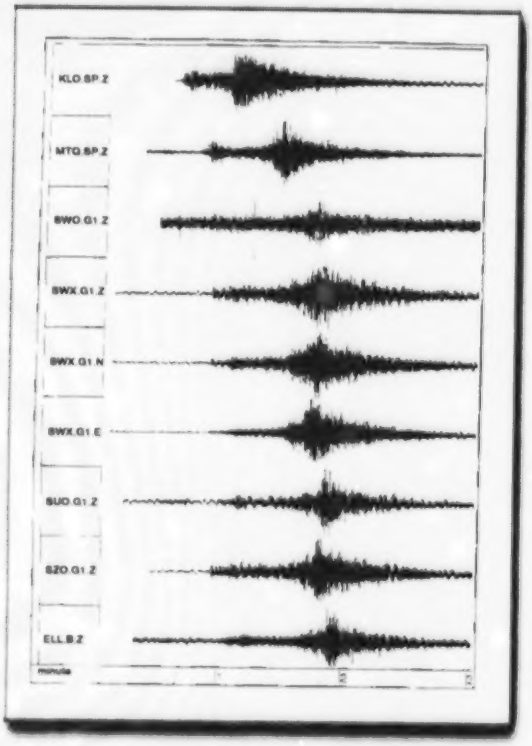

3.7 Conclusion

Following the upgrade of the Sudbury Local Telemetered Network and the expansion of the CANMET Digital Seismograph Network, the network was now composed of seven single-component and one three-component seismograph stations. The new single-component stations are located in Kirkland Lake, Ontario, and Matagami and Val d'Or in Quebec. The three-component station was installed in the Dowling area of the Sudbury Basin.

The additional coverage provided by the expanded CDSN has significantly increased the quality of magnitude determinations for mine-induced events occurring in the mines of northeastern Ontario and northwestern Quebec.

Figure 3.16 Source location and magnitude determination for the Dec. 25, 1994, small earthquake in the Kapuskasing area

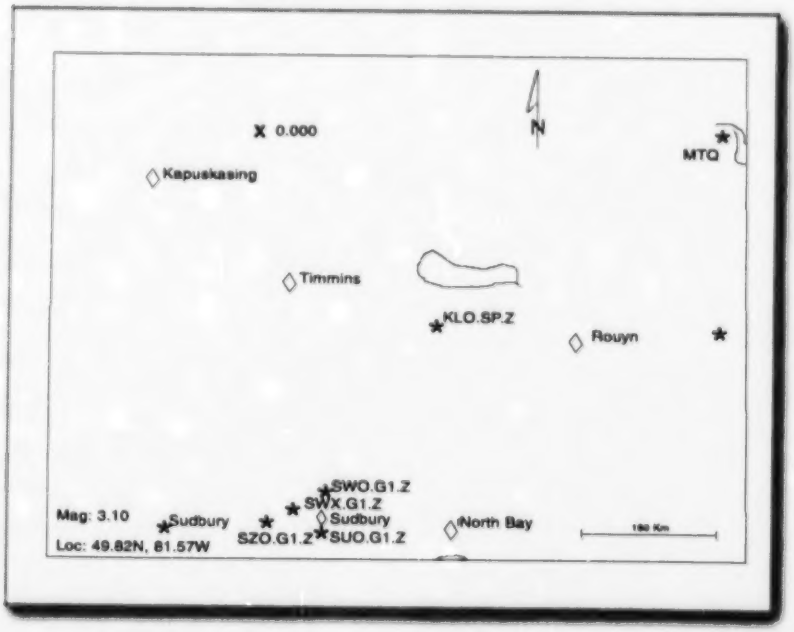

Table 3.1 Mine-induced seismic events (m_N >1.5) in Northern Ontario from September 3, 1992, to June 15, 1993
The first column shows the results of the CANMET macroseismic systems (operational at the Creighton, Macassa and Campbell mines) and the fifth column shows the results from the GSC seismograph network (data courtesy of C.A. Galley and R.J. Wetmiller).
Notes – NR: event not recorded; NC: GSC was not contacted, typically m_N<2; IMP: magnitude determination was impossible based on the available data.

Date	Local Time	Mine Location	Magnitude (m_n) CANMET– macro	Magnitude (m_n) GSC
Sept. 3, 1992	22:39:06	Creighton	2.4	2.7
Sept. 4, 1992	09:13:23	Creighton	1.5	1.5
Sept. 5, 1992	01:21:08	Creighton	1.8	1.5
Sept. 7, 1992	16:33:16	Creighton	1.6	1.7
Sept. 11, 1992	07:11:03	Creighton	1.5	1.4
Sept. 11, 1992	18:22:26	Creighton	1.6	1.7
Sept. 12, 1992	01:26:03	Creighton	1.6	1.5
Sept. 16, 1992	22:50:00	Creighton	1.8	NR
Sept. 17, 1992	17:51:27	Creighton	1.5	NR
Sept. 23, 1992	11:00:00	Falconbridge 5 shaft	–	2.0
Sept. 23, 1992	11:01:00	Falconbridge 5 shaft	–	2.4
Oct. 1, 1992	02:22:36	Creighton	1.8	1.8
Oct. 1, 1992	10:53:09	Macassa	1.5	NR
Oct. 4, 1992	21:29:24	Creighton	1.7	2.1
Oct. 8, 1992	14:06:56	Creighton	1.6	1.9
Oct. 20, 1992	18:37:28	Creighton	2.3	2.6
Oct. 22, 1992	15:54:57	Campbell	1.5	NR
Oct. 28, 1992	10:26:20	Macassa	2.1	2.3
Oct. 28, 1992	10:35:08	Macassa	2.3	2.6
Oct. 28, 1992	22:32:21	Creighton	1.7	1.9
Oct. 29, 1992	06:19:45	Creighton	1.6	1.5
Oct. 29, 1992	20:02:07	Creighton	1.9	2.1
Oct. 31, 1992	12:04:25	Creighton	1.8	2.1
Nov. 7, 1992	05:38:13	Creighton	1.9	2.0
Nov. 9, 1992	11:55:49	Macassa	1.5	NR
Nov. 30, 1992	21:58:51	Creighton	2.1	IMP
Dec. 4, 1992	15:42:12	Creighton	2.0	2.0
Dec. 4, 1992	16:19:10	Creighton	2.7	2.8
Dec. 9, 1992	22:14:15	Creighton	2.3	2.2
Dec. 10, 1992	05:15:51	Creighton	1.3	1.5
Dec. 11, 1992	21:36:24	Creighton	1.6	NR
Dec. 17, 1992	13:21:38	Creighton	2.1	2.6
Feb. 6, 1993	10:03:03	Creighton	1.6	1.8
Feb. 7, 1993	03:11:06	Creighton	1.4	1.9
Feb. 21, 1993	22:07:40	Creighton	1.6	1.6
Mar. 16, 1993	02:22:02	Creighton	2.0	2.2
Mar. 16, 1993	02:24:29	Creighton	1.5	NR
Mar. 17, 1993	15:51:21	Campbell	2.1	NR
Mar. 17, 1993	15:52:15	Campbell	1.6	NR
Mar. 24, 1993	01:39:39	Creighton	1.6	NR
Mar. 29, 1993	01:23:51	Creighton	NR	1.6
Apr. 1, 1993	19:14:03	Creighton	2.2	2.1
Apr. 2, 1993	14:23:13	Creighton	2.9	2.9
Apr. 2, 1993	14:27:43	Creighton	1.5	NR
Apr. 3, 1993	15:47:49	Campbell	1.5	NR
Apr. 3, 1993	22:25:59	Creighton	1.5	NR
Apr. 15, 1993	00:07:16	Campbell	1.7	NR
Apr. 28, 1993	08:03:23	Creighton	1.5	2.2
Apr. 29, 1993	15:26:12	Creighton	1.8	NR
May 8, 1993	14:57:12	Creighton	1.9	1.9
May 8, 1993	20:12:41	Creighton	2.6	2.5
May 12, 1993	21:03:21	Creighton	1.5	NR
May 14, 1993	08:05:12	Creighton	1.8	NR
May 14, 1993	08:07:12	Creighton	1.8	NR
June 5, 1993	22:13:06	Creighton	1.5	NR
June 8, 1993	17:02:10	Creighton	1.5	2.0
June 15, 1993	14:32:39	Creighton	2.6	2.7

Table 3.2 Mine-induced seismic events (m_N >1.5) in Northern Ontario from June 15, 1993, to December 31, 1993
They were recorded by the CANMET macroseismic monitoring systems, the CANMET Digital Seismograph Network and the GSC network, respectively.
Notes – NR: event not recorded; NC: GSC was not contacted, typically m_N<2; IMP: magnitude-determination was impossible based on the available data.

Date	Local Time	Mine Location	Magnitude (m_N) CANMET – macro	Magnitude (m_N) CANMET – CDSN	Magnitude (m_N) GSC
June 15, 1993	14:32:39	Creighton	2.6	NR	2.7
June 15, 1993	22:43:29	Creighton	1.5	NR	NC
June 22, 1993	07:50:48	Creighton	1.8	NR	NR
July 5, 1993	19:02:11	Creighton	1.4	NR	1.5
July 5, 1993	08:17:30	Creighton	1.5	NR	1.4
July 27, 1993	02:00:11	Creighton	NR	NR	2.3
July 28, 1993	14:33:04	Creighton	1.7	NR	2.4 (blast and burst)
Aug. 5, 1993	22:39:51	Creighton	3.1	NR	2.9
Aug. 6, 1993	06:48:22	Creighton	1.6	NR	NC
Aug. 7, 1993	21:18:36	Creighton	2.1	NR	2.2
Aug. 10, 1993	02:51:10	Creighton	1.7	NR	NR
Aug. 11, 1993	02:29:46	Creighton	1.5	NR	NC
Aug. 13, 1993	18:24:08	Creighton	1.7	NR	NR
Aug. 15, 1993	01:03:18	Creighton	1.5	NR	NR
Aug. 19, 1993	22:49:11	Creighton	2.0	1.5	1.7
Aug. 23, 1993	00:35:55	Creighton	1.6	1.6	1.4
Sept. 3, 1993	14:00:25	Creighton	1.9	1.9	NR
Sept. 9, 1993	04:52:07	Creighton	1.6	NR	NC
Sept. 13, 1993	23:59:07	Creighton	SD	2.4	2.3
Sept. 22, 1993	16:05:50	Creighton	1.6	NR	NC
Sept. 25, 1993	20:37:24	Creighton	1.9	NR	1.8
Sept. 27, 1993	08:25:21	Creighton	1.5	1.5	NC
Oct. 2, 1993	00:06:39	Creighton	1.9	2.3	NR
Oct. 9, 1993	16:55:48	Campbell	1.5	NR	NR
Oct. 12, 1993	16:19:54	Creighton	2.6	2.4	2.6
Oct. 17, 1993	04:44:30	Creighton	2.1	1.9	1.5
Oct. 19, 1993	22:23:04	Creighton	2.0	2.0	2.2
Oct. 22, 1993	08:58:09	Creighton	1.8	2.1	NR
Oct. 26, 1993	20:56:17	Creighton	1.0	2.1	NR
Nov. 5, 1993	03:43:21	Creighton	1.8	2.3	2.4
Nov. 5, 1993	22:23:22	Creighton	2.8	2.9	2.8
Nov. 7, 1993	09:15:47	Fraser	–	2.4	NR
Nov. 19, 1993	15:54:34	Creighton	1.5	NR	NR
Nov. 20, 1993	03:56:34	Campbell	1.9	NR	NR
Nov. 23, 1993	23:22:23	Lockerby	–	2.0	1.8
Nov. 26, 1993	08:20:38	Macassa	2.4	2.9	2.8
Nov. 26, 1993	08:20:45	Macassa	2.1	2.4	2.5
Nov. 26, 1993	08:20:47	Macassa	1.7	1.7	1.7
Nov. 30, 1993	17:28:51	Creighton	1.5	1.7	1.9
Dec. 2, 1993	12:36:13	Creighton	2.2	2.2	2.5
Dec. 2, 1993	12:31:34	Creighton	2.4	2.4	2.6
Dec. 6, 1993	16:11:40	Stobie	–	2.3	2.4
Dec. 7, 1993	23:32:16	Stobie	–	1.6	NR
Dec. 20, 1993	02:41:11	Creighton	1.6	NR	1.6
Dec. 31, 1993	12:31:34	Creighton	2.3	NR	NR

Table 3.3 Mine-induced seismic events (m_N >1.5) in Northern Ontario from January 1, 1994, to December 31, 1994
They are recorded by the CANMET macroseismic monitoring systems, the CANMET Digital Seismograph Network and the GSC network, respectively.
Notes – NR: event not recorded; NC: GSC was not contacted, typically m_N<2; IMP: magnitude determination was impossible based on the available data.

Date	Local time	Mine location	Magnitude (m_N) CANMET – macros	Magnitude (m_N) CANMET – CDSN	Magnitude (m_N) GSC
Jan. 1, 1994	19:57:27	Frood-Stobie area	–	1.8	1.5
Jan. 6, 1994	10:31:26	Creighton	1.8	1.8	NC
Jan. 7, 1994	22:30:17	Onaping	–	2.6	2.5
Jan. 8, 1994	23:35:20	Frood-Stobie area	–	1.8	NR
Jan. 10, 1994	06:24:42	Frood-Stobie area	–	2.1	2.1
Jan. 19, 1994	01:18:26	Creighton	1.8	NR	NC
Jan. 19, 1994	09:08:00	Kerr Addison	–	NR	2.4
Jan. 19, 1994	09:10:00	Kerr Addison	–	NR	2.2
Jan. 19, 1994	14:28:18	Creighton	1.7	NR	NC
Jan. 25, 1994	17:05:44	Creighton	2.0	NR	NR
Mar. 13, 1994	20:32:02	Creighton	1.8	NR	NC
Mar. 19, 1994	21:05:26	Creighton	1.6	NR	NC
Mar. 23, 1994	21:09:26	Campbell	2.2	NR	2.3
Mar. 23, 1994	21:22:04	Campbell	1.9	NR	NR
Mar. 31, 1994	08:11:08	Creighton	2.5	2.2	2.3
Apr. 2, 1994	08:26:30	Creighton	2.3	NR	2.0
Apr. 2, 1994	13:32:28	Creighton	1.5	NR	NC
Apr. 13, 1994	05:13:54	Kidd Creek	–	2.9	2.8
Apr. 20, 1994	03:45:20	Campbell	1.5	NR	NR
May 14, 1994	12:59:35	Creighton	2.4	2.6	2.6
May 17, 1994	01:03:44	Creighton	1.6	1.9	NC
June 7, 1994	03:05:30	Creighton	1.6	1.9	NC
June 13, 1994	11:50:30	Strathcona	–	1.9	NR
Aug. 7, 1994	00:44:16	Creighton	1.6	NR	NC
Aug. 7, 1994	23:17:47	Creighton	1.8	NR	1.6
Aug. 9, 1994	11:06:53	Creighton	1.7	1.6	NC
Aug. 13, 1994	01:00:58	Creighton	1.7	1.9	NC
Aug. 30, 1994	14:58:07	Creighton	2.0	NR	1.7
Aug. 30, 1994	15:34:27	Creighton	1.5	NR	NC
Aug. 31, 1994	03:17:04	Creighton	2.9	2.9	3.1
Sept. 10, 1994	14:33:09	Macassa	1.5	NR	NC
Sept. 20, 1994	09:13:08	Creighton	3.2	2.9	2.9
Sept. 20, 1994	09:13:22	Creighton	2.0	1.9	NR
Sept. 20, 1994	21:15:45	Creighton	1.6	NR	NC
Sept. 21, 1994	02:26:19	Creighton	–	2.9	2.5
Oct. 3, 1994	00:55:24	Creighton	2.9	3.0	2.9
Oct. 3, 1994	10:13:28	Creighton	1.6	NR	NC
Oct. 9, 1994	22:18:09	Creighton	1.5	NR	NC
Oct. 23, 1994	04:54:51	Creighton	2.5	2.5	2.1
Oct. 23, 1994	23:19:47	Creighton	1.6	1.5	NC
Oct. 26, 1994	23:45:03	Campbell	1.5	NR	NR
Oct. 31, 1994	15:42:52	Campbell	2.6	NR	2.8
Nov. 2, 1994	09:15:44	Creighton	1.6	NR	NC
Nov. 24, 1994	20:00:14	Creighton	1.5	NR	NC
Dec. 5, 1994	08:24:37	Creighton	2.7	2.7	2.6
Dec. 9, 1994	08:52:46	Creighton	1.9	2.0	NC
Dec. 18, 1994	17:50:22	Creighton	3.0	2.7	2.8
Dec. 19, 1994	11:02:42	Creighton	2.1	1.7	NR
Dec. 19, 1994	23:50:29	Creighton	2.4	1.6	NC
Dec. 20, 1994	15:09:00	Kidd Creek	–	2.2	2.2
Dec. 20, 1994	16:19:16	Creighton	1.5	NR	NC
Dec. 25, 1994	07:56:35	Macassa	2.3 at 2 sites	2.7	2.5

3.8 References

Hedley, D.G.F. (1992). *Rockburst Handbook for Ontario Hardrock Mines.* CANMET Special Report SP 92-1E, 305 pages.

Mottahed, P. (1991). *A Report on the Seismograph Stations Operated by CANMET and a Proposal for Modification and Communication of Data.* CANMET Internal Report.

Plouffe, M., Cajka, M.G., Wetmiller, R.J. and Andrew, M.D. (1990). "The Sudbury Local Telemetered Network." Proceedings of the 2nd International Symposium on Rockbursts and Seismicity in Mines, pp. 221-226.

Pritchard, C.J. and Talebi, S. (1994). *The Upgraded Sudbury Local Telemetered Network (SLTN): The First Year of Operation (93-94).* CANMET Report MRL 94-053(TR), p. 33.

Talebi, S., Pritchard, C.J. and Mottahed, P. (1994). *Rockburst Activity in Northern Ontario: September 1992 - December 1994.* CANMET Report MRL 94-071 (TR), p. 15.

CANMET's Macroseismic System and Waveform Analysis Software

4.1 Introduction

The microseismic monitoring systems which had been installed at mine sites for local coverage of the seismic events, prior to initiation of the first phase of rockburst research, had several limitations. Although the system provided reliable first arrival times for seismic-source location, these were not designed to capture seismic waveforms and provide reliable magnitude determination of seismic events.

One of CANMET's mandates was to fulfil this need by designing and installing a new generation of seismic monitoring systems, called Macroseismic Monitoring Systems. Through the first phase of the rockburst research, these systems were installed at five different mining camps in Ontario: Falconbridge's Strathcona Mine and Inco's Creighton Mine, both in the Sudbury Basin; Rio Algom's Quirke Mine at Elliot Lake; Placer Dome's Campbell Mine at Balmerton; and Lac Minerals' Macassa Mine in Kirkland Lake.

These systems were designed as a research tool to better understand the rockburst phenomenon based on the recording of the complete seismic waveforms. Their purpose was also to provide source-location calculation and magnitude determination and to allow the study of seismic-source parameters.

4.2 CANMET's Macroseismic System

In concordance with the design, fabrication and installation of the new macroseismic system, a suite of software was written to facilitate the recording and analysis of the day-to-day data captured. This chapter discusses these two main topics: the macroseismic system and the waveform analysis package.

4.2.1 An Historical Review of Macroseismic Systems in Ontario

Originally, these systems were based on five triaxial sensors located about one kilometre away from the rockburst-prone areas of a mine. The magnitude range targeted, without sensor saturation, was from 0.5 to 2.5 m_N, while the frequency response range was typically between 1- and 2500-Hz. The data-acquisition unit was located at the mine site and all recorded data were processed at CANMET's Elliot Lake Laboratory and, subsequently, at the Sudbury Laboratory. These systems were remotely accessible via modems, allowing data-file transfer and remote-system control.

In March 1987, the first macroseismic monitoring system was installed on the surface at Rio Algom's Quirke Mine near Elliot Lake. It was developed by the Noranda Research Centre of Noranda Mines Ltd. (Labuc et al., 1987). Initially, the system consisted of five surface-mounted triaxial ADR-711 accelerometers during the period March 1987 to June 1987 (Kestle, 1983). After this date,

several lightning strikes destroyed the sensors and they were replaced with Geospace GS-40B 8-Hz geophones with a sensitivity of 0.27 V/cm/sec, having the capability of case-to-coil motion of 0.18 cm.

Signals from sensors were frequency modulated, multiplexed and sent along fibre-optic links to a central location where the signal was converted from optical to electrical, demultiplexed, filtered and then digitized by a mini-computer (16-bit accuracy) at 1000 points per sec for 0.8 sec, including a 0.2 sec pretrigger. Events were considered valid and were saved if the trigger levels of at least 9 of the 15 channels exceeded the set threshold. In that case, the 15 channels of data were stored in ASCII format as one file to allow the subsequent interactive analysis on the mini-computer.

During the same period, the second macroseismic system was installed at the Strathcona Mine. The system consisted of five triaxial accelerometers, Model S-100, manufactured by Teledyne Geotech, with a frequency response from 0.01-2000 Hz. The output sensitivity of the accelerometer/amplifier assembly was 20 V/g. Three sensors were located on surface and two underground at the 2375 and 2750 levels, and the seismic signals were transmitted by electric cable to the processing unit located on the surface. This system was developed by Kanata-based Instantel Inc. The data-acquisition system consisted of five individual signal-processing units, and the signal from each sensor was digitized at 4 kHz/channel, 12-bit accuracy and temporarily stored in a buffer. A serial multiplexer was used to interface each slave processor to an IBM-AT micro-computer responsible for event-handling and data storage.

The Macassa and Campbell mines' macroseismic systems were installed in September 1988 and August 1989, respectively. The design of both systems was identical. It consisted of five strong-motion triaxial velocity gauges, Model 1130, manufactured by Electro-Lab, including programmable sensor amplifier form 0-60 dB. All sensors were located underground. Their sensitivity was 0.30 V/cm/sec, while the frequency response ranged from 1- to 2700-Hz.

For these sites, the seismic signals were amplified at each sensor and transmitted by electric cable to the recording unit, located on surface. The signals were then conditioned by anti-aliasing filters and recorded. However, both the triggering and the recording mechanism were based on the Gould technology, which was not designed for this type of application. The system was based on only 8-bit accuracy, and was designed to trigger on only one pre-selected channel. In several cases, its use resulted in the system not recording large seismic events.

The last seismic monitoring system at Creighton was installed in March 1991. The design of this system is primarily similar to that of the Macassa and Campbell systems, with the main differences being that (a) the Creighton system used dual amplification to provide a larger dynamic range in order to prevent saturation of larger seismic events; and (b) data were transmitted through fibre-optic cable in one of the Creighton Mine shafts, with a multiplexer and demultiplexer located at both ends of the fibre-optic cable (Figure 4.1.) The system utilized five strong-motion triaxial sensors, which were installed between the 5400 and 7000 levels to cover primarily the 400 and 403 ore bodies.

Several problems occurred during the installation of the Creighton macroseismic system. The installation of the fibre-optic cable took almost two years to complete, leading to the late installation of the system. Additionally, the system — and, more specifically, the recording unit, designed by Electro-Lab — failed to work adequately. After several months, the unit was replaced with the Gould unit.

Figure 4.1 CANMET's macroseismic system overview – Creighton Mine

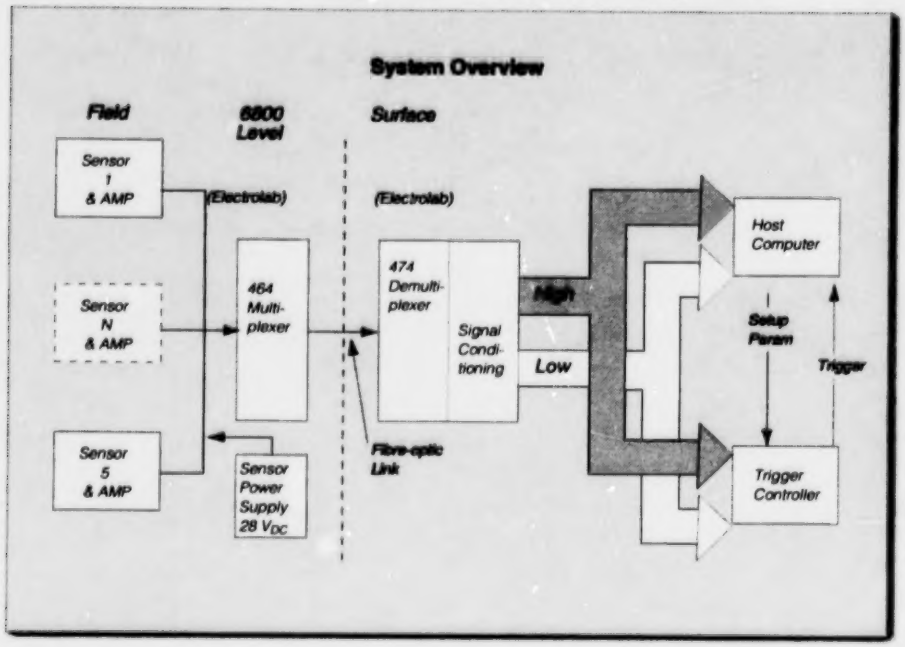

4.2.2 An Historical Review of Macrosesmic Systems: Its Origin

As described earlier, the design of the systems installed was based on the amalgamation of different technologies: fibre-optic cables versus electrical cables; accelerometers versus velocity gauges; dual-gain or single-gain amplifier; accuracy of A/D converters ranging from 8 bits to 16 bits; several different triggering mechanisms; host computer ranging from IBM-PC to mini-computer; surface or underground sensor installation; various manufacturers; various software. The diversity of the components of the systems in use made the maintenance of the systems very difficult.

The main handicap of these systems related to their limitations and, in some cases, their complexity. None of them were able to meet the main expectations of reliability, flexibility, efficiency and simplicity. This warranted a new approach to the monitoring of seismic signals.

Based on the experience and expertise gained from the installed systems, it was decided to design and fabricate a macroseismic system capable of fulfilling the outlined expectations, which included improving the output sensitivity and eliminating the problems at CANMET's Elliot Lake Laboratory. The main design requirement of this new system was as follows:

- intelligent triggering mechanism;
- programmable system parameters;
- electrical spike elimination;
- continuous and non-continuous mode of data acquisition;
- reliable communication package for remote access;
- high performance, real-time operating system;

- accuracy, expandability;
- adaptability for various sensor types;
- real-time, automatic magnitude calculation; and
- user-friendliness for the seismic-waveform-analysis software.

In May 1991, the first version of the proposed system was successfully completed and tested. It was followed by the design of the centralized version, portable and intrinsically safe for coal-mine use.

4.2.3 Upgrade of the Ontario Macroseismic Systems

In May 1991, the obsolete Gould waveform recorders, which were used as triggering and recording units, were replaced by the new CANMET triggering board, a 12-bit A/D converter board for better accuracy and by a more powerful computer as a recording and storage unit. In addition, a new high-performance 32-bit, real-time multi-tasking/multi-use operating system called QNX was implemented as the new computer operating system. This system provided a more reliable environment for remote communication. The Creighton macroseismic system was also successfully upgraded in February 1992 based on the same technology. Out of the five systems installed in Ontario mines, two were discontinued by November 1992. The imminent closure of Rio Algom's Quirke Mine led to the shutdown of the macroseismic system. Negotiations with the Rio Algom and Denison mines (the second mine was also destined to be closed by June 1993) were to no avail and the system was decommissioned in May 1991. As with Falconbridge's Strathcona Mine, the upgraded system was hampered by many problems, partly due to operational constraints, and did not fulfil its objective. The closure of the mine dictated the decommissioning of the system by November 1992. It must be emphasized that the system installed did capture the early full-waveform data from this site, which was used by Queen's University in the focal mechanism project (Trifu et al., 1995).

4.2.4 Macroseismic Data Collection

In 1992, the last three remaining systems — the Macassa, Campbell and Creighton mines — were completely upgraded based on CANMET technology, improving the capability of data capture. Since February 1992, at Creighton Mine, the CANMET system has recorded more than 925 seismic events with magnitude values ranging from 0.5 to 3/5 m_N (see Appendix II) and as many as 5500 events generated by blasting. The magnitude values are determined from seismic-energy integration, recorded from the triaxial sensors. The calculated value is corrected for distance and then converted to an empirical Nuttli magnitude scale. As shown in Appendix II, the magnitude values provided by the CANMET system (first column) are comparable with those published by GSC's Geophysics Division in Ottawa in the early days, and later with the CANMET Digital Seismograph Network values (second column) showing the consistency of the data deduced.

For the same period, Macassa's system recorded more than 220 seismic events, of which 175 events had magnitude values ranging from 0.0 to 2.9 m_N (see Appendix II) and 2950 events were blast-generated. For Campbell Mine, the figure is more than 4700, with 78 seismic events having a magnitude ranging from 0.0 to 2.8 m_N and more than 4625 events generated by blasts (Appendix II). All collected data files, including blasts, were transferred to CANMET's Elliot Lake Laboratory and subsequently to the Sudbury Laboratory via modem for analysis, and the results were communicated to the mine site for their use. Under the agreement, CANMET was also responsible for the upkeep and maintenance of all the systems, as well as the update and publication of the data bank.

4.2.5 Upgrade of the CANMET Seismic System

Since November 1994, the CANMET seismic system has been greatly improved, with the system being capable of expanding from 16 to 32 channels-plus, by simply adding extra A/D converter and triggering boards in the host computer. Real-time automatic arrival-time picking, source location and magnitude determination are now part of the system's data acquisition. A data-analysis package which has been ported to the QNX Windows platform could also be added to the system. In addition, the CANMET system is capable of accommodating a wide variety of transducers (accelerometers, velocity gauges and hydrophones), both uniaxial and triaxial. The ability to mix different types of sensors on the same system provides the flexibility needed for a wide range of applications.

In the past, the sensors used with the system were mainly manufactured by Electro-Lab or Teldyne Geotech. Now, however, the seismology group at CANMET is capable of the design and manufacture of programmable sensor/amplifier velocity transducers and numerous units have been designed, manufactured and installed in different mining environments.

4.2.6 Technical Details of the CANMET Seismic System

4.2.6.1 Hardware Requirements

The hardware is designed to operate on any 386 family or faster IBM-PC-compatible computer having a minimum of two ISA slots and one hardware interrupt (from 3-7) available. For systems having more than 16 channels, a rack-mounted PC is recommended. This approach provides plenty of ISA slots for upgrades up to 64 channels and allows easy CPU upgrade by simply replacing the CPU board.

Table 4.1 shows the basic recommended computer hardware requirements.

Although the minimum requirements are adequate for a small system, it is highly advisable to consider a more powerful platform to exploit the full capabilities of the system. This is especially true if continuous data acquisition is needed (with no downtime between successive events).

Memory and hard-drive selections should be based on the desired sampling rate, event time-window and acquisition mode, all of which determine the size of the event file.

Table 4.1 Basic recommended computer hardware requirements

Resource	Minimum	Recommended
CPU	386DX 20 MHz	486DX2 66 MHz
Memory	4 Megabytes	8 Megabytes
Hard drive	200 Megabytes	500 Megabytes
Floppy	3½", 1.4 Megabytes	same
Ports	1 serial, 1 parallel	same
*Printer	24 pin dot matrix	same
*Plotter	PostScript	same
*Modem	9600 baud	14,400 or 28,800 baud

*=> optional

4.2.6.2 Triggering Mechanism

One of the unique features of the CANMET data-acquisition system is its triggering mechanism. Designed and developed in-house, the mechanism is based on a triggering time-window which is initiated by any channel hit by a signal exceeding the minimum triggering level specified in the system configuration. Once the time-length window has elapsed, the number of channels hit is then compared to the minimum number of channels preset for a valid trigger. If both requirements are met, the event is recorded.

This triggering technique was developed to eliminate the recording of very small seismic events. It prevented mining-equipment noise or induced electrical spikes from triggering the system, while allowing significant seismic events to be recorded and stored on hard disk.

The triggering mechanism has the following software configurable parameters:

- triggering level from 5 to 90% of A/D range;
- triggering time-window from 25 to 500 msec; and
- number of channels for a trigger 1 to 15.

4.2.6.3 Acquisition Software

The acquisition software runs under QNX© version 4.21 and is entirely written in C language. Although it may be run within the QNX Windows environment, it has been designed to run as a stand-alone application for portability and use in embedded systems, as in the portable version.

The complete package consists of several program modules, as shown in Table 4.2. The first four modules are required to run the acquisition, while the remaining program modules are used off-line to configure the system and perform maintenance functions.

The primary acquisition program (DAC) is the heart of the system. It performs all initializations and starts up the other three modules to activate acquisition, and is hence responsible for detecting and storing events in memory.

The secondary acquisition program (DAC_SON) is called by DAC to store events from memory to disk once they are acquired.

The demux task (DEMUX) is then called to read the raw data from disk and reformat them with a proper header file so they can be read and displayed on-screen by the analysis software (SEI-CAN) or by the display utility (DISP). The locate module (LOCATE), used during the demultiplexing process, provides a real-time, automatic arrival-time picking for source-location calculation and magnitude determination of the event.

The data flow and interaction which occur between these various program modules are shown on Figure 4.2. Each program runs as a stand-alone task on a priority basis, with the higher priority tasks being at the top of the table.

The configuration program (DAC_CONFIG) allows the user to set up all acquisition hardware and software parameters for the specific needs of the application. Configuration is performed either in operator mode or engineering mode. Operator mode is used only to set the sensitivity of the system by changing the trigger level and the trigger channels. The engineering mode has password access and is used when commissioning the system to set system-specific parameters such as sampling rate, event size and duration, pretrigger, trigger window, acquisition mode, anti-aliasing filters and other parameters, including sensor co-ordinates and calibration factors. The acquisition parameters are set by the user via an intelligent menu-driven program which alerts the user if incompatible parameters are selected.

Figure 4.2 Flow chart depicting the data-acquisition software and the interaction between different program modules

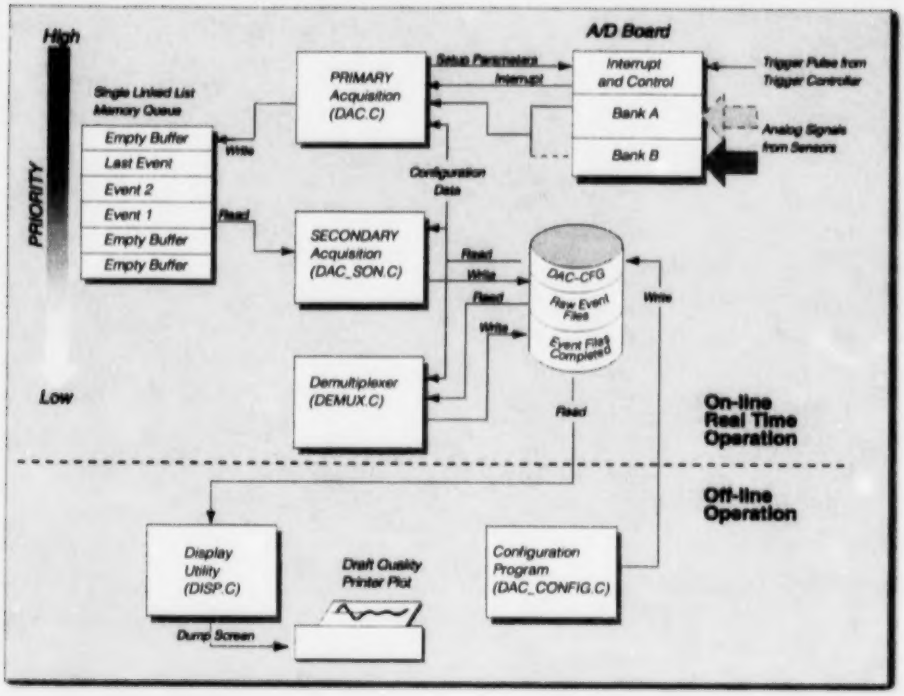

The last five modules (*) are optional and are used for maintenance and troubleshooting.

4.2.6.4 System Commands

The seismic data-acquisition unit uses several operating-system resources to provide powerful system-maintenance tools.

Remote system access relies entirely on system commands to handle model link-up, login procedures, file transfers and scheduling. The multi-tasking environment allows those tasks to occur without interrupting the data acquisition. Table 4.3 lists the most important system commands used.

Table 4.2 Data flow and interaction between various program modules

Program	Description
DAC	Primary acquisition
DAC_SON	Secondary acquisition
DEMUX	Event demultiplexer
LOCATE	Source location and magnitude
DAC_CONFIG	Configuration
*SIMUL	Event simulator
*USER_EXEC	Main menu executive
*MONITOR	Audio monitoring utility
*DISP	Basic troubleshooting display utility
*ARCHIVER	Packing and archiving utility

Table 4.3 List of most important system commands used

Command	Description
modem	Monitors and controls all modem-related functions
qtalk	Allows communication and terminal emulation via a modem
qcp	Provides efficient file-transfer protocol
ditto	Allows remote interactive shared access to any console (take over screen and keyboard)
cron	Provides scheduling utility to initiate commands at specified times

The "modem" command is normally installed at boot time in the system initialization process and remains active at all times.

The "qtalk" is used as required by the user to initiate a link-up to a remote system (could be a DOS machine).

The "qcp" is a QNX© specific file-transfer protocol but the popular "X-Y-ZMODEM" from the DOS environment is also supported.

The "ditto" command is an interesting feature, as it allows a remote user to literally take over control of a system console (virtual screen with associated keyboard). The remote user can perform any task while at the other location, such as system-parameter configuration and data-acquisition control, including booting the remote machine. Only programs such as waveform analysis (SEI-CAN) and waveform display utilities (DISP) cannot be remotely run since they operate in graphics mode. This command is also particularly convenient to check the status of the data-acquisition system, as well as the summary of the recorded activity which includes the data-acquisition parameter settings, the data and time of the recorded events, their locations, magnitude values and more. This information is displayed on the main console while the data-acquisition programs are being executed.

The "cron" command provides a convenient method for executing commands at specific times without operator intervention. It requires that the timer administrator be running in background.

The system also provides an automatic process of "booting" the system which initializes all data-acquisition functions after any power failure. Furthermore, it provides a password system which can prevent the files from being tampered with by inexperienced users.

4.2.6.5 Transducers

Sensor selection is determined by the type of application and the characteristics of the seismic events to be recorded. The CANMET seismic system accommodates a wide variety of acoustic transducers (accelerometers, velocity gauges or hydrophones), both uniaxial and/or triaxial. The ability to mix different types of sensors on the same system provides the flexibility to meet the needs of a wide range of applications.

Sensors and field-amplifier installations often represent a significant portion of the total system cost. To keep the costs down, CANMET has developed the capability of designing and building its own programmable sensor/amp velocity fabricating transducers for ease of installation with the possibility of retrieval of the unit, if so desired. This ensures compatibility with the data-acquisition system.

The transducers may be used for either single- or dual-gain systems with programmable gain from 6 to 64 dB in eight increments, with the possibility of drain either with jumpers at the site or directly from the system software, depending on the number of pairs of electrical wires available to the site.

4.3 Automatic Source Location and Magnitude Determination

The CANMET seismic system provides on-site, real-time automatic source location and magnitude determinations for seismic events. Source-location determination (LOCATE) is based on the algorithm developed by CANMET (see Chapter 5).

In addition to the event co-ordinates, several quality factors related to the accuracy and reliability of the given source location are also provided. These factors include residual sensitivity and event rank.

The event residual is a total effect of mismatch between the observed and calculated arrival times, which is the most important criterion for measuring the source-location accuracy. Sensitivity measures the stability of the solution, which is defined as the distance between a located source and its associated position obtained by assuming 10% lower velocity. For both parameters, a lower value indicates a better solution. The rank, which is a combination of these quality factors, also takes into account the hit sequence. This quality factor, which cannot be displayed on-screen, compares the observed and calculated hit sequences and determines the seriousness of the mismatch. The rank is categorized into five classes (A, B, C, D, Z), where A indicates a very good rating and Z means that the event is impossible to locate.

The magnitude calculation is based on the seismic-energy integration recorded from the triaxial sensors. The calculated value is corrected for distance and then converted to an empirical Nuttli magnitude scale. For systems without triaxial transducers, corrected seismic energy for distance is provided.

Appendix I depicts the circuit diagram for the CANMET macroseismic system.

4.4 Waveform Analysis Software

As a part of the first and second phases of the rockburst research program, CANMET embarked upon development of seismic-waveform-analysis software. The software exhibits a number of features to include source location, magnitude determination and the capability to calculate the seismic parameter as a result of the mine-induced source of the event. This research tool is mine-driven and is very user-friendly. The software, which was developed to analyze the seismic data collated by the macroseismic units developed by CANMET, has several interesting features:

- the software allows waveform display;
- manual arrival-time picking;
- source-location optimization and seismic-parameter determination;
- magnitude, seismic-energy and peak-particle calculations;
- menu selection for event distribution histograms as a function of time and/or magnitude values; and
- the plotting of seismic-event locations on the screen, provided that mining plans are available in an AutoCAD file format.

The software has been successfully implemented on several mini-computers, such as a DEC-VAX© station running under the VAX© operating system, MASSCOMP 5400, CONCURRENT 6350 and a SUN station, all running under UNIX© WINDOWS System V operating system. The software has been also written for micro-computers, such as 386 or 486 computers, running SCO UNIX© WINDOWS System

V operating system or QNX4 WINDOWS, being an abridged version of the seismic-waveform-analysis software. As a part of the data-acquisition package, the software has been ported to QNX4 WINDOWS, a Windows environment, the software is mouse menu-driven and easy to use.

CANMET's waveform-analysis software consists of several executable programs grouped in four categories:

1. **Data Sorting**
2. **Data Conversion**
3. **Waveform Analysis**
4. **Mine Display**

The **Data Sorting** program is used to quickly discard blasts from seismic event data-files recorded at the mine sites. A limited amount of waveform analysis can be done with this program.

Data Conversion programs are used to convert the raw binary data-files recorded from different mines to a standard ASCII file format prior to the analysis.

Waveform Analysis software provides full-waveform-analysis capability. The graphic utility's menu is designed to operate with a mouse.

Among the main features of this program, is that, regardless of the type of input (whether velocity gauges, accelerometers or both), original waveforms can be displayed in five modes: acceleration, velocity, displacement, radial-transverse and P-SV-SH. Energy values are automatically calculated and stored in the parameter file, and, if requested by the user, can be displayed on-screen.

The waveform-analysis program also provides various techniques for source location, such as least-squares methods based on "P" and "S-P" arrival times, as well as CANMET's source location. Figure 4.3 depicts the various options offered by this software.

Spectral analysis of the input signal in frequency domain is displayed for displacement mode in a log-log scale and for acceleration mode in log-log and lin-log scales. Seismic parameters are also calculated in time domain (Beardswood, 1993, 1994) and values are automatically stored in time-domain parameter file, with polarization of seismic waveforms so they can be used to study seismic waveforms.

The software offers two different versions of focal mechanism: focmec and focal. Focmec algorithm, written by Virginia Technical College, searches the focal sphere for acceptable solutions based on polarities and/or (SV/P) amplitude ratios (Snoke et al., 1994). To cover the focal sphere, the azimuth will vary from 0° to 360°and the dip from 0° to 90°. All possible focal mechanisms (up to 50) will then be included if Herrmann's X axis varies from 0° to 180°, which represents the lower part of the focal sphere. Solutions in the second quadrant are the same as ones in the first, except for the sign of the slip direction (Figure 4.4).

The focal version has been developed at the Geological Survey of Canada in Ottawa (Wetmiller, 1984). The theoretical approach used is very similar to focmec; however, two major differences characterize focal, and, contrary to focmec, only the best focal mechanism solution is kept from the computation process. The user has the opportunity to adjust or fit the proposed solution with regard to in situ rockmass observations through a series of menu choices.

The **Mine Display** program allows the user to access the level-plan layout of several mines. The user can plot one or several level plans, zoom and plot seismic activities and sensor location.

Figure 4.3 Flow chart depicting the available options in CANMET's waveform-analysis software

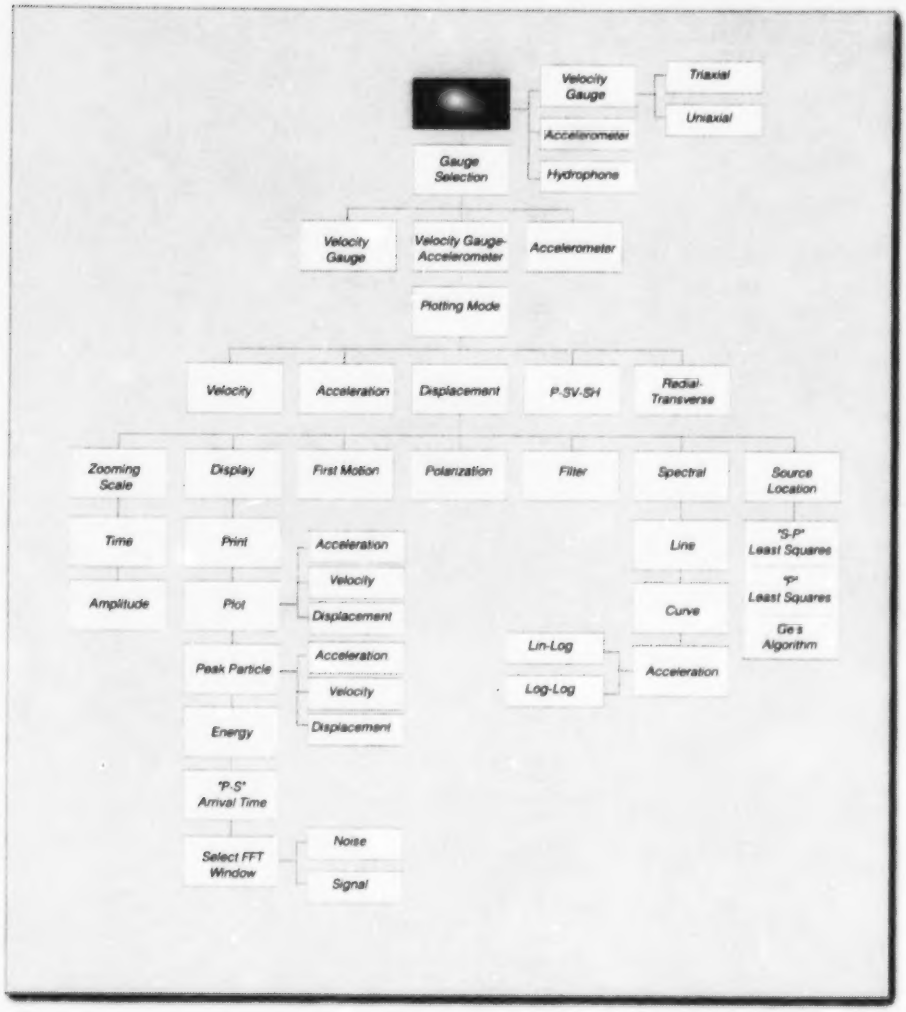

Histograms of seismic events can also be produced based on any time-length window and magnitude range. Finally, hard copy of any screen display can be obtained (figures 4.5 and 4.6). Appendix I provides the details and mode of operation of this software package.

Figure 4.4 Focal mechanism plot for Creighton data using Virginia Technical College algorithm

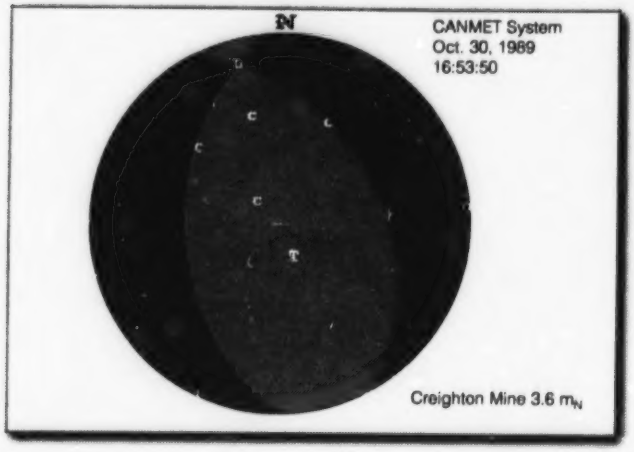

Figure 4.5 Histogram showing magnitude of events versus times for Creighton data

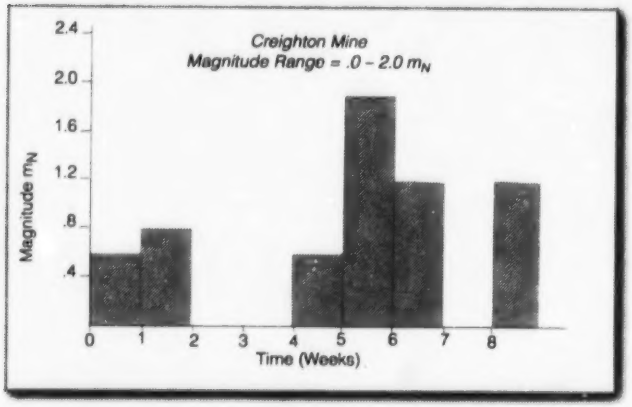

Figure 4.6 Histogram showing number of events versus times for Creighton data

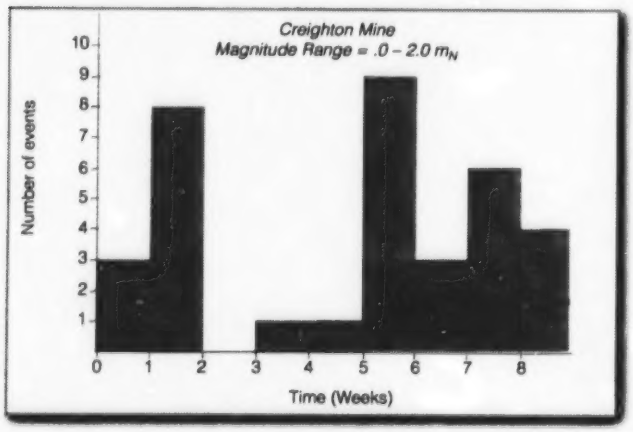

4.5 References

Beardwood, F. (1993). *A Study of Wave Polarization.* Sudbury Laboratory, CANMET Internal Report, 33 pages.

Beardwood, F. (1994). *A Study of Wave Polarization: Application to Macroseismic Data from Creighton Mine.* Sudbury Laboratory, CANMET Internal Report, 57 pages.

Kestle, A.M. (1983). "A Practical High Resolution Geophone." 53rd Meeting of the Society of Exploration Geophysicists, Las Vegas.

Labuc, V., Bawden, W. and Kitzinger, F. (1987). "Seismic Monitoring System Using Fibre Optic Signal Transmission." Proceedings of the 6th International Rock Mechanics Congress, Montréal, Quebec.

Snoke, J.A., Munsey, J.W., Teague, A.G. and Bollinger, G.A. (1994). "A Program for Focal Mechanism Determination by Combined Use of Polarity and SV-P Amplitude Ratio Data." *Earthquake Notes* 55(3):15.

Trifu, C.I., Urbancic, T.I. and Young, R.P. (1995). "Source Parameters of Mining-Induced Seismic Events: An Evaluation of Homogeneous and Inhomogeneous Faulting Models for Assessing Damage Potential." *Pure and Applied Geophysics* 145(1):3-27.

Wetmiller, R.J. Pers. Comm. 1984 M.S. dissertation, University of California, Los Angeles.

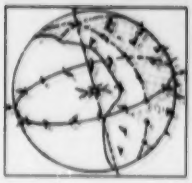

Microseismic Source Location

5.1 Introduction

The location of seismic events is extremely important in rockburst research. When a rockburst takes place, the first question asked is: "Where did it occur?" This piece of information is the key for taking many important subsequent decisions, such as implementing a rescue plan and other emergency measures. Microseismic source-location data are also important for mine design and planning. It has been standard practice for many rockburst-prone mines to evaluate the effectiveness of ground-control measures based on the pattern of the locations of seismic events. Furthermore, accurate source locations are required for all advanced studies, such as magnitude determinations, source mechanism and parameter assessments. This information, together with the knowledge of mining and geology, enables one to determine the likely causes of the rockbursts and to search for the optimum mine design and planning which will alleviate future occurrences.

Because of the importance of accurately locating microseismic events, CANMET initiated a comprehensive research program to improve source-location techniques during the second phase of the Canadian Rockburst Research Program. The program included basic research on the theory of automated data analysis and location of source, developing an innovative automatic source-location technique and implementing this technique in the mining industry. The program has been very successful and has provided the Canadian mining industry with state-of-the-art source-location technology for its daily monitoring of rockbursts.

This chapter presents a brief review of the theory and methods of the microseismic source-location technology, including the advanced automated source-location technique recently developed by CANMET.

5.2 Background

The location of microseismic events encompasses a wide range of technologies, such as instrumentation, transducer array geometry, data processing, source-location methods and reliability analysis. In this chapter, the principle of microseismic source location will first be illustrated through a simple example. Next, a number of important concepts will be discussed in order to establish a perspective view of the technique. Following this, several typical source-location methods will be presented. Finally, the factors affecting the source-location accuracy will be discussed, especially the quality of input data and transducer array geometry.

5.2.1 Source-Location Principles

Although there are different source-location approaches, the most widely used is the arrival-time-difference approach, which has been used almost exclusively in geotechnical studies (Hardy, 1986). It is therefore representative to use this approach to illustrate the principles of source location.

The concept of the arrival-time-difference approach is relatively simple. For it to be used, a number of single element transducers are needed, installed at suitable positions where microseismic activity can be effectively detected. A source position can then be calculated from the difference of arrival times detected at each transducer, the velocity model and the co-ordinates of the transducers.

Mathematically, this approach is initially described by a set of non-linear equations which has the form

$$((x_i - x)^2 + (y_i - y)^2 + (z_i - z)^2)^{1/2} = v(t_i - t) \qquad (1)$$

where the unknowns, x, y and z, are the co-ordinates of the source; t is the origin time of the source; x_i, y_i, and z_i are the co-ordinates of the ith transducer; ti is the arrival time at the ith transducer; v is stress-wave propagation velocity; and i=1, 2, ..., N+1, ..., M. Here, N denotes the geometric dimension of the problem and M denotes the number of equations. In order to solve for the unknowns, it is clear that the condition

$$M \geq N+1$$

must be satisfied, since there are N+1 unknowns (x, y, z, t).

5.2.2 Important Concepts

The discussion of the source-location method involves a number of general concepts in addition to the mathematical scheme which is used to search for the final solution. A good understanding of these concepts allows one to have some perspective of the methods and to avoid much of the confusion experienced by both researchers and practitioners.

5.2.2.1 Experimental Set-up and Source-Location Approach

In order to understand a source-location method, one has to know the experimental set-up associated with it. Microseismic-source-location technology contains two principal experimental set-ups. The most popular approach is to use arrival times of P- and/or S-waves detected from single-element and/or triaxial transducers. With this approach, each arrival time will allow one to establish an equation similar to Equation 1. The location can then be found by solving the resulting set of simultaneous equations.

The other approach uses both arrival times and amplitudes obtained from triaxial transducers. The general idea is that the spatial location of an event can be expressed by the distance and the relative azimuth to the transducer. The distance can be calculated from the arrival-time difference of P- and S-wave arrivals, and the relative azimuth can be determined in terms of the amplitudes of three mutually orthogonal components of the transducer. A detailed discussion of the mathematical procedure is given by Ge (1988). The major advantage of the approach is that the source location can be carried out with a single transducer, although there is a 180° ambiguity. The problem in using it in the mining environment is the high uncertainty associated with amplitudes because of extremely complicated geological structures, mine openings and backfill material. Sometimes it is also difficult to determine S-wave arrivals. Its application for daily monitoring is, therefore, very limited.

5.2.2.2 Optimization Methods

When there are more equations than unknowns, such as the case of microseismic source location, the solution must be defined statistically. This is usually done by using an

optimization method, which is actually the mathematical definition of the total error. The solution with the minimum error is considered as being the best solution or best fit. There are two principal optimization methods that are often used, the most popular one being the least-squares method. The other is called the absolute-value method, which has gained increased attention in recent years.

The least-squares method, statistically known as L2 norm approach, defines the total error as the sum of the squares of individual errors. The least-squares method has long been used in science and engineering to obtain the so-called "best fit" for over-determined problems in which the number of equations exceeds the number of variables. Based on statistical considerations, the best fit is unbiased only for linear approximations, with the assumption that the errors associated with each variable follow a normal probability distribution (Hines and Montgomery, 1980; Burden et al., 1981). It is understood from the assumption that more observations will yield a better fit since the probability for a larger group of observations to bias its normal distribution is much smaller. This is why using more transducers than necessary can lead to better accuracy in source location.

The absolute-value method, or L1 norm approach, defines the total error as the sum of the absolute values of the individual errors. The argument for using the absolute-value method is that the errors may not follow a normal distribution and, as such, a large error may dominate the calculation when the number of observations is small and the least-squares method is used.

It is important to understand that the fundamental difference between different optimization methods is in the definition of the total error. It is this difference which causes the difference in the estimation of individual errors, the calculation procedure and, finally, the best fit. A detailed theoretical discussion of the difference between the least-squares method and the absolute-value method is given by Ge (1995).

It is also important to understand that a best fit given by an optimization method is only the best for the given data set, and that the best fit could be meaningless if the given data set is poor. Furthermore, one should never expect to use an optimization method to try to extract information which does not physically exist in the given data set. For example, if an array is two-dimensionally arranged, it is inherently difficult to have good source-location accuracy in the third direction. The use of an optimization method, therefore, is not necessarily a guarantee of finding a reliable solution. The best solution will be found only when the input data are reasonably accurate and the experimental set-up (array geometry) is compatible with the problem to be solved.

5.2.2.3 Iterative Solution and Direct Solution

The final solution for the location of a microseismic event can be sought in two different ways: iteratively or directly.

The iterative approach to a solution is a method of searching numerically for the final solution. Normally, a trial solution (e.g. the co-ordinates and the origin time) is needed to initiate the calculation. Following certain schemes, this guess solution is updated in the next iteration. The process is repeated until an updated solution from a single iteration finally satisfies the pre-set error criteria.The result is then considered to be the true solution. In general, it is more flexible to use an iterative approach to search for the final solution because of the non-linear nature of the source-location problem. Typical examples of this

approach are Geiger's method and the Simplex method, both of which will be discussed later on.

The direct-solution approach is different from the iterative-solution approach in the sense that the final solution is obtained analytically. With this approach, neither a trial solution nor an iteration process is involved in the calculation procedures. For the direct-source location approach, the first step is to linearize the non-linear equations. The unknown parameters are then obtained by simultaneously solving the linearized equations. The USBM method, which has been widely used by mines, is representative of this approach.

5.2.2.4 Velocity Model

In microseismic source location, a suitable velocity model is one of the most critical factors affecting the accuracy of locating a source. It is also the most difficult one to determine.

Ideally, the velocity model should be able to characterize the major features of the real velocity field. In reality, however, it is very difficult to establish such a model. The geological structures and materials near the surface are very complicated and, in the mining environment, this is further complicated by the numerous openings and backfilling materials. To precisely identify the various velocity zones and their boundaries under such conditions is extremely difficult. Furthermore, according to Snell's law, the wave path is sensitive to a number of factors, which include the orientation of the velocity zone boundaries, the ratio of the velocities on the two sides of the boundary and the incident angle. A small deviation in these factors could produce a major error in later calculations. Because of these difficulties, the commonly used velocity models are highly simplified.

Several velocity models are available for microseismic source location. These models are the half-space model, the multi-layer model, the unique velocity model and the anisotropic half-space model.

The half-space model is also called the constant velocity model. In this model it is assumed that the geologic medium is continuous, isotropic and homogeneous, and, consequently, that the ray path is considered to be a straight line. The half-space velocity model is the basic velocity model used in microseismic source location because of its simplicity and the reasonable result one can normally expect. It is important, however, to know to what degree this simplified velocity model affects the accuracy of source location and how to reduce the impact of the initial velocity error caused by this highly simplified model.

The multi-layer velocity model assumes that there are a number of perfectly horizontal layers and that each layer is associated with a specific velocity value. This velocity model is mainly used in geophysics to simulate the crustal structure of the Earth for the location of local earthquakes. It is not clear how well this model can be used in the mining environment. Hardy and Mowrey (1981), based on a two-layer model and a half-space model, analyzed 26 major events recorded at an underground gas-storage reservoir in New Haven, Michigan. The study showed that both velocity models gave essentially similar results and, therefore, no critical evaluation could be made. Crosson and Peters (1974) have studied three different models theoretically, involving four layers, two layers and a single layer. According to their study, the three models gave similar source-location accuracies for sources lying outside the array boundaries. For events inside the array, the four-layer model was not perceptibly better than the two-layer model, but both of these models were better than the single-layer model.

In the unique velocity model, which is not specifically concerned with the details of the velocity field itself, it is assumed that a unique velocity exists between each transducer and the region of interest. The unique velocity model may work more effectively than the other models when the potential region of microseismic activity can be predetermined.

5.2.3 Source-Location Method

This section discusses several major source-location methods, along with their advantages and disadvantages. Although a source-location procedure includes a broad range of topics, such as processing input data, calculating event locations and evaluating the reliability of solutions, it is traditionally conceived as an algorithm to search for the final solution based on the constraints resulting from the experimental set-up. Therefore, the discussion of source-location methods in this section will be restricted to this tradition, and data processing and reliability evaluation will be given in the later sections.

5.2.3.1 Geiger's Method

Geiger's method (Geiger, 1910, 1912) is well known, and is almost universally used for the location of local earthquakes. It is also very popular in microseismic analysis. With Geiger's method, the final solution is numerically approached in an iterative process. In each iteration, the adjustment vector (Δx, Δy, Δz, Δt) is calculated based on the least-squares method and is then added to the previous solution to form a new solution. The iterative process is continued until the adjustment vector fulfils a pre-set error criterion. Geiger's method is an example of the Gauss-Newton method for optimization (Lee and Stewart, 1981).

Geiger's method, if the solution converges, usually produces very accurate results within a few iteration steps. The method can be used for different velocity models, such as the half-space velocity model, the unique velocity model and the discontinuous model. The major problem associated with the method is that convergence cannot be guaranteed. Although some remedial measures have been proposed (Smith, 1976; Buland, 1976; Lee and Stewart, 1981; Anderson, 1982; Lienert and Frazer, 1983), implementing these is usually very complicated and requires considerable experience.

5.2.3.2 Thurber's Method

Thurber's method (Thurber, 1985) is a modification of Geiger's. The method uses both the first- and the second-order partial derivatives to calculate the adjustment vector, while only the first-order partial derivatives are used for Geiger's method. Theoretically, Thurber's method appears more appropriate since source location, as shown by Equation 1, is inherently a non-linear problem. From a computational point of view, Thurber's method is identical to Newton's method.

Both Thurber's and Geiger's methods possess similar advantages and disadvantages. Although the method should be able to tolerate more complex source-location conditions, divergency could still be a problem.

5.2.3.3 Simplex Method

The Simplex source-location method was introduced by Prugger and Gendzwill (Prugger and Gendzwill, 1988; Gendzwill and Prugger, 1989). The mathematical procedures and related concepts in error estimation for this method have been discussed by Ge (1995).

The method uses a curve-fitting technique known as the Simplex algorithm (Caceci and Cacheris, 1984) to search for a solution. Conceptually, the Simplex source-location method consists of three important aspects: error space, Simplex figure and error estimation. The method starts from the idea that, for a given set of arrival times at a set of transducers, an error can be calculated for any point by comparing the observed and the calculated arrival times. An error space is thus one in which every point is defined by an associated error. It is easy to understand from the definition of the error space that the point with the minimal error is the location of the source of the event.

The process of searching for the point of minimum error with the Simplex method is unique. The solution is said to be found when a Simplex figure falls into the depression in the error space. The Simplex is a geometric figure which contains one more vertex than the dimension of the space in which it is used. Its movement is controlled by a set of rules. The ones adopted by Prugger and Gendzwill (1988) were originally given by Caceci and Cacheris (1984).

The search for the final solution with the Simplex source-location method involves four general steps:

- setting an initial Simplex figure;
- calculating errors for vertices;
- moving Simplex figures; and
- examining the status of convergency.

In general, the last three steps have to be repeated many times in order to arrive at the final solution.

The Simplex method is very flexible in the use of different velocity models, a feature which is essential for the accommodation of the event-based velocity model. The method is also flexible in the use of the optimization method. These features are not unique and can also be found in other iterative methods, such as Geiger's and Thurber's, which are popularly used by seismologists.

The main advantage of the Simplex method over the other iterative methods is that it is less vulnerable. There has not been a single case of divergency found in the several thousands of events analyzed by the Automatic Data Analysis and Source Location System (CADASLS) developed at CANMET, which makes use of this algorithm. One possible explanation is that the Simplex figure will not leave the lowest error point which has been found unless a better one is located. The Simplex method, therefore, will always keep the best solution which has been found; whereas, in others, it may be lost in iteration processes. The calculation speed of the Simplex method is considerably slower than that for Geiger's, Thurber's and the USBM methods.

5.2.3.4 USBM Method

The USBM method was developed in the early 1970s at the United States Bureau of Mines. The development of this method was part of the Bureau of Mines' effort to make the acoustic emission/microseismic (AE/MS) technique an effective engineering tool for determining the stability of rock structures. The method was first published in 1970 and was further modified in 1972 (Leighton et al., 1970, 1972). Since then, it has become the major mine-oriented AE/MS source-location method used in North America.

The USBM method is a non-iterative method and solutions are found directly. With this method, the time of origin is first eliminated by subtracting the first equation from the rest. The resulting equations are then linearized, and can then be solved by either the least-squares or the absolute-value methods. It is important to note that the USBM method requires at least one more equation than the number of unknowns.

The USBM method is easy to use and offers the fastest solution of all of the analytical source-location methods. Users do not need to worry about choosing the guess solution, setting the convergency criterion and especially the divergence problem. Either the least-squares or the absolute-value methods can be easily incorporated into this source-location method.

While the method is not suitable for handling events with many S-wave arrivals, it has been found to be often quite effective in dealing with large-energy events which may have problems with a few channels. These problems could be obvious errors, or even S-wave arrivals. For this reason, the USBM method has been included in CANMET's ADASLS.

5.2.4 Factors Affecting the Accuracy of Source Location

The accuracy of source location is affected by many factors, such as the quality of input parameters (velocity, arrival time and transducer co-ordinates); the complexity of velocity structure; background noise; location method; optimization method; array size; and array geometry. Although all of these factors could significantly affect the accuracy of source location, the most important ones are the quality of the input data and the geometry of the transducer array.

5.2.4.1 Quality of Input Data

A major difficulty existing in determining microseismic source location is that not all input parameters, such as velocity, arrival time and the transducer co-ordinates, as shown in Equation 1, can be precisely determined. Among these parameters, only the transducer co-ordinates can be determined accurately, and, in some cases (e.g. transducers in deep boreholes), this may be difficult. The velocity model and the arrival times usually include a certain number of errors which can be very significant. For example, it is frequently reported that the percentage standard deviation of the propagation velocity, as determined in the field, can be over 10%. Such errors definitely affect the accuracy of source location. Therefore, the first priority of any source-location project is always to improve the quality of the input data.

5.2.4.2 Transducer Array Geometry

It is important to realize, however, that it is almost impossible to obtain the perfect data set and that there are always some existing errors. This is mainly because it is beyond our capability to precisely model the real velocity structure.

How would the initial errors affect the accuracy of source location? A theoretical study (Ge, 1988; Ge and Hardy, 1988) shows that it all depends on the geometry of the transducer array. A poor geometry of the array would make the final solution extremely vulnerable to any initial errors, while a good one would effectively reduce the impact of any initial errors. Because of the unavoidable nature of the errors associated with the input data, the optimization of the array geometry becomes one of the most significant means of improving the accuracy of source location. A recent rockburst monitoring experience in Canada has demonstrated that an accurate determination of a source location is impossible at a mine site without a carefully designed array (Ge, 1992, 1993, 1994, 1996). Those mines in which the

arrays have been optimized have all enjoyed a significant improvement in the accuracy of locating the sources of seismic events.

5.3 Theoretical Developments at CANMET

The daily monitoring programs which began in the early 1980s by the Canadian mining industry were truly historic events in the application of microseismic techniques. For the first time, this technique was used on a large industrial scale in the geotechnical area on a daily basis. In general, it was a very successful step. From a theoretical point of view, it provided the basic scientific data that were needed to study the rockburst phenomenon: the mechanisms; the relationships with geological structures and mining activity; and the critical conditions which might cause the problem. From a practical point of view, mine operators had a unique tool with which to assess the whole mine's stability relative to the time and spatial distributions of rockbursts and microseismic activity; to identify those seismic-prone structures; and to evaluate the suitability of mining sequences and mine planning.

Since this was the first time the microseismic monitoring technique had been used on a large industrial scale on a daily basis, it also brought along a number of very difficult problems. New theories and approaches needed to be developed in order to resolve these very challenging problems.

5.3.1 Assessment of Source-Location Problems in the Canadian Mining Industry

The major problem encountered by the mining industry was inaccurate locations, and this was especially true for small events. The significance of this problem was that it often led to the wrong pattern of microseismic activity in a mine. For example, it was almost a systematical phenomenon at the Creighton mine that events in the hanging wall were located as being in the footwall when the traditional approach was used (Ge and Kasier, 1991; Ge, 1993).

In order to improve the accuracy of source location, several problems had to be solved. The first one was the physical status of arrival times. The microseismic system used by most mines for daily monitoring is the Electrolab MP250 system. This system does not record waveforms; it only records arrival times. The origin of the arrival times detected by MP250 systems is complex. In addition to P-wave arrival picks, which is almost exclusively assumed by users, there are many S-wave picks as well as outliers (arrivals attributed to noise or interference of other seismic activity). In reviewing many microseismic systems used in mines, this has been one of the key problems causing inaccurate location.

Next, there are massive microseismic events which have to be processed automatically each day at those seismic-active mines, and the location accuracy varies widely, from good to meaningless. Unfortunately, there is no evaluation process which can be used to assess the reliability of the results, so all solutions were accepted on an as-is basis. This often significantly contaminated the final seismic activity picture.

The geometry of the transducer array is one of the most important factors affecting source-location accuracy. This largely remained as an academic issue, however, and received little attention in the mining industry in 1980s. An investigation at a number of Ontario mines showed that the array geometry was one of two major problems responsible for inaccurate source locations (Ge, 1992, 1993, 1994; Ge and Kaiser, 1989, 1991). It was strategically important, therefore, for the mining industry to understand this and to develop an efficient plan to optimize array configurations.

In addition, there were several other theoretical problems which had to be solved, such as error estimation and analysis of location method. The efficiencies of the automated daily monitoring programs would depend greatly upon resolving these problems. This became an important part of CANMET's work. This section discusses the several critical problems in data processing that were resolved by CANMET scientists. The optimization of arrays will be discussed later in a separate section.

5.3.2 Identification of the Physical Status of Arrival Picks

The arrival times picked by a microseismic system at a mine site are complicated. In addition to arrivals of P-waves, there are also many arrivals of S-waves and noise. For the accurate location of sources, it is essential that one be able to identify the physical status of each arrival. Traditionally, the identification of the types of arrivals has been based on a manual analysis of the full waveforms being captured. Although there has been research on automatic picking based on the waveform analysis for many years, there is no reliable technique for continuous daily analysis. Furthermore, most of the rockburst-prone mines use the MP250 system for their daily monitoring. These only record arrival times, with no waveforms. Thus, because of a lack of ability to analyze the types of arrival times, all mines have had to use an unrealistic assumption that all of the arrivals were P-waves. As a result, accuracy was poor and the utility of data was low.

In order to solve this problem, a theory for the interpretation of the types of arrival picks without waveforms had been developed (Ge, 1988; Ge and Hardy, 1988; Ge and Kaiser, 1990; Ge and Mottahed, 1994). Based on this theory, it is possible to discriminate between P- and S-wave arrivals, as well as noise picks.

The theory includes the analysis of the difference in arrival times and residual analysis. The general idea is that the physical status of an arrival pick, although unknown when judged by the arrival time alone, will manifest itself in connection with other related parameters. Such connections may be found in the observed arrival time differences relative to the distances of the associated transducers, in the array size and density. They may also be found in the size and sign of channel residuals relative to the assumed arrival type and in the observed arrival-time differences. Hence, it may be possible to identify the arrival type through an analysis of these connections. Readers may refer to Appendix III for several case studies.

5.3.2.1 Arrival-Time-Difference Analysis

The arrival-time-difference analysis deals with the theory of the consistency of arrival times. While a detailed discussion of this topic has been given previously (Ge, 1988; Ge and Hardy, 1988), a brief description of the concept is provided here for the sake of completion.

Locating a seismic event in a three-dimensional space involves four unknowns, x, y, z and t; where x, y and z are the co-ordinates of the source and t is the origin time of an event. The exact time of origin is often not given in the final solution, as it is of little practical value for most applications. In some instances, the velocity is treated as an unknown. This practice is not recommended when the types of arrival picks are not clear. In this report, the unknowns for the location of a seismic event are the three co-ordinates and the origin time of the event.

The governing equation for source location based on a half-space velocity model, as given earlier, is:

$$((x_i - x)^2 + (y_i - y)^2 + (z_i - z)^2)^{1/2} = v(t_i - t) \qquad (1)$$

where the unknowns, x, y, and z are the co-ordinates of the source; t is the origin time of the event; x_i, y_i and z_i are the co-ordinates of the ith transducer; t_i is the arrival time at the ith transducer; and v is stress-wave propagation velocity.

Equation 1 may be rearranged in the following way to extract some of the information which is needed for this study. Subtracting the ith from the ith equation leads to:

$$((x_i - x)^2 + (y_i - y)^2 + (z_i - z)^2)^{1/2} - ((x_j - x)^2 + (y_j - y)^2 + (z_j - z)^2)^{1/2} = v(t_i - t_j) \quad (2)$$

This equation defines a hyperboloid. Locating a source within a half-space velocity model, therefore, is the process of finding the common intersection of hyperboloids. A hyperbola, the trace of a hyperboloid on the x-y plane, is shown in Figure 5.1.

A very important fact resulting from Equation 2 is that, once the positions of two transducers are given, the shape and the position of a hyperboloid depend only on the arrival-time difference. If the distance between two transducers is 2c, the arrival-time difference may vary over the range of:

$$0 \leq | t_i - t_j | \leq 2c/v \quad (3)$$

The implications of this equation are as follows:

- If the arrival-time difference is zero, the source is on the central plane. The central plane is defined as such that the distances from any point on this plane to the two transducers are equal.
- The smaller the value of the arrival-time difference, the closer the source is to the central plane. This can be seen from the hyperbolic field shown in Figure 5.2. The arrival-time difference from each hyperbola to the two transducers is equal to dD/v, where dD is the distance along the transverse axis between this hyperbola and its mirror image about the central plane. In Figure 5.2, this plane is represented by the central line. Hyperbolas representing higher arrival-time differences are further from the central line.

Figure 5.1 Hyperbola determined by the difference of arrival times at two transducers

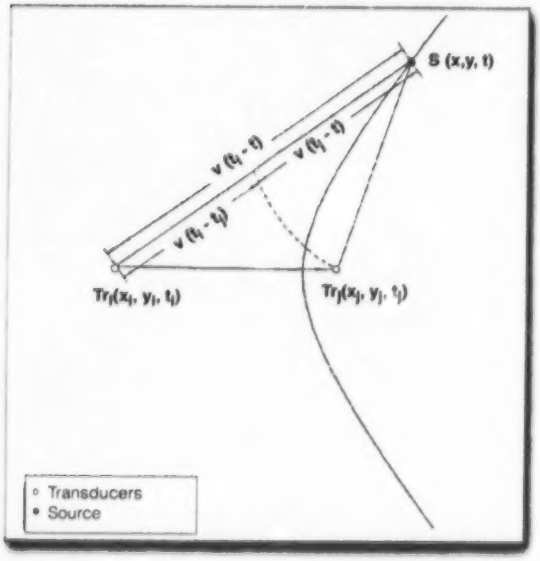

Figure 5.2 Hyperbolic field associated with two transducers

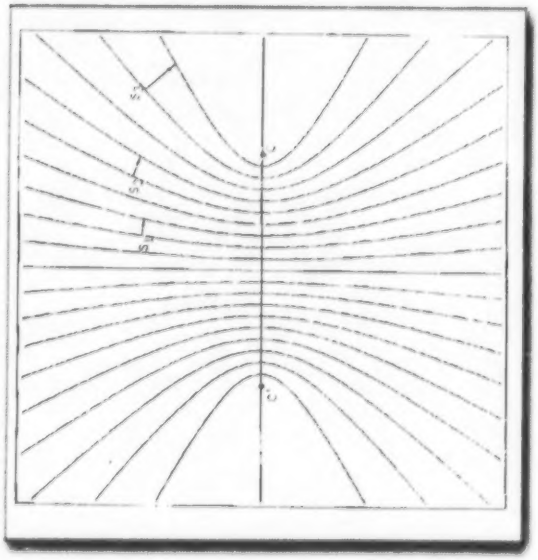

- The theoretical limit of the arrival-time difference for a half-space velocity model is 2c/v, where 2c is the distance between two transducers, and v is the velocity. Mathematically, the implication is that:

$$2c/v \geq t_i - t_j \qquad (4)$$

- A conclusion, which follows immediately from Equation 4, is that no solution can be found in the real domain to satisfy an arrival-time difference that is greater than the theoretical limit of arrival-time difference when a half-space velocity model is assumed.
- A source must be located at the first transducer location or on the extension of the line connecting two transducers (transverse axis) when the theoretical limit 2c/v is reached. In general, this limit should not be reached since it would be a rare occurrence that a source is either at a transducer position or on the extension of the line connecting two transducers.

An important concept emerging from the previous discussion is the theoretical limit of the arrival-time difference at two transducers. For a half-space velocity model, this limit can be found easily by substituting an appropriate velocity in Equation 4. For the situation where the triggering-wave phases are different at the two transducers, the limit can also be determined as long as the ground can be assumed to be homogeneous and isotropic. Four theoretical limits that are critical for locating microseismic sources are summarized in Table 5.1.

Table 5.1 provides a theoretical guideline for examining the types of arrival picks. For example, if the observed arrival-time difference at two transducers exceeds the theoretical limit of the associated P-wave arrival-time difference, either the second one, or both, must be triggered by an S-wave arrival. A comprehensive analysis of the original arrival-time data based on the arrival-time difference theory can positively identify those P- and S-wave arrival picks, as well as outliers, in most cases. Readers may refer to Ge and Kaiser (1990, 1992) for a detailed discussion of this problem.

Table 5.1 Theoretical limits for differences between arrival times at two transducers for four combinations of wave types

First Arrival	Second Arrival	Theoretical Limit
P	P	$2c/v_p$
S	S	$2c/v_s$
S	P	$2c/v_p$
P	S	∞

5.3.2.2 Residual Analysis

Residual analysis is the theory about the constitution of channel residuals and the interpretation of these in terms of their associated physical phenomena. It starts with the analysis of the constitution of the channel residual. According to the theory of the least-squares solution (Ge, 1994), the channel residual can be expressed as:

$$\gamma_i = t_i - tt_i - \Sigma\, t_i/n + \Sigma\, tt_i/n \qquad (5)$$

where: γ_i is the channel residual, t_i is the observed arrival time; tt_i is the calculated travel time; n is the number of observations; $\Sigma\, t_i/n$ is the average observed arrival time; $\Sigma\, tt_i/n$ is the average calculated travel time.

Since the analysis of residuals is carried out after the arrival-time analysis and, hence, well-defined S-wave channels and outliers have been detected, it is reasonable to assume that the last two terms in Equation 5 will not be significantly altered if only a few problem channels

remain. The channel residual is then basically a function of the travel time since the observed arrival-time, t_i, is not affected by calculations. If the channel residual has a positive sign, the travel time is too short or the velocity assigned to this channel is too high. By the same logic, a negative sign indicates that the assigned velocity is too low. Now, if we further consider the channel status, the physical cause of the channel residual may be found. For example, if a channel has been assigned P-wave velocity status and its channel residual has a positive sign, this channel could be an S-wave channel, since the positive sign means that the velocity is too high.

A summary of channel residual interpretations is given in Table 5.2. There are five possible situations, of which the first has just been discussed. The second represents a case where the velocity is still too low even though the P-wave velocity was used. This is physically impossible unless the channel has been triggered by another source early in the time window of the event. The third situation represents a low assigned S-wave velocity. This may be due to a delayed pick of an S-wave arrival. Since it would be arbitrary to assign another velocity to this channel, it must be deleted. In the fourth situation, the assigned S-wave velocity is too low and can be corrected by assigning the P-wave velocity. The last situation is one where the magnitude of the residual remains almost unchanged but the sign changes when the velocity is changed from P- to S- or from S- to P-wave velocity. Intermediate picks are clearly some kind of erroneous picks.

Table 5.2 Channel residual interpretation

Original Channel Velocity	Sign of Channel Residual	Assessment of Original Velocity	Correction Measures and Remarks
P	+	Too high	Use S-wave velocity
P	-	Too low	Delete the channel; possible outlier
S	+	Too high	Delete the channel; delayed pick or outlier
S	-	Too low	Use P-wave velocity
P	+	Too high or too low	Intermediate pick if magnitudes of channel residuals are close
S	-		

The analysis of residuals supplements the analysis of arrival times and detects S-wave channels and outliers which have been missed in the previous stage of the analysis of differences in arrival times.

5.3.2.3 Event-based Velocity Model

Based on the analysis of differences in arrival times and the analysis of residuals, it is possible to establish an event-based velocity model which specifies the physical status of each channel. P- and S-wave velocities will be assigned to P- and S-wave channels, respectively, and channels with erroneous triggering will be dropped. In comparison with the traditional P-wave velocity model, the event-based velocity model has two distinctive features. First, it is not a pre-assumed model, but is constructed based on the analysis of the physical status of the arrival picks. Second, this velocity model recognizes the variations of types of arrival picks, and, therefore, is event-oriented. The event-based velocity model allows the location of sources to be carried out on a realistic basis.

The theory of the interpretation of the physical status of the arrival picks without waveforms has been extremely successful in the analysis of daily microseismic events, and forms the theoretical base for the data analysis and source-location code ADASLS software developed by CANMET and widely used by the Canadian mining industry. Users may refer to Appendices IV and V for the detailed case studies.

5.3.3 Error Estimation

One of the important aspects of the theory of locating microseismic sources is error estimation. Traditionally, this has been done almost exclusively by the least-squares method (the L2 method). Since the 1980s, the absolute-value method (the L1 method) has been introduced for error estimation. There is, however, some confusion about the concepts and how these methods should be incorporated into the procedures for locating sources. Gendzwill and Prugger (1989), for example, suggested the use of the station residual derived from the L2 method as the station residual for the L1 method when they introduced the Simplex.

In order to solve this problem, a theoretical study was carried out at CANMET. As the result, formulae for the estimation of the time of origin and the station residual were derived for the Simplex method. These were based on both the least-squares and the absolute-value methods. The study demonstrated that the station residual defined by the absolute-value and the least-squares methods take completely different forms. It was deduced that the station residual is not a concept independent of misfit norms, but that it is defined by the misfit norm being used. The study also demonstrated that the Simplex method cannot avoid the problems associated with ill-conditioned matrices, even though no derivative information is needed. The results of this study were published in the Bulletin of the Seismological Society of America (Ge, 1995).

5.3.4 Reliability Analysis

The accuracy of microseismic source location is affected by many factors. For those vast amounts of daily collected events, the accuracy may vary significantly. One of the important tasks in determining microseismic source location, therefore, is to determine the reliability of the locations calculated.

The most common criterion used to measure the accuracy of source locations is the residual, which is the total effect of the differences between the calculated and the observed times of arrival. Since the essence of most source-location methods is the searching of the location for which the calculated times of arrival best match the observed times of arrival, the event residual, a measure of mismatch, naturally deserves the most attention.

However, there are some drawbacks when the residual is used alone to measure the accuracy of locating sources. One of the most important reasons is that the actual error in the location may vary significantly for the same residual, depending on the array geometry and the relative position of the source with the array of sensors. When the source is far distant from the array, the residual may be a terrible measurement of the accuracy of source location. Furthermore, this could lead to a practice of using the smaller events since an event with fewer channels is likely to have a smaller residual. Practical experience has indicated that the locations of the large-energy events are generally more reliable.

A comprehensive analysis procedure was developed to assess the reliability of the locations of sources. This analysis is carried out in two stages. The first is associated with the raw data, in which the data are systematically analyzed. The channels with significant errors, or identified as outliers, are dropped from further calculations. If an event is so noisy that the number of channels remaining are not sufficient to obtain an analytical solution, it will be dropped. Those events are very small, typically involving only five channels. They would significantly contaminate the source-location picture if they were not detected and subsequently dropped.

The second stage is an analysis of the solutions of source locations. This analysis involves a number of aspects, of which the primary ones are event residual, sensitivity and hit sequence. In addition, head residual, energy level and the number of channels are also considered for special applications.

The index of the sensitivity is a measurement of the stability of a solution. This is defined as the distance between a source which has been located and the position that would be obtained by assuming velocities that are 10% lower. The index of the sensitivity takes into account the effect of the array geometry. A solution with a large sensitivity index is mathematically unstable and should not be used for the further analysis.

Analysis of hit sequence assesses the reliability of a source location's feasible region. The sequence of hits, together with the velocity model and the array arrangement, defines the feasible region where the event could have occurred. A mismatch between the observed and the calculated hit sequences simply means that the source located is not within the feasible region. The seriousness of a mismatch is judged relative to the associated difference in arrival times. One of the main advantages of the analysis of hit sequence is that it provides a means for an intuitive evaluation. It is also a means of assessing the velocity model.

As the result of this comprehensive procedure of analysis, a ranking system was developed in which event locations are ranked from A to E (or 1 to 5), based on reliability. The event-ranking system provides mine operators with a convenient way to use the location data for ground-control purposes.

5.3.5 Hybrid Source-Location Method

The Simplex method is efficient in handling the event-based velocity model. It almost always provides a better solution in comparison with the USBM method when there are a substantial number of S-channels. On the other hand, it has been found from the calibration data (rockburst or blast events for which the locations are precisely known) that the USBM method offers comparable accuracy for main events, where most or all channels have P-wave status. Sometimes the solutions from the USBM method are even better. An important advantage of the USBM method, which was observed in the calibration study, is that it can effectively handle the erroneous channels when the number of such channels is very limited. The Simplex method, on the other hand, may be very sensitive to them.

The Hybrid method is designed to take advantage of the two previous methods and to discount their disadvantages. It determines which solution is more reliable based on both theoretical and empirical considerations. The analysis is carried out in two stages. In the first, the relevance of the original data to the source-location method is analyzed. The second stage is a reliability analysis which is mainly based on three criteria: the sensitivity index, the event residual and the head residual. The sensitivity measures the stability of a solution. The event residual measures the overall effect of the difference between the observed and the calculated times of arrival. The head residual, on the other hand, examines how well the observed times of arrival of the first several channels have been matched by the calculated arrival times.

The head residual is a critical concept in the Hybrid method. The emphasis of the residuals associated with the first several channels is based on the fact that the errors in arrival times are not randomly distributed among the channels. In general, the channels triggered earliest should have the smallest errors. This is not difficult to understand for practical reasons. The key is the distance. The earliest triggered transducers are closer to the source, and this effectively reduces the uncertainties associated with the velocity model. The shorter distance also means a higher energy level, and thus sharper arrivals, which reduce the timing errors. The calibration study shows that solutions with smaller head

residuals are more reliable. Appendix V contains examples showing the effectiveness of the Hybrid method.

5.4 Computer Code ADASLS

As a result of the theoretical development, a sophisticated software package called the Automatic Data Analysis and Source Location System was developed at CANMET. The code was designed for general application in the mining industry where a rapid, scientific and comprehensive analysis of the data to locate microseismic source is required. A general discussion of the code was given by Ge and Mottahed (1993, 1994).

5.4.1 General

ADASLS offers an advanced analysis of data and technology to locate the sources of events. The most attractive feature of the code is an ability to identify the type of arrival picks (i.e., P-wave, S-wave and outliers) without waveforms. This feature, which cannot be found in other conventional methods, makes it possible for one to analyze MP250 data on a scientific basis. The source-location algorithm used in the code is also unique. It analyzes the results of both the Simplex and USBM methods and searches for the most reliable one. The algorithm is called the Hybrid method.

The other distinctive feature of the code is the reliability analysis. With this capability, the code provides not only the location of the source, but also the confidence associated with it. The code has been developed for general use with the following important features:

- It is a user-friendly, manual-driven code, in that it is controlled by more than 130 parameters. These assess the local conditions for locating sources and determine the optimum analysis procedure. These parameters are contained in three data-files, and are adjustable.
- All of the data-analysis techniques are written in the form of digital filters (i.e., each data analysis technique functions as a special digital filter), and can be used both conveniently and flexibly for general purposes.
- The code utilizes a unique method of locating sources, developed at CANMET, which is called the Hybrid method. This enables the code to automatically include the advantages of the Simplex and the USBM algorithms.
- The code provides a wide choice of techniques for the analysis of data and locating sources. For locating sources, one may use any of three methods: Simplex, USBM or Hybrid. For each method, one may use either of two principal optimization approaches, namely, the least-squares and the absolute-value methods. Furthermore, there is the option of back-calculating the velocity for each method.
- The code was written based on a broad range of the first-hand experience in locating sources that was gained at the Campbell Mine (Placer Dome); the dense array at Creighton Mine (Inco); the North Mine (Inco); the Kidd Creek Mine (Falconbridge); the mine-wide array at Creighton Mine (Inco); and Homestake Mine. It is a mature technique.

Table 5.3 shows some general technical features of the code.

5.4.2 Application

ADASLS has been tested extensively and has shown a performance which is superior to that of other methods. It is now used, not only by CANMET as its primary source-location code, but also at many

Table 5.3 Technical features of ADASLS

GENERAL	
Code size (line)	5200
Number of routines	78
Manual-driven *	
Continuous-analysis mode	
Detailed-analysis mode	
User-control mode	
RAW DATA ANALYSIS	
Data-analysis techniques written in the form of digital filters	
Number of data-analysis techniques	33
SOURCE LOCATION	
Hybrid location method	
Simplex location method	
USBM location method	
Least-squares optimization	
Absolute-value optimization	
Velocity back-calculation	
RELIABILITY ANALYSIS	
Residual analysis	
Sensitivity analysis	
Hit-sequence analysis	
Head residual analysis	
Small-event analysis	
Large-event analysis	
OUTPUT OPTIONS	
Store detailed result	
Print detailed result	
Store concise result	
Store concise result and print detailed result	

* *Essential feature for general use. The ADASLS can easily adopt local conditions.*

rockburst-prone mines for their daily data-processing purposes. In 1993, ADASLS was registered as the intellectual property of the Canadian government.

An example which demonstrates the performance of ADASLS is given in Figure 5.3, where the locations of a rockburst and 20 after-shock events, as determined by ADASLS and by a conventional method used by the mine, are compared. With one exception, the locations of the after-shock events calculated by ADASLS were all in the immediate vicinity of the main event. In contrast, those determined by the conventional method were scattered over a very large area. Thirteen of those were shifted significantly to the east, while eight had their locations flopped from hanging wall to the footwall.

The cause of the large errors associated with the conventional method may be seen from Table 5.4, which contains somewhat more detailed information about this rockburst and its after-shock events. The numbers in the first column are the sequence numbers of the events, as these appeared in the original data file. Number 36 was the main event. The second column contains the rank of the ADASLS solutions. The numbers given in the third column show the number of channels on which the events were detected. In the fourth column are shown the velocity models as determined by ADASLS, where P, S and D stand for P-, S- and dropped channel, respectively.

The locations that were determined by ADASLS are given in the next three columns. The solutions as determined by the mine's method are then shown in the last three columns. The actual location of the main event is shown at the top of the table, above event No. 36. The solutions with major errors are shown in bold type for easy distinction. A very interesting pattern which can be observed from the table is that the poor solutions given by the conventional method are always associated with those events having a number of S-wave channels. This explains the cause of the failure of the conventional method considering all arrival times being P-waves.

5.5 Optimization of Transducer Array Geometry

The significance of the geometry of the array is that it determines how the errors associated with the input data, such as the timing error and the error caused by the simplified velocity model, err in finding the location of the source. A good geometry of the array will effectively minimize the impact of the initial

Figure 5.3 A comparison of the location of rockburst RB1097 and its aftershock events as given by a conventional method and ADASLS

(a) Locations calculated by a conventional method

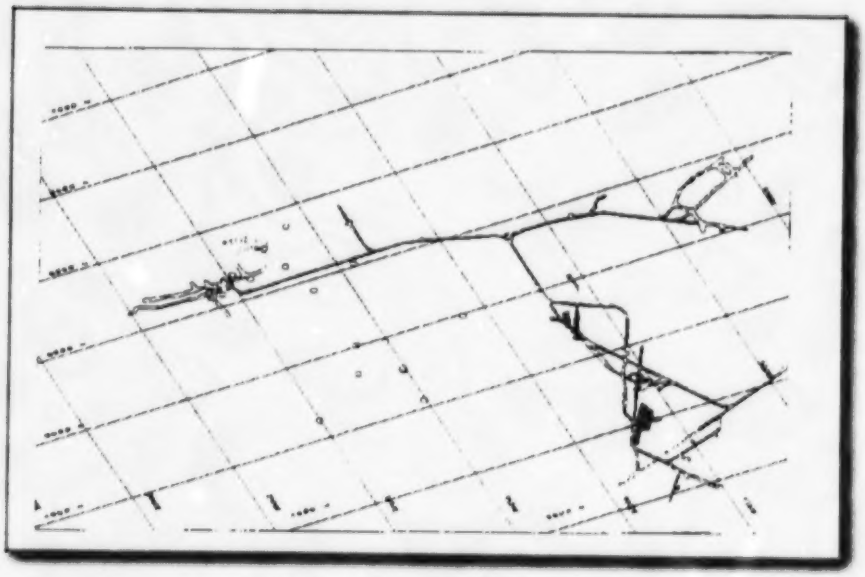

(b) Locations calculated by ADASLS

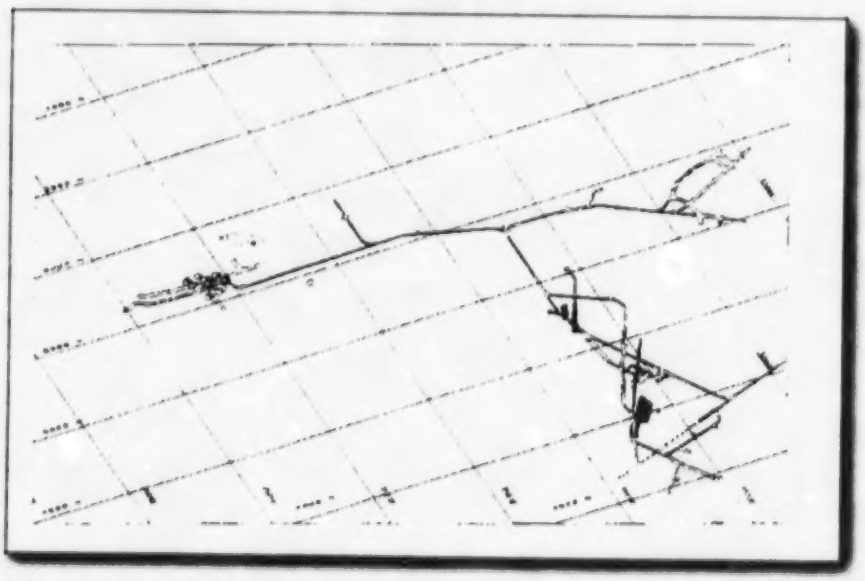

errors, while a poor one will maximize their effect. Since the initial errors are unavoidable, a good array geometry is always essential.

The importance of the geometry of the transducer array, however, was not well understood by the mining industry prior to the second phase of the rockburst research program. In many cases, the geometry of the arrays used by the industry could not meet the monitoring objectives. Therefore, one of the major tasks in improving the accuracy of source location was to help the industry understand the importance of the geometry of the transducer array, and to help those mines with microseismic monitoring systems to optimize their arrays. CANMET took several steps in this regard.

Table 5.4 A comparison of locations by ADASLS and a conventional method for rockburst RB1097 and its after-shock events

Event No.	Rank	Total Chanel	Velocity Model	ADASLS			Conventional Method		
				X	Y	Z	X	Y	Z
			Blast Location	2907	5615	5253	2907	5615	5252
36	A	16	PPPPPPPPPPPPPPP	2886	5635	5293	2879	5624	5307
37	C	8	PSSSPSSS	2929	5650	5273	**3319**	**5426**	5250
38	A	16	PPPPPPPDPPPDPPPD	2884	5632	5309	2868	5608	5309
39	A	11	PSSPSPSSPDS	2928	5566	5320	**3469**	**4759**	5318
40	B	13	PSSSPPPSPSDSS	2920	5604	5297	**3476**	**4771**	5330
41	B	13	PPPPSSPPSPSDS	2854	5550	5417	**3475**	**4532**	5318
46	A	16	PPPSPPPPSSPSPPSS	2869	5700	5287	3081	5624	5337
48	C	11	DPPPSPSPPPP	**3325**	**5441**	**5439**	**3270**	**4822**	**5629**
49	A	13	PSSSPPPSPSSDS	2945	5649	5299	**3264**	5630	5428
50	A	16	PPPPPPPPDPPPPPPP	2819	5652	5399	2875	5584	5376
52	B	11	PPSSPPSPDSS	2978	5614	5304	**3338**	**5003**	5172
53	A	16	PPPPPPPPPSPSPSPS	2880	5570	5314	2859	5577	5322
54	A	9	PPSSPSPSD	2943	5672	5279	**3379**	**5880**	**5027**
55	C	16	PPPPPPPPPPPPPPP	2975	5626	5278	3015	5679	5236
56	A	7	PSPSPSS	2965	5625	5283	**3222**	5784	5288
57	A	12	PPPSSPSDSPDS	2941	5578	5299	**3560**	5519	**5632**
58	B	7	PPSSPSPDS	2869	5624	5303	**3875**	**4985**	5268
59	B	16	PPPPPPPPPPPPPPP	2935	5595	5284	2920	5577	5306
60	B	13	PPPSSPPSPPSSS	2910	5560	5352	2976	**4605**	5276
61	A	13	PPPPSSPSPDSSD	2808	5687	5361	**3478**	**4972**	5267
62	C	16	PPPPPPPPPDPPPPPP	2909	5660	5324	2976	5623	5284

First, an extensive study on the impact of the array geometry on the source-location accuracy was carried out. This was based on the actual microseismic data collected from the mine sites. The typical cases which vividly showed the effects of the array geometry on accuracy were documented (Ge, 1992, 1993, 1994), and were then conveyed and explained to the companies. Since the data originated at these companies, there were no difficulties in appreciating the results.

At the Onaping Mine of Falconbridge Ltd., for example, a major rockburst occurred on January 7, 1994. The mine could not determine the location of this rockburst, and this severely restricted its ability to assess the ground conditions. CANMET was approached to assist in solving the problem. After studying some 340 events, CANMET was able to provide the approximate location of the rockburst. It also concluded that the array geometry caused one of the major problems in locating the event. At the time, the array used by the mine was in a plane almost coincident with the footwall contact, making it difficult to determine perpendicular locations. This conclusion was confirmed by the widely scattered locations of the 340 events in this direction (Figure 5.4). The much poorer solutions given by the mine were also due to the unrealistic assumption of P-wave picks for the arrivals.

As a result of the study, many mines have asked CANMET to design or to redesign their monitoring arrays as a primary means of improving the accuracy of source location. At the Kidd Creek Mine, the redesigned array has resulted in a major improvement in accuracy.

To facilitate daily monitoring operations, a set of guidelines for the optimization of arrays has been developed for mine operators. These are:

- The volumes to be monitored should be covered three-dimensionally. Transducers should be placed both inside and outside volumes to be monitored.
- The surrounding transducers should be some distance away from the target area, since there are often unstable zones in the vicinity of the surrounding transducers. Therefore, it is poor practice to put all the transducers inside the volume to be monitored.
- The array should be balanced. Locations are over-weighted if transducers are crowded.
- Two-dimensional arrays should be avoided. This type of array gives very poor accuracy in directions perpendicular to the plane.
- Special pairs of transducers may be designed to reinforce coverage in certain directions at particular locations.

The guidelines also include several criteria for the monitoring of site selection. These are:

- accessibility;
- not shielded by large openings, or by major discontinuities, or by loose materials, such as backfill; and
- the rocks should be competent and make a good coupling effect achievable.

Figure 5.4 Location of rockburst of January 7, 1994, and associated events at the Onaping Mine

(a) Locations originally determined by the mine

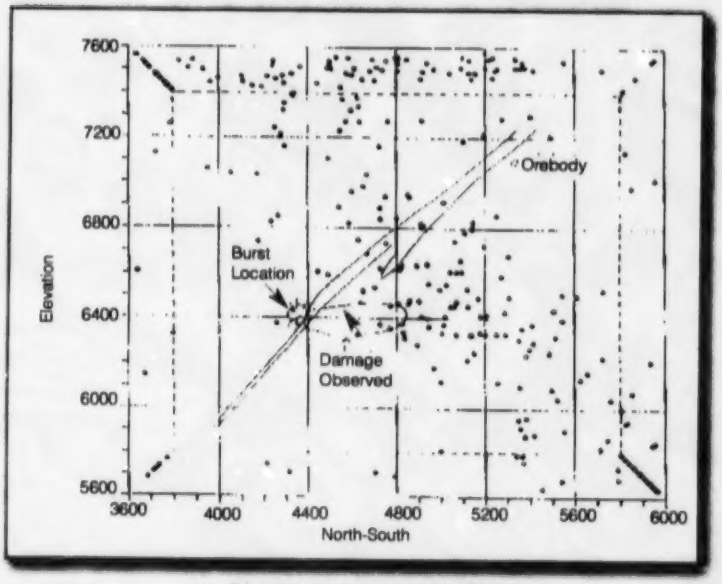

(b) Locations determined by ADASLS

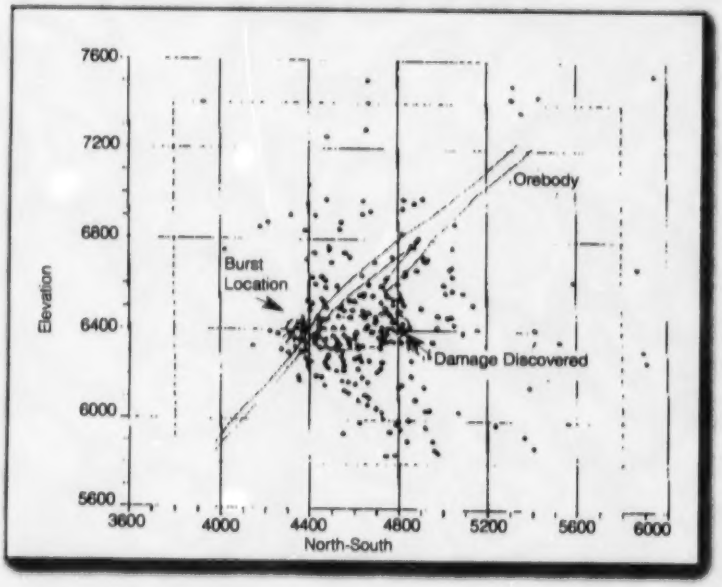

Because of CANMET's efforts, the mining industry now has a much better understanding of the role of the geometry of monitoring arrays in microseismic monitoring. Many mines have benefited from the improved arrays which have resulted. More importantly, they have begun to look after the array problems by themselves. Through the training provided by CANMET, some operators are able to adjust the transducer locations for their daily operations.

5.6 References

Allen, R.V. (1989). A letter to S.G. Wesnousdy, Associate Editor of *Bull. Seism. Soc. Am.*, Menlo Park, California.

Anderson, K.R. (1982). "Robust Earthquake Location Using M-Estimates." *Phys. Earth Planet Interiors* 30:119-130.

Bharti Engineering Associates Inc. (1993). *A Technological Review of the Seismic and Microseismic Monitoring Systems in Ontario Mines.* Final report to Mining Research Directorate, Ontario.

Buland, R. (1976). "The Mechanics of Locating Earthquakes." *Bull. Seism. Soc. Am.* 66:173-187.

Burden, R.L., Faires, J.D. and Reynolds, A.C. (1978). *Numerical Analysis.* Prindle, Weber & Schmidt, Boston, Massachusetts.

Caceci, M.S. and Cacheris, W.P. (1984). "Fitting Curves to Data (the simplex algorithm is the answer)." *Byte* 9:340-362.

Crosson, R.S. and Peters, D.C. (1974). "Estimates of Miner Location Accuracy: Error Analysis in Seismic Location Procedures for Trapped Miners." *Seismic Detection and Location of Isolated Miners*, Vol. 2, A.D. Little Inc., Cambridge, Massachusetts.

Ge, M. (1996). *Use of ADASLS at Homestake Mine.* Final report to Homestake Inc., 142 pages.

Ge, M. (1995). Comment on "Microearthquake Location: A Nonlinear Approach that Makes Use of a Simplex Stepping Procedure." *Bull. Seism. Soc. Am.* 85:375-377.

Ge, M. and Mottahed, P. (1994). "Automated AE/MS Source Location Technique Used by Canadian Mining Industry." Proceedings of the 12th International Acoustic Emission Symposium, Sapporo, Japan, pp. 417-424.

Ge, M. (1994). *Analysis of Locations of January 7 Rockburst and Associated Events.* Final report to Onaping Mine, Falconbridge Limited, 17 pages.

Ge, M. and Mottahed, P. (1993). "An Automatic Data Analysis and Source Location System." Proceedings of the 3rd International Symposium on Rockbursts and Seismicity in Mines, Kingston, Ontario, pp. 343-348.

Ge, M. (1993). *Analysis of Kidd Creek Source Location Data.* Final report to Kidd Creek Mine, Falconbridge Limited, 150 pages.

Ge, M. and Kaiser, P.K. (1992). "Practical Application of an Innovative Microseismic Source Location Procedure." *Geotechnical and Geological Engineering* 10:163-184.

Ge, M. (1992). *Analysis of Mine-Wide Array Microseismic Data.* Final report to Inco Limited, 116 pages.

Ge, M. and Kaiser, P.K. (1991). *Microseismic Source Location Study at Creighton and North Mine.* Final report to Inco Limited, 66 pages.

Ge, M. and Kaiser, P.K. (1990). "Interpretation of Physical Status of Arrival Picks for Microseismic Source Location." *Bull. Seism. Soc. Am.* 80:1643-1660.

Ge, M. and Kaiser, P.K. (1989). *Use of Campbell Microseismic Data in Mine Design: Part I – Seismic Data Validation.* Final report to Campbell Mine, 158 pages.

Ge, M. and Hardy, H.R. Jr. (1988). "The Mechanism of Array Geometry in the Control of AE/MS Source Location Accuracy." Proceedings of the 29th U.S. Symposium on Rock Mechanics, Minneapolis, Minnesota, pp. 597-605.

Ge, M. (1988). *Optimization of Transducer Array Geometry for Acoustic Emission/Microseismic Source Location.* Ph.D. Thesis, Pennsylvania State University, Department of Mineral Engineering, 237 pages.

Geiger, L. (1910). "Herbsetimmung bei erdbeben aus den ankunfzeiten." *K. Gessell. Wis. Goett.* 4:331-349.

Geiger, L. (1912). "Probability Method for the Determination of Earthquake Epicenters from the Arrival Time Only" (translated from Geiger's 1910 German article), *Bulletin of St. Louis University* 8(1):56-71.

Gendzwill, D. and Prugger, A. (1989). "Algorithms for Micro-Earthquake Location." Proceedings of the 4th Conference on Acoustic Emission/Microseismic Activity in Geologic Structures, Pennsylvania State University, 1985, pp. 601-616.

Hardy, H.R., Jr. and Mowrey, G.L. (1981). *A Microseismic Study of an Underground Natural Gas Storage Reservoir, Volume II — Field Data Analysis and Results*. American Gas Association, Inc., Arlington, Virginia. A.G.A Cat. No. L51396, 343 pages.

Hines, W. and Montgomery, W. (1980). *Probability and Statistics in Engineering and Management Science*. John Wiley & Sons, Inc., New York.

Kijko, A. (1995). A letter to CANMET scientist M. Ge. Western Levels, Republic of South Africa.

Lee, W.H.K. and Stewart, S.W. (1981). "Principles and Applications of Microearthquake Networks." *Adv. Geophys.* Suppl. 2.

Leighton, F. and Blake, W. (1970). *Rock Noise Source Location Techniques*. USBM RI 7432, 14 pages.

Leighton, F. and Duvall, W.I. (1972). *A Least Squares Method for Improving Rock Noise Source Location Techniques*. USBM RI 7626, 19 pages.

Lienert, B.R. and Frazer, L.N. (1983). An Improved Earthquake Location Algorithm. *EOS*, Trans. Am. Geophys. Union 64, 267 pages.

Mori, Y. (1994). A letter on behalf of the organizing committee and program and papers committee of the 12th International Acoustic Emission Symposium to M. Ge, a research scientist, CANMET. Chiab, Japan.

Prugger, A. and Gendzwill, D. (1988). "Microearthquake Location: A Non-Linear Approach that Makes Use of a Simplex Stepping Procedure." *Bull. Seism. Soc. Am.* 78: 799-815.

Smith, E.G.C. (1976). "Scaling the Equations of Condition to Improve Conditioning." *Bull. Seism. Soc. Am.* 66:2075-2076.

Thurber, C.H. (1985). "Nonlinear Earthquake Location: Theory and Examples." *Bull. Seism. Soc. Am.* 75:779-790.

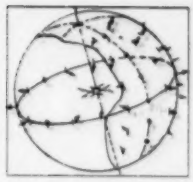

Source Studies Over a Broad Magnitude Range

6.1 Introduction

This chapter summarizes the results of the research project entitled Source Studies of Mine-Induced Seismic Events Over a Broad Magnitude Range ($-4 < M < 4$) sponsored by the Mining Research Directorate of Ontario on behalf of the Canadian Rockburst Research Program (CRRP).
The project deals with the analysis of the source properties of mine-induced seismic events that were recorded over a broad range of magnitude covered by full-waveform recording equipment. This consists of data recorded by the seismographic network, the macroseismic system and the microseismic system operating at Inco's Creighton mine. The project started in 1992 as one component of a three-component project regarding an analysis of the source mechanism of mine-induced seismic events. A preliminary report dealt with data processing for this project (Talebi, 1993). The final report was submitted to the CRRP in December 1994 (Talebi, 1994).

In the next section we present a description of the project — the objectives, the mine site under study, the available full-waveform recording equipment and the scaling relations. The basic definitions of the topics related to rockburst research are presented at the end of this report and will not be repeated in this chapter. The data available and the results of the data processing (i.e. attenuation correction, source-parameter determinations, their scaling relations) will be presented in the next section. The conclusions will follow.

6.2 Description of the Project

6.2.1 Objectives

The main objective of this project is to contribute to the clarification of the nature of the scaling relations; i.e. whether or not seismic events have the same behaviour, over a broad range of magnitude, regardless of their strength. Indeed, similar behaviour of large and small mine-induced seismic events would allow the approximation of such parameters as peak particle parameters obtained for small events to those expected for large events, and vice-versa. This approach has important practical consequences for the study of rockbursts and hazard estimation. The techniques employed in this approach are purely seismological, and the results are of significance from scientific and engineering points of view for ground-motion estimations in hard-rock mines.

6.2.2 The Mine Site

The choice of a specific site for the present study had to fulfill two basic requirements. The first consisted of the necessity of focusing on an active mine site where chances of recording mine-induced seismicity over a broad magnitude range was high, and the second requirement was the possibility of recording the full magnitude range of events being considered in this project. Out of the Sudbury and

Elliot Lake mining districts, the most active mining areas within Ontario in the last decade, the Sudbury Basin fulfilled both requirements (all but one mine in Elliot Lake had stopped operation). Creighton mine, the most seismically active mine within the Sudbury Basin, was chosen as the site for the present study.

6.2.3 Full-Waveform Recording Systems

Three types of full-waveform recording systems which are extensively used in Canada cover three magnitude ranges of mine-induced seismic events (see Section 2.2.4). These are commonly called seismographic, macroseismic and microseismic systems, and are designed to record large seismic events, medium-sized events and small microseismic events, respectively. The seismographic systems, particularly the CANMET Digital Seismograph Network (CDSN) is fully described in Chapter 3 (see also Talebi et al., 1994). In this section, we describe the macroseismic and microseismic systems used in this study.

6.2.3.1 Macroseismic System

CANMET has been developing a macroseismic system for operation in Canadian mines for a number of years (see Chapter 4). The original system was based on using five triaxial sensors installed in boreholes on the surface or underground, or a combination of both. To prevent saturation of the sensors by noise, these are usually installed 0.5 to 1.0 km from the active mine workings. Typically, macroseismic systems record seismic signals in the 1 to 2000 Hz frequency range. They are capable of detecting seismic events of magnitude greater than 0 and recording up to two seconds of complete waveforms of seismic events.

The macroseismic system installed at Creighton Mine uses five triaxial sensors located around the active mining area. The differential signals are amplified and transmitted to an underground multiplexer unit where these are multiplexed and sent to the surface via a single fibre-optic link. A demultiplexer unit on the surface then reconstructs the signals before they pass through signal conditioning and recording systems. The anti-aliasing filter is set at 1500 Hz at 72 dB/octave. The sampling rate is 4500 points per second and per channel, and the sensor amplifiers are dual gain with both a low and a high output for each axis. This allows for a larger system dynamic range, recording both small and large seismic events. The selected outputs are then routed to both a triggering detection-controller and a data-acquisition board located in a PC-compatible host computer. The DC power necessary for the field sensors and amplifiers is provided from the multiplexer located underground.

The operating system employed is QNX, chosen for its versatility as a multi-user, multi-tasking system and for its fast execution, efficiency, remote-access capability and its PC hardware-environment compatibility (Section 4.2.6.3). The acquisition software consists of three main modules — a primary and a secondary acquisition module along with a demultiplexing task, all running concurrently on a priority basis. A configuration module and a basic display module are also provided for configuring the system operation and displaying event waveforms in the field. Additionally, a communication task is also included in the system to handle remote access via modem. Macassa and Campbell mines are using a similar system to that of Creighton Mine.

System calibration of the three-component sensors of the macroseismic system at all sites has been performed by generating a sine wave of known amplitude and frequency at each step of the input of preamplifiers and recording it as an event. Three to four frequencies of 300, 600, 900 and 1200 Hz are used. The amplitude of the recorded signal is then measured and

compared to the measurements of the original signal, and the calibration factor is hence calculated. The amplification factors measured in this manner for the 15 components of recording are plotted versus frequency, and the best-fit curve to the results for each component is used for calibration purposes.

6.2.3.2 Microseismic System

Several full-waveform microseismic systems developed at the Engineering Seismology Laboratory of Queen's University are also currently in use in Ontario mines. The first such system was installed in Falconbridge's Strathcona Mine in 1987 to complement an ElectroLab MP250. This system used two acquisition computers to record signals from different types of sensors. The first computer recorded signals from five triaxial accelerometers installed around the active mining area, whilst the second computer recorded 15 one-component accelerometers of the ElectroLab MP250 system. The data set recorded in this way was used for a multi-aspect analysis of mine-induced seismicity, including the determinations of the location, mechanism and parameters characterizing the events (Talebi and Young, 1990).

In 1990, a number of microseismic systems were planned for installation at Creighton mine as part of projects, including the Source Mechanism and the Mine Design projects. The initial plan consisted of the addition of six triaxial sensors: three at depth, one close to the proposed Neutrino observatory and two in the upper levels, but borehole drilling requirements prevented a fully operational system from being installed until 1992 (Urbancic et al., 1993). The original plan was modified to include additional seismic monitoring projects. A detailed description of the situation with regard to microseismic hardware installation at Creighton mine has been described by Urbancic et al. (1993 and 1994).

6.2.4 Scaling Relations

Scaling relations of seismic sources are the relationship between the two first types of source parameters, i.e. those between source strength and source dimensions. More precisely, a source scaling relation describes the manner in which source duration or source dimension increases with increasing seismic moment. In the studies of source parameters, for a large number of seismic events, over a broad range of magnitude, it has been observed that stress drop is roughly independent of the magnitude and ranges mostly between 0.1 and 10 MPa (Gibowicz, 1990b). This pattern has been confirmed by many studies of seismic and volcanic events, after-shock sequences, mine tremors in South Africa and Poland, etc. A constant stress drop model implies a "self-similar" rupture process regardless of the scale of the seismic events, implying in simple terms that earthquakes, mine tremors and microseismic events are generated in a similar manner, but along failure areas of different sizes. Scholz et al. (1986) have observed higher levels of stress drop between large interplate and intraplate earthquakes (Figure 6.1).

Figure 6.1 Difference in stress drop between large intraplate and interplate earthquakes

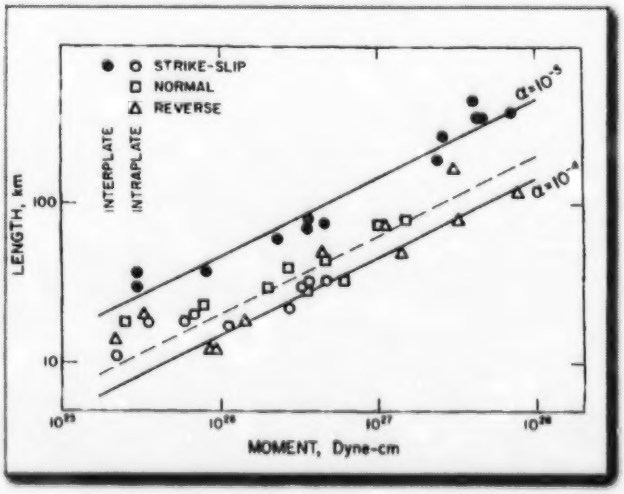

Figure 6.2 Example of signals recorded by the macroseismic system of CANMET at the Creighton mine

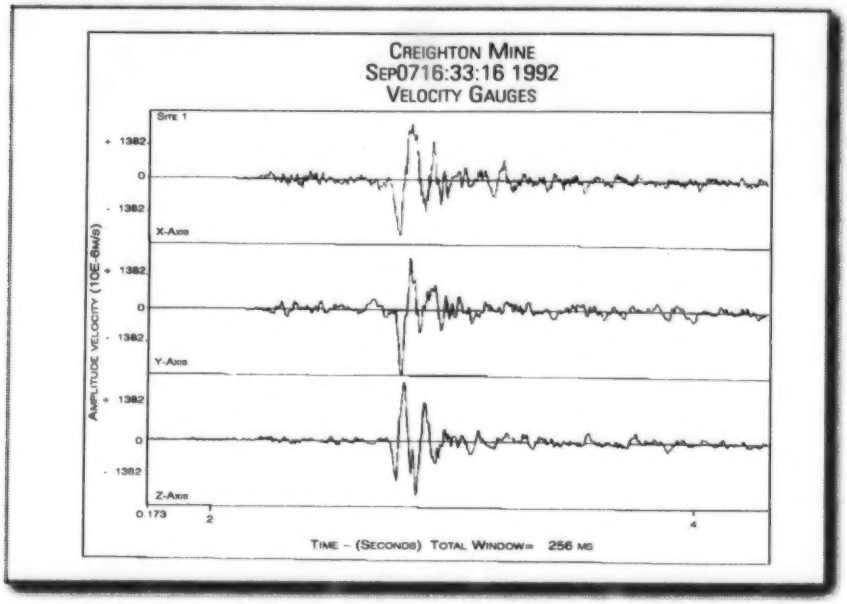

In contrast to the general observation of similarity of the seismic events, over a broad range of magnitude, there is growing evidence of a breakdown in similarity for very small events observed by a marked decrease of stress drop with decreasing seismic moment. This could be explained by any phenomenon at the source, in the earth or by the recording system, which reduces the influence of high frequencies in the recorded signals. Seismologists have proposed two different explanations for this observation, provided the influence of the recording system can be neglected. Hanks (1982) attributes this to a propagation effect and argues that there is a maximum frequency limit, f_{max}, to what can be detected due to the high attenuation close to the Earth's surface. Aki (1984), on the other hand, argues that this represents a true source effect and that there is a minimum to the dimension of the source (Scholz, 1990). Chapter 2 provided a more detailed description of this subject.

6.3 Processing of the Full-Waveform Data

This section presents the results of signal processing of data. Initially, the description of the available data will be presented, followed by the procedure used for spectral analysis of the data and the implementation of attenuation correction for the macroseismic data set. This will be followed by the results of the source-parameter determinations and their scaling relations.

6.3.1 The Available Data

Data from the microseismic and macroseismic systems have been treated in this study. The macroseismic data set consisted of more than 150 events recorded during the period of November 1992 to June 1993, and an example of these types of signals at Creighton Mine is shown in Figure 6.2. Figure 6.3 depicts the plan view projections and vertical section of the locations of the five

three-component sensors and event source-locations for the data set recorded by the macroseismic system. The microseismic data set used consists of 91 events recorded following a post-production blast. The result of their processing is reported by Urbancic et al. (1994).

6.3.2 Spectral Analysis

Spectral analysis was performed using interactive computer graphics which allowed the choice of signal and noise windows on any seismic channel. The time series were tapered, using a cosine function, prior to the calculation of the spectra using a Fast Fourier Transform (FFT) algorithm. The spectra were corrected for instrumental response prior to the calculation of spectral parameters. Attenuation effects on each spectrum were approximated using the methodology described in the next section and corrected spectra for attenuation were used for source-parameter determinations. The spectra of noise observed prior to each signal was calculated and plotted on the same graph. Figure 6.4 shows examples of observed displacement spectra. The traces on these figures are, respectively, from the bottom to the top, those of the noise prior to the signal arrival, the original S-wave signal and the S-wave signal corrected for attenuation effects. The details of the calculations are described in the following sections.

Figure 6.3 Plan view (a) and vertical section (b) showing sensors and event-source locations at Creighton Mine

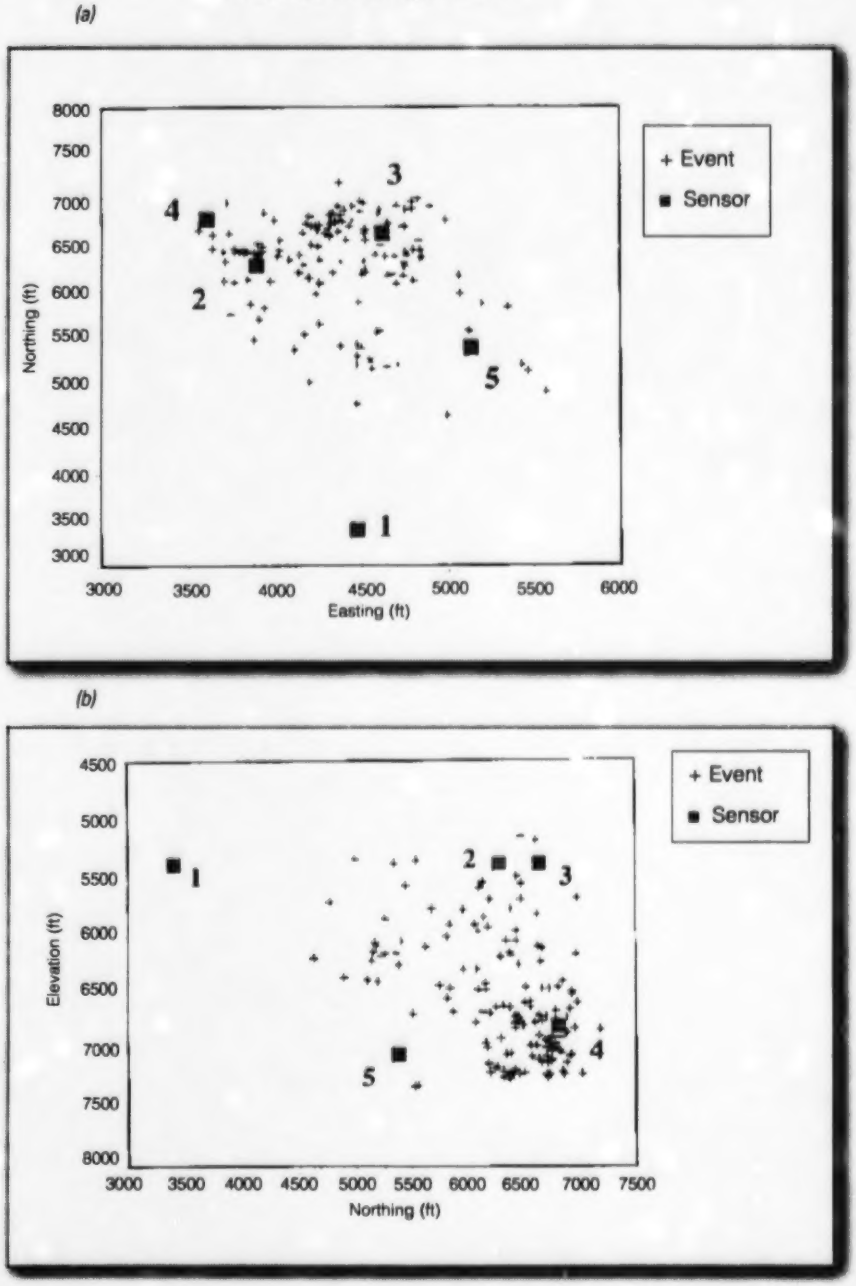

6.3.2.1 *Attenuation Correction*

Seismic spectra must be corrected for attenuation caused by wave propagation along the source-sensor path. Such corrections are of utmost importance for proper retrieval of source parameters of small events, even if they are recorded at short distances (Gibowicz, 1990b). The effects of attenuation on seismic and microseismic signals and the need for proper correction have been pointed out by several authors (Talebi and Cornet, 1987; Cranswick and

Sembera, 1989). To correct for attenuation along the path, the spectra should be multiplied by the exponential term $\exp(\pi f R / C Q)$ where:

f is the frequency considered,

R is the source-sensor distance,

C is the velocity of the body wave,

Q is the quality factor of the body wave.

This latter parameter is the one most commonly used in attenuation measurements. A related parameter also used in this study is Kappa (K). In the absence of local site effects or when such effects can be neglected, (K) is defined as follows:

$$K = \pi R / C Q \qquad (1)$$

As mentioned earlier, the high-frequency descending trend of the displacement spectrum, according to Brune's model, has a fall-off slope of -2. A number of authors have confirmed this observation (Hanks and McGuire, 1981). The slope observed in the displacement spectra from seismic events is usually equal to or less than -2. The difference between the value of the observed slope and -2 is usually attributed to the attenuation and a number of authors have used this property for attenuation measurements (Feustel et al., 1993; Spottiswoode, 1993).

The approach adopted in this study is compatible with the above methodology. The procedure consists, in the first instance, of measuring the observed slope of the high-frequency descending trend of the displacement spectra. The presence of f_{max}, in some cases, and other effects at frequencies above 1 kHz, in others, caused some irregularities of the spectra at very

Figure 6.4 Example of displacement spectra observed for a macroseismic event

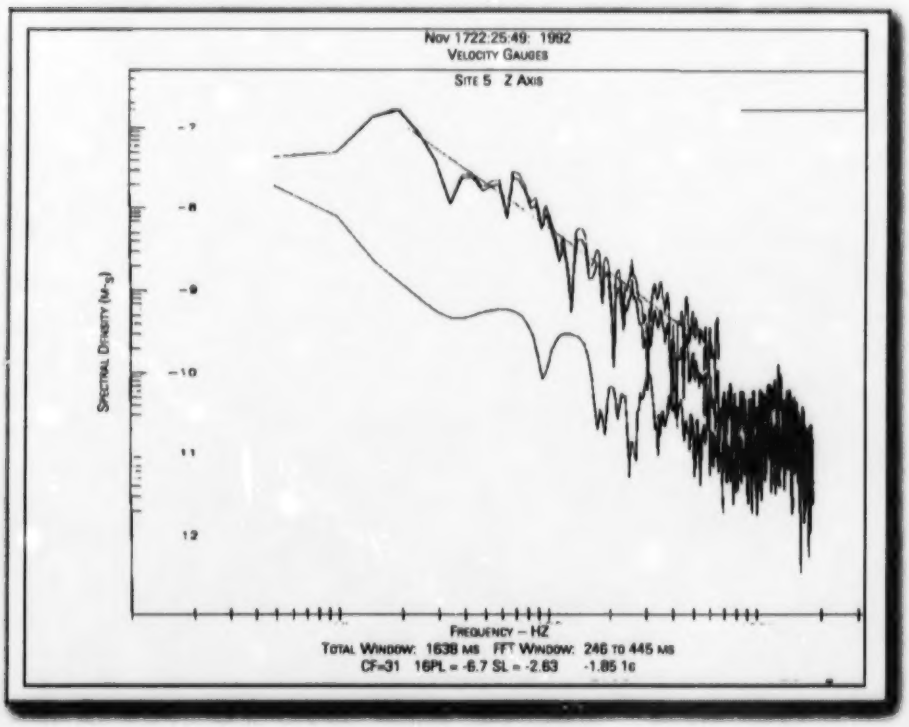

high frequencies (see Figure 6.4). This caused difficulty in the utilization of the entire frequency window up to 1500 Hz, as this would result unrealistic estimates. A window on the displacement spectra was defined for attenuation measurements, which was limited between a low and a high frequency (f_L and f_H), typically about a few Hz and a few hundred Hz, respectively. The corner frequency (f_0), where the spectrum starts to decline, was then estimated and the best-fit line between this frequency and f_H was calculated. The Q factor is calculated according to the following relationship:

$$Q = \frac{\pi \log_e R\,(f_H - f_0)}{C[2\log(f_0/f_H) + \log(U(f_0)/U(f_H))]} \qquad (2)$$

where: $\log_e$ is a logarithmic conversion factor

$U(f_0)$ and $U(f_H)$ are amplitudes of displacement spectrum at f_0 and f_H

C is the velocity of the S-wave, being 3658 m/s

Reasonable estimates of Q factor were found in the majority of cases where attenuation measurements were attempted, although the choice of the high-frequency limit (f_H) seemed to affect the final results to some extent. Q_S measurements were attempted for more than 150 macroseismic events for each individual channel of recording with a reasonable signal-to-noise ratio. Figure 6.5 shows a histogram of the results. It can be seen from this figure that the maximum concentration in Q_S occurs in the 50-150 range and that there seems to be an upper limit of about 500.

The results of attenuation measurements for the five different sensor sites are presented in Figure 6.6. In this figure, the Kappa factor has been plotted versus source-sensor distance in a log-log scale, where lines of constant Q_S are drawn and each point is the average value of up to three measurements. The lower and upper bounds of Q_S are clearly 20 and 500. The results of Q_S for individual sites are given by Talebi (1993). The comparison between these two sets of results seems to confirm the upper bound limit of 500 for all the sensors, although the range of hypocentral distances involved varies from sensor to sensor. Typically, this distance is within the range 80 m to 800 m, with the exception of sensor 1, for which distances are around 1 km. This result partly explains the lower number of measurements for the first sensor, relative to others. Accordingly, the lower bound limit for the results of sensor 1 is higher than the limit of 20 observed for the other sensors. The broadest range of the distances are observed for sensors 2 and 4, but the same general trends are

Figure 6.5 Histogram showing the results of measurements of the quality factor of S-waves (Q_s)

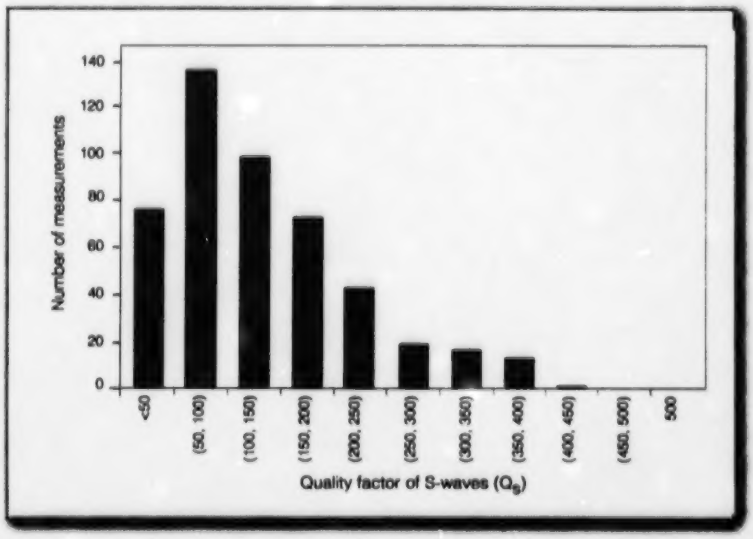

Figure 6.6 Attenuation factor of S-waves (Kappa) as a function of source-sensor distance on a log-log scale for the five sensor sites (S1 to S5)

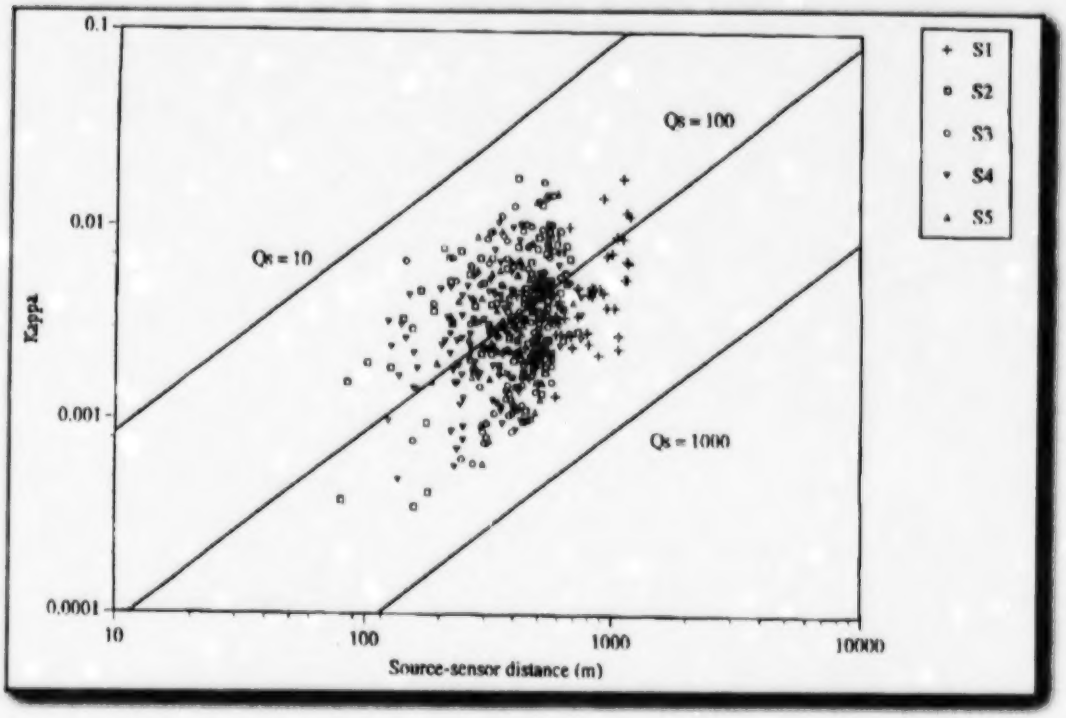

observed. The value of Kappa is in the range 0.0004 and 0.02 for all units. Anderson and Hough (1984) have carried out a similar analysis on S-wave signals of an earthquake in California. Their observations, and those reported by other authors, seem to indicate that at least part of the attenuation observed using the parameter Kappa (K) can be attributed to the near-sensor effects, particularly when the sensors are placed near the surface in such a case. The equation (1) can be rewritten as follows:

$$K = K_0 + \pi R / C Q \qquad (3)$$

In the study of Anderson and Hough (1984), the determination of the value of K_0 for stations placed on different types of rock medium showed distinct values of 0.066, 0.065 and value of 0.04, respectively, for alluvium, consolidated sediments and rock, although a slightly different K factor was used. Likewise, when the results of Kappa measurements were plotted versus distance, a steeper slope was found for stations on rock than those on alluvium.

In an attempt to investigate such effects in the present case, Kappa measurements were plotted versus distance on a linear scale for all of the sensors (Figure 6.7). The upper bound of the results at a value of 500 is shown and, clearly, a lower bound exists at about 20. Two more observations can be made from this figure. The data are rather scattered due to the fact that raypaths have to pass through areas of fractured rock, back-fill, etc. and are heavily affected by them. Besides, the results will be well described if no local or near-site effects were present within the window Q_s = 20 to 500. This observation was substantiated by examining the results for individual sensors. One obvious observation from these results is the degree of the scatter of the data. It is interesting to observe that the scatter is at minimum for sensor 1, which is farthest away from the activity, meaning that the raypaths would traverse mostly the undisturbed rock mass. In this case, the local site effects are obviously negligible. The scatter

Figure 6.7 Attenuation factor of S-waves (Kappa) as a function of source-sensor distance on a linear scale for the five sensor sites (S1 to S5)

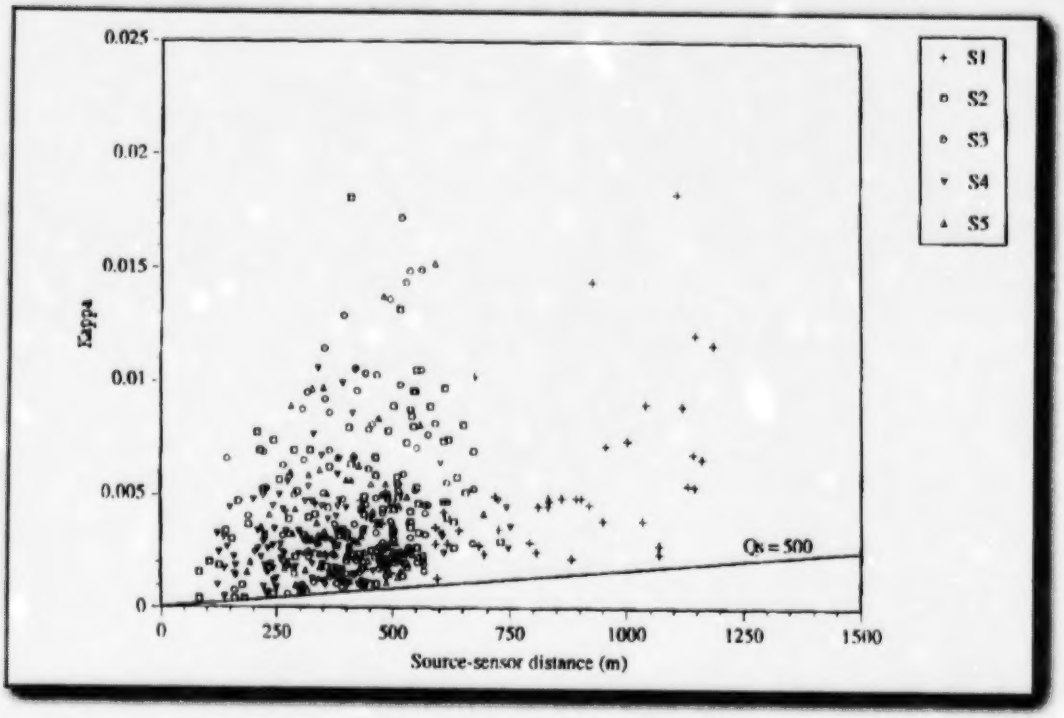

in the data makes it difficult to quantify any local site effects for the other sensor sites and as any such effects appear to be negligible, they are not considered for the rest of this study.

As mentioned earlier, the scatter in the results can be explained by the presence of zones of fractured rock and back-fill within the mine. These zones contribute a great deal to body wave attenuation, even if the distances involved are rather small, as observed in this case. These results also indicate that using an average value for the attenuation parameter for the whole mine, as assumed in some studies, will have severe consequences for the determination of seismic-source parameters, as such estimates will be unreliable unless the attenuation corrections are made for each case individually.

6.3.2.2 Source-Parameter Determinations

Two independent parameters were calculated directly from the displacement spectra of S-waves corrected for attenuation:

Ω_0, the level of the low-frequency constant trend of the displacement spectra,

J_C, the energy flux, the integral of the square of ground velocity for the S-wave window.

The method used is that of Snoke (1987), used successfully by Gibowicz et al. (1991). Two frequencies (f_1 and f_2) are defined in this approach as the limits of the spectral bandwidth over which the calculation of energy flux is performed. The method assumes a constant spectral amplitude of the displacement spectrum for frequencies below f_1 and an f^{-2} fall-off

for frequencies above f_2. The details of this procedure can be found in Gibowicz (1990a and b).

Corner frequencies can then be calculated from the following relationship:

$$f_0 = (J_C / 2 \pi^3 \Omega_0^2)^{1/3} \quad (4)$$

where the estimates of Ω_0 and J_C were available, the corner frequencies were determined for each sensor. The low-frequency spectral levels were calculated for each sensor as the vector sum of the determinations for the three components of recording on that particular sensor, the energy flux for each sensor being the sum of the measurements of the three components. The results of corner frequency determinations using the automatic approach showed an overestimation of corner frequencies in a number of cases. DiBona and Rovelli (1988) report that the effects of bandwidth on the estimations of source parameters could be significant when corner frequencies are not in the middle of the selected frequency band. Based on this postulation, the data falling in this category had to be excluded from the data set and manual picks were used in cases where corner frequencies were higher than the middle of the frequency band. The parameters characterizing the source are calculated using the methodology and equations described by Talebi (1993 and 1994).

Table 6.1 summarizes the average results of source-parameter determinations for all the events analyzed in this study. The following is the range of some source parameters from this table.

Moment magnitude:	0.4 to 2.6
Seismic moment:	3.6 to 7470 GNm
Source radius:	8.8 to 152.9 m
Stress drop:	0.03 to 10.6 MPa

Table 6.1 Results of source-parameter determinations

m_N is Nuttli magnitude, M is moment magnitude, R_v is peak velocity parameter, M_0 is seismic moment, r_0 is source radius and $\Delta\sigma$ is stress drop. All results have been corrected for attenuation along the ray path.

Event	m_N	M	R_v(m²/S)	M_0(GNm)	r_0(m)	$\Delta\sigma$(MPa)	Event	m_N	M	R_v(m²/S)	M_0(GNm)	r_0(m)	$\Delta\sigma$(MPa)
1	2.1	2.0	4.17	980.0	49.7	6.48	47		1.1	0.58	48.5	19.8	3.57
2		1.3	0.51	82.0	24.5	2.24	48		0.9	1.21	22.5	11.3	6.38
3		1.4	0.55	146.1	26.5	2.08	49		1.6	0.58	238.0	34.6	4.19
4	2.8	2.4	7.43	4606.0	88.1	3.67	50		1.7	1.08	382.0	36.6	4.06
5		1.4	2.16	144.2	21.7	4.32	51		1.2	0.60	70.6	21.4	5.63
6		1.4	1.21	115.6	18.9	6.29	52		1.4	0.63	119.0	21.6	7.15
7		1.8	0.70	426.5	58.6	1.65	53		1.1	0.61	40.2	17.5	4.34
8		0.9	1.13	20.0	24.8	0.56	54	1.6	1.7	1.18	359.0	32.3	6.27
9		1.2	0.91	62.2	12.0	1.92	55		1.1	1.35	49.0	12.1	6.55
10		1.2	1.83	66.1	17.0	6.00	56		0.8	0.56	18.7	32.5	0.24
11		1.3	0.36	79.3	18.4	5.66	57		0.9	0.69	25.7	14.7	3.97
12		0.9	0.40	19.6	12.0	5.67	58		1.3	0.80	91.2	22.2	3.87
13		1.4	0.49	113.0	21.5	3.99	59		0.9	0.91	23.7	15.3	4.87
14		1.4	0.63	146.0	24.1	4.07	60		1.5	1.17	169.0	38.7	1.38
15		0.8	0.91	13.6	13.9	4.30	61		1.0	1.16	33.1	17.4	3.85
16		1.2	0.96	73.5	22.7	4.26	62		1.0	0.87	31.3	27.3	1.27
17		1.0	0.97	28.0	13.3	6.14	63		1.0	0.36	30.9	18.0	2.40
18	2.2	1.7	0.75	356.0	35.1	3.79	64		1.1	0.50	48.7	21.4	5.37
19		1.4	1.02	136.0	15.0	9.55	65		1.5	0.34	169.0	44.0	1.30
20		1.6	3.02	295.0	31.5	3.93	66		1.3	0.65	98.9	23.6	4.55
21		1.3	1.05	89.8	23.4	3.97	67		1.4	0.91	115.0	26.6	4.10
22	2.0	1.9	2.90	675.0	44.9	3.90	68		1.3	0.33	95.2	29.2	4.33
23	2.8	2.6	6.72	7470.0	128.4	1.81	69		1.2	0.26	62.3	17.4	5.58
24		1.0	0.47	26.7	24.0	1.09	70		1.5	0.77	207.0	30.1	4.79
25		1.0	0.64	34.9	27.0	0.93	71		1.0	0.33	37.0	15.1	5.45
26		1.1	0.74	40.1	82.8	0.03	72		1.6	0.72	285.0	47.2	1.59
27		1.4	0.89	135.0	35.4	2.88	73		1.3	0.88	105.0	25.2	3.50
28		0.8	0.27	16.7	24.8	2.62	74		1.3	1.51	99.4	15.1	9.52
29		1.4	0.74	121.0	26.0	3.47	75		0.7	0.36	11.8	16.9	1.09
30		1.5	0.95	205.0	35.3	2.96	76		0.7	0.55	12.3	13.2	3.10
31		1.3	0.84	85.8	66.7	0.39	77		1.1	1.01	42.3	14.9	7.20
32		1.7	0.73	393.0	27.9	1.05	78		1.8	0.86	540.0	58.3	0.99
33	2.2	1.9	3.14	754.0	60.4	4.81	79		1.1	0.41	45.3	17.4	4.92
34	1.5	1.7	0.75	319.0	152.9	0.05	80		1.6	1.20	293.0	57.0	3.90
35		1.9	1.11	692.0	61.4	2.30	81		1.7	0.63	306.0	51.5	1.33
36	2.6	2.2	2.60	1810.0	87.9	1.66	82		1.5	1.11	202.0	24.6	5.18
37		1.1	1.01	46.4	56.8	0.51	83		1.0	0.32	31.5	13.5	7.80
38		1.3	2.08	90.8	30.5	1.54	84		1.3	0.87	79.7	19.3	5.54
39		0.7	0.33	11.2	35.5	0.47	85		0.9	0.60	21.8	13.0	5.86
40		0.4	0.33	3.6	26.1	1.70	86		1.2	0.52	56.5	30.1	0.73
41		0.8	0.59	18.5	33.2	0.82	87		1.5	0.60	194.0	30.8	3.95
42		0.7	1.08	12.1	27.0	1.81	88	2.7	2.3	4.41	2550.0	80.5	2.73
43		1.0	0.48	28.6	21.2	2.26	89		1.3	0.87	91.3	19.2	6.77
44	1.8	1.9	1.55	757.0	62.4	2.57	90		1.5	0.90	192.0	46.2	1.73
45	1.9	1.9	0.74	609.0	51.1	5.05	91		1.3	0.55	99.2	35.8	1.52
46		1.2	0.41	72.6	28.0	2.93	92		1.5	0.82	165.0	15.1	9.34

Table 6.1 (cont'd.)

Event	m_N	M	R_v(m²/S)	M_o(GNm)	r_o(m)	Δσ(MPa)	Event	m_N	M	R_v(m²/S)	M_o(GNm)	r_o(m)	Δσ(MPa)
93		1.4	0.75	137.0	24.8	4.19	121		0.7	0.81	9.8	9.3	7.08
94		1.2	0.50	72.7	18.8	3.21	122		1.3	0.83	90.1	33.6	0.41
95		1.4	0.75	119.0	24.4	4.40	123		1.1	1.10	52.5	11.3	8.89
96		1.1	1.10	52.4	16.5	4.66	124		0.9	0.52	25.0	14.0	5.16
97		0.7	0.79	13.1	10.6	5.23	125		1.2	0.53	56.0	29.5	2.0
98	2.2	2.1	2.17	1310.0	41.4	6.48	126		1.1	0.77	47.6	46.7	0.04
99		1.5	1.21	209.0	21.9	5.93	127		1.6	2.24	214.0	29.0	3.82
100		1.4	0.56	108.0	19.4	6.48	128		0.8	0.45	16.9	11.6	5.6
101		1.3	1.11	102.0	21.1	4.16	129		1.1	0.56	43.7	55.7	0.34
102		1.2	0.87	68.6	16.4	6.78	130	2.0	1.9	3.03	771.0	81.3	0.64
103		1.5	1.63	178.0	23.2	4.85	131		1.5	0.74	172.0	37.4	2.39
104		1.3	0.67	89.3	26.8	2.13	132		1.5	1.76	165.0	25.1	2.97
105		1.4	1.35	143.0	22.2	5.54	133		1.5	1.76	190.0	24.1	6.05
106		1.2	0.74	71.1	29.6	3.39	134		1.0	0.52	27.4	10.3	10.64
107		1.3	0.63	77.4	22.7	4.9	135		1.2	0.55	59.9	16.3	5.93
108		1.4	1.13	127.0	21.3	7.51	136		1.5	1.21	161.0	28.4	3.81
109		0.9	0.49	23.8	10.6	9.15	137		1.7	0.40	341.0	42.0	4.6
110		1.2	1.25	72.3	15.9	7.57	138		1.0	0.41	26.7	21.9	1.68
111		1.9	2.62	674.0	58.6	1.16	139		0.8	0.80	18.3	31.0	0.27
112		1.5	1.43	197.0	29.3	5.08	140		0.7	0.34	12.7	27.8	0.54
113	2.5	2.1	8.01	1250.0	57.7	1.04	141		0.7	0.32	13.2	14.8	4.75
114		1.5	0.82	186.0	33.4	3.34	142		0.4	0.32	4.0	28.6	0.88
115		1.1	0.82	37.8	18.6	3.6	143		0.7	0.53	10.0	10.8	3.43
116		1.1	0.55	48.7	17.0	6.5	144		1.7	1.13	397.0	64.3	1.28
117		1.5	3.78	202.0	24.8	9.3	145		1.3	0.92	94.9	25.6	4.27
118		1.2	1.03	60.8	20.0	1.66	146		0.6	0.99	9.4	28.8	0.31
119		0.9	0.34	23.0	12.0	4.33	147		1.2	0.44	53.3	40.2	1.22
120		0.8	0.36	13.7	8.8	5.06	148		1.3	0.75	98.1	28.6	1.54

6.3.3 Scaling Relations

With the source parameters from all the data having been calculated, it is possible to proceed with the analysis of the scaling relation using these data. The most interesting exercise is to compare the result from this study with those of other authors as far as the dependence of stress drop on source dimensions is concerned. Figure 6.8 depicts the graph of seismic moment versus source radius for the present study. A large majority of the results show a stress drop within the 0.1-10.0 MPa range, as described in the previous section, thus confirming the previous observations reported in the literature. However, there is a tendency for stress drops to be rather in the higher side of the above window. The detailed examination of this graph does not allow drawing any clear conclusion as to the moment-dependence of stress drop. Although some decrease in seismic moment is observed at the lower end of the spectrum, the large majority of the points follow a typical dependence expected for similar source behaviour.

Figure 6.9 depicts the graph of peak velocity parameter (R_v) versus seismic moment M_o for the present study. McGarr (1984) has analyzed a large number of earthquakes and mine-induced events recorded over a large range of magnitude and has reported a slope of 0.44 for the best-fit line (Figure 6.9). However, most models (Brune, 1970 and 1971; McGarr, 1981) have a slope of 0.33 for this scaling, making this a model-independent observation. McGarr (1984) shows in his study that indeed

Rv scales as $M_0^{1/3}$, as expected, and attributes the discrepancies to several factors such as crustal stress and focal depth or local site conditions. Interestingly, the best-fit line for the present data set shows a slope of 0.33, compatible with a self-similar rupture process. Hence, it can be safely concluded, from the present macroseismic results, that seismic sources involved here show a self-similar behaviour.

In order to examine the validity of these observations at lower magnitudes, two other data sets were considered. Figure 6.10 shows seismic moment versus source radius for the present case, as well as for the results of Gibowicz et al. (1991) and Urbancic et al. (1994). The latter results were obtained from the analysis of a sequence of microseismic events recorded at the Creighton mine following a post-production blast in October 1992. The results of Urbancic et al. are comparable to the present results in many respects. The dominant mechanism of energy loss is intrinsic attenuation with a dominant quality factor of about 100, although a different measurement method was used. Moreover, their results indicate clearly a self-similar source behaviour, as stated in their report.

The results of Gibowicz et al. (1991) were obtained from the analysis of a collection of microseismic events recorded at AECL's Underground Research Laboratory (URL), during the period that the shaft was extended from the 300 level to the 420 level (Talebi and Young, 1992). The rock mass under study at the URL is a homogeneous granitic rock where a number of the complications related to local geology and the presence of back-fill areas that would be encountered in a typical mining environment can safely be neglected.

The data processed by Gibowicz et al. (1991) were composed of two parts: one set of data had known focal mechanism determinations, while average values were used for the other set since focal mechanisms were not known. The estimates of seismic moment and source radius had to be modified to make it compatible with the present results by using average values of radiation coefficients used in Brune's (1970) model. It is noteworthy that the main conclusions of Gibowicz et al. (1991) remain valid after these modifications, as demonstrated by two observations on Figure 6.10.

Stress drop estimates are somewhat lower than those generally reported and they tend to depend on seismic moment, compatible with a non-similar behaviour

Figure 6.8 Seismic moment versus source radius for the present results. The straight lines represent constant values of stress drop

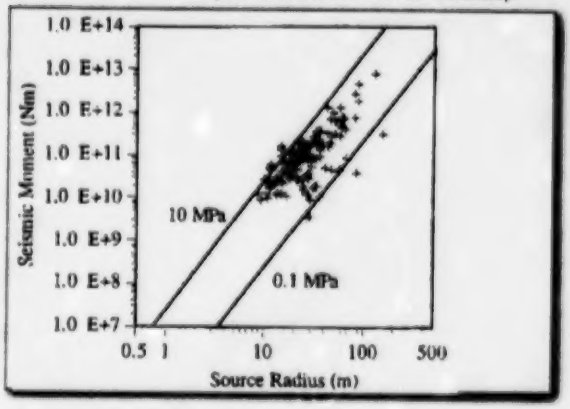

Figure 6.9 Peak velocity parameter (R_v) as a function

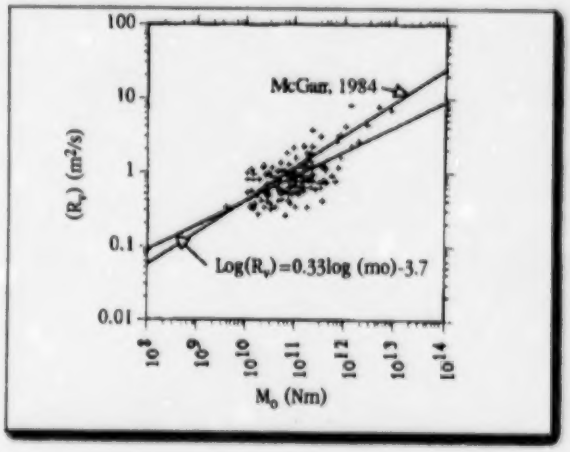

Figure 6.10 Seismic moment versus source radius

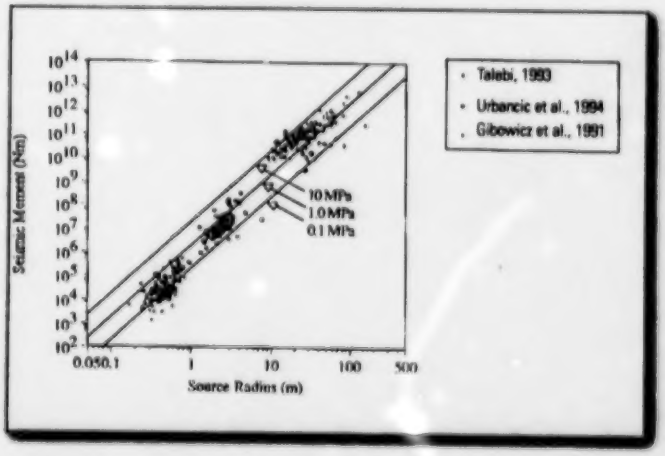

observed for small mining tremors. The examination of Figure 6.10 indicates that the majority of the results show stress drops within the 0.1-100 MPa range expected for self-similar sources. However, the results of Gibowicz et al. (1991) at the lower end of the spectrum seem to be slightly different from the two other cases. It should be noted that this data set has been recorded in a different mining environment and at much higher frequencies than the two other data sets. It is also noteworthy that a significant proportion of these events seemed to have a non-double-couple focal mechanism, i.e. shear failure accompanied by a component of tensile failure.

6.4 Conclusion

Attenuation along the source-sensor path plays a major effect on recorded signals and estimates of source parameters of mine-induced events. Such estimates should be made after correction of spectra for system response and attenuation effects.

The attenuation parameter, Kappa, varied strongly for each sensor while local site effects were negligible to absent. The amount of scatter observed was thought to be due to the presence of areas of fractured rock, back-fill, etc., in the mine. The results showed that using an average value for attenuation parameter for a whole mine will have severe consequences for source-parameter determinations, and attenuation corrections need to be made for each case individually.

The S-wave attenuation factor, Q_S, varied in the range 20 - 500 in the present case, the peak being observed between 50 and 150.

A spectral analysis of macroseismic data provided the following ranges of the source parameters:

Moment magnitude:	0.4 to 2.6
Seismic moment:	3.6 to 7470 GNm
Source radius:	8.8 to 152.9 m
Stress drop:	0.03 to 10.6 MPa

The results of this study show that the large majority of estimations of stress drops are within the 0.1-10.0 MPa range, compatible with the results that have been reported by other authors in the literature. A typical dependence of source parameters, as expected from theoretical shear models, was observed; between seismic moment and source radius on one hand, and between peak velocity parameter and seismic moment on the other. This strongly indicates a self-similar source behaviour, compatible with the reported results in the literature.

6.5 References

Aki, K. (1984). "Asperities, Barriers and Characteristics of Earthquakes." *J. Geophys. Res.* 89:5867-5872.

Anderson, J.G. and Hough, S. (1984). "A Model for the Shape of the Fourier Amplitude Spectrum of Acceleration at High Frequencies." ***Bull. Seism. Soc. Am.*** 74(5):1969-1993.

Brune, J.N. (1970). "Tectonic Stress and the Spectra of Seismic Shear Waves from Earthquakes." *J. Geophys. Res.* 75:4997-5009.

Brune, J.N. (1971). "Correction." *J. Geophys. Res.* 76-5002.

Cranswick, E. and Sembera, E. (1989). "Earthquake Site/Source Studies in the AE/MS Domain." Proceedings of the 4th Conference on AE/MS Activity in Geological Structures and Materials. Trans-Tech Publications, pp. 375-402.

DiBona, M. and Rovelli, A. (1988). "Effects of the Bandwidth Limitation on Stress Drops Estimated from Integrals of the Ground Motion." ***Bull. Seism. Soc. Am.*** 78(5):1818-1825.

Feustel, A.J., Urbancic, T.I. and Young, R.P. (1993). "Estimates of Q Using the Spectral Decay Technique for Seismic Events with M < 1.0." Proceedings of the 3rd International Symposium on Rockbursts and Seismicity in Mines, pp. 337-342.

Gibowicz, S.J. (1990a). "Keynote Lecture: The Mechanism of Seismic Events Induced by Mining: A Review." Proceedings of the 2nd International Symposium on Rockbursts and Seismicity in Mines, pp. 3-27.

Gibowicz, S.J. (1990b). ***Determination of Source Parameters of Small Seismic Events: Report on Methods and Applications to Seismicity Induced by Mining***. Internal Report #RP001Q, Queen's University, 33 pages.

Gibowicz, S.J., Young, R.P., Talebi, S. and Rawlence, D.J. (1991). "Source Parameters of Seismic Events at the Underground Research Laboratory in Manitoba, Canada: Scaling Relations for Events with Moment Magnitude Smaller than -2". ***Bull. Seism. Soc. Am.*** 81(4):1157-1182.

Hanks, T.C. (1982). "$\dot{u}_{max}$". ***Bull. Seism. Soc. Am.*** 72:1867-1880.

Hanks, T.C. and McGuire, R.R. (1981). "The Character of High-Frequency Strong Ground Motion." ***Bull. Seism. Soc. Am.*** 71:2071-2096.

McGarr, A. (1981). "Analysis of Peak Ground Motion in Terms of a Model of Inhomogeneous Faulting." *J. Geophys. Res.* 86:3901-3912.

McGarr, A. (1984). "Scaling of Ground Motion Parameters, State of Stress, and Focal Depth." *J. Geophys. Res.* 89(B8):6969-6979.

Scholz, C.H. (1990). ***The Mechanics of Earthquakes and Faulting***. Cambridge University Press, p 439.

Scholz, C.H., Aviles, C. and Wesnousky, S. (1986). "Scaling Differences Between Large Intraplate and Interplate Earthquakes." ***Bull. Seism. Soc. Am.*** 76:65-70.

Spottiswoode, S.M. (1993). "Seismic Attenuation in Deep-Level Mines." Proceedings of the 3rd International Symposium on Rockbursts and Seismicity in Mines, pp. 409-414.

Snoke, J.A. (1987). "Stable Determination of (Brune) Stress Drop." ***Bull. Seism. Soc. Am.*** 77(2):530-538.

Talebi, S. (1993). ***Source Studies of Mine-Induced Seismic Events Over a Broad Magnitude Range (- 4 < M < 4)***. CANMET Client Report MRL 93-046(CL), 72 pages.

Talebi, S. (1994). ***Source Studies of Mine-Induced Seismic Events Over a Broad Magnitude Range (- 4 < M < 4)***. CANMET Client Report MRL 94-030(CL), 55 pages.

Talebi, S. and Cornet, F.H. (1987). "Analysis of the Microseismicity Induced by a Fluid Injection in a Granitic Rock Mass." ***Geophys. Res. Lett.*** 14(3):227-230.

Talebi, S., Pritchard, C.J. and Mottahed, P. (1994). ***Rockburst Activity in Northern Ontario: September 1992 – December 1994***. CANMET Divisional Report MRL94-071(TR).

Talebi, S. and Young, R.P. (1990). "Characterizing Microseismicity Associated with Stope Development." Proceedings of the 2nd International Symposium on Rockbursts and Seismicity in Mines, pp. 189-194.

Talebi, S. and Young, R.P. (1992). "Microseismic Monitoring in Highly Stressed Granite: Relation between Shaft-Wall Cracking and In Situ Stress." *Int. J. Rock Mech. Min. Sci. & Geomech. Abstr.* 29(1):25-34.

Urbancic, T.I., Bowes, R. and Young, R.P. (1993). *Monitoring of Seismicity with QMS Systems at Creighton Mine, Sudbury, Ontario.* Report #MRD005, 34 pages.

Urbancic, T.I., Feustel, A.J. and Marisett, S. (1994). *Source Studies of Mining-Induced Seismicity at Creighton Mine, Sudbury, Canada: Analysis of Seismicity Related to the m_N 2.1 Rockburst Sequence of October 29, 1992.* ESG Report to PMC-CRRP, 71 pages.

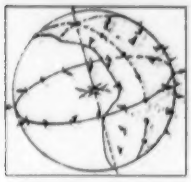

CANMET's Macroseismic Analysis Software – Layout and Description

Chapter 4 discussed CANMET's macroseismic system and its associated software. This appendix addresses the graphic program associated with this system.

(I) Graphic Program

Once the data file name to be analyzed has been read, the program first displays the MAIN MENU selection (Figure 1) on the left side of the screen. In order to proceed, the user must use the mouse to select the appropriate menu when the following message locator input required is displayed on the screen, or via the keyboard when keyboard input requested appears on the top left corner of the screen.

Figure 1 Main menu

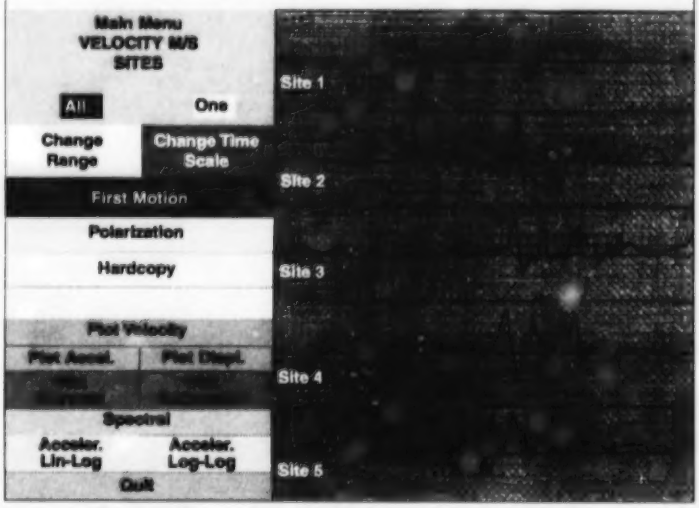

Figure 2 Menu 4 – Plot channel – channel relocation

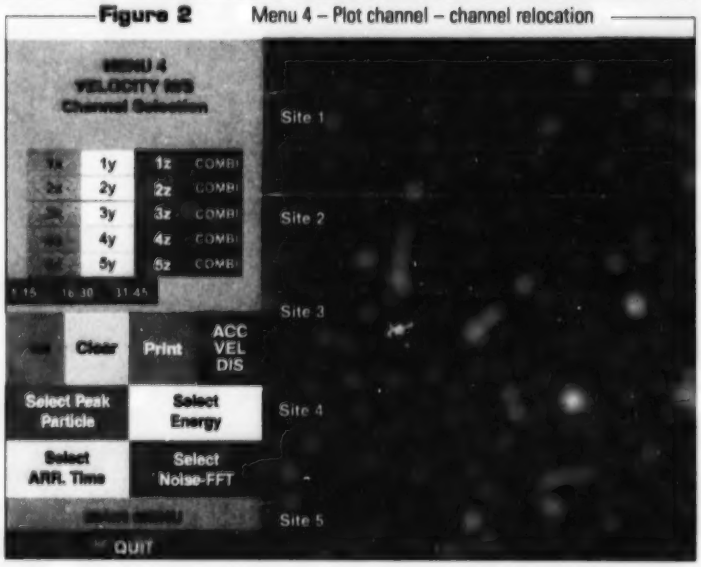

(II) MENU DESCRIPTION

(i) Main Menu - PLOT CHANNELS (MENU 4)

The Menu 4 selection (Figure 2) is used to display PLOT and print PRINT waveform, clear screen CLEAR and plot on the same screen acceleration, velocity and displacement mode for a particular channel ACC/VEL/DIS. A maximum of five windows can be used or selected. Triaxial, uniaxial or both could be selected. Triaxial sensors are identified by two characters, a number for site identification and a letter for axis. Uniaxial sensors are identified by a number only. For triaxial sensors, waveforms can be displayed as a single axis or multi-axes if COMBI menu is selected, with up to three waveforms displayed in the same window. The PRINT menu produces a dump of the current graphics screen to the printer. The seismic-waveform-analysis software can handle up to 60 channels per bank of 15 channels at a time, i.e. 1-15, 16-30, 31-45

and 46-60. If the data file contains more than 15 channels, channel bank menu will be displayed, allowing the user to select any available channels.

(ii) Main Menu – CHANGE RANGE (MENU 3)

To change the range of the vertical axis, CHANGE RANGE menu box (Figure 3) must be selected. Menu 3 will then display several options for range selection. The percentage range amplitude selected appears at the bottom of Menu 3 just below REPLOT box. The default range is set at 25%. The high and low limits for each plot are equal to the percentage range selected times the highest value read from the input file. This value appears on Menu 3 below the amplitude-range title. The range scale may be changed as often as required by the user. The percentage range will increase or decrease, depending on whether + 10%, + 1%, -10%, / 10, or *10 menu is selected. To plot the waveforms with the new range, the user must select the REPLOT box menu. If a new range has been selected and the user selects a new menu prior to replot, the waveforms will be replotted automatically before displaying the new menu.

Figure 3 Menu 3 – Change range

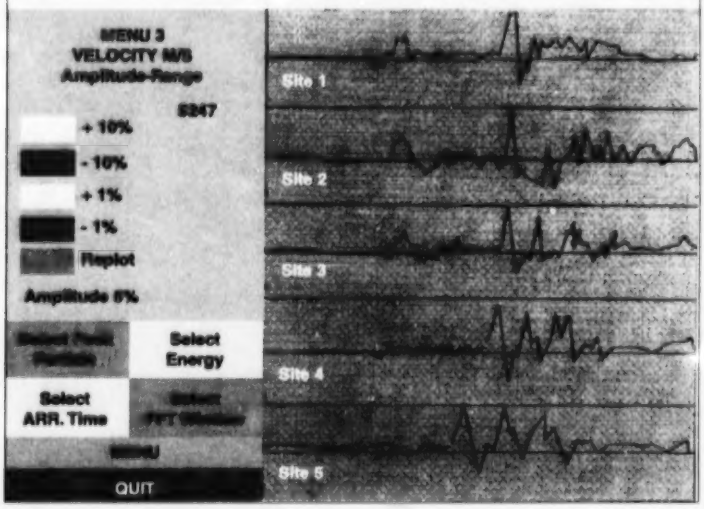

Figure 4 Menu 5 – Change time scale

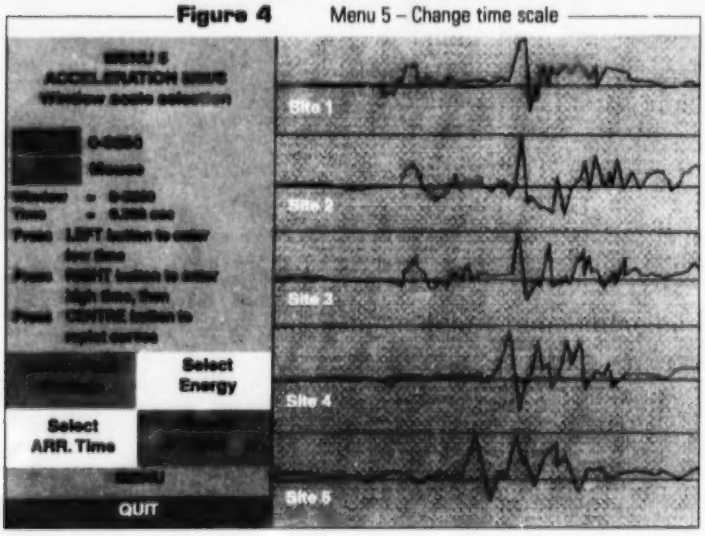

(iii) Main Menu – CHANGE TIME SCALE (MENU 5)

The time scale or horizontal axis of the plots can be changed by selecting the CHANGE TIME SCALE menu box (Figure 4). Menu 5 will display two menu boxes labelled 0-xxxx and MOUSE, where xxxx is the total number of points per channel read from the input data file.

When the 0-xxxx box selected, the entire waveform is replotted. To expand any portion of the plots, the user must select the MOUSE menu box and then position the mouse to redefine the new lower and upper limits of the time scale. When the new limits are selected, the new window is then redrawn. The new limits will be written on the menu side of the screen in both seconds and digitized point number. A short help menu is written on the menu side of the screen to guide the user on how to proceed with the mouse to define a new window.

(iv) Main Menu – POLARIZATION

Waveforms produced by seismic events often show two distinct waves: Primary or "P" waves and shear or "S" waves. In the P-wave, the particle motion is in the direction of the wave motion; while for the S-wave, the particle motion is perpendicular to the direction of the wave motion. The shear wave is often broken down again into two components, termed the "SV" and "SH" waves, where "V" and "H" refer to vertical

and horizontal, respectively. These two components are usually mixed when the waveforms are recorded by a sensor.

Because the motion of P- and S-waves is perpendicular to each other, it is possible to rotate the waveform so that all of the energy from the P-wave is placed on the x-axis and all of the energy from the S-wave is placed on the y and z axes.

The POLARIZATION menu option plots the particle motion of the wave on the "P-SV", "P-SH" and "SV-SH" planes and can be used to analyze P- and S- wave polarization.

(v) Main Menu – SOURCE LOCATION (MENU 8)

Once the arrival-times have been entered, the user can locate the epicentre of the recorded event by selecting the SOURCE LOCATION menu option (Figure 5). Three source-location techniques are provided: the least-squares method based on P arrival times; the "S-P" least-squares method; and, finally, CANMET's algorithm (Section 5.4).

First, the user is prompted to select the location technique, i.e. SP, P or GE, and then the channels to be used for source location. The LOCATE menu will calculate the co-ordinates of the source and display the results on the screen. If the required arrival times have not been entered, the user will be prompted accordingly and the selected channel will not be part of the solution. A warning will also be displayed if a minimum number of channels or arrival times is not met.

P- and S-velocity can be changed by selecting P, S, + or - menu selection. For any velocity change, new values are displayed on the screen. The ACCEPT LOCATION menu will store the co-ordinates of the source in a parameter file.

In addition to the event co-ordinates, several quality factors related to the accuracy and the reliability of the given source location are also provided. These factors include the residual, the sensitivity and the event rank (Section 5.3.4).

The event residual is a total effect of mismatch between the observed and calculated arrival times, which is the most important criterion for determining the source-location accuracy. Sensitivity measures the stability of the solution, which is defined as the distance between a located source and its associated position obtained by assuming 10% lower velocity. For both parameters, a lower value indicates a better solution. The rank, which is a combination of these quality factors, also takes into account the hit sequence. This quality factor, which cannot be displayed on-screen, compares the observed and calculated hit sequences and determines the seriousness of the mismatch. The rank is categorized into five classes (A, B, C, D, Z), where A indicates a very good rating while Z means that the event is impossible to locate.

Figure 5 Menu 8 – Source location

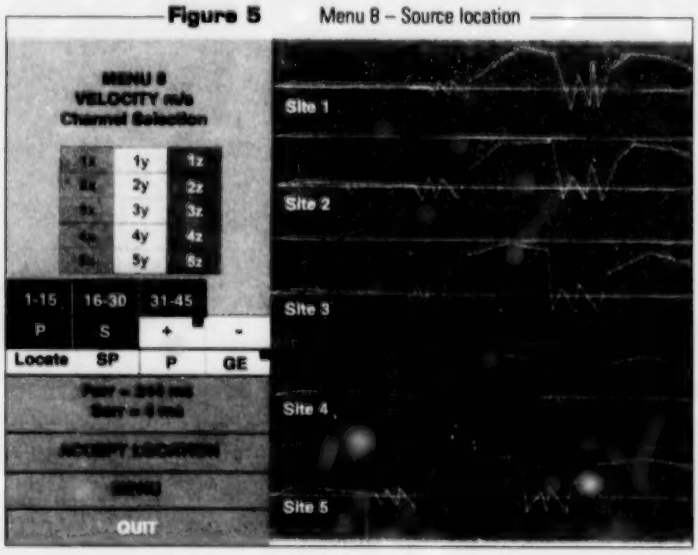

(vi) Main Menu – FIRST MOTION (MENU 11)

In order to proceed with focal-mechanism analysis of seismic events, the first motion of each waveform must be defined. The first motion is either up or down for each wave. The menu

box "+" is used to define an upward motion, while the "-" menu box defines a downward motion. Based on a proper in situ calibration, the polarity of an upward motion is related to a compression mode, while a downward motion represents a dilatation mode, or vice versa. The first motion selection is stored in an external parameter file which is used as an input for focal-mechanism analysis.

(vii) Main Menu – SPECTRAL LINE

Spectral analysis of seismic waveforms in the frequency domain is used to obtain information on source mechanisms. The seismic signal, in the form of a displacement wave, is transformed into a frequency distribution using a Fast Fourier Transform. The spectral density is plotted against frequency in a logarithmic format. Plateau and corner frequency obtained from the graph are used to calculate seismological parameters, such as seismic moment, stress drop, source radius, etc.

When the SPECTRAL menu box has been selected, the screen displays a signal menu area on the left and a plotting area on the right. From the menu, the user can select any channel, get slope, plateau and corner frequency and store them in a parameter file STORE, display the Fast Fourier Transform of the background noise NOISE, correct the curve for attenuation ATTENUATION, apply filter F1 and F2, draw least-squares curve LEAST SQUARE on the original curve (black curve) and/or corrected curve for attenuation (red curve), replot the graph REPLOT, print PRINT or exit the program EXIT.

(viii) Main Menu – SPECTRAL CURVE

This menu option allows the user to perform an extensive study of seismic-wave polarization. The various menu selections, as well as the theory and the procedures to use the software, have been extensively documented in Beardwood (1993 and 1994) reports[1].

(ix) Main Menu – ACCELERATION LIN-LOG

This menu selection displays the Fast Fourier Transform of the recorded wave in acceleration mode. The curve is displayed on a linear-logarithmic graph in order to obtain various seismological parameters, such as Kappa and slope. This particular feature of the program has been used, so far, as a research tool. No provision has been made to save the calculated results.

(x) Main Menu – ACCELERATION LOG-LOG

This menu selection displays the Fast Fourier Transform of the recorded wave in acceleration mode. The curve is displayed on a log-log scale in order to obtain various seismological parameters, such as slope, plateau and corner frequency. As with the acceleration lin-log menu, this particular feature has also been used as a research tool. No provision has been made to save the calculated results.

(xi) Secondary Menu – SELECT PEAK PARTICLE (MENU 6)

The utility SELECT PEAK PARTICLE (Figure 6) allows the user to calculate the peak particle acceleration, velocity and/or displacement, based on the display mode selected from the main menu (acceleration, velocity or displacement). When selected, Menu 6 displays the highest vector sum value of the peak found for each site or channel displayed on the screen. If desired, peak particle value can

---

[1] Beardwood, F. (1993). *A Study of Wave Polarization*. Sudbury Laboratory. CANMET Internal Report, 33 pages.

Beardwood, F. (1994). *A Study of Wave Polarization: Application to Macroseismic Data from Creighton Mine*. Sudbury Laboratory. CANMET Internal Report, 57 pages.

also be calculated for any particular window. To proceed, the user must first select the SELECT WINDOW menu located in the middle of the menu screen and then define the window time. The window time limits, as well as the calculated value, will be displayed on the screen.

Peak particle values are automatically stored in a parameter file. They represent the highest vector sum calculated for each site and for the whole window. All other values calculated through the SELECT WINDOW menu are not stored.

Figure 6 Menu 6 – Select peak particle

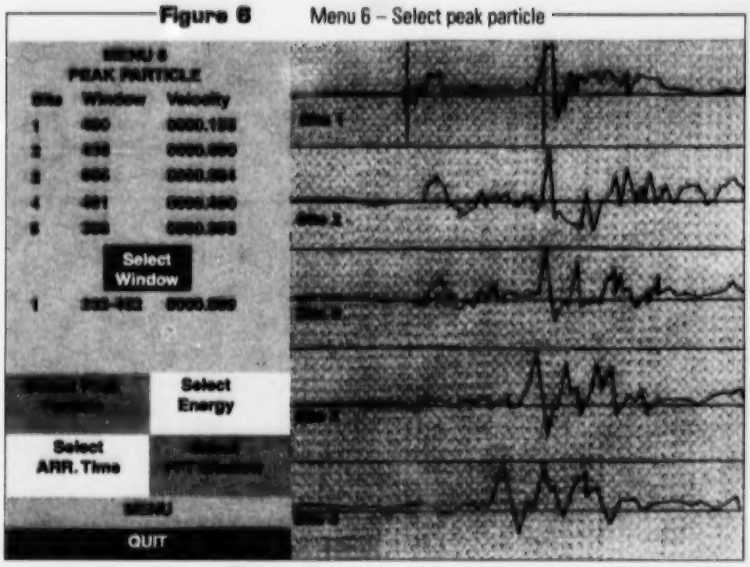

(xii) Secondary Menu – SELECT ENERGY (MENU 7)

The energy calculation assumes that the location of the event is known. If it is unknown, the user will be prompted to determine the location of the event prior to proceeding.

This particular SELECT ENERGY menu (Figure 7) is quite similar to Menu 6. The top screen of Menu 7 displays the total energy of the whole waveform, in kjoules, for the selected channels displayed on the screen. If desired, energy value can also be calculated for any particular window. To proceed, the user must first select the SELECT WINDOW menu located in the middle of the menu screen and then define the window time. The window time limits, as well as the calculated value, will be displayed on the screen.

Energy values are automatically stored in a parameter file. They are calculated for each site and for the whole window. All other values calculated through the SELECT WINDOW menu are not stored.

Figure 7 Menu 7 – Select energy

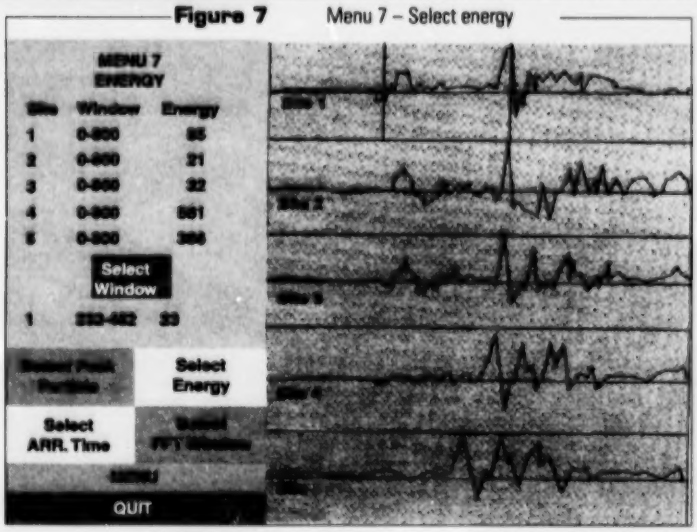

(xiii) Secondary Menu – SELECT ARRIVAL TIME (MENU 2)

The SELECT ARRIVAL TIME menu (Figure 8) allows the user to manually pick, check and/or adjust the arrival time of both the P- and S- waves of a specified event for source-location purposes. Once in Menu 2, a help menu, instructing the user on how to proceed, appears on the screen.

Figure 8 Menu 2 – Select arrival time

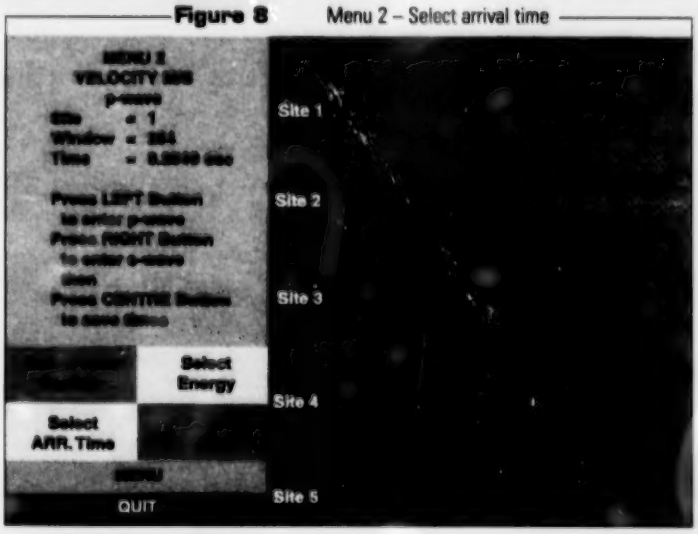

From the mouse selection, the arrival-time picking, as well as site or channel identification, will be displayed on the screen. If requested by the user, the arrival times can be stored in a parameter file.

Figure 8 Menu 9 – Select noise FFT

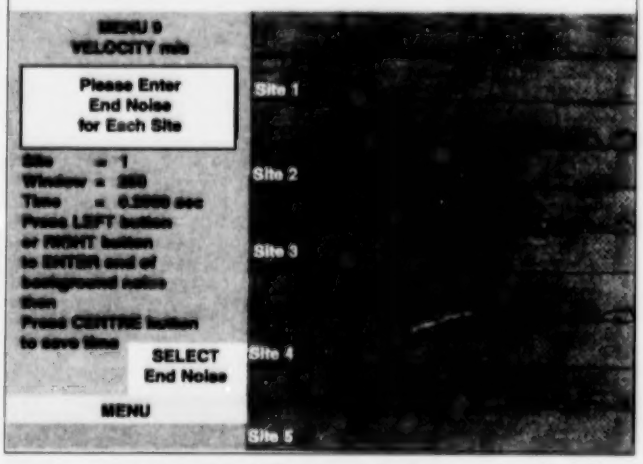

(xiv) Secondary Menu – SELECT NOISE-FFT (MENU 9)

This utility is used to define a time-window for spectral analysis (Figure 9). Two window types can be defined; one for the spectral analysis of the recorded signal (i.e. P, S or the entire signal) and, if required, a second for the spectral analysis of the background noise.

When MENU 9 is selected, a user help menu appears on the screen on how to use the mouse to proceed. The time window may be altered as often as required by the user.

(xv) Secondary Menu – MENU

The MENU option from the secondary menu bar recalls and displays the main menu selection.

(III) PARAMETER FILE 'p'

The 'p' file, called parameter file (MmmDD:HH:SSp), contains the summary of the various parameters calculated and stored from the STORE menu option, if not automatically stored by the software itself (Table (i)). These parameters include the file identification and its occurrence, the updated date of the analysis, the P- and S-wave arrival times for each site as selected by the operator, the time window used for the spectral analysis of the background noise, the azimuth and the emergence of each sensor, the source location of the event according to the mine co-ordinate system, the velocity used to calculate seismic parameters, the FFT time window, the energy, the peak particle acceleration, velocity and displacement, as well the distance from the source to each site. Peak particle accelerations are calculated only if input data are recorded from accelerometers.

For each axis, seismic parameters are calculated at the site and include site axis identification, first motion, corner frequency, plateau, slope, source radius, seismic moment and stress drop. For the triaxial sensor only, source radius, seismic moment and stress drop are also calculated from the corner frequency average and the vector sum of the plateau. Slope average is also calculated.

(IV) FAX FILE 'f'

The 'f' file (MmmDD:HH:SSf), called fax file, contains the data sent to mine operators (Table (ii)). The file, which is presented in a more formal format, is simply a reorganization of the 'p' file values. In addition, the 'f' file has an option for identifying the user, and provides both the estimated magnitude based on the energy values and the magnitude of the event recorded by the CANMET Digital Seismograph Network (CDSN).

Table I An output example of "p" file

```
Oct2018:37:28 92
 Updated on Wed Oct 21 08:44:34 1992
 Arrival Times (p, s)      NOISE          AZ    EM
                           (msec)        (deg) (deg)
 Site  1
       288        401        266          182   61
 Site  2
       219        278        185          275   24
 Site  3
       209        264        188            5   15
 Site  4
       189        227        171          300   82
 Site  5
       179        213        161          147   85


 p - Direct Solution :- (x, y, z)      VELOCITY (ft/sec)
        4581.00    6228.00    6934.00        12000.00


 SITE                  1          2          3          4          5

 FFT WINDOW      1890-4668  1358-6298  1295-3476  1124-4726  1059-3261
 ENERGY (KJ)       27240.      5686.      8328.     12512.      8353.
 PPV (mm/s)         3.662      2.120      3.295      5.009     10.149
 PPD (mm)           0.026      0.020      0.020      0.053      0.024
 DISTANCE (m)         985        520        491        351        308


      Site  Parameters

 SITE   CORNER   PLATEAU     SLOPE                SOURCE   SEISMIC   STRESS
 Nbr    Freq.    (10-9)                           Radius   Moment    Drop
          (Hz)   (m-sec)                           (m)    (GN.m)    (KPa)
 1 x      17.2    633.88    -2.142          0.     79.2    1954.9    1723.5
 1 y      17.7   1272.41    -2.149          0.     77.0    3924.1    3762.9
 1 z      15.8    482.01    -2.101          0.     86.5    1486.5    1006.2
          16.9   1501.05    -2.131          0.     80.7    4629.2    3857.4

 2 x      15.6    782.31    -2.327          0.     87.3    1274.6     838.1
 2 y      16.2    729.78    -2.370          0.     84.3    1189.0     868.1
 2 z      15.6    715.18    -2.328          0.     87.6    1165.2     758.6
          15.8   1286.88    -2.342          0.     86.4    2096.7    1423.5

 3 x      19.9    664.42    -2.173          0.     68.5    1021.9    1391.9
 3 y      17.4    962.82    -2.247          0.     78.4    1480.9    1346.8
 3 z      20.5    371.38    -2.194          0.     66.4     571.2     854.6
          19.3   1227.36    -2.205          0.     70.7    1887.8    2336.6

 4 x      15.8   2366.20    -2.592          0.     86.3    2598.1    1766.3
 4 y      16.3   4967.18    -2.560          0.     83.6    5453.9    4077.3
 4 z      17.3    611.01    -2.529          0.     78.6     670.9     603.5
          16.5   5535.80    -2.561          0.     82.7    6078.2    4693.0

 5 x      18.8    466.06    -1.981          0.     72.3     449.9     520.0
 5 y      21.7    292.41    -2.079          0.     62.8     282.3     497.9
 5 z      20.9    790.50    -1.969          0.     65.2     763.2    1203.6
          20.5    963.12    -2.010          0.     66.6     929.8    1379.5
```

Table ii An output example of "fax" file

```
WAVEFORM ANALYSIS DONE BY:
SEISMIC EVENT Oct2018:37:28 92 MAGNITUDE ESTIMATED FROM ENERGY: 2.3 Mn
                               MAGNITUDE FROM OTTAWA/CDSN     : 2.6 Mn
Arrival Times (p, s)     NOISE          AZ    EM
          (msec)         (msec)        (deg) (deg)
SITE  1   288     401     268           182   -61
SITE  2   219     278     268             5   -15
SITE  3   209     264     268           275   -24
SITE  4   189     227     268           300   -82
SITE  5   179     213     268           147    85

SOURCE LOCATION FROM    CREIGHTON MINE   :   4581.E     6228.N     6934.ELEV.
VELOCITY  12000. (ft/sec); WAVEFORM ANALYSIS DONE ON  "SHEAR" WAVES
SITE                 1          2          3          4          5
FFT WINDOW      1890-4668  1358-6298  1295-3476  1124-4726  1059-3261
ENERGY (KJ)       27240.      5068.      9345.     12512.     23790.
PPV (mm/s)         3.662      2.120      3.295      5.009     12.562
PPD (mm)           0.026      0.019      0.025      0.063      0.046
DISTANCE (m)         985        491        520        351        308

     Site  Parameters
SITE   CORNER  PLATEAU   SLOPE              SOURCE   SEISMIC   STRESS
Nbr    Freq.   (10-9)                       Radius   Moment    Drop
        (Hz)   (m-sec)                       (m)     (GN.m)    (KPa)
1 x    17.2     633.9    -2.14        0.     79.2     1954.9    1721.8
1 y    20.6    1930.6    -2.15        0.     66.1     5954.0    9009.3
1 z    15.8     482.0    -2.10        0.     86.2     1486.5    1014.9
       17.9(1)2088.4(2)  -2.13(3)     0.     76.2(4)  6440.6(4) 6358.3(4)

2 x    15.6     782.3    -2.33        0.     87.3     1203.3     790.7
2 y    16.2     729.8    -2.37        0.     84.1     1122.5     826.0
2 z    15.6     715.2    -2.33        0.     87.3     1100.0     722.9
       15.8(1)1286.9(2)  -2.34(3)     0.     86.2(4)  1979.4(4) 1351.4(4)

3 x    19.9     664.4    -2.17        0.     68.5     1082.5    1476.7
3 y    17.4     962.8    -2.25        0.     78.3     1568.7    1430.4
3 z    20.5     371.4    -2.19        0.     66.4      605.1     902.3
       19.3(1)1227.4(2)  -2.20(3)     0.     70.7(4)  1999.7(4) 2475.5(4)

4 x    15.8    2366.2    -2.59        0.     86.2     2598.1    1773.8
4 y    16.3    4967.2    -2.56        0.     83.6     5453.9    4088.4
4 z    17.3     611.0    -2.53        0.     78.7      670.9     601.3
       16.5(1)5535.8(2)  -2.56(3)     0.     82.7(4)  6078.2(4) 4697.6(4)

5 x    18.8     466.1    -1.98        0.     72.5      449.9     517.5
5 y    21.7     292.4    -2.08        0.     62.8      282.3     499.3
5 z    20.9     790.5    -1.97        0.     65.2      763.2    1206.0
       20.5(1)  963.1(2)  -2.01(3)     0.     66.6(4)   929.8(4) 1379.8(4)
(1): AVERAGE FROM X,Y,Z          (2):  VECTOR SUM FROM X,Y,Z
(3): AVERAGE FROM X,Y,Z          (4):  CALCULATED FROM (1) and (2)
```

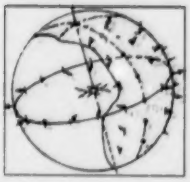

List of Rockbursts Recorded in Ontario Mines by CANMET's Macroseismic Systems

TABLE i Recorded seismic events in Ontario mines — Campbell Mine from 1/01/92 to 12/31/95 (updating: 12/31/95)

No.	Date	Time	Magnitude	Mine	No.	Date	Time	Magnitude	Mine
1	7/03/92	13:15:22	0.6	Campbell	40	10/26/94	23:45:03	1.5	Campbell
2	7/13/92	15:45:48	0.6	Campbell	41	10/26/94	23:45:10	0.7	Campbell
3	7/13/92	20:28:35	0.6	Campbell	42	10/31/94	15:42:52	2.8	Campbell
4	8/14/92	19:02:34	1.3	Campbell	43	11/04/94	15:23:37	1.0	Campbell
5	9/01/92	19:46:30	0.7	Campbell	44	12/10/94	06:36:57	1.3	Campbell
6	9/29/92	06:03:17	0.7	Campbell	45	12/21/94	17:46:53	0.9	Campbell
7	10/17/92	02:05:26	0.7	Campbell	46	12/31/94	13:30:03	1.2	Campbell
8	10/22/92	15:54:57	1.5	Campbell	47	1/21/95	19:54:52	0.7	Campbell
9	10/23/92	03:31:45	0.5	Campbell	48	2/09/95	03:28:24	1.9	Campbell
10	10/23/92	16:41:35	0.0	Campbell	49	2/16/95	02:52:28	1.0	Campbell
11	10/23/92	19:37:20	0.8	Campbell	50	2/20/95	20:42:41	1.0	Campbell
12	10/23/92	20:21:59	0.0	Campbell	51	3/03/95	22:03:20	0.7	Campbell
13	10/24/92	06:39:55	0.0	Campbell	52	3/22/95	15:28:56	2.2	Campbell
14	10/28/92	03:33:46	0.7	Campbell	53	3/23/95	16:37:56	2.1	Campbell
15	11/21/92	06:35:17	1.3	Campbell	54	3/29/95	15:36:42	0.9	Campbell
16	12/04/92	21:27:30	0.9	Campbell	55	4/12/95	15:26:41	1.2	Campbell
17	12/08/92	14:22:40	0.0	Campbell	56	5/18/95	15:32:49	1.0	Campbell
18	3/17/93	15:51:21	2.1	Campbell	57	5/18/95	19:31:30	1.1	Campbell
19	3/17/93	15:52:15	1.6	Campbell	58	5/18/95	22:46:03	0.5	Campbell
20	4/03/93	15:47:49	1.5	Campbell	59	5/28/95	09:57:56	2.5	Campbell
21	4/15/93	00:07:16	1.7	Campbell	60	7/17/95	11:35:03	0.2	Campbell
22	6/25/93	08:10:17	0.8	Campbell	61	7/18/95	03:55:08	0.7	Campbell
23	10/09/93	16:12:52	0.8	Campbell	62	8/08/95	08:41:55	1.2	Campbell
24	10/09/93	16:15:46	0.9	Campbell	63	8/20/95	08:51:20	0.4	Campbell
25	10/09/93	16:55:48	1.5	Campbell	64	8/22/95	22:12:05	0.7	Campbell
26	11/10/93	15:47:26	1.0	Campbell	65	9/13/95	00:55:47	1.3	Campbell
27	11/20/93	03:56:34	2.0	Campbell	66	9/16/95	19:34:31	0.9	Campbell
28	11/25/93	16:09:19	1.0	Campbell	67	9/29/95	05:45:05	0.2	Campbell
29	12/27/93	10:44:18	1.2	Campbell	68	9/29/95	05:45:20	0.2	Campbell
30	2/17/94	12:22:09	1.1	Campbell	69	10/07/95	15:18:03	0.2	Campbell
31	3/18/94	03:51:25	1.2	Campbell	70	10/07/95	15:18:23	0.3	Campbell
32	3/23/94	21:99:26	2.2	Campbell	71	10/07/95	16:54:50	0.0	Campbell
33	3/23/94	21:22:94	1.9	Campbell	72	10/07/95	18:20:29	1.0	Campbell
34	4/20/94	03:45:20	1.5	Campbell	73	10/22/95	15:09:53	0.0	Campbell
35	4/21/94	18:30:11	0.7	Campbell	74	10/22/95	15:11:08	1.1	Campbell
36	5/31/94	07:38:27	1.2	Campbell	75	10/22/95	15:11:11	1.2	Campbell
37	8/13/94	17:07:48	1.2	Campbell	76	10/22/95	15:11:12	1.2	Campbell
38	9/25/94	03:53:46	0.9	Campbell	77	10/22/95	18:07:31	0.5	Campbell
39	10/20/94	15:25:38	0.8	Campbell	78	11/16/95	03:07:40	0.0	Campbell

TABLE ii Recorded seismic events in Ontario mines — Macassa Mine from 5/01/91 to 11/31/95 (updating: 11/31/95)

No.	Date	Time	Magnitude	Mine	No.	Date	Time	Magnitude	Mine
1	6/23/91	01:33:30	2.5	Macassa	62	10/29/92	15:23:11	0.1	Macassa
2	7/21/91	09:01:38	2.0	Macassa	63	11/09/92	11:54:18	1.2	Macassa
3	7/21/91	09:02:03	1.8	Macassa	64	11/09/92	11:55:49	1.5	Macassa
4	7/21/91	19:45:11	1.8	Macassa	65	11/19/92	13:18:38	0.7	Macassa
5	8/06/91	16:11:35	2.1	Macassa	66	12/20/92	08:49:38	1.4	Macassa
6	9/15/91	16:17:39	1.7	Macassa	67	12/22/92	10:31:55	0.4	Macassa
7	9/25/91	17:53:41	1.9	Macassa	68	1/12/93	16:12:32	0.2	Macassa
8	10/08/91	00:22:36	1.3	Macassa	69	1/12/93	23:41:58	1.4	Macassa
9	11/06/91	10:31:48	0.4	Macassa	70	1/21/93	01:51:54	0.0	Macasse
10	11/12/91	00:07:29	0.5	Macassa	71	1/31/93	05:52:13	0.0	Macassa
11	12/20/91	14:19:13	0.8	Macassa	72	2/18/93	03:14:53	0.6	Macassa
12	12/20/91	14:19:30	0.5	Macassa	73	4/02/93	19:45:12	0.0	Macassa
13	1/03/92	01:04:22	1.5	Macassa	74	4/03/93	17:19:20	0.0	Macassa
14	1/16/92	21:54:14	0.6	Macassa	75	4/16/93	03:32:24	1.9	Macassa
15	1/17/92	07:39:36	0.7	Macassa	76	4/27/93	22:33:41	0.3	Macassa
16	1/19/92	20:52:52	0.5	Macassa	77	5/14/93	23:05:07	0.6	Macassa
17	1/27/92	13:01:14	0.6	Macassa	78	5/29/93	00:28:39	0.0	Macassa
18	2/08/92	23:19:45	1.9	Macassa	79	5/29/93	00:47:20	0.0	Macassa
19	2/24/92	20:35:44	1.0	Macassa	80	6/02/93	04:23:57	1.1	Macassa
20	3/06/92	08:04:47	1.2	Macassa	81	6/26/93	00:10:00	1.1	Macassa
21	4/22/92	03:08:50	2.8	Macassa	82	6/30/93	10:27:35	0.6	Macassa
22	4/22/92	03:11:55	0.8	Macassa	83	7/12/93	12:40:20	1.5	Macassa
23	4/22/92	03:16:39	0.9	Macassa	84	7/13/93	01:14:23	0.0	Macassa
24	4/26/92	00:18:17	0.9	Macassa	85	7/24/93	00:40:30	0.6	Macassa
25	8/23/92	14:37:44	1.4	Macassa	86	7/24/93	01:33:39	0.3	Macassa
26	8/23/92	14:38:08	2.3	Macassa	87	7/27/93	14:51:12	0.7	Macassa
27	8/23/92	19:01:14	0.8	Macassa	88	7/30/93	05:33:22	0.7	Macassa
28	9/18/92	02:52:14	0.7	Macassa	89	8/17/93	17:37:44	0.3	Macassa
29	9/30/92	20:28:09	0.9	Macassa	90	8/18/93	03:09:36	0.9	Macassa
30	9/30/92	20:29:58	0.7	Macassa	91	8/27/93	03:15:12	1.7	Macassa
31	10/01/92	08:35:30	0.5	Macassa	92	8/28/93	00:09:47	0.6	Macassa
32	10/01/92	10:53:09	1.5	Macassa	93	9/19/93	21:14:19	0.0	Macassa
33	10/01/92	14:00:14	0.0	Macassa	94	9/20/93	15:58:55	1.1	Macassa
34	10/02/92	19:55:39	1.0	Macassa	95	9/20/93	16:42:42	1.2	Macassa
35	10/02/92	22:39:27	0.0	Macassa	96	9/23/93	16:00:13	0.0	Macassa
36	10/09/92	23:56:06	0.9	Macassa	97	9/27/93	00:24:00	0.0	Macassa
37	10/10/92	04:14:39	0.2	Macassa	98	9/28/93	03:29:07	0.9	Macassa
38	10/11/92	15:25:44	0.0	Macassa	99	9/28/93	13:28:21	0.0	Macassa
39	10/14/92	18:56:12	0.0	Macassa	100	9/29/93	04:02:23	0.0	Macassa
40	10/16/92	14:53:05	0.0	Macassa	101	10/07/93	03:51:19	0.4	Macassa
41	10/17/92	23:06:01	0.0	Macassa	102	10/27/93	14:02:30	0.4	Macassa
42	10/28/92	10:26:20	2.3	Macassa	103	11/19/93	11:12:36	0.0	Macassa
43	10/28/92	10:26:23	0.7	Macassa	104	11/20/93	00:00:04	1.3	Macassa
44	10/28/92	10:26:25	0.0	Macassa	105	11/25/93	01:38:58	0.8	Macassa
45	10/28/92	10:26:28	0.0	Macassa	106	11/26/93	08:20:38	2.8	Macassa
46	10/28/92	10:26:31	0.0	Macassa	107	11/26/93	08:20:45	2.1	Macassa
47	10/28/92	10:26:38	0.0	Macassa	108	11/26/93	08:20:47	1.7	Macassa
48	10/28/92	10:26:56	0.0	Macassa	109	12/04/93	19:36:59	1.2	Macassa
49	10/28/92	10:28:07	0.0	Macassa	112	7/19/94	04:32:14	0.7	Macassa
50	10/28/92	10:31:36	0.0	Macassa	113	7/19/94	08:10:29	0.0	Macassa
51	10/28/92	10:35:08	2.5	Macassa	114	7/20/94	15:29:34	0.0	Macassa
52	10/28/92	10:35:12	0.0	Macassa	115	9/10/94	14:33:09	1.5	Macassa
53	10/28/92	10:35:30	0.0	Macassa	116	9/10/94	14:38:44	0.5	Macassa
54	10/28/92	10:52:44	0.0	Macassa	117	9/12/94	21:29:55	1.2	Macassa
55	10/28/92	11:43:22	0.0	Macassa	118	10/08/94	05:06:15	0.1	Macassa
56	10/28/92	11:51:17	0.0	Macassa	119	10/08/94	05:06:19	1.1	Macassa
57	10/28/92	13:37:59	0.0	Macassa	120	10/08/94	08:46:34	1.2	Macassa
58	10/28/92	16:33:38	0.0	Macassa	121	10/22/94	16:11:32	1.0	Macassa
59	10/28/92	21:14:07	0.0	Macassa	122	12/25/94	07:56:35	2.5	Macassa
60	10/29/92	06:16:04	0.0	Macassa	123	2/01/95	16:16:03	2.9	Macassa
61	10/29/92	09:34:24	0.0	Macassa	124	2/01/95	16:44:58	1.2	Macassa

TABLE ii (cont'd.)

No.	Date	Time	Magnitude	Mine	No.	Date	Time	Magnitude	Mine
125	2/05/95	13:04:50	1.3	Macassa	152	7/21/95	21:14:31	0.7	Macassa
126	2/12/95	01:38:19	1.0	Macassa	153	7/26/95	16:16:26	0.0	Macassa
127	3/10/95	15:48:58	0.7	Macassa	154	7/27/95	16:56:41	0.8	Macassa
128	3/18/95	03:22:44	0.0	Macassa	155	7/28/95	00:34:31	1.9	Macassa
129	3/24/95	22:11:09	2.1	Macassa	156	8/26/95	15:15:37	2.7	Macassa
130	3/24/95	22:11:57	0.0	Macassa	157	8/26/95	15:16:34	1.2	Macassa
131	3/25/95	00:11:43	0.0	Macassa	158	8/26/95	15:31:04	0.2	Macassa
132	3/25/95	05:19:10	0.3	Macassa	159	8/26/95	16:26:49	0.7	Macassa
133	4/01/95	16:24:28	0.1	Macassa	160	8/26/95	17:44:57	0.0	Macassa
134	4/01/95	16:25:43	1.0	Macassa	161	8/26/95	18:12:29	0.4	Macassa
135	4/01/95	16:37:13	0.0	Macassa	162	8/27/95	15:02:28	2.4	Macassa
136	4/01/95	16:39:53	0.2	Macassa	163	8/28/95	10:02:56	2.9	Macassa
137	4/01/95	16:40:07	1.1	Macassa	164	8/28/95	10:03:48	1.1	Macassa
138	4/01/95	17:29:30	0.0	Macassa	165	8/28/95	10:05:24	0.3	Macassa
139	4/01/95	20:35:36	0.8	Macassa	166	8/28/95	10:11:56	0.8	Macassa
140	4/05/95	15:59:39	0.8	Macassa	167	8/29/95	02:52:35	1.2	Macassa
141	4/12/95	13:35:56	0.3	Macassa	168	8/29/95	22:00:26	1.1	Macassa
142	5/09/95	09:50:36	0.0	Macassa	169	9/15/95	16:44:38	0.4	Macassa
143	5/20/95	16:45:00	0.0	Macassa	170	9/18/95	01:11:46	0.7	Macassa
144	6/08/95	03:15:20	2.6	Macassa	171	9/18/95	15:40:45	1.4	Macassa
145	6/20/95	04:06:06	2.6	Macassa	172	9/23/95	03:13:32	0.4	Macassa
146	6/20/95	04:06:11	1.2	Macassa	173	10/30/95	03:19:08	1.0	Macassa
147	7/15/95	12:37:28	1.5	Macassa	174	10/11/95	21:38:54	0.2	Macassa
148	7/15/95	13:39:30	1.3	Macassa	175	10/16/95	23:04:30	0.4	Macassa
149	7/15/95	13:39:53	0.6	Macassa	176	10/29/95	01:38:10	0.2	Macassa
150	7/15/95	13:40:27	0.3	Macassa	177	10/29/95	11:51:21	0.3	Macassa
151	7/19/95	16:33:04	0.5	Macassa					

TABLE III Recorded seismic events in Ontario mines — Creighton Mine from 2/12/92 to 11/20/95 (updating: 11/20/95)

No.	Date	Time	Magnitude	Mine	No.	Date	Time	Magnitude	Mine
1	2/21/92	08:46:20	1.3-1.5	Creighton	62	6/07/92	22:28:55	0.5	Creighton
2	2/21/92	10:16:45	1.2-1.9	Creighton	63	6/08/92	06:42:29	0.7	Creighton
3	2/26/92	06:18:48	1.5-1.8	Creighton	64	6/10/92	01:40:53	0.6	Creighton
4	2/27/92	22:46:53	1.8-2.1	Creighton	65	6/10/92	09:29:18	1.0	Creighton
5	2/28/92	03:06:06	0.6	Creighton	66	6/10/92	09:36:54	1.4-1.8	Creighton
6	2/28/92	03:39:33	1.0	Creighton	67	6/11/92	18:44:25	0.8	Creighton
7	3/01/92	09:51:04	0.9	Creighton	68	6/20/92	10:53:15	1.1	Creighton
8	3/08/92	11:10:31	1.2-1.4	Creighton	69	6/21/92	00:16:33	1.0	Creighton
9	3/15/92	14:05:32	1.7-1.9	Creighton	70	6/21/92	10:58:10	1.0	Creighton
10	3/24/92	12:49:34	1.6-1.6	Creighton	71	6/23/92	14:05:52	0.8	Creighton
11	3/24/92	14:39:58	0.0	Creighton	72	6/23/92	14:05:54	0.7	Creighton
12	3/26/92	06:13:55	0.0	Creighton	73	6/29/92	01:45:27	1.1	Creighton
13	3/28/92	22:40:01	1.0	Creighton	74	7/01/92	22:17:41	1.2	Creighton
14	4/01/92	15:04:40	1.5-1.5	Creighton	75	7/03/92	14:17:23	0.8	Creighton
15	4/03/92	04:11:37	1.3	Creighton	76	7/04/92	04:05:50	0.9	Creighton
16	4/06/92	15:11:56	1.9-2.0	Creighton	77	7/07/92	04:50:33	0.6	Creighton
17	4/06/92	23:17:30	1.0-1.5	Creighton	78	7/08/92	12:57:41	1.4-1.4	Creighton
18	4/07/92	02:16:30	0.0	Creighton	79	7/29/92	07:57:28	0.5	Creighton
19	4/07/92	06:08:58	1.8-2.1	Creighton	80	7/29/92	20:28:33	0.6	Creighton
20	4/10/92	04:20:26	0.9	Creighton	81	8/02/92	02:47:56	0.8	Creighton
21	4/11/92	07:00:03	0.9	Creighton	82	8/09/92	01:15:50	0.8	Creighton
22	4/23/92	00:20:53	2.2-2.4	Creighton	83	8/20/92	01:38:11	1.1-1.4	Creighton
23	4/23/92	05:40:00	1.5-1.7	Creighton	84	8/20/92	21:50:10	0.6	Creighton
24	4/25/92	11:03:38	2.2-2.6	Creighton	85	8/23/92	04:26:33	0.6	Creighton
25	4/26/92	00:31:23	1.0	Creighton	86	8/23/92	06:58:16	0.7	Creighton
26	4/26/92	05:17:28	1.0	Creighton	87	8/23/92	16:00:56	0.8	Creighton
27	4/26/92	10:20:50	1.0	Creighton	88	8/28/92	04:11:01	1.1	Creighton
28	4/27/92	11:43:27	1.3	Creighton	89	8/28/92	10:56:15	0.3	Creighton
29	4/28/92	04:58:30	1.0	Creighton	90	9/02/92	21:10:47	1.0	Creighton
30	5/02/92	17:24:32	1.3	Creighton	91	9/03/92	18:49:34	0.6	Creighton
31	5/06/92	05:38:57	0.9	Creighton	92	9/03/92	22:39:06	2.2-2.4	Creighton
32	5/06/92	13:07:31	1.2	Creighton	93	9/03/92	22:39:13	0.9	Creighton
33	5/09/92	04:52:25	2.0-2.2	Creighton	94	9/03/92	22:39:36	1.2	Creighton
34	5/09/92	05:32:42	1.7	Creighton	95	9/04/92	09:11:07	0.9	Creighton
35	5/09/92	05:57:23	0.0	Creighton	96	9/04/92	09:13:23	1.5-1.5	Creighton
36	5/10/92	08:53:15	2.0-2.0	Creighton	97	9/05/92	01:21:08	1.8-1.5	Creighton
37	5/11/92	09:17:42	1.0-1.6	Creighton	98	9/06/92	03:49:58	1.0	Creighton
38	5/14/92	02:58:21	1.1	Creighton	99	9/06/92	22:54:36	0.6	Creighton
39	5/14/92	10:37:11	1.1-1.3	Creighton	100	9/07/92	99:19:16	0.6	Creighton
40	5/16/92	09:47:56	0.7	Creighton	101	9/07/92	16:33:16	1.6-1.7	Creighton
41	5/16/92	13:16:44	0.8	Creighton	102	9/11/92	07:11:03	1.5-1.4	Creighton
42	5/20/92	05:04:59	0.8	Creighton	103	9/11/92	14:23:08	1.0	Creighton
43	5/21/92	11:41:59	0.8	Creighton	104	9/11/92	18:22:26	1.6-1.7	Creighton
44	5/21/92	15:59:00	0.8	Creighton	105	9/11/92	19:40:21	0.9	Creighton
45	5/23/92	04:38:48	0.0	Creighton	106	9/12/92	01:26:03	1.6	Creighton
46	5/23/92	04:42:00	1.6	Creighton	107	9/15/92	10:52:10	0.7	Creighton
47	5/25/92	01:10:00	2.8-2.6	Creighton	108	9/15/92	12:37:33	0.7	Creighton
48	5/27/92	06:46:49	1.5-1.9	Creighton	109	9/15/92	19:28:59	0.9	Creighton
49	5/31/92	15:37:28	0.5	Creighton	110	9/16/92	22:50:00	1.8-2.4	Creighton
50	6/01/92	16:12:41	1.2	Creighton	111	9/17/92	17:51:27	1.5	Creighton
51	6/04/92	02:26:55	1.2-1.5	Creighton	112	9/18/92	03:20:21	0.6	Creighton
52	6/04/92	03:09:49	1.5-1.7	Creighton	113	9/18/92	17:43:31	0.9	Creighton
53	6/04/92	09:33:40	1.1	Creighton	114	9/18/92	18:20:35	1.2	Creighton
54	6/04/92	17:00:28	0.9	Creighton	115	9/18/92	23:44:41	0.8	Creighton
55	6/04/92	19:58:36	1.2	Creighton	116	9/22/92	15:13:45	0.7	Creighton
56	6/05/92	09:44:20	0.5	Creighton	117	9/22/92	21:30:00	1.4	Creighton
57	6/05/92	18:08:48	0.7	Creighton	118	9/23/92	07:22:19	1.0	Creighton
58	6/06/92	18:03:29	2.1-2.5	Creighton	119	9/24/92	09:26:39	1.4	Creighton
59	6/06/92	22:54:12	1.4-1.5	Creighton	120	9/24/92	10:45:26	1.3	Creighton
60	6/06/92	22:56:32	1.1	Creighton	121	9/27/92	11:56:46	1.1	Creighton
61	6/07/92	22:16:37	1.1	Creighton	122	9/28/92	15:26:02	0.9	Creighton

TABLE iii (cont'd.)

No.	Date	Time	Magnitude	Mine
123	9/29/92	16:07:08	1.2	Creighton
124	9/29/92	17:19:05	1.3	Creighton
125	9/30/92	14:57:13	0.9	Creighton
126	9/30/92	15:45:22	0.8	Creighton
127	9/30/92	15:58:31	0.5	Creighton
128	9/30/92	18:40:02	0.6	Creighton
129	10/01/92	02:22:36	1.8-1.8	Creighton
130	10/02/92	21:10:55	1.0	Creighton
131	10/03/92	03:28:32	0.4	Creighton
132	1/03/92	07:02:06	0.8	Creighton
133	10/03/92	10:15:38	0.9	Creighton
134	10/04/92	21:29:24	1.7-2.1	Creighton
135	10/06/92	15:57:36	1.2	Creighton
136	10/06/92	15:57:53	1.0	Creighton
137	10/06/92	16:18:41	0.7	Creighton
138	10/07/92	01:38:23	1.1	Creighton
139	10/08/92	14:06:56	1.6-1.9	Creighton
140	10/10/92	03:05:20	0.9	Creighton
141	10/10/92	20:59:06	1.1	Creighton
142	10/10/92	22:41:20	1.2	Creighton
143	10/11/92	15:10:07	0.0	Creighton
144	10/15/92	09:27:10	0.8	Creighton
145	10/17/92	10:37:23	0.8	Creighton
146	10/20/92	18:37:28	2.2-2.6	Creighton
147	10/20/92	19:14:45	0.8	Creighton
148	10/21/92	22:03:41	0.6	Creighton
149	10/22/92	21:47:59	1.0	Creighton
150	10/23/92	01:33:22	0.7	Creighton
151	10/23/92	07:41:53	0.8	Creighton
152	10/23/92	10:49:19	1.0	Creighton
153	10/23/92	11:21:01	0.7	Creighton
154	10/23/92	15:20:32	0.8	Creighton
155	10/26/92	09:18:52	0.8	Creighton
156	10/27/92	22:01:41	0.9	Creighton
157	10/28/92	21:09:24	1.0	Creighton
158	10/28/92	22:32:21	1.7-1.9	Creighton
159	10/29/92	06:19:45	1.6-1.5	Creighton
160	10/29/92	14:45:04	1.0	Creighton
161	10/29/92	17:29:43	0.9	Creighton
162	10/29/92	20:02:07	1.9-2.1	Creighton
163	10/31/92	12:04:25	1.8-2.1	Creighton
164	10/31/92	21:34:50	0.8	Creighton
165	11/01/92	18:54:16	1.1	Creighton
166	11/02/92	09:32:48	0.9	Creighton
167	11/03/92	05:19:37	1.4	Creighton
168	11/05/92	22:26:05	0.5	Creighton
169	11/06/92	09:13:36	0.8	Creighton
170	11/07/92	05:38:13	1.9-2.0	Creighton
171	11/07/92	05:50:17	1.2	Creighton
172	11/07/92	15:21:09	1.4	Creighton
173	11/08/92	12:46:13	1.4	Creighton
174	11/11/92	20:59:55	0.6	Creighton
175	11/13/92	21:18:14	0.9	Creighton
176	11/17/92	20:09:08	1.1	Creighton
177	11/17/92	22:25:49	1.2	Creighton
178	11/17/92	22:37:04	0.7	Creighton
179	11/19/92	17:11:43	0.6	Creighton
180	11/20/92	17:30:35	1.1	Creighton
181	11/20/92	17:31:20	0.5	Creighton
182	11/20/92	19:51:09	0.5	Creighton
183	11/20/92	19:51:09	0.5	Creighton
184	11/22/92	22:41:24	0.0	Creighton
185	11/24/92	04:16:07	0.4	Creighton
186	11/25/92	22:08:03	1.4	Creighton
187	11/27/92	23:49:12	1.2	Creighton
188	11/28/92	09:55:29	1.0	Creighton
189	11/28/92	15:14:13	0.8	Creighton
190	11/30/92	21:58:51	2.1	Creighton
191	11/30/92	22:45:15	1.1	Creighton
192	12/01/92	09:00:45	1.1	Creighton
193	12/04/92	15:42:12	2.0	Creighton
194	12/04/92	16:19:10	2.7-3.0	Creighton
195	12/04/92	16:19:16	0.8	Creighton
196	12/04/92	16:19:56	0.9	Creighton
197	12/04/92	21:38:26	0.9	Creighton
198	12/05/92	02:21:04	1.1	Creighton
199	12/05/92	18:25:37	0.6	Creighton
200	12/05/92	20:56:17	1.1	Creighton
201	12/06/92	01:26:20	1.1	Creighton
202	12/07/92	22:55:47	1.1	Creighton
203	12/08/92	01:18:00	0.7	Creighton
204	12/09/92	22:14:15	2.3-2.2	Creighton
204	12/10/92	21:36:24	1.6	Creighton
206	12/17/92	13:21:38	2.1-2.6	Creighton
207	12/17/92	22:38:18	1.1	Creighton
208	12/19/92	16:05:57	1.4	Creighton
209	12/21/92	08:01:42	0.4	Creighton
210	12/21/92	21:18:04	0.3	Creighton
211	12/24/92	17:23:17	0.6	Creighton
212	12/27/92	07:18:14	0.9	Creighton
213	12/29/92	08:15:21	0.5	Creighton
214	1/01/93	05:42:50	0.7	Creighton
215	1/03/93	18:27:05	0.8	Creighton
216	1/05/93	21:17:40	0.6	Creighton
217	1/09/93	16:29:56	0.7	Creighton
218	1/09/93	20:15:38	0.4	Creighton
219	1/11/93	06:34:51	0.6	Creighton
220	1/11/93	10:11:25	0.9	Creighton
221	1/11/93	19:02:27	1.1	Creighton
222	1/12/93	06:13:42	1.3	Creighton
223	1/12/93	23:32:54	0.8	Creighton
224	1/15/93	00:07:22	0.7	Creighton
225	1/23/93	21:16:16	1.2	Creighton
226	1/29/93	11:19:28	0.6	Creighton
227	2/06/93	10:03:03	1.6-1.8	Creighton
228	2/07/93	03:11:06	1.4-1.9	Creighton
229	2/09/93	02:21:29	0.8	Creighton
230	2/09/93	05:19:01	0.8	Creighton
231	2/09/93	17:57:45	0.8	Creighton
232	2/10/93	20:32:55	0.9	Creighton
233	2/10/93	22:56:05	1.1	Creighton
234	2/11/93	00:39:49	1.4	Creighton
235	2/11/93	00:39:55	0.8	Creighton
236	2/16/93	06:32:24	1.2	Creighton
237	2/16/93	16:28:49	1.0	Creighton
238	2/18/93	18:06:58	1.1	Creighton
239	2/20/93	20:33:56	0.8	Creighton
240	2/21/93	22:07:40	1.6-1.6	Creighton
241	2/22/93	13:32:05	1.3	Creighton
242	2/23/93	09:54:16	1.2	Creighton
243	2/23/93	20:24:34	0.7	Creighton
244	2/25/93	12:50:11	0.8	Creighton
245	2/25/93	22:00:13	1.2	Creighton
246	2/26/93	22:57:18	1.1	Creighton

TABLE iii (cont'd.)

No.	Date	Time	Magnitude	Mine
247	2/27/93	11:35:56	0.9	Creighton
248	2/27/93	19:12:57	1.2	Creighton
249	2/27/93	19:13:17	1.0	Creighton
250	3/01/93	00:00:41	1.0	Creighton
251	3/01/93	23:22:14	1.3	Creighton
252	3/03/93	10:49:50	1.1	Creighton
253	3/04/93	21:33:45	0.6	Creighton
254	3/05/93	01:52:17	1.2	Creighton
255	3/10/93	04:31:03	1.2	Creighton
256	3/13/93	04:03:37	0.8	Creighton
257	3/16/93	02:22:02	2.0-2.2	Creighton
258	3/16/93	02:24:29	1.5	Creighton
259	3/16/93	13:33:13	0.9	Creighton
260	3/21/93	10:42:21	1.1	Creighton
261	3/21/93	10:52:18	1.0	Creighton
262	3/24/93	01:39:39	1.6	Creighton
263	3/26/93	03:46:18	0.9	Creighton
264	3/29/93	18:09:58	1.2	Creighton
265	3/30/93	03:02:21	1.0	Creighton
266	4/01/93	19:14:03	2.1-2.1	Creighton
267	4/01/93	20:51:22	1.1	Creighton
268	4/02/93	02:14:51	1.2	Creighton
269	4/02/93	14:23:13	2.9-2.9	Creighton
270	4/02/93	14:27:43	1.5	Creighton
271	4/02/93	14:35:28	1.3	Creighton
272	4/02/93	22:55:24	1.3	Creighton
273	4/03/93	02:16:59	0.8	Creighton
274	4/03/93	09:56:25	1.1	Creighton
275	4/03/93	22:25:59	1.5	Creighton
276	4/03/93	22:50:57	0.7	Creighton
277	4/04/93	06:21:48	0.6	Creighton
278	4/05/93	14:27:18	0.7	Creighton
279	4/05/93	21:56:12	1.0	Creighton
280	4/18/93	04:15:33	0.8	Creighton
281	4/18/93	08:36:49	1.2	Creighton
282	4/19/93	23:12:57	0.9	Creighton
283	4/23/93	16:31:20	1.4	Creighton
284	4/28/93	08:03:23	1.5	Creighton
285	4/29/93	02:45:32	1.4	Creighton
286	4/29/93	15:26:12	1.8	Creighton
287	4/29/93	17:02:55	0.7	Creighton
288	5/06/93	06:49:25	1.1	Creighton
289	5/07/93	01:01:30	1.2	Creighton
290	5/07/93	14:15:26	0.5	Creighton
291	5/08/93	13:44:26	1.3	Creighton
292	5/08/93	14:57:12	1.9-1.9	Creighton
293	5/08/93	15:17:49	1.4	Creighton
294	5/08/93	20:12:41	2.6-2.5	Creighton
295	5/11/93	22:36:36	1.2	Creighton
296	5/12/93	21:03:21	1.5	Creighton
297	5/13/93	04:37:55	0.9	Creighton
298	5/13/93	12:40:10	0.7	Creighton
299	5/14/93	08:05:12	1.8	Creighton
300	5/14/93	08:07:12	1.8	Creighton
301	5/14/93	10:11:45	1.1	Creighton
302	5/16/93	18:35:10	0.7	Creighton
303	5/22/93	07:42:45	0.5	Creighton
304	5/23/93	10:16:33	0.8	Creighton
305	5/24/93	01:59:03	1.1	Creighton
306	5/25/93	01:58:29	1.0	Creighton
307	5/26/93	19:27:55	1.0	Creighton
308	5/30/93	18:05:06	0.5	Creighton
309	6/03/93	03:20:11	1.1	Creighton
310	6/04/93	04:40:44	1.2	Creighton
311	6/05/93	22:13:06	1.5	Creighton
312	6/06/93	22:19:45	0.4	Creighton
313	6/07/93	04:41:37	0.9	Creighton
314	6/07/93	13:31:47	0.9	Creighton
315	6/08/93	17:02:10	1.5-2.0	Creighton
316	6/08/93	18:47:32	0.6	Creighton
317	6/09/93	21:56:28	1.4	Creighton
318	6/10/93	03:06:26	1.1	Creighton
319	6/10/93	12:13:27	1.3	Creighton
320	6/11/93	19:55:42	0.5	Creighton
321	6/11/93	21:03:34	1.4	Creighton
322	6/14/93	06:56:22	0.7	Creighton
323	6/14/93	07:05:38	0.9	Creighton
324	6/15/93	00:39:38	1.1	Creighton
325	6/15/93	14:32:39	2.6-2.7	Creighton
326	6/15/93	15:15:48	1.0	Creighton
327	6/15/93	22:43:29	1.5	Creighton
328	6/18/93	07:41:44	0.8	Creighton
329	6/22/93	07:50:48	1.8	Creighton
330	6/22/93	10:44:04	0.6	Creighton
331	6/22/93	15:37:01	0.6	Creighton
332	6/22/93	15:46:12	0.8	Creighton
333	6/23/93	03:36:41	0.0	Creighton
334	7/05/93	08:17:30	1.5-1.4	Creighton
335	7/05/93	19:02:11	1.4-1.5	Creighton
336	7/07/93	08:13:14	1.2	Creighton
337	7/09/93	20:24:50	1.2	Creighton
338	7/10/93	10:29:11	1.1	Creighton
339	7/27/93	11:52:43	—	Creighton
340	7/28/93	14:33:04	1.7-2.3	Creighton
341	8/01/93	01:05:54	1.0	Creighton
342	8/04/93	07:03:35	1.1	Creighton
343	8/05/93	17:55:02	1.2	Creighton
344	8/05/93	22:39:51	3.1-2.9	Creighton
345	8/05/93	22:41:36	1.3	Creighton
346	8/06/93	04:40:53	0.8	Creighton
347	8/06/93	06:48:22	1.6	Creighton
348	8/07/93	21:18:36	2.1-2.2	Creighton
349	8/08/93	20:02:41	1.0	Creighton
350	8/09/93	10:17:16	0.9	Creighton
351	8/09/93	10:51:21	1.0	Creighton
352	8/10/93	00:58:59	0.3	Creighton
353	8/10/93	02:51:10	1.7	Creighton
354	8/10/93	11:57:23	0.9	Creighton
355	8/10/93	21:16:58	0.9	Creighton
356	8/11/93	00:43:17	1.0	Creighton
357	8/11/93	02:29:46	1.5	Creighton
358	8/11/93	04:35:36	1.2	Creighton
359	8/11/93	09:07:08	1.0	Creighton
360	8/12/93	09:26:57	1.3	Creighton
361	8/12/93	22:44:37	1.2	Creighton
362	8/13/93	11:11:19	1.3	Creighton
363	8/13/93	18:24:08	1.7	Creighton
364	8/15/93	01:03:18	1.5	Creighton
365	8/17/93	02:58:06	1.3	Creighton
366	8/19/93	22:49:11	2.0-1.7	Creighton
367	8/19/93	22:50:12	1.4	Creighton
368	8/21/93	01:05:35	1.2	Creighton
369	8/23/93	08:35:55	1.6	Creighton
370	8/25/93	00:01:23	1.3	Creighton
371	8/25/93	00:08:22	1.1	Creighton
372	8/26/93	03:58:24	1.1	Creighton

TABLE iii (cont'd.)

No.	Date	Time	Magnitude	Mine
373	8/27/93	13:38:16	0.8	Creighton
374	8/27/93	17:33:58	1.1	Creighton
375	8/28/93	07:58:07	0.9	Creighton
376	8/29/93	12:57:32	0.9	Creighton
377	8/29/93	12:57:32	1.2	Creighton
378	9/03/93	14:00:25	1.9	Creighton
379	9/03/93	14:16:25	0.9	Creighton
380	9/03/93	22:47:48	1.4	Creighton
381	9/04/93	05:39:18	1.4	Creighton
382	9/04/93	06:08:28	1.2	Creighton
383	9/06/93	01:58:44	1.3	Creighton
384	9/06/93	03:12:22	1.3	Creighton
385	9/09/93	03:17:48	1.3	Creighton
386	9/09/93	04:52:07	1.6	Creighton
387	9/13/93	23:59:07	2.3	Creighton
388	9/15/93	07:58:45	1.0	Creighton
389	9/15/93	15:24:21	0.9	Creighton
390	9/16/93	02:02:43	0.4	Creighton
391	9/16/93	21:50:15	0.7	Creighton
392	9/17/93	05:42:32	1.4	Creighton
393	9/19/93	13:17:44	0.5	Creighton
394	9/22/93	14:39:40	1.1	Creighton
395	9/22/93	14:57:06	0.8	Creighton
396	9/22/93	16:05:50	1.6	Creighton
397	9/22/93	19:16:39	1.0	Creighton
398	9/25/93	11:34:43	0.4	Creighton
399	9/25/93	13:12:55	1.1	Creighton
400	9/25/93	20:37:24	1.9-1.8	Creighton
401	9/27/93	03:28:29	1.4	Creighton
402	9/27/93	08:25:21	1.5	Creighton
403	9/27/93	23:48:28	1.1	Creighton
404	9/30/93	02:43:55	0.7	Creighton
405	9/30/93	11:52:19	1.0	Creighton
406	9/30/93	15:48:56	1.2	Creighton
407	10/01/93	14:20:22	0.8	Creighton
408	10/01/93	22:41:23	0.7	Creighton
409	10/02/93	00:40:28	0.9	Creighton
410	10/02/93	00:06:39	1.9	Creighton
411	10/02/93	03:28:47	1.4	Creighton
412	10/04/93	21:01:26	1.2	Creighton
413	10/04/93	22:18:27	0.7	Creighton
414	10/05/93	16:10:04	1.2	Creighton
415	10/05/93	17:09:53	0.9	Creighton
416	10/05/93	20:12:12	0.7	Creighton
417	10/06/93	15:15:14	0.8	Creighton
418	10/07/93	22:38:23	0.7	Creighton
419	10/08/93	16:18:17	1.1	Creighton
420	10/08/93	19:46:22	0.8	Creighton
421	10/09/93	13:43:56	1.0	Creighton
422	10/11/93	23:24:31	0.9	Creighton
423	10/12/93	16:19:54	2.6-2.6	Creighton
424	10/13/93	00:27:50	1.2	Creighton
425	10/14/93	06:47:23	0.7	Creighton
426	10/14/93	09:41:58	1.4	Creighton
427	10/14/93	21:20:26	1.0	Creighton
428	10/14/93	22:01:40	1.0	Creighton
429	10/15/93	21:38:55	0.6	Creighton
430	10/16/93	18:09:30	1.4	Creighton
431	10/17/93	04:44:30	2.1-1.5	Creighton
432	10/18/93	12:03:34	1.2	Creighton
433	10/19/93	22:23:04	2.0-2.2	Creighton
434	10/20/93	21:53:07	1.0	Creighton
435	10/22/93	08:58:09	1.8	Creighton
436	10/22/93	17:47:07	1.0	Creighton
437	10/23/93	02:26:55	1.2	Creighton
438	10/25/93	06:30:44	0.8	Creighton
439	10/26/93	04:50:27	1.1	Creighton
440	10/26/93	20:56:17	1.8	Creighton
441	10/26/93	20:57:39	0.9	Creighton
442	10/29/93	05:30:09	0.9	Creighton
443	10/29/93	05:32:44	0.7	Creighton
444	11/01/93	23:15:25	1.1	Creighton
445	11/03/93	02:34:37	0.7	Creighton
446	11/03/93	17:17:01	0.9	Creighton
447	11/05/93	03:43:21	1.8-2.4	Creighton
448	11/05/93	04:54:39	0.9	Creighton
449	11/05/93	13:10:23	1.0	Creighton
450	11/05/93	22:23:22	2.8-2.8	Creighton
451	11/05/93	22:23:28	1.1	Creighton
452	11/05/93	22:24:21	1.0	Creighton
453	11/05/93	22:25:33	0.7	Creighton
454	11/05/93	23:00:12	1.3	Creighton
455	11/06/93	06:11:39	0.8	Creighton
456	11/06/93	06:12:04	1.1	Creighton
457	11/06/93	10:37:31	1.3	Creighton
458	11/07/93	04:12:14	1.3	Creighton
459	11/07/93	05:17:10	1.1	Creighton
460	11/08/93	00:14:57	1.2	Creighton
461	11/08/93	00:36:58	1.0	Creighton
462	11/09/93	12:47:35	0.7	Creighton
463	11/10/93	13:08:55	1.0	Creighton
464	11/11/93	08:05:22	1.1	Creighton
465	11/12/93	20:59:00	0.9	Creighton
466	11/14/93	10:16:05	0.9	Creighton
467	11/16/93	21:42:18	0.7	Creighton
468	11/18/93	15:35:34	0.3	Creighton
469	11/19/93	15:54:34	1.5	Creighton
470	11/20/93	07:22:39	1.4	Creighton
471	11/22/93	13:26:14	1.3	Creighton
472	11/24/93	08:42:19	1.1	Creighton
473	11/24/93	13:42:00	0.7	Creighton
474	11/24/93	22:31:07	1.0	Creighton
475	11/24/93	22:47:05	0.6	Creighton
476	11/25/93	14:10:33	1.0	Creighton
477	11/25/93	14:18:46	1.3	Creighton
478	11/29/93	23:47:19	0.7	Creighton
479	11/30/93	01:09:34	0.4	Creighton
480	11/30/93	17:28:51	1.5-1.9	Creighton
481	12/02/93	12:06:13	2.2-2.5	Creighton
482	12/02/93	13:41:10	2.4-2.6	Creighton
483	12/03/93	00:31:07	1.4	Creighton
484	12/03/93	10:24:13	0.6	Creighton
485	12/08/93	19:49:21	1.0	Creighton
486	12/11/93	11:06:00	1.3	Creighton
487	12/11/93	13:29:00	0.8	Creighton
488	12/20/93	02:41:11	1.6	Creighton
489	12/20/93	15:01:10	0.7	Creighton
490	12/21/93	08:34:35	0.7	Creighton
491	12/28/93	03:52:33	0.8	Creighton
492	12/29/93	09:59:14	1.0	Creighton
493	12/29/93	22:33:06	0.8	Creighton
494	1/05/94	08:21:24	0.9	Creighton
495	1/06/94	10:31:26	1.8	Creighton
496	1/18/94	12:31:55	1.4	Creighton
497	1/18/94	12:40:20	0.9	Creighton
498	1/19/94	01:18:26	1.8	Creighton
499	1/19/94	14:28:18	1.7	Creighton

TABLE iii (cont'd.)

No.	Date	Time	Magnitude	Mine	No.	Date	Time	Magnitude	Mine
500	1/22/94	22:41:40	1.0	Creighton	563	6/18/94	03:26:26	0.5	Creighton
501	1/25/94	17:05:44	2.0	Creighton	564	6/21/94	17:41:02	1.0	Creighton
502	2/03/94	01:04:00	1.2	Creighton	565	6/24/94	06:56:03	0.6	Creighton
503	2/15/94	01:42:23	0.4	Creighton	566	6/30/94	01:43:02	0.4	Creighton
504	2/16/94	07:55:58	1.2	Creighton	567	6/30/94	01:44:57	1.0	Creighton
505	3/07/94	13:46:05	0.6	Creighton	567	6/30/94	16:54:36	1.0	Creighton
506	3/09/94	11:01:30	1.2	Creighton	568	7/01/94	14:57:11	1.1	Creighton
507	3/09/94	22:11:17	1.4	Creighton	569	7/05/94	13:51:54	1.1	Creighton
508	3/13/94	20:32:02	1.8	Creighton	570	7/11/94	10:56:54	1.1	Creighton
509	3/14/94	09:37:30	0.3	Creighton	571	7/11/94	22:47:57	1.2	Creighton
510	3/17/94	18:32:22	0.3	Creighton	572	7/28/94	05:45:10	1.2	Creighton
511	3/19/94	04:44:39	0.8	Creighton	573	7/28/94	13:10:42	1.0	Creighton
512	3/19/94	21:05:26	1.6	Creighton	574	7/28/94	22:50:02	1.4	Creighton
513	3/22/94	22:12:21	1.1	Creighton	575	7/30/94	06:42:05	0.8	Creighton
514	3/25/94	22:24:48	0.2	Creighton	576	7/30/94	20:41:25	1.1	Creighton
515	3/26/94	13:09:07	1.4	Creighton	577	8/01/94	23:43:39	1.1	Creighton
516	3/28/94	07:28:06	1.3	Creighton	578	8/06/94	06:11:36	1.0	Creighton
517	3/31/94	08:11:08	2.5-2.3	Creighton	579	8/07/94	00:44:16	1.6	Creighton
518	3/31/94	14:02:11	0.8	Creighton	580	8/07/94	01:02:56	0.4	Creighton
519	4/01/94	03:57:48	1.1	Creighton	581	8/07/94	15:25:06	1.2	Creighton
520	4/01/94	06:17:55	1.0	Creighton	582	8/07/94	23:08:18	0.0	Creighton
521	4/02/94	08:26:30	2.3-2.0	Creighton	583	8/07/94	23:17:47	1.8-1.6	Creighton
522	4/02/94	13:32:28	1.5	Creighton	584	8/08/94	15:41:05	0.4	Creighton
523	4/16/94	01:46:16	0.8	Creighton	585	8/09/94	11:06:53	1.7	Creighton
524	4/22/94	04:04:49	0.3	Creighton	586	8/09/94	15:36:34	0.9	Creighton
525	4/26/94	04:20:59	0.7	Creighton	587	8/09/94	18:39:11	0.5	Creighton
526	4/30/94	17:58:30	0.9	Creighton	588	8/11/94	14:10:33	1.4	Creighton
527	5/07/94	00:33:17	0.6	Creighton	589	8/12/94	23:15:02	1.4	Creighton
528	5/09/94	13:31:21	0.7	Creighton	590	8/13/94	01:00:58	1.7	Creighton
529	5/10/94	23:07:41	0.8	Creighton	591	8/15/94	20:51:42	1.2	Creighton
530	5/12/94	14:52:05	0.5	Creighton	592	8/16/94	22:51:01	0.5	Creighton
531	5/13/94	06:17:48	1.1	Creighton	593	8/18/94	22:44:22	1.0	Creighton
532	5/14/94	02:39:22	0.7	Creighton	594	8/22/94	10:59:55	0.5	Creighton
533	5/14/94	12:59:35	2.4-2.6	Creighton	595	8/23/94	22:52:14	0.7	Creighton
534	5/14/94	15:49:16	1.3	Creighton	596	8/24/94	13:34:14	0.0	Creighton
535	5/14/94	23:35:00	1.0	Creighton	597	8/24/94	19:22:07	0.8	Creighton
536	5/15/94	06:14:59	0.7	Creighton	598	8/25/94	03:46:49	1.3	Creighton
537	5/16/94	03:23:44	1.3	Creighton	599	8/25/94	07:43:24	1.0	Creighton
538	5/16/94	03:23:50	1.0	Creighton	600	8/26/94	08:17:15	0.5	Creighton
539	5/16/94	09:08:18	1.4	Creighton	601	8/26/94	08:19:35	0.6	Creighton
540	5/17/94	01:03:44	1.6-1.9	Creighton	602	8/30/94	12:10:54	0.8	Creighton
541	5/18/94	08:50:03	0.8	Creighton	603	8/30/94	12:18:54	1.2	Creighton
542	5/19/94	03:26:33	0.9	Creighton	604	8/30/94	14:58:07	2.0-1.7	Creighton
543	5/20/94	13:42:11	0.9	Creighton	605	8/30/94	15:34:27	1.5	Creighton
544	5/23/94	04:05:28	0.8	Creighton	606	8/30/94	21:35:45	0.7	Creighton
545	5/23/94	18:05:06	1.2	Creighton	607	8/31/94	03:17:04	2.9-3.1	Creighton
546	5/24/94	19:05:39	0.5	Creighton	608	8/31/94	18:17:17	1.2	Creighton
547	5/26/94	14:49:13	0.8	Creighton	609	9/01/94	11:11:12	0.9	Creighton
548	5/28/94	12:46:13	0.7	Creighton	610	9/04/94	11:51:43	1.2	Creighton
549	5/28/94	12:49:30	0.4	Creighton	611	9/04/94	15:07:35	1.0	Creighton
550	6/02/94	12:39:06	0.9	Creighton	612	9/05/94	05:33:53	0.8	Creighton
551	6/06/94	22:05:11	0.5	Creighton	613	9/05/94	21:41:50	0.9	Creighton
552	6/07/94	03:05:30	1.6	Creighton	614	9/07/94	03:29:52	0.9	Creighton
553	6/07/94	07:53:22	0.7	Creighton	615	9/07/94	18:44:50	1.4	Creighton
554	6/08/94	10:30:28	0.3	Creighton	616	9/08/94	23:04:48	0.8	Creighton
555	6/09/94	21:08:14	1.2	Creighton	617	9/08/94	23:11:43	0.7	Creighton
556	6/11/94	05:45:55	1.0	Creighton	618	9/09/94	12:29:23	0.9	Creighton
557	6/11/94	14:01:16	1.1	Creighton	619	9/10/94	17:43:44	0.6	Creighton
558	6/11/94	17:17:31	1.2	Creighton	620	9/11/94	02:27:57	1.2	Creighton
559	6/11/94	18:14:36	1.2	Creighton	621	9/15/94	13:30:25	1.4	Creighton
560	6/11/94	21:07:36	0.7	Creighton	622	9/15/94	23:12:33	1.3	Creighton
561	6/15/94	18:39:15	0.7	Creighton	623	9/17/94	10:07:58	1.2	Creighton
562	6/17/94	23:51:36	0.8	Creighton	624	9/20/94	09:13:08	3.2-3.0	Creighton

TABLE iii (cont'd.)

No.	Date	Time	Magnitude	Mine
625	9/20/94	09:13:22	2.0	Creighton
626	9/20/94	09:13:43	0.9	Creighton
627	9/20/94	09:26:51	0.9	Creighton
628	9/20/94	09:31:15	0.6	Creighton
629	9/20/94	18:00:20	0.9	Creighton
630	9/20/94	21:15:45	1.6	Creighton
631	9/20/94	21:16:51	1.2	Creighton
632	9/20/94	21:39:52	0.9	Creighton
633	9/21/94	02:26:19	2.5	Creighton
634	9/21/94	02:28:33	1.0	Creighton
635	9/21/94	02:57:18	0.4	Creighton
636	9/21/94	22:15:44	1.1	Creighton
637	9/23/94	21:01:37	0.8	Creighton
638	9/23/94	22:36:30	0.7	Creighton
639	9/24/94	01:04:37	1.1	Creighton
640	9/24/94	01:11:03	0.6	Creighton
641	9/24/94	01:52:01	0.9	Creighton
642	9/25/94	13:08:23	0.8	Creighton
643	9/28/94	15:34:48	1.3	Creighton
644	9/29/94	00:54:58	0.7	Creighton
645	9/30/94	06:52:12	0.9	Creighton
646	9/30/94	20:06:38	1.0	Creighton
647	10/01/94	10:34:59	0.8	Creighton
648	10/02/94	04:21:55	0.8	Creighton
649	10/02/94	21:37:51	1.0	Creighton
650	10/02/94	23:27:48	1.2	Creighton
651	10/03/94	00:55:24	3.0-2.9	Creighton
652	10/03/94	00:55:34	1.3	Creighton
653	10/03/94	01:44:13	1.0	Creighton
654	10/03/94	01:46:34	1.4	Creighton
655	10/03/94	02:17:26	0.9	Creighton
656	10/03/94	02:19:30	1.0	Creighton
657	10/03/94	04:06:44	1.4	Creighton
658	10/03/94	06:34:08	0.9	Creighton
659	10/03/94	06:35:25	1.1	Creighton
660	10/03/94	08:22:05	1.1	Creighton
661	10/03/94	10:13:28	1.6	Creighton
662	10/03/94	13:02:13	0.7	Creighton
663	10/05/94	11:17:35	1.2	Creighton
664	10/05/94	12:44:33	1.0	Creighton
665	10/05/94	21:44:47	0.6	Creighton
666	10/05/94	22:50:48	1.4	Creighton
667	10/05/94	23:05:24	0.6	Creighton
668	10/06/94	06:38:41	1.2	Creighton
669	10/07/94	08:45:54	1.4	Creighton
670	10/07/94	09:46:41	1.1	Creighton
671	10/07/94	22:56:39	0.8	Creighton
672	10/08/94	03:07:41	1.2	Creighton
673	10/08/94	04:44:30	1.0	Creighton
674	10/08/94	18:26:45	0.7	Creighton
675	10/09/94	18:24:10	1.3	Creighton
676	10/09/94	22:18:09	1.5	Creighton
677	10/11/94	07:39:03	1.4	Creighton
678	10/12/94	13:48:39	0.6	Creighton
679	10/12/94	15:24:41	1.1	Creighton
680	10/13/93	09:16:29	1.0	Creighton
681	10/14/94	07:29:55	1.1	Creighton
682	10/15/94	23:25:21	1.0	Creighton
683	10/16/94	22:00:45	1.0	Creighton
684	10/18/94	22:52:34	0.5	Creighton
685	10/19/94	03:40:22	0.9	Creighton
686	10/21/94	04:54:34	1.2	Creighton
687	10/23/94	04:54:51	2.5-2.5	Creighton
688	10/23/94	23:19:47	1.6-1.5	Creighton
689	10/26/94	15:36:02	1.2	Creighton
689	10/26/94	19:56:39	0.6	Creighton
690	11/01/94	19:38:13	0.8	Creighton
691	11/02/94	09:15:44	1.6	Creighton
692	11/03/94	17:35:32	1.0	Creighton
693	11/14/94	17:16:29	1.0	Creighton
694	11/15/94	03:36:07	0.2	Creighton
695	11/18/94	14:52:22	1.0	Creighton
696	11/20/94	15:12:06	0.9	Creighton
697	11/20/94	17:54:29	0.8	Creighton
698	11/20/94	23:14:02	0.4	Creighton
699	11/21/94	15:01:06	1.2	Creighton
700	11/23/94	02:52:42	0.6	Creighton
701	11/23/94	02:56:46	0.7	Creighton
702	11/23/94	20:41:19	1.1	Creighton
703	11/23/94	22:33:38	1.3	Creighton
704	11/23/94	22:48:42	0.6	Creighton
705	11/24/94	20:00:14	1.5	Creighton
706	11/25/94	02:39:35	1.0	Creighton
707	11/30/94	19:37:28	0.8	Creighton
708	12/05/94	08:24:37	2.7-2.6	Creighton
709	12/05/94	08:24:43	1.1	Creighton
710	12/07/94	01:44:27	1.1	Creighton
711	12/07/94	05:35:40	0.9	Creighton
712	12/09/94	08:52:46	1.9-2.0	Creighton
713	12/10/94	00:38:22	0.7	Creighton
714	12/11/94	11:10:53	1.2	Creighton
715	12/13/94	22:58:26	1.1	Creighton
716	12/18/94	17:50:54	3.0-2.8	Creighton
717	12/19/94	11:02:41	2.1-1.6	Creighton
718	12/19/94	23:50:39	2.4-1.6	Creighton
719	12/19/94	23:51:16	0.9	Creighton
720	12/20/94	16:19:16	1.5	Creighton
721	12/22/94	03:27:36	1.1	Creighton
722	12/22/94	04:56:34	1.1	Creighton
723	12/22/94	08:15:45	0.4	Creighton
724	12/24/94	06:57:23	0.6	Creighton
725	1/05/95	04:06:01	0.7	Creighton
726	1/07/95	14:03:36	0.8	Creighton
727	1/ 9/95	11:17:48	0.9	Creighton
728	1/13/95	12:24:42	1.1	Creighton
729	1/13/95	21:30:46	1.4	Creighton
730	1/15/95	11:11:06	0.5	Creighton
731	1/15/95	11:26:12	0.9	Creighton
732	1/17/95	10:58:57	0.7	Creighton
733	1/30/95	20:09:22	1.0	Creighton
734	1/30/95	20:16:19	0.7	Creighton
735	2/03/95	06:05:33	1.0	Creighton
736	2/04/95	10:12:57	1.1	Creighton
737	2/05/95	10:25:18	1.4	Creighton
738	2/07/95	21:24:59	1.2	Creighton
739	2/09/95	21:49:47	1.3	Creighton
740	2/10/95	15:15:22	1.8-1.9	Creighton
741	2/11/95	12:35:53	1.2	Creighton
742	2/13/95	04:23:29	0.7	Creighton
743	2/14/95	05:52:52	0.0	Creighton
744	2/15/95	13:44:01	0.9	Creighton
745	2/16/95	07:19:11	0.5	Creighton
746	2/16/95	12:23:47	0.2	Creighton
747	2/16/95	21:32:26	0.2	Creighton
748	2/20/95	18:11:38	1.0	Creighton
749	2/20/95	21:14:29	1.6	Creighton

TABLE iii (cont'd.)

No.	Date	Time	Magnitude	Mine	No.	Date	Time	Magnitude	Mine
750	2/20/95	22:16:19	1.2	Creighton	812	5/06/95	21:41:03	1.5-1.7	Creighton
751	2/21/95	15:51:02	1.6	Creighton	813	5/09/95	05:11:39	1.4-1.5	Creighton
752	2/23/95	05:53:32	1.0	Creighton	814	5/09/95	20:56:20	1.4	Creighton
753	2/23/95	15:13:30	0.7	Creighton	815	5/10/95	10:44:07	1.6	Creighton
754	2/23/95	21:21:08	0.9	Creighton	816	5/10/95	10:16:45	1.0	Creighton
755	2/25/95	11:40:43	1.1	Creighton	817	5/12/95	04:34:57	1.7-1.8	Creighton
756	2/26/95	21:04:30	0.7	Creighton	818	5/21/95	19:39:22	1.2	Creighton
757	2/28/95	02:03:08	0.9	Creighton	819	5/24/95	02:48:14	0.7	Creighton
758	2/28/95	16:22:13	0.6	Creighton	820	5/24/95	09:04:02	0.4	Creighton
759	2/28/95	23:06:53	1.5	Creighton	821	5/25/95	08:14:56	1.7-1.8	Creighton
760	3/02/95	04:47:54	3.7-3.6	Creighton	821	5/25/95	16:06:21	1.3	Creighton
761	3/02/95	05:46:08	0.8	Creighton	822	5/26/95	09:41:27	1.1	Creighton
762	3/02/95	05:51:09	1.1	Creighton	823	5/27/95	19:36:25	1.0	Creighton
763	3/02/95	07:33:22	1.5	Creighton	824	5/27/95	20:52:58	1.3	Creighton
764	3/02/95	08:57:15	1.9	Creighton	825	6/01/95	21:14:15	2.0-2.0	Creighton
765	3/02/95	09:46:07	1.5	Creighton	826	6/01/95	21:14:56	1.2	Creighton
766	3/03/95	14:38:25	0.8	Creighton	827	6/04/95	04:38:08	1.0	Creighton
767	3/04/95	18:58:14	1.0	Creighton	828	6/06/95	08:27:52	1.7-2.2	Creighton
768	3/04/95	19:05:56	1.3	Creighton	829	6/06/95	21:37:03	1.3	Creighton
769	3/05/95	11:31:05	0.7	Creighton	830	6/12/95	17:03:21	1.1	Creighton
770	3/06/95	12:05:05	0.9	Creighton	831	6/13/95	15:07:52	1.0	Creighton
770	3/06/95	12:05:35	0.9	Creighton	833	6/14/95	16:30:36	1.2	Creighton
771	3/06/95	15:11:48	0.5	Creighton	834	6/17/95	22:55:36	0.7	Creighton
772	3/06/95	16:21:10	0.8	Creighton	835	6/18/95	20:19:35	0.6	Creighton
773	3/07/95	11:51:39	0.9	Creighton	836	6/19/95	01:52:04	1.0	Creighton
774	3/07/95	15:47:05	1.7	Creighton	837	6/19/95	04:08:11	0.9	Creighton
775	3/08/95	14:13:08	0.8	Creighton	838	6/21/95	23:05:07	0.9	Creighton
776	3/08/95	14:19:39	0.5	Creighton	839	6/25/95	09:16:54	1.7-1.9	Creighton
777	3/09/95	07:04:54	1.2	Creighton	840	6/28/95	02:37:43	0.7	Creighton
778	3/09/95	10:23:45	1.6	Creighton	841	7/07/95	00:00:25	1.0	Creighton
779	3/10/95	01:22:10	1.5	Creighton	842	7/07/95	05:52:28	1.0	Creighton
780	3/10/95	04:58:47	0.4	Creighton	843	7/08/95	14:22:22	1.0	Creighton
780	3/10/95	11:17:52	1.4	Creighton	844	7/16/95	05:38:20	1.3	Creighton
781	3/10/95	22:25:44	2.1-2.3	Creighton	845	7/24/95	21:26:47	1.4	Creighton
782	3/11/95	05:29:41	2.1-2.4	Creighton	846	7/27/95	04:08:13	0.7	Creighton
783	3/11/95	06:39:52	1.0	Creighton	847	7/29/95	06:12:48	0.8	Creighton
784	3/11/95	09:53:59	2.5-2.3	Creighton	848	7/31/95	05:45:30	0.9	Creighton
785	3/11/95	19:31:25	2.1-1.6	Creighton	849	7/31/95	11:33:33	1.5	Creighton
786	3/14/95	05:42:26	1.4	Creighton	850	7/31/95	13:41:05	1.4	Creighton
787	3/15/95	22:01:23	1.0	Creighton	851	8/01/95	06:21:22	0.7	Creighton
788	3/16/95	15:47:03	0.4	Creighton	852	8/01/95	14:26:03	1.1	Creighton
789	3/16/95	20:06:25	0.9	Creighton	853	8/02/95	05:08:06	0.8	Creighton
790	3/17/95	02:05:19	0.7	Creighton	854	8/02/95	08:09:11	1.6	Creighton
791	3/17/95	09:50:10	0.8	Creighton	855	8/06/95	00:25:55	1.9-1.8	Creighton
792	3/17/95	12:47:18	0.9	Creighton	856	8/06/95	02:25:26	1.0	Creighton
793	3/17/95	17:15:17	1.3	Creighton	857	8/08/95	12:14:37	1.2	Creighton
794	3/18/95	05:07:07	1.0	Creighton	858	8/09/95	10:53:38	1.7	Creighton
795	3/20/95	08:35:10	2.0-2.3	Creighton	859	8/09/95	16:04:10	0.9	Creighton
796	3/20/95	13:38:45	1.3	Creighton	860	8/10/95	02:39:45	1.7	Creighton
797	3/22/95	06:50:58	0.9	Creighton	861	8/11/95	08:06:27	0.8	Creighton
798	3/23/95	07:49:56	1.7	Creighton	862	8/12/95	07:42:48	1.3	Creighton
799	3/23/95	12:03:54	1.4	Creighton	863	8/13/95	21:52:38	1.6	Creighton
800	3/24/95	14:51:25	1.2	Creighton	864	8/16/95	07:51:15	0.9	Creighton
801	3/24/95	20:40:16	1.1	Creighton	864	8/16/95	16:47:55	1.3	Creighton
802	3/29/95	04:01:54	1.3	Creighton	865	8/18/95	01:13:45	1.2	Creighton
803	3/29/95	10:52:58	0.3	Creighton	866	8/18/95	11:39:37	2.7-2.8	Creighton
804	4/26/95	18:02:37	1.0	Creighton	867	8/18/95	18:17:56	1.1	Creighton
805	4/27/95	11:18:33	1.0	Creighton	868	8/20/95	02:21:48	1.8-1.6	Creighton
806	4/30/95	19:35:06	0.7	Creighton	869	8/22/95	07:57:33	0.9	Creighton
807	5/01/95	21:20:20	0.9	Creighton	870	8/23/95	05:13:44	0.4	Creighton
808	5/02/95	18:34:48	1.9	Creighton	871	8/23/95	21:12:20	1.2	Creighton
810	5/05/95	04:36:49	1.2	Creighton	872	8/24/95	14:43:47	0.9	Creighton
811	5/06/95	11:01:47	1.3	Creighton	873	8/25/95	17:05:24	1.6	Creighton

TABLE iii (cont'd.)

No.	Date	Time	Magnitude	Mine	No.	Date	Time	Magnitude	Mine
874	8/25/95	18:54:43	1.6	Creighton	902	9/25/95	00:56:47	1.2	Creighton
875	8/25/95	18:56:55	1.1	Creighton	903	9/25/95	00:57:33	1.0	Creighton
876	8/29/95	10:55:29	1.7	Creighton	904	9/26/95	06:50:20	1.3	Creighton
877	8/30/95	12:50:20	0.6	Creighton	905	9/26/95	11:10:44	1.1	Creighton
878	9/01/95	02:18:41	0.9	Creighton	906	9/27/95	17:18:27	0.9	Creighton
879	9/01/95	14:34:55	1.2	Creighton	907	9/29/95	07:12:44	1.3	Creighton
880	9/02/95	05:38:53	1.1	Creighton	908	10/02/95	01:48:43	1.8	Creighton
881	9/02/95	08:11:55	1.1	Creighton	909	10/02/95	11:46:56	0.9	Creighton
882	9/02/95	09:02:26	1.4	Creighton	910	10/06/95	12:06:29	1.5	Creighton
883	9/02/95	09:24:48	1.1	Creighton	911	10/07/95	17:57:42	0.8	Creighton
884	9/02/95	09:54:59	1.0	Creighton	912	10/16/95	21:58:24	0.9	Creighton
885	9/02/95	20:38:14	1.0	Creighton	913	10/19/95	03:12:04	1.6	Creighton
886	9/03/95	01:18:10	1.8-1.5	Creighton	914	10/20/95	20:11:59	1.2	Creighton
887	9/04/95	06:28:40	1.3	Creighton	915	10/25/95	08:25:42	1.8-2.0	Creighton
888	9/04/95	14:35:35	1.1	Creighton	916	10/25/95	08:25:58	1.0	Creighton
889	9/04/95	21:34:33	1.6	Creighton	917	10/29/95	02:40:36	1.1	Creighton
890	9/04/95	23:36:32	1.5	Creighton	918	11/03/95	13:06:21	1.1	Creighton
891	9/05/95	07:53:32	1.1	Creighton	919	11/04/95	06:42:18	1.8-1.8	Creighton
892	9/06/95	06:26:14	1.7-1.5	Creighton	920	11/05/95	10:07:19	1.3	Creighton
894	9/07/95	13:21:57	1.7	Creighton	921	11/06/95	09:10:29	1.9-2.2	Creighton
895	9/07/95	22:29:13	1.1	Creighton	922	10/06/95	23:35:11	1.1	Creighton
896	9/08/95	10:41:13	1.3	Creighton	923	11/09/95	07:34:48	1.1	Creighton
897	9/18/95	16:46:09	1.5	Creighton	924	11/10/95	08:11:36	0.9	Creighton
898	9/21/95	04:38:11	0.8	Creighton	925	11/18/95	01:22:12	1.3	Creighton
899	9/21/95	13:33:31	1.9	Creighton	926	11/18/95	21:07:06	1.0	Creighton
900	9/21/95	22:51:00	1.0	Creighton	927	11/19/95	03:57:48	1.0	Creighton
901	9/23/95	20:21:29	1.2	Creighton	928	11/19/95	09:14:29	1.4	Creighton

Case Studies of S-Wave Picks

A criterion which is widely used to determine the arrival times of an acoustic emission/microseismic signal is threshold crossing; that is, the time at which a signal crosses a preset threshold is considered the arrival time of that signal. This criterion is also adopted by MP250 systems. The origin of the arrivals picked by a microseismic system based on this criterion is complex. In addition to P-wave picks, there are many S-wave and noise picks. Based on the investigations conducted at a number of mine sites in Canada and the United States, S-wave picks account for about 40%, hence it is imperative to identify S-wave arrivals in order to obtain a meaningful source-location result.

This appendix demonstrates the existence of S-wave picks and the significance of detecting them by a number of case studies. Although the intention is not to explain how to identify S-wave picks, the analysis presented should give clear evidence that S-wave picks can be studied scientifically in many ways in addition to the inspection of waveforms.

Case 1

The threshold and the time window are the two basic criteria used for automatic event recognition. With MP250 systems an event is declared to have occurred if there has been at least a specified number of arrivals, with signal voltages exceeding the threshold level, during a prescribed period. This event recognition mechanism will result in an S-wave pick if its voltage level is above the threshold and its preceding P-wave arrival is below the threshold. This phenomenon can be seen clearly from the waveforms of a microseismic event recorded in the field (Figure 1).

This figure shows that the amplitude of S-wave arrivals is significantly higher than that of P-wave arrivals for six of ten channels. If the threshold level were chosen to be the magnitude of the P-wave arrival at the first channel, these six channels (1, 2, 4, 8, 9, 10) would more likely be activated by S-wave rather than P-wave arrivals. In any case, channel 4 would always be triggered by the S-wave arrival regardless of the threshold setting as the P-wave arrival is not detectable. The higher amplitude of S-wave arrivals at some transducers may be due to such factors as source mechanism, travel path, frequency content, attenuation characteristics of the medium, transducer characteristics and the relative orientation of the transducer (single-unit velocity gauge or accelerometer-type transducers) with respect to the direction of the particle motion.

Figure 1 Example of signals from a microseismic event

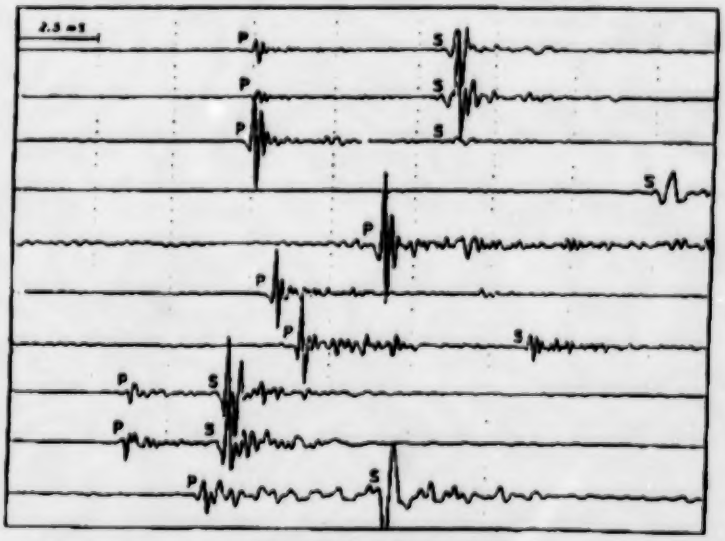

(After Talebi and Young, 1989)

Case 2

One of the best approaches to assess the reliability of the event-based velocity model (the physical status of each channel is determined based on the theory of arrival-time difference and residual analysis discussed in Chapter 5 of the report) is the calibration study, which provides the actual location error for each given velocity model. The following example demonstrates that the detection of S-wave picks may play a major role in the accurate location of an event. It also demonstrates that retaining S-wave channels is necessary in many cases, especially for small events. The elimination of these channels may cause the collapse of the location process. The event under consideration was blast-related, recorded at the Kidd Creek Mine site, Falconbridge Limited, on April 19, 1991. The information for the event is documented in tables i to iv. Table i contains the transducer co-ordinates and arrival times. The observed arrival-time differences, as well as the associated theoretical limits of P-wave arrival-time differences (in italics), are compared in Table ii. The main source-location results, as well as the real location of the event, are presented in Table iii. The details of the channel residuals are given in Table iv. Three solutions are presented in Table iii. In the first solution, P-wave arrival picks are assumed, and the location of this event is some 290 m away from the blast site, indicating the erroneous nature of the assumption.

Table i Transducer co-ordinates and arrival times for event 89

Transducer No.	9	29	31	11	23
X (m)	65614	65629	65636	65649	65675
Y (m)	65542	65610	65500	65438	65628
Z (m)	2728	2546	2544	2727	2566
Arrival time (10 µs)	0	715	1000	1410	2005

Table ii Arrival-time difference table for event 89 (10 µs)

	1	2	3	4	5
1P	*0*	*3897*	*3800*	*2194*	*3865*
	0	715	1000	1410	2005
2P	*3897*	*0*	*2204*	*5009*	*1065*
	715	0	285	695	1290
3P	*3800*	*2204*	*0*	*3873*	*2712*
	1000	285	0	410	1005
4P	*2194*	*5009*	*3873*	*0*	*5007*
	1410	695	410	0	595
5PS	*3865*	***1065***	*2712*	*5007*	*0*
	2005	**1290**	1005	595	0

Nota: The numbers in the first row and column represent channel numbers in terms of the triggering sequence. The number at the top of each cell is the theoretical limit of the P-wave arrival-time difference, and the one below is the observed arrival-time difference of the two channels denoted by the row and column numbers.

Table iii Source-location result for event 89

Solution	Velocity Model	Co-ordinate (m)			Event Residual (10 µs)	Sensitivity (m)	Error (m)
		X	Y	Z			
Blast site		65663	65552	2643			
1	PPPPP	65374	65553	2664	428	30	290
2	PPPPS	65647	65573	2656	58	13	29
3	PPPPD	65476	65568	2656	0	70	187

In the second solution, it is assumed that channel 23 (the last channel in the event) is triggered by an S-wave arrival. There are two reasons for this assumption. First, this channel has been identified as a possible S-wave channel, as the observed arrival-time difference with the second channel in the event (1290) exceeds the associated theoretical limit (1065) (Table ii). Second, this channel has the largest residual in the first solution (Table iv), which is the sign of an S-wave channel according to the theory of residual analysis. The location of the event, as determined by this solution, was 29 m away from the blast site — which, from a practical point of view, appears to be very reasonable. It is also noticed that this solution has a very small event residual: 0.58 ms.

In the third solution the fifth channel is dropped, and the location of the event is some 187 m away from the blast site. The cause of this inaccurate solution is in the wrong geometry of the array. With the original-event array, the five transducers form a curve with a relatively small radius in the X-Y plan, and the blast site is on the concave side of the curve, as shown in Figure 2. From a theoretical point of view, the event can be located without major difficulties. The remaining transducers, however, are almost on a vertical plane after the drop of the last channel. The standard deviation of the best-fit plane is only 14 m, with the normal of the plane in the X direction (the direction cosines of the plane are 0.97, 0.21 and 0.09, respectively). This array geometry makes it extremely difficult to control the accuracy in the X-direction. This point can be clearly seen from the sensitivity analysis, which shows that the sensitivity (m) in X, Y and Z directions are 70, 0 and -1 metres, respectively. The actual location errors (m) in these directions are 187, 16 and 13, respectively.

Table iv Channel residual for event 89 (10 μs)

Transducer No.	9	29	31	11	23
Solution 1	-163	-211	-54	121	307
Solution 2	-22	38	-25	24	-14
Solution 3	0	0	0	0	0

Figure 2 The array geometry for event 89 and the locations resulting from three different velocity models

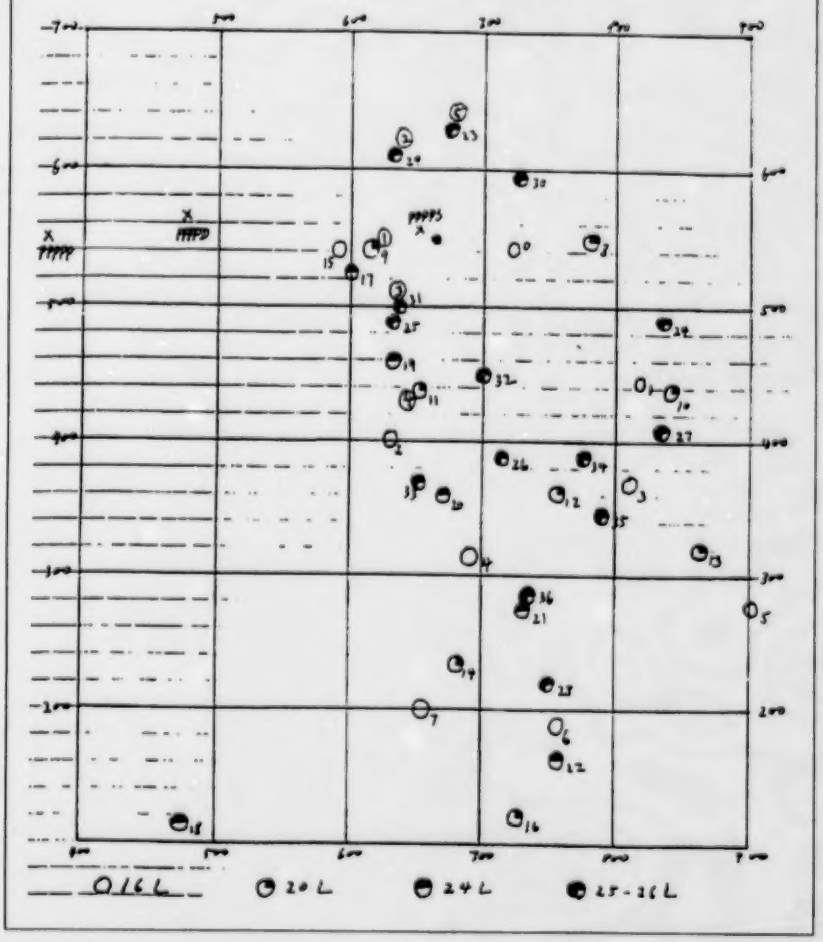

Case 3

The existence of the S-wave pick, as well as its impact on the overall solution of the source location, has been clearly demonstrated in Case 2. Although the case itself is a detailed calibration study of a single event, it does not represent an unusual phenomenon. According to investigations conducted by the author at a number of mines, S-wave picks account for about 40%. The ability to detect S-wave picks is, therefore, critical to obtain a meaningful pattern of seismicity. In

the present case, the existence of S-wave picks will be further demonstrated in a calibration study of a group of rockburst events. In particular, it is to show that the conventional methods, which assume P-wave arrivals for all picks, may lead to false patterns of seismicity.

Rockburst RB1097 occurred at the Creighton Mine on February 17, 1992. Its actual location in the local co-ordinate system (ft.) was 2907, 5615 and 5252. Table v contains the locations of this rockburst as determined by ADASLS, as well as a conventional method, considering all arrival times being P-waves, used by the mine. These data also include the locations for 20 after-shock events. The sequence numbers of these events, as they appeared in the original data file (RBDADA), are given in the first column, where 36 was the main event. The characters given in the second column are the rank of the solutions from ADASLS. The number of channels associated with each event is given in the third column. The associated velocity models used by ADASLS are listed in the fourth column, where P, S and D represent P-wave, S-wave and dropped channels, respectively. The precise locations determined by ADASLS are given in the next three columns. The mine's solutions are shown in the last three columns. The actual location of the main event was located directly above the main event (No. 36).

Figure 3 A comparison of the locations of rockburst RB1079 and its after-shock events as given by a conventional method and ADASLS (The actual location of RB1079 is shown by the solid cicle. Open circles represent the calculated locations.)

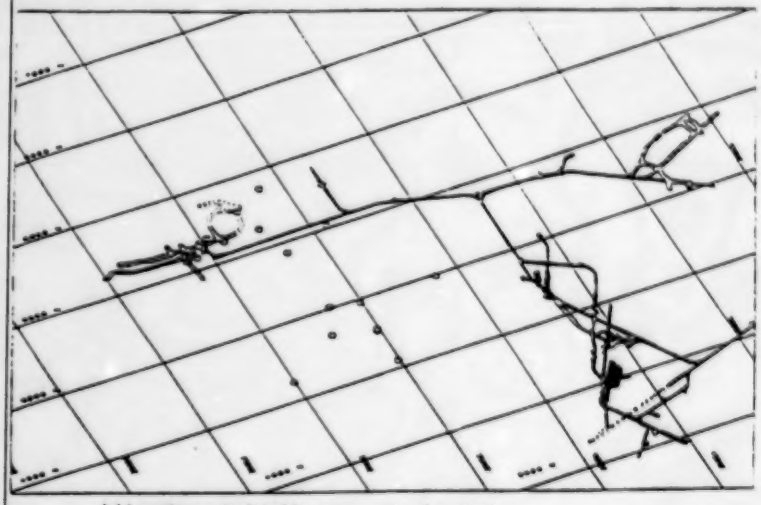

(a) Locations calculated by a conventional method

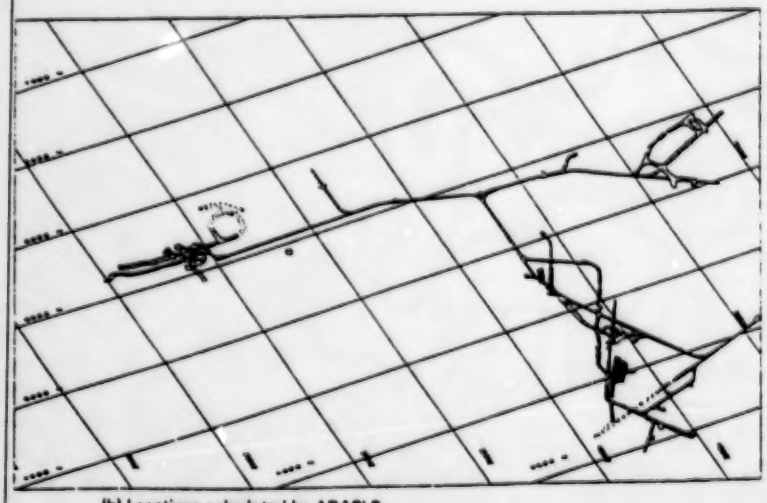

(b) Locations calculated by ADASLS

By comparing each co-ordinate of the actual location to the rest of the values in the column, it is immediately evident that significant errors were involved in the mine's solution. The typical error is about 500 ft. in the X-direction, and in the order of 1000 ft. in the Y-direction. Out of 21 events, 9 have their locations switched from the hanging wall to the footwall. In contrast, the solutions given by ADASLS are much more reliable, with only one having an error of about 500 ft. For easy comparison, the numbers with major errors are shown in bold print. Figure 3 shows the locations of the events given by ADASLS and the conventional method.

A very interesting pattern which can be observed from Table v is that the poor solutions given by the conventional method are always associated with those events which have a number of S-wave channels, which explains the cause of

failure with the conventional method. At this mine site, the data from both the dense array and the mine-wide array, the two main microseismic systems used at the site, have shown that the conventional method has a tendency to switch the hanging-wall events to the footwall because of P-wave-arrival assumption. This problem is eliminated by using ADASLS.

Case 4

A positive approach to examine an S-wave pick is to test its consistency with all other arrivals. For an event with many channels, an S-wave channel can be tested if the location results with and without this channel are identical.

On November 9, 1991, a relatively large event, with the energy number of 145, was recorded at the Creighton Mine site. The sequence number of this event on the mine's daily file is 175. The triggering-time period for this 16-channel event is very short, about 38.85 ms, which usually indicates reliable timings. The source-location information of this event is presented in tables vi to viii.

According to the theory of the arrival-time difference analysis discussed in Chapter 5 of the main report, channel 59 (the 13th triggered channel) was not activated by a P-wave arrival. The observed arrival-time differences with the first two channels (30.30 ms and 27.05 ms) are significantly higher than the associated theoretical limits of P-wave arrival-time differences (22.92 ms and 12.17 ms). Channel 59 is therefore either an outlier or an S-wave channel. However, it is more likely for this channel to have been triggered by an S-wave arrival, since there are no signs which are usually associated with outliers. There is no evidence based on the theory of arrival-time difference that any of the other channels were triggered by S-wave arrivals.

Table v A comparison of locations by ADASLS and a conventional method for rockburst RB1097 and its after-shock events

Event No.	Rank	Total Channel	Velocity Model	ADASLS			Mine		
				x	y	z	x	y	z
			Blast Location	2907	5615	5253	2907	5615	5252
36	A	16	PPPPPPPPPPPPPPP	2886	5635	5293	2879	5624	5307
37	C	8	PSSSPSSS	2929	5650	5273	**3319**	**5426**	5250
38	A	16	PPPPPPPDPPPDPPPD	2884	5632	5309	2868	5608	5309
39	A	11	PSSPSPSSPDS	2928	5566	5320	**3469**	**4758**	5318
40	B	13	PSSSPPPSPSDSS	2920	5604	5297	**3476**	**4771**	5330
41	B	13	PPPPSSPPSPSDS	2854	5550	5417	**3475**	**4532**	5318
46	A	16	PPPSPPPPSSPSPPSS	2869	5700	5287	3081	5624	5337
48	C	11	DPPPSPSPPPP	**3325**	**5441**	**5439**	**3270**	**4822**	**5629**
49	A	13	PSSSPPPSPSSDS	2945	5649	5299	**3284**	5630	5428
50	A	16	PPPPPPPPDPPPPPPP	2819	5652	5399	2875	5584	5376
52	B	11	PPSSPPSPDSS	2978	5614	5304	**3338**	**5003**	5172
53	A	16	PPPPPPPPPSPSPSPS	2880	5570	5314	2859	5577	5322
54	A	9	PPSSPSPSD	2943	5672	5279	**3379**	**5880**	**5027**
55	C	16	PPPPPPPPPPPPPPP	2975	5626	5278	3015	5679	5236
56	A	7	PSPSPSS	2965	5625	5283	**3222**	5784	5288
57	A	12	PPPSSPSDSPDS	2941	5578	5299	**3560**	5519	**5632**
58	B	7	PPSSPSPDS	2869	5624	5303	**3875**	**4985**	5268
59	B	16	PPPPPPPPPPPPPPP	2935	5595	5284	2920	5577	5306
60	B	13	PPPSSPPSPPSSS	2910	5560	5352	2976	**4805**	5276
61	A	13	PPPPSSPSPDSSD	2808	5687	5361	**3478**	**4972**	5267
62	C	16	PPPPPPPPPDPPPPP	2909	5660	5324	2976	5623	5284

In the first solution, channel 59 was excluded from the calculation, and all other channels were assumed to be P-wave picks. The event residual for this solution was extremely small; only 1.27 ms.

The sensitivity was 33 ft., which implied a stable solution. Therefore, it was reasonable to conclude that the assumption of P-wave picks was right for all except channel 59.

Table vi Transducer co-ordinates and arrival times for event 175

Transducer No.	31	22	8	21	62	48	18	30	23	50	63	61	59	1	26	16
x (ft)	4577	4655	4578	4603	4687	4549	4846	4582	4784	3920	4078	3920	4791	4541	3938	4499
y (ft)	5386	5441	5266	4961	5452	5937	5847	5720	5884	5786	5836	5637	5446	6069	5909	6107
z (ft)	5972	6171	5768	6168	5774	5972	6371	5574	6172	5973	5776	5771	6373	5974	6171	6371
Arrival time (10 μs)	5	330	980	370	1225	2405	2410	2430	2725	2885	2840	2845	3035	3120	3305	3885

Table vii Source-location result for event 175

Solution	Velocity Model	Co-ordinate (ft.)			Event Residual (10 μs)	Sensitivity (ft.)
		x	y	z		
1	PPPPPPPPPPPPDPPP	4471	5279	6061	127	33
2	PPPPPPPPPPPPSPPP	4471	5279	6061	121	30
3	PPPPPPPPPPPPPPPP	4439	5293	6004	383	30

Table viii Channel residuals for solutions of event 175

Transducer No.	31	22	8	21	62	48	18	30	23	50	63	61	59	1	26	16
Solution 1	-34	-174	48	-2	65	-101	-48	-68	112	-102	-22	83	0	-32	-24	300
Solution 2	-33	-173	49	-1	65	-101	-48	-68	113	-103	-22	83	0	-32	-24	299
Solution 3	-137	-518	106	-353	60	-160	-240	20	-93	-45	89	222	1077	-91	-49	114

In the second solution, the 13th channel was tested for being triggered by an S-wave arrival. The hypothesis was that we would have no reason to reject the assumption of an S-wave triggering of channel 59 if the second solution gave a result identical to the first. The results of the two solutions are strikingly similar. The locations of the event given by the two solutions had the same co-ordinates; furthermore, even the channel residuals for these two solutions resemble each other in an accuracy of 0.01 ms (i.e., the difference of channel residuals for any channel was less than 0.01 ms). From a source-location point of view, the resemblance of the channel residuals can only be attributed to the fact that the S-wave pick for channel 59 was highly consistent with the P-wave picks for the other channels.

The third solution, in which the P-wave pick was assumed for all channels, is presented for comparison purposes. This solution has a relatively large residual, as expected, and it is also noticed that a considerable amount of residuals are transferred from channel 59 to the two earlier triggered channels, channels 22 and 21.

Case 5

This case is designed to demonstrate the existence of S-wave picks from three different perspectives: by showing that the solution which recognizes the S-wave arrival is more accurate; by demonstrating that the S-wave arrival pick is consistent with P-wave picks at other channels; and by presenting the physical evidence of the P-wave arrival time at the S-wave channel.

The event under study occurred at the Creighton Mine site on April 14, 1992. It was a blast-related event recorded two seconds after the main event. The location of the blast on the mine's local co-ordinate system (ft.) was 4600, 6100 and 6300. The actual information for the event is given in tables ix to xiii.

Based on the theory of the arrival-time difference analysis, the last channel was not triggered by a P-wave arrival. The observed arrival-time differences were found to be significantly higher than the corresponding theoretical limits for the five associated channels (Table x), with the largest difference being about 16 ms.

There are three possible ways to deal with the last channel:

- exclude it from the calculation;
- use it as an S-wave channel; or
- use it as a P-wave channel.

In all of these cases, P-wave arrival picks are assumed for the other channels. The corresponding solutions for these event-based velocity models are numbered sequentially as 1, 2 and 3 in tables xi and xii.

In comparison with the actual location of the blast, the first two solutions appear more reasonable. These were 28 and 27 ft. away from the blast site, whereas it was 49 ft. for the third solution, in which P-wave arrivals were assumed for all channels. The residual of the third solution is much larger than those of the first two solutions. Furthermore, it is noticed that the channel residuals associated with the second and first solutions are very similar — solid evidence of the consistency of the S-wave arrival pick with all other P-wave arrival picks. The P-wave arrival time at the last channel can be estimated from the main event (event 200), taking place two seconds earlier. The main event and the one under study have very similar arrival times, showing that the P-wave arrival time for the last channel (channel 24) should be around 22 ms, as shown in Table xiii.

Table ix Transducer co-ordinates and arrival times for event 201

Transducer No.	9	10	34	13	3	16	2	14	18	20	23	6	47	48	19	24
x (ft)	4581	4436	4436	4472	4634	4499	4952	4302	4346	4088	4784	4857	4668	4549	5300	4489
y (ft)	6143	6036	6128	5951	6409	6107	6312	5895	5847	6039	5884	5519	6549	5937	6125	6012
z (ft)	6783	6783	6560	6992	6568	6371	6568	7020	6371	6782	6172	6779	7178	5972	5357	6170
Arrival time (10 μs)	5	545	845	1220	1335	1520	1865	1945	2150	2520	2530	2780	2820	3125	3480	4260

Table x Comparison of OAD and TLP for several channels associated with channel 24*

Associated Channel	9	10	34	16	18
TLP (10 μs)	3166	3078	2050	1112	1481
OAD (10 μs)	4255	3715	3415	2740	2110

*TLP: theoretical limit of P-wave arrival-time difference
OAD: observed arrival-time difference*

Table xi Source-location results for event 201

Solution	Velocity Model	Co-ordinate (ft.)			Event Residual (10 μs)	Sensitivity (ft.)	Error (ft.)
		X	Y	Z			
	Blast site	4600	6100	6300			
1	PPPPPPPPPPPPPPD	4620	6086	6716	135	23	28
2	PPPPPPPPPPPPPPS	4620	6087	6718	130	25	27
3	PPPPPPPPPPPPPPP	4635	6093	6763	501	25	49

Table xii Channel residuals for solutions of event 201 (10 μs)

Transducer No.	31	22	8	21	62	48	18	30	23	50	63	61	59	1	26	16
Solution 1	-64	-59	26	-77	-30	95	137	-46	47	235	-78	97	-45	-279	41	0
Solution 2	-57	-58	19	-71	-34	84	133	-42	38	235	-89	95	-38	-291	35	39
Solution 3	-13	-132	-225	8	-159	-194	68	-16	216	132	-329	64	96	-567	-561	540

Table xiii A comparison of arrival times between events 200 and 201

Transducer No.	Arrival Times (10 μs)	
	Event 200	Event 201
9	5	5
10	550	545
34	770	845
13	1215	1220
5	1320	1335
11	1325	1520
2	1600	1865
14	1940	1945
18	2075	2150
24	**2215**	–
20	2295	2520
23	2360	2530
6	2695	2780
47	2750	2820
48	3045	3125
1	3075	–
19	–	3480
24	–	4260

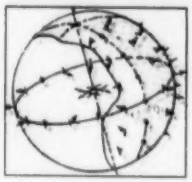

Case Studies of Outliers

Outliers are those channels which are not triggered by the physical source triggering the majority of channels during an event-time window. In the case of the mining environment, interference with seismic events and other noises, such as those caused by blasting, drilling, mining machines and fans, are the primary sources of outliers.

According to investigations conducted at several mine sites in Canada and the United States, outliers account for about 10% of the total channels. Since the presence of one such channel in an event will, in general, completely ruin the source-location solution, the detection of outliers is one of the critical steps for the effective use of automatically determined microseismic events.

This appendix is designed to demonstrate a number of typical outliers, as well as their severe impact on source location.

Case 1

Many small events as defined by MP250 systems are not real, in the sense that each of these events is triggered by two or more physical sources and the number of channels triggered by a single source is not sufficient to obtain an analytical solution. Since those events which cannot be used for source-location account for at least 20% of the total recorded events, based on the investigations at several Ontario mines, their detection is important for a meaningful use of MP250 data. Otherwise, these events could have a great detrimental effect on the solution for the source location.

A typical example of such an event is given in Table i. The event was recorded by the mine-wide array at Creighton Mine on April 13, 1992. It is noticed from this table that a very large time gap, 71 ms, is found between transducer 63 and transducer 50. A large time difference between two very close transducers implies that the source would be remote. In this case, it would be far beyond the footwall in the solid rock. This is an unreal situation. Furthermore, it is noticed that the co-ordinates of transducer 49 (the first triggered channel) are very different from others. The distances from this transducer to the rest, as shown in Table ii, are about 2000 ft. In fact, transducer 49 is located in an isolated ore body, and the triggering pattern as shown by this 'event' is practically impossible. If an event had taken place in the local area and it had been large enough to activate the very remote transducers, several other local transducers would have been triggered at the same time.

Table i Transducer co-ordinates and arrival times for event 24

Transducer No.	49	61	63	50	36
x (ft.)	2494	3920	4078	3920	4411
y (ft.)	5149	5637	5836	5786	4833
z (ft.)	4768	5771	5776	5973	5176
Arrival time (μs)	5	740	1590	8735	9160

Table ii Distances from transducer 49 to others in event 24

Transducer No.	61	63	50	36
Distance (ft.)	1810	1999	1973	1985

Based on the above analysis, it can be concluded that at least three physical sources were involved in this 'event'. Channel 49 was associated with the first one; channels 61 and 63 with the second; and channels 50 and 36 with the third.

Case 2

Outliers are found in major events, as well as in small ones. The danger of outliers is their extraordinary power to damage source-location solutions. One outlier in an event is often enough to ruin the final solution, regardless of the size of the event.

On April 29, 1991, four 12-channel events, caused by a nearby blast, were recorded at the Kidd Creek Mine site during a six-second period. These were all major events, characterized by very short triggering-time periods, approximately 20 ms, if the effect of outliers is ignored. The original data of these four events are given in tables iii to vi.

Among the four events, three are contaminated by outliers. In event 39, channel 15, the first one triggered, is an outlier characterized by a very large time-event gap, (68 ms) with the next one. For the same reason, in event 40, channel 30 is an outlier. In event 41, channel 52 is an outlier, which is explained in Table vii where the triggering patterns for the four events are compared. From this, it is not difficult to see that all four events had a very similar pattern of arrival times, indicating that they originated in a very restricted volume. Based on the triggering pattern given by events 39 and 40, channel 52 should be one of the earliest triggered channels, instead of the last.

The source-location results are summarized in Table viii. The first column gives the sequence numbers of these events in the original data file. The velocity models used by ADASLS are given in the second column, where P and D represent P-wave and dropped channels, respectively. The locations determined by ADASLS are given in the next three columns and those by a conventional method in the last three columns. The locations as given by ADASLS are very consistent. They are contained in a 19 x 24 x 12 ft. block. In contrast, the solutions from the conventional method, which ignores the existence of outliers, are completely meaningless. The number 99999 indicates that the calculated co-ordinate has at least six digits, which clearly signals a wrong solution.

Table iii Transducer co-ordinates and arrival times for event 39

Transducer No.	X (m)	Y (m)	Z (m)	Arrival Time (10 μs)
15	65588	65545	2850	0
52	65709	65572	2102	6820
57	65692	65559	2038	7325
49	65714	65555	2140	7555
59	65648	65654	1964	7620
47	65604	65635	2142	7940
50	65584	65629	2102	7960
45	65706	65559	2197	8125
53	65639	65533	2099	8130
60	65724	65555	1964	8380
43	65639	65555	2196	8715
44	65596	65607	2197	8810

Table iv Transducer co-ordinates and arrival times for event 40

Transducer No.	X (m)	Y (m)	Z (m)	Arrival Time (10 μs)
30	65726	65597	2542	0
52	65709	65572	2102	6055
57	65692	65559	2038	6130
47	65604	65635	2142	6380
59	65684	65654	1964	6445
50	65584	65629	2102	6790
53	65639	65533	2099	6885
60	65724	65555	1964	6920
45	65706	65559	2197	7245
44	65596	65607	2197	7390
40	65628	65559	2276	8030
41	65662	65581	2271	8185

Table v Transducer co-ordinates and arrival times for event 41

Transducer No.	X (m)	Y (m)	Z (m)	Arrival Time (10 μs)
57	65692	65559	2038	0
59	65684	65654	1964	185
47	65604	65635	2142	245
50	65584	65629	2102	495
53	65639	65533	2099	590
60	65724	65555	1964	1070
43	65639	65555	2196	1210
44	65596	65607	2197	1245
41	65662	65581	2271	1570
40	65628	65559	2276	1970
39	65608	65615	2272	2165
52	65709	65572	2102	3250

Table vi Transducer co-ordinates and arrival times for event 43

Transducer No.	X (m)	Y (m)	Z (m)	Arrival Time (10 μs)
49	65714	65555	2140	0
59	65684	65654	1964	15
57	65692	65559	2038	170
47	65604	65635	2142	400
50	65584	65629	2102	430
53	65639	65533	2099	560
45	65706	65559	2197	565
60	65724	65555	1964	725
43	65639	65555	2196	1020
44	65596	65607	2197	1195
41	65662	65581	2271	1655
40	65628	65559	2276	2110

Table vii A comparison of triggering patterns

Event	Channel Numbers (in triggering sequence)*												
39	**15**	52	57	49	59	47	50	45	53	60	43	44	–
40	**30**	52	57	47	59	50	53	60	45	44	40	41	–
41	–	57	59	47	50	53	60	43	44	41	40	39	**52**
43	–	49	59	57	47	50	53	45	60	43	44	41	40

**Bold numbers represent the identified outliers*

Table viii A comparison of locations given by ADASLS and a conventional method assuming all P-wave picks

Event	Event Velocity Model Given by ADASLS	Location Given by ADASLS (m)			Location Given by a Conventional Method (m)		
		X	Y	Z	X	Y	Z
39	DPPPPPPPPPP	65720	65651	2080	99999	99999	99999
40	DPPPPPPPPPP	65717	65669	2084	99999	99999	99999
41	PPPPPPPPPPD	65727	65663	2092	–	29421	-70801
43	PPPPPPPPPP	65736	65675	2088	65736	65675	2088

Case 3

One of the important causes of outliers is the interference of seismic events themselves. The present case demonstrates this phenomenom by showing that an MP250 defined event is the result of the merger of two events.

Event 94, show in Table ix, occurred on April 19, 1991, at the Kidd Creek Mine site. It is clear from the table that the transducers triggered in the time window of event 94 fall into two distinct groups regarding their general locations. Transducers 8, 23, 30, 11 and 10 are located in the top levels of the mine; the rest are in the deep levels. This type of triggering pattern is impossible due to a single physical source based on the mine layout and transducer arrangement.

These two groups of transducers are actually related to two different blasts. Event 94A (transducers 8, 23, 30, 11 and 10) was caused by a blast which occurred 25 seconds earlier. The main event of this blast has the triggering sequence of **8, 30, 23**, 31, 29, **10**, 25, 19, 26, 9, **11**, 0, which is very similar to that of event 94A. The locations of the main event and event 94A are (663, 552, 2643), and (713, 633, 2697), respectively. It seems that a major error has been involved in the solution of event 94.

Event 94B (transducers 52, 57, 47, 50, 49, 53) was caused by another blast taking place six seconds earlier. The triggering sequence for the main event is **52, 47, 57, 43, 50, 49**, 59, 23 and 29. These two events have the locations of (694, 654, 2108), and (718, 660, 2076), respectively, which are very close: only 40 m apart.

Table ix Transducer co-ordinates and arrival times for event 94

Transducer No.	X (m)	Y (m)	Z (m)	Arrival Time (10 μs)
8	**65779**	**65550**	**2722**	0
23	**65675**	**65628**	**2586**	160
52	65709	65572	2102	330
57	65692	65559	2038	810
30	**65726**	**65597**	**2542**	915
47	65604	65635	2142	1070
50	65584	65629	2102	1625
11	**65849**	**65438**	**2727**	1835
10	**65840**	**65438**	**2720**	2010
49	65714	65555	2140	2965
53	65639	65533	2099	3650

PART A Case Studies on Hybrid Source-Location Methods

and

PART B Statistics on Source-Location Accuracy

PART A Case Studies on Hybrid Source-Location Methods

This appendix is organized into two parts. Part A deals with the case studies on hybrid source-location methods and Part B compares lists of tables of the location of the seismic source determined by ADASLS and a conventional method.

The hybrid method utilizes the Simplex and USBM algorithms and assesses the reliability of solutions given by these methods based on the analysis of raw event data, as well as the information contained in the solutions.

An important concept used in the hybrid method is head residual, which examines how well the observed arrival times of the first several channels can be matched by the calculated arrival times. The emphasis of the residuals associated with the first several channels is based on the fact that arrival-time errors; are not randomly distributed. In general, the channels triggered earlier should have the smaller errors; this is not difficult to understand from practical reasons. The key here is the distance. The earlier triggered transducers are closer to the source, which will effectively reduce the uncertainties associated with the velocity model. The shorter distance also means a higher energy level and thus sharper arrival, which reduces the timing errors. The calibration study shows that solutions with smaller head residuals are more reliable. In this appendix, two cases are presented to demonstrate the principle of the hybrid method.

Case 1

The event specified in Table i was related to a drift blast at the Kidd Creek Mine site recorded on May 7, 1991 (Julian day 127). All channels were triggered by P-wave arrivals based on the analysis of arrival-time differences. The Simplex and USBM solutions, as well as the location of the blast site, are given in Table ii. Although the event residual for the USBM solution is somewhat larger than that for the Simplex solution, the actual location error for the USBM solution is much smaller; about 35 m. In contrast, the location error for the Simplex solution is 129 m. If we carefully examine the distribution of channel, residuals as shown in Table iii, it is not difficult to understand why the USBM algorithm yields the better solution in this case: the smaller residuals are associated with the earlier triggered channels while the relatively larger residuals are associated with the later ones. From the earlier discussion, it is understood that this pattern is highly desirable from a practical point of view. In comparison, the channel residuals for the Simplex solution exhibit a reverse pattern with large residuals associated with the first several channels.

Table i Transducer co-ordinates and arrival times for event 72

Transducer No.	X (m)	Y (m)	Z (m)	Arrival Time (10 μs)
41	65662	65581	2271	0
40	65628	65559	2276	75
43	65539	65555	2196	135
44	65696	65607	2197	260
39	65608	65615	2272	285
48	65655	65530	2146	760
47	65604	65635	2142	1035
45	65706	65559	2197	1245
50	65584	65629	2102	1545
49	65714	65555	2140	1985

Table ii	Source-location result for event 72						
Algorithm	Velocity Model*	Co-ordinate (m)**			Event Residual (10 μs)	Head Residual (10 μs)	Error (m)
		X	Y	Z			
	(Blast site)	65658	65608	2221			
Simplex	PPPPPPPPPPP	65559(99)	65527(81)	2241(10)	269	343	129
USBM	PPPPPPPPPPP	65635(23)	65585(23)	2235(14)	293	58	35

* *P represents P-wave channels*
** *Numbers in parentheses represent errors*

Table iii	Channel residual for event 72									
Transducer No.	41	40	43	44	39	48	47	45	50	49
Simplex (10 μs)	-509	292	103	179	71	-61	-143	-1	-57	127
USBM (10 μs)	50	36	80	8	126	-436	-238	499	-510	383

Case 2

The event discussed in this case is an after-shock of rockburst RB1097, which took place at Creighton Mine on February 17, 1992. The source-location data for this event are given in tables iv to vi, in very similar formats to those discussed in Case 1.

The duration of this event was first noticed to be quite long — about 100 ms. Experience in mine sites indicates that the duration of an event is normally less than 30 ms if all the channels are triggered by P-waves. With this in mind, it is not surprising to note the presence of so many S-wave channels. The actual number is six, based on the arrival-time difference and residual analysis. Because of the major presence of S-wave channels, the USBM algorithm was not expected to produce any reasonable result. As a matter of fact, there would be a very large location error — about 500 ft. — if the method were used. With ADASLS, the USBM algorithm is ignored for events like this which have many S-wave channels.

With the Simplex algorithm there are two possible solutions (see Table v), with the difference being the input data related to channel 2. The first solution considers the channel triggered by a P-wave, while the second solution considers an S-wave. Although the event residuals of the two solutions are similar, the head residuals are very different. The one with the smaller head residual (0.64 ms) only has an error of 46 ft., while the one with the relatively large head residual (2.37 ms) has an error of 363 ft.

Table iv	Transducer co-ordinates and arrival times for event 37			
Transducer No.	X (ft.)	Y (ft.)	Z (ft.)	Arrival Time (10 μs)
32	2990	5678	5371	5
40	3041	5596	4979	2070
25	3241	5711	5574	3090
52	2566	5546	4722	5085
63	4078	5836	5776	5520
49	2494	5149	4768	6120
54	2479	5106	4565	7825
50	3920	5786	5973	9770

Table v Source-location result for event 37

Algorithm	Velocity Model*	Co-ordinate (m)**			Event Residual (10 μs)	Head Residual (10 μs)	Error (m)
		X	Y	Z			
	(Blast site)	2907	5615	5252			
Simplex	PPSSPSSS	2665(242)	5715(100)	5504(363)	295	237	363
Simplex	PSSSPSSS	2929(22)	5650(35)	5273(21)	280	64	46
USBM	PPPPPPPP	3352(445)	5674(59)	5040(212)	2497	1933	496

* *P and S represent P- and S-wave arrivals, respectively*
** *Numbers in parentheses represent errors*

Table vi Channel residual for event 37 (10 μs)

Algorithm	Velocity Model	32	40	25	52	63	49	54	50
Simplex	PPSSPSSS	-276	269	-140	10	-213	-78	78	350
Simplex	PSSSPSSS	-98	-47	22	132	-332	-182	172	384
USBM	PPPPPPPP	-3288	-404	-482	-44	-549	67	1259	3442

PART B Statistics on Source-Location Accuracy

This section consists of six tables. Tables vii to xii contain the locations determined by ADASLS and a conventional method for six sets of blast data. Each table is organized in the following manner. In the first column are the sequence numbers of the events as they appeared in the original data file. The characters given in the second column are the rank of the solutions from ADASLS. Readers may refer to Chapter 5 of the main report for an explanation of the rank system. The number of triggered channels is given in column three. The velocity models used by ADASLS are listed in the fourth column, where P, S and D represent P-wave, S-wave and dropped channels, respectively. The precise locations determined by ADASLS as well as the associated errors are given in the next four columns. The mine's solutions are shown in the last four columns. The actual location of each blast is also given in the table.

Table vii A comparison of locations given by ADASLS and a conventional method for events related to a drift blast on February 19, 1992[1]

Event No.	Rank	Total Channel	Velocity Model	ADASLS (m)				Conventional Method (m)			
				X	Y	Z	E**	X	Y	Z	E**
			Blast Location	**5699**	**5532**	**2663**		**5699**	**5532**	**2663**	
1	B	12	PPPPPPPPPPP	5676	5532	2660	23	5674	5535	2659	25
2	A	12	PPPPPPPPPPP	5689	5519	2657	17	5554	5532	2639	147
3	B	12	PDPPPPSDPDPP	5682	5331	2662	17	5540	5528	2823	226
4	D	6	D*PDSPP	5693	5427	2671	105	5254	5108	2413	664
5	C	12	PDPDPPPPDPPP	5695	5511	2682	29	5554	5588	2761	184
6	C	12	PPDDPPDPPPPP	5669	5505	2693	50	5789	4532	3217	730
7	C	12	PPPDDPPDPPSS	5678	5451	2669	84	5441	5322	2706	335
8	D	8	D*PDPPDPP	5676	5451	2669	63	5441	5322	2706	457
10	C	12	PPPPDSPPPPDD	5691	5508	2666	25	5639	5560	2696	74
11	C	12	PPPDDPPPPPS	5696	5539	2684	22	5790	5953	3311	778
12	C	12	PPPPSSPSSDPS	5713	5532	2626	40	5648	5551	2715	75
13	C	12	D*PPDDPPPPSPP	5695	5554	2685	31	5506	5515	2714	200
14	C	10	PPPPDDDSSD	5669	5530	2674	32	5611	5611	2280	166
15	A	12	PPDDPPPPSSSD	5669	5530	2674	41	5611	5611	2780	172
16	D	6	D*PPPPP	5469	5175	2571	434	5045	5102	2531	794
17	C	5	D*PPPS	5714	5514	2643	30	5262	5074	2287	736

[1] *Events from data file MCG. Data provided by Kidd Creek Mine*
* *Identified outliers*
** *Distance from event location to blast site, an error estimate*

Table viii A comparison of locations given by ADASLS and a conventional method for events related to a drift blast on January 15, 1992[1]

Event No.	Rank	Total Channel	Velocity Model	ADASLS (m)				Conventional Method (m)			
				X	Y	Z	E**	X	Y	Z	E**
			Blast Location	5778	5273	2590		5778	5273	2590	
40	A	12	PPPDPPPPPPP	5745	5276	2591	33	5368	521	2654	419
45	C	12	D*PPPPPPPPP	5769	5267	2572	21	5598	5360	2617	202
53	C	10	PPPPPPPPP	5782	5224	2518	87	5772	5221	2516	90

[1] *Events from data file MCG. Data provided by Kidd Creek Mine*
* *Identified outliers*
** *Distance from event location to blast site, an error estimate*

Table ix A comparison of locations given by ADASLS and a conventional method for events related to a drift blast on May 6, 1992[1]

Event No.	Rank	Total Channel	Velocity Model	ADASLS (m)				Conventional Method (m)			
				X	Y	Z	E**	X	Y	Z	E**
			Blast Location	5762	5513	2631		5762	5513	2631	
1	A	12	PPPPPPPPPPP	5749	5498	2644	24	5749	5595	2646	27
2	C	12	PPPPPPPPPPP	5768	5495	2633	29	5775	5496	2628	22
3	C	12	PPPPPPPPPPP	5766	5513	2631	4	6260	5424	2182	676
4	C	8	PPPPPPPP	5712	5523	2665	61	5672	5472	2643	114
5	C	12	PPPPPPPPPPP	5770	5496	2621	21	5773	5496	2620	23
6	C	12	D*D*PPPPPPPPP	5771	5518	2622	14	5589	5328	2748	279
7	C	12	PPPPPPPPPPD	5754	5512	2641	23	5769	5525	2649	23
8	C	12	PPPPPPPPPPD	5754	5512	2641	15	5745	5514	2653	28
9	C	12	PPPPPPPPPPP	5790	5519	2623	30	5799	5518	2618	40
10	C	12	PPPPPDDPPDPP	5907	5467	2433	249	5807	5504	2626	46
11	A	12	PPPPPPPPPPP	5759	5499	2640	17	5164	5499	2637	15
12	C	12	PPPPPPPPPPP	5767	5504	2618	17	5783	5506	2611	31
13	C	12	PPPPPPPPSPP	5760	5497	2627	17	5769	5507	2626	10
14	C	12	PPPPPPPPPPP	5842	5537	2590	93	5821	5543	2599	74

[1] *Events from data file Drift91. Data provided by Kidd Creek Mine*
* *Identified outliers*
** *Distance from event location to blast site, an error estimate*

Table x A comparison of locations given by ADASLS and a conventional method for events related to a drift blast on May 29, 1991[1]

Event No.	Rank	Total Channel	Velocity Model	ADASLS (m)				Conventional Method (m)			
				X	Y	Z	E**	X	Y	Z	E**
			Blast Location	5690	5559	2722		5690	5559	2722	
25	B	12	PPPPPPPPPPP	5685	5568	2712	11	5675	5555	2716	17
26	C	12	PPPPPPPPPPP	5679	5576	2711	23	5657	5596	2750	51
27	C	12	PPPPPPPPPPP	5740	5555	2709	53	5785	5524	2677	111
28	C	9	PPPPPPPPS	5662	5549	2689	44	5778	5531	2622	136
29	D	6	PPPSPP	5688	5739	2741	181	5759	5525	2629	121
30	C	12	PPPPPPSSSSPS	5701	5546	2710	21	5684	5588	2724	29
31	C	12	D*D*PPPPPPPPP	5684	5572	2718	14	5726	5624	2634	115
32	C	12	PPPPPPPPPSSP	5691	5560	2722	1	5776	5539	2686	95
33	C	12	PPPPPPPPPPDD	5716	5578	2731	33	5801	5530	2670	126
34	C	12	PPPPPPPPPSPP	5641	5592	2722	59	5770	5562	2692	85
35	C	5	PPPDP	5697	5551	2412	310	5066	5718	2270	710
36	C	12	PPPPPPPPPPP	5713	5538	2724	31	5706	5547	2728	21
37	C	7	PPPPD*PP	5765	5507	2672	104	5680	5503	2619	117
38	C	12	PPPPPPPPSSS	5719	5506	2700	64	5750	5498	2674	98
39	B	12	PPPPPPPPDDD	5682	5525	2727	35	5815	5513	2660	149
40	C	12	PPPPPPPPPPD*	5739	5555	2685	61	5734	5558	2681	56
41	B	12	PPPPPPPPPSP	5691	5575	2719	16	5717	5554	2719	28
42	C	12	PPPPPPPSSPS	5698	5551	2743	24	5689	5552	2744	23
43	D	6	PPPPD	5691	5540	2691	36	5663	5486	2679	89
44	C	12	PPPPPPPPPSP	5703	5579	2723	24	5729	5546	2715	42
45	D	7	D*PPPPP	5710	5659	2730	102	5717	5655	2746	103

[1] *Events from data file Drift91. Data provided by Kidd Creek Mine*
* *Identified outliers*
** *Distance from event location to blast site, an error estimate*

Table xi A comparison of location given by ADASLS and a conventional method for events related to a drift blast on May 7, 1991[1]

Event No.	Rank	Total Channel	Velocity Model	ADASLS (m)				Conventional Method (m)			
				X	Y	Z	E**	X	Y	Z	E**
			Blast Location	5658	5608	2221		5658	5608	2221	
71	A	12	PPPPPPPPPSS	5657	5594	2215	15	5654	5580	2225	29
72	C	10	PPPPPPPPP	5635	5585	2235	35	5636	5581	2232	40
73	C	11	PPPPPPPSSSD	5662	5595	2203	23	5719	5616	2208	63
74	A	8	D*PPPPD*SS	5568	5584	2204	95	5131	5380	2216	574
75	C	7	D*PPPPPP	5663	5648	2209	42	5667	5644	2217	37
76	C	7	PPPPSSD*	5613	5570	2212	60	5529	5545	2190	146
77	C	7	PPPPPPP	5538	5566	2178	134	5619	5623	2168	67
78	C	11	PPPPPPPPDDD*	5625	5567	2222	53	5648	5570	2212	40
79	C	7	PPPPPPP	5660	5628	2211	24	5399	5189	2384	519
80	A	12	PPPPPPPPPDD	5648	5594	2227	18	5643	5591	2225	23
81	C	11	PPPPPPPPPP	5664	5620	2189	34	5662	5616	2187	35
82	A	7	DPPPPPS	5564	5504	2231	141	5489	5511	2294	208
83	C	10	PPPPPPPPD	5667	5610	2209	14	5664	5613	2209	14

[1] *Events from data file Drift91. Data provided by Kidd Creek Mine*

* *Identified outliers*

** *Distance from event location to blast site, an error estimate*

Table xii A comparison of locations given by ADASLS and a conventional method for events related to a drift blast on April 19, 1991[1]

Event No.	Rank	Total Channel	Velocity Model	ADASLS (m)				Conventional Method (m)			
				X	Y	Z	E**	X	Y	Z	E**
			Blast Location	5663	5552	2643		5663	5552	2643	
66	A	12	PPPPPPPPPPP	5814	5590	2600	162	5699	5504	2629	63
67	C	8	D*PPD*SSD*D	5754	5541	2627	93	5771	5224	2282	500
68	D	7	PPPPSSD	5885	5485	2728	170	5868	5366	2577	285
70	D	7	PDSPSD*S	5577	5861	2490	645	5724	5541	2721	100
71	C	6	PPPPPD	5679	5574	2665	35	5698	5537	2662	43
72	D	6	PPPPPD	5712	5597	2739	117	5720	5580	2739	110
74	C	5	PPPPD	5667	5534	2581	65	5791	5506	2736	165
75	C	7	D*D*PPPPS	5691	5589	2733	101	5658	5501	2726	100
76	C	12	PPPPSSSSSSSS	5792	5630	2477	224	5645	5570	2574	74
78	C	5	PPPPD*	5779	5455	2607	162	5777	5453	2600	163
80	B	8	PPPPPSSP	5639	5563	2663	33	5699	5548	2641	36
82	C	6	PPPPPP	5666	5577	2657	28	5664	5513	2613	49
83	A	8	D*D*PPPPPP	5638	5513	2618	53	5638	5203	2092	653
84	C	9	PPPPPPPPD	5645	5480	2644	74	5758	5539	2654	97
85	D	5	PPPPP	5597	5470	2395	269	5831	5643	2865	293
86	C	8	PPPPPPDD*	5668	5542	2635	20	5625	5537	2633	42
87	C	6	D*PPPPD	5654	5563	2671	31	5703	5464	2618	100
88	A	8	D*PPPPPDD	5668	5412	2609	144	6030	6163	2788	727
89	A	5	PPPPS	5647	5573	2656	29	4921	5569	2665	743
91	C	5	DPPPP	5684	5539	2689	52	5691	5519	2665	49
92	C	7	PPPPPDD*	5660	5560	2633	13	5677	5528	2636	29
93	D	7	PPPPPPD*	5604	5530	2611	71	5856	5530	2697	202
95	C	5	PPPPP	5677	5561	2703	62	5693	5520	2671	52
96	C	12	D*PPPPPPPPPP	5678	5533	2655	39	5698	5510	2646	55
97	D	12	PPPPPPPSPPPP	5691	5531	2659	38	5687	5542	2641	26
98	A	12	PPPPPPPSPPPP	5691	5531	2659	39	5712	5529	2651	55
100	C	12	PPPPPPSPPSSS	5700	5540	2665	45	5753	5528	2645	93
101	C	10	PPPPPPPPPP	5695	5527	2642	41	5695	5521	2642	45
102	C	5	PPPPP	5668	5551	2685	42	5693	5514	2657	50
103	A	8	D*PPPPSP	5651	5527	2635	29	6324	5671	2556	687
104	C	7	PPPPDDD	5638	5590	2641	46	5666	5468	2651	84
105	D	6	D*PPPPP	5699	5633	2619	92	5701	5627	2620	87
106	C	12	PPPPPSSSPPSS	5676	5507	2639	47	5725	5529	2646	66
107	C	8	PPPPPPPP	5669	5542	2571	79	5668	5543	2577	67
108	C	11	PPPPPPPPPPD	5693	5509	2644	56	5633	5501	2663	62
109	C	5	PPPPD	5637	5527	2643	36	5633	5512	2645	50

[1] *Events from data file Blast91. Data provided by Kidd Creek Mine*

* *Identified outliers*

** *Distance from event location to blast site, an error estimate*

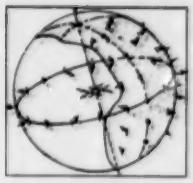

List of Publications on Induced Seismology by CANMET's Mining Research Laboratories Personnel Related to Phase II of the Canadian Rockburst Research Program, 1990-1995

Arjang, B. (1991). *Utilization of Stiff Backfill in Alleviation of Rockbursts Part 1: Pre-Mining Ground Stress Determinations at the Macassa Mine.* CANMET Report MRL 91-089 (TR).

Arjang, B. and Stevens, K. (1992). *Utilization of Stiff Backfill in Alleviation of Rockbursts Part 2A: Laboratory Scale Dilatometer Testing of Cemented Rockfill.* CANMET Report MRL 92-096 (TR).

Arjang, B. and Swan, G.(1995). "Mechanical Characteristics of Stiff Backfills Under Confinement." CAMI '95: 3rd Canadian Conference on Computer Applications in the Mineral Industry.

Côté, M., Talebi, S. and Plouffe, M. (1994). *Preliminary Analysis of the Seismic Activity Recorded at Phalen Colliery, Sydney, Nova Scotia.* CANMET Report MRL 94-055 (TR).

Forrester, D., Cain, D.P., Corbett, G. and Plouffe, M. (1994). *CBCRL Monitoring of Outburst Incident at Phalen Colliery of September 28, 1994.* CANMET Report MRL 94-052 (CF).

Gagnon, L.P., Plouffe, M. and Côté, M. (1994). *Analyse de l'activite séismique a la mine Sigma, Val d'Or, Quebec, Decembre 1992-Avril 1994.* CANMET Report MRL 94-019 (TR).

Galley, C.A. and Wetmiller, R.J. (1992). *The History of Mining-Induced Seismic Events in Sudbury Mines.* Special Report, GSC.

Ge, M. (1991). *Microseismic Source Location Methods.* CANMET Internal Report, 29 pages.

Ge, M. (1992). *Analysis of Mine-Wide Array Microseismic Data.* Final report to Inco Limited, 116 pages.

Ge, M. (1992). *Automatic Data Analysis and Source Location System.* CANMET Internal Report, p. 9.

Ge, M. (1993). *Analysis of Kidd Creek Source Location Data.* Final report to Kidd Creek Mine, Falconbridge Limited, 150 pages.

Ge, M. (1994). *Analysis of Locations of January 7 Rockburst and Associated Events.* Technical Report to Onaping Mine, Falconbridge Limited, p. 16.

Ge, M. (1995). "Comments on "Microearthquake Location: A Nonlinear Approach that Makes Use of a Simplex Stepping Procedure" by A. Prugger and D. Gendzwill. *Bull. Seism. Soc. Am.* 85:375-377.

Ge, M. and Kaiser, K.P. (1992). "P-Wave Velocity Back-Calculation with Automatically Determined Microseismic Event Data." 33rd U.S. Symposium on Rock Mechanics, Santa Fe, pp. 1071-1078.

Ge, M. and Mottahed, P. (1993). "An Automatic Data Analysis and Source Location System." Proceedings of the 3rd International Symposium on Rockbursts and Seismicity in Mines, Kingston, Ontario, pp. 343-348.

Ge, M. and Mottahed, P. (1994). "An Automated AE.MS Source Location Technique Used by Canadian Mining Industry." Paper invited by the 12th International Acoustic Emission Symposium, pp. 147-424.

Hedley, D.G.F. (1991). *A Five-Year Review of the Canada – Ontario – Industry Rockburst Project.* CANMET Special Report, SP90-4E.

Hedley, D.G.F. (1992). *Rockburst Handbook for Ontario Mines.* CANMET Special Report SP92-1E.

Laverdure, L. (1992). *Analysis of Time and Frequency Domain of Mining-Induced Seismicity at Kidd Creek Mine, Ontario.* CANMET Report MRL 92-195 (TR), 1992, p. 167.

Laverdure, L. (1994). *Wave Attenuation of Mining Induced Seismic Events: Part I-Bibliography.* CANMET Report MRL 94-000 (TR), p. 73.

Laverdure, L. and Plouffe, M. (1991). *Full Waveform Analysis at Kidd Creek Mine — Progress Report.* CANMET Report MRL 91-104 (TR), 21 pages.

Laverdure, L. and Rochon, P. (1991). *Spectral Analysis of Sudbury Basin Data for the Proposed Neutrino Laboratory Site in Creighton Mines, Sudbury, Ontario.* CANMET Report MRL 91-131 (TR), p. 167.

Plouffe, M. (1990). *A Local Seismic Survey at Creighton Mine.* CANMET Report MRL 90-076 (TR).

Plouffe, M. (1992). *Preliminary Local Magnitude Scales for Mining-Induced Seismicity at Some Mines in the Sudbury Basin.* CANMET Report MRL 92-109 (TR).

Plouffe, M. (1992). *Preliminary Report on Magnitude Scaling of Mining-Induced Seismicity at Kirkland Lake.* CANMET Report MRL 92-113 (TR).

Plouffe, M. (1993). *Rapport préliminaire: levé séismique à la mine Agnico-Eagle, Joutel, Québec.* CANMET Report MRL 93-002 (CF).

Plouffe, M. and Côté, M. (1993). La Macroséismicité: un outil pour le design minier. 8e journée d'échanges en contrôle de terrain de l'Association minière du Québec, Val d'Or.

Plouffe, M., Lachance, D.V., Asudeh, I., Aguila, R. and Turgeon, L. (1993). "The Agnico-Eagle Mine Seismic Survey." *Proceedings of the 3rd International Symposium on Rockbursts and Seismicity in Mines,* Kingston, Ontario. CANMET Report MRL 93-009 (TR).

Plouffe, M., Mottahed, P., Lebel, D. and Côté, M. (1993). "Monitoring of Large Mining-Induced Seismic Events." *Proceedings of the 3rd International Symposium on Rockbursts and Seismicity in Mines,* Kingston, Ontario.

Pritchard, C. and Talebi, S. (1994). *The Upgraded Sudbury Local Telemetered Network (SLTN): The First Year of Operation (93-94).* CANMET Report MRL 94-053 (TR).

Rochon, P., Lebel, D., Plouffe, M. and Côté, M. (1995). "Rockburst Phenomenon. Data Acquisition and Analysis Using Multi-Tasking and Multi-User Operating Systems." 3e Conférence canadienne sur les applications informatiques dans l'industrie minérale (CAMI'95), Montréal, Quebec.

Stevens, K. (1992). *The Influence of Continuous Structures on Ground Stability at the Fraser Mine, Sudbury Basin.* CANMET Report MRL 92-126 (TR), p.72.

Swan, G., Arjang, B. and Hedley, D.G.F. (1993). "On the Use of Rockfills in Overhand Cut-and-Fill Mining." Proceedings International Congress on Mine Design, Kingston, Ontario.

Talebi, S. (1993). *Source Studies of Mine-Induced Seismic Events Over a Broad Magnitude Range ($-4 < m_N < 4$).* Report MRL 93-046(CL) to CRRP.

Talebi, S. (1994). *Source Studies of Mine-Induced Seismic Events Over a Broad Magnitude Range ($-4 < M < 4$).* MRL 94-030 (CL).

Talebi, S., Ge, M., Rochon, P. and Mottahed, P. "Analysis of Induced Seismicity in a Hard-Rock Mine in the Sudbury Basin, Ontario, Canada." Proceedings of the First North America Rock Mechanics Symposium, pp. 937-944.

Talebi, S., Mottahed, P. and Corbett, G. (1995). "Outburst Monitoring Using Microseismic Techniques in the Phalen Colliery, Sydney, Nova Scotia, Canada." Paper to be presented at the International Symposium on Management and Control of High Gas Emission and Outbursts in Underground Coal Mines, Wollongong, Australia.

Talebi, S., Mottahed, P. and Plouffe, M. (1995). Overview of Mine-Induced Seismicity at CANMET. Workshop on Induced Seismicity, Conference of the Canadian Union of Geophysics, Banff, Alberta.

Talebi, S., Pritchard, C. and Mottahed, P. (1995). "Rockburst Monitoring in Mining Camps of Ontario and Quebec Using CANMET's Digital Seismograph Network." CIM General Meeting, Halifax, Nova Scotia.

Talebi, S. and Young, R.P. (1992). *Source Studies of Mining-Induced Seismic Events Over a Broad Magnitude Range ($-4 < m_N < 4$).* MRD-SM001, 28 pages.

Talebi, S. and Young, R.P. (1993). "Design of a Microseismic Monitoring System for the Investigation of Tunnel Excavation Damage." Proceedings of the 3rd International Symposium on Rockbursts and Seismicity in Mines, Kingston, Ontario, pp. 423-428.

Wetmiller, R.J., Galley, C.A. and Plouffe, M. (1993). "Post-Closure Seismicity at a Hard-Rock Mine." *Proceedings of the 3rd International Symposium on Rockbursts and Seismicity in Mines,* Kingston, Ontario.

Wetmiller, R.J., McNeil, W. and Plouffe, M. (1992). Canada's Largest Rockburst. 33rd U.S. Symposium on Rock Mechanics, Santa Fe, U.S.

Wetmiller, R.J., Galley, C.A. and North, R.G. (1992). "The Role of the National Seismograph Network in Monitoring Mining-Induced Seismicity in Canada." Montréal, Quebec.

LIST OF TABLES

LIST OF FIGURES

Figures in the Appendices

Tables in the Appendices

Glossary of Seismological Terms

Acoustic emission (AE): High-frequency emissions generated by rocks under high stress levels. When this phenomenon is audible, it is also called rock noise.

AE/MS: Simplified term for acoustic emission/microseismic.

Apparent stress: A model-independent estimate of dynamic stress release at the source.

Algebraic Reconstruction Technique (ART): An iterative technique in tomography where a starting model is progressively modified until it converges to a solution.

Asperities: Regions/patches along a fault with strong resistance to shear failure; i.e. regions of highest stress release and seismic energy radiation.

Attenuation (or absorption): Absorption of part of the energy of seismic waves as they travel in an inelastic medium, i.e. selective filtering of the frequency content of seismic waves causing wave distortion.

B- (or Null) axis: The axis corresponding to the intersection of the two nodal planes of a focal mechanism (the movement along this axis is null).

b-value: The slope of the distribution of the logarithm of the number of events versus their magnitude. This parameter can be used as a precursory parameter.

Barriers: Regions/patches along a fault which resist the rupture front and remain unbroken following a rupture sequence.

Body waves: Mechanical waves that propagate through an unbounded continuum. These are of two kinds: P- and S-waves.

Coda waves: The portion of waveforms where vibrations are still being detected long after the passage of seismic waves.

Corner frequency: The frequency corresponding to the intersection of the low- and high-frequency trends of the FFT displacement spectra of radiated P- and S-waves of shear events.

Diffraction tomography: Tomographic imaging using waves scattered by discontinuities within an object.

Displacement spectra: FFT spectra of the displacement of radiated P- or S-waves.

Double couple: A point force system consisting of two superimposed opposing couples having a null momentum. This is the model used to describe shear events in the far field.

Dynamic stress drop: Stress drop based on far-field ground velocity and acceleration.

Earthquake (physical) prediction: The forecasting of the place, size and time of an expected earthquake. Based on the primary information considered, one can distinguish statistical and tectonic predictions. Also, depending on the period of interest, prediction is broken into short-term, intermediate-term and long-term components.

Elastic: An elastic solid recovers its original form following a sequence of loading and unloading; i.e. with no loss of energy during such a process.

Energy flux: The integral of the squared particle velocity of the radiated body waves.

Epicentre: The projection of the hypocentre onto the surface of the Earth.

Error space: 3D distribution of a misfit function, calculated based on residuals, characterizing the error in source location (i.e. a spatial error distribution).

Far field: Area around a source with distances from the source much larger than the actual wavelengths considered; i.e. several wavelengths away from the source.

Fault-slip events: Events caused by slip along pre-existing faults.

FFT: Fast Fourier Transform.

f_{max}: The maximum frequency limit of seismic spectra that can be recorded.

Focal mechanism (or fault plane solution): Radiation pattern for a double couple source, consisting of two quadrants of dilatation and two quadrants of compression.

Focus: Synonym for hypocentre.

Foreshocks: Lower magnitude seismic activity observed prior to earthquakes.

Fractal behaviour: A special type of complexity of a physical phenomenon where the mutual relationship of the elements is the same regardless of the level of observation.

Geometrical spreading (or spherical divergence): Propagation of an expanding spherical wavefront causing the wave amplitude to decrease with distance while the total energy remains the same.

Geophysics: A branch of earth science with the objective of studying the Earth by using the methods and tools available in physics.

Geotomography: Tomographic imaging used in geophysics with the objective being the extraction of useful information about the internal structure of the Earth.

Green's function: A function representing the response of the Earth to slip during the generation of seismic events.

High-frequency systems: Portable data-acquisition systems usually monitoring acoustic emissions in the magnitude range from -6 to -3.

Homogeneous model: A model describing a shear-failure seismic source for which there is a homogeneous stress release along the fault when the rupture is completed.

Homogeneous: A medium where properties are the same at all points.

Hypocentre: The geometrical point where rupture initiates and the earliest P-waves are radiated.

Induced Seismicity: Seismicity caused by human activity, i.e. not directly originating from natural processes (e.g. mining, tunnelling, fluid injection/extraction, dams, etc.)

Inhomogeneous model: A model describing a shear-failure seismic source for which the release of stress along the fault is not homogeneous at the completion of the rupture.

Isotropic: Exhibiting equal physical properties or actions in all directions.

Kinematic model: A model describing a shear-failure seismic source for which the time history of dislocation along the fault has been assumed (e.g. Brune's model).

Macroseismic systems: Data acquisition systems usually monitoring seismic events in the magnitude range from 0 to 3.

Magnitude: An estimate of the strength of an event, usually calculated based on the maximum amplitude of a seismic wave at a particular frequency.

Microseismic systems: Data acquisition systems usually monitoring microseismic events in the magnitude range from - 4 to 0.

Mine-induced events (or tremors): Seismic events generated as a result of mining operations.

Mine-induced seismicity: Seismicity generated as a result of mining operations.

MLTWA (Multiple Lapse (Time Window Analysis): An attenuation measurement method allowing one to estimate the relative importance of intrinsic and scattering components of seismic wave attenuation.

Moment magnitude: An estimate of the strength of an event using its seismic moment.

Near field: Area around a seismic source where distances from the source are smaller than the actual wavelengths considered.

Nodal planes: Two orthogonal planes separating the quadrants of dilatation and compression in a focal mechanism. One of these planes corresponds to the actual fault plane, while the other is called an auxiliary plane.

Nuttli Magnitude: Magnitude based on the maximum amplitude of seismic waves on a logarithmic scale, used for seismic events in the eastern part of North America.

P- (or Pressure) axis: The axis along which the dilational movement of a focal mechanism is a maximum.

P-wave: First type of body waves also called dilatational, compressional, longitudinal, irrotational and Primary wave. The latter name indicates that this type of wave is generally the first one recorded following an earthquake.

Path effects: Distortion of seismic-waveforms due to wave propagation in the Earth.

PCA (Principal Component Analysis): A statistical method used to detect planar features in the distribution of event-source locations.

Polarization: Particle motion in a medium during the passage of a seismic wave.

Porosity: A parameter defining the void ratio in rocks or other materials.

Precursory phenomena: Anomalous occurrences recorded prior to earthquakes. These phenomena can be modelled using nucleation or dilatancy models.

Q- (Quality) factor: A parameter characterizing the attenuation of seismic waves.

Quasi-dynamic model: A model describing a shear-failure seismic source for which the rupture velocity along the fault has been assumed and the time history of dislocation is calculated based on this assumption (e.g. Madariaga's model).

Radiation pattern: The pattern of radiation of the waves generated by seismic sources over different directions of the space.

Residuals: Differences between calculated and observed P- and S-wave arrival times from a seismic source to sensors. This concept is used in source-location techniques.

Rockburst: A mine-induced seismic event, which causes injury or damage to equipment or the displacement of more than five tonnes of rock (Hedley, 1992).

S-wave: Second type of body wave also called shear, transverse, rotational and secondary wave. The latter name indicates that this type of wave arrives generally after the arrival of primary waves of an earthquake.

Scaling relations: Relationships between estimates of source strength and dimensions.

Scattering: Reflection and/or refraction of body waves on discontinuities within a rock mass causing part of the seismic energy to be lost.

Seismic energy: The energy of P- and S-waves radiated by a seismic source.

Seismic event: Instability within a rock mass often caused by rock fracturing at different scales. At the lower end of the seismic scale, these events are sometimes called microseismic or macroseismic events.

Seismic hazard: Hazard caused by potential seismicity in a certain area of the Earth.

Seismicity: Generation of seismic events because of instabilities within the Earth.

Seismogram:	Recorded waveform at a sensor location following a seismic event.
Seismographic systems:	Data acquisition systems usually monitoring seismic events having magnitudes larger than 2.5.
Seismology:	The science of studying earthquakes using their seismograms. Different branches of this science deal with different situations, such as Earthquake seismology, Mine (-induced) seismology, Exploration seismology, etc.
Self-similar rupture process:	Rupture process implied by a constant stress drop model; i.e. seismic events are generated in a similar manner but along different-sized failure areas.
SH-wave:	The horizontal component of a decoupled S-wave.
Shear-wave splitting (or birefringence):	Decoupling of S-wave into two components travelling at two different speeds within an isotropic media.
Simplex:	A geometric figure with one more vertex than the dimensions of the space to search.
Simultaneous Iterative Reconstruction Technique (SIRT):	An iterative process where a starting model is progressively modified until it converges to a solution.
Slip function:	A function describing the fault displacement during the generation of seismic events.
Source-location techniques:	Techniques used to determine the location of seismic events. They can be divided into direct methods (e.g. USBM method) and iterative methods (e.g. Geiger's and Simplex methods).
Source location:	Equivalent to hypocentre; i.e. the point of rupture initiation.
Source parameters:	Seismic parameters, calculated in time and frequency domains, characterizing the properties of the seismic source.
Source region (or focal region):	The zone of rupture associated with a seismic event.
Spectral analysis:	Analysis of radiated seismic waves using their FFT spectra.
Static stress drop:	The average difference between the initial and final stress levels over a fault plane following a rupture sequence.
SV-wave:	The component of a decoupled S-wave polarized in a vertical plane and perpendicular to the seismic ray.
T- (or Tension) axis:	The axis along which the compressional movement of a focal mechanism is a maximum.

Tomography: Reconstruction of some property within an object, along a cross-section or in a volume, by measuring, on the perimeter of the object, the energy passing through it and then using inversion techniques.

Tomographic imaging: Producing an image of some property within an object using tomography.

Transmission tomography: Tomographic imaging using waves directly transmitted from sources to receivers on the perimeter of an object.

Velocity model: A model of the distribution of seismic velocities within an area of the Earth used in source-location determinations.

Nomenclature

A	Seismic source area
A_1, A_2	Wave amplitude at points 1 and 2
C	P- or S-wave velocity
C_p	P-wave velocity
C_s	S-wave velocity
f	Frequency
f_0	Corner frequency
f_1, f_2	Low- and high-frequency limits of the spectral bandwidth
F_C	P- or S-wave radiation coefficient
f_{max}	Maximum frequency limit of seismic spectra
J_C	Energy flux
M	Moment magnitude
M_0	Seismic moment
M_L	Richter magnitude
m_N	Nuttli magnitude
M_S	Magnitude calculated based on surface waves
M_A	Magnitude calculated based on maximum acceleration
M_D	Magnitude calculated based on duration of coda waves
Q	Quality factor of P- or S-waves
r_0	Source radius (radius of a planar circular source)
R	Source-sensor distance
R_C	Free surface amplification factor
u	Average slip on the fault plane
α	Attenuation parameter
$\Delta\sigma$	Static stress drop
λ	Lamé constant
μ	Shear modulus of rigidity of rock
ρ	Rock density
σ_d	Dynamic stress drop
σ_{rms}	rms stress drop
Ω_0	Plateau level of displacement spectra
ω	Angular frequency ($= 2 \pi f$)